Christoph M. Augustin

Classical and All-floating FETI Methods with Applications to Biomechanical Models

Monographic Series TU Graz

Computation in Engineering and Science

Series Editors

G. Brenn	Institute of Fluid Mechanics and Heat Transfer
G. A. Holzapfel	Institute of Biomechanics
W. von der Linden	Institute of Theoretical and Computational Physics
M. Schanz	Institute of Applied Mechanics
O. Steinbach	Institute of Computational Mathematics

Monographic Series TU Graz

Computation in Engineering and Science Volume 27

Christoph M. Augustin

Classical and All-floating FETI Methods with Applications to Biomechanical Models

---

This work is based on the dissertation *"Classical and All-floating FETI Methods with Applications to Biomechanical Models"*, presented by Christoph M. Augustin at Graz University of Technology, Institute of Computational Mathematics (Math D) in 2012.
Supervisor: Steinbach, Olaf, (Graz University of Technology)
Reviewer: Holzapfel, Gerhard (Graz University of Technology)
Meyer, Arnd (TU Chemnitz, Germany)

© 2015 Verlag der Technischen Universität Graz

Cover photo	Vier-Spezies-Rechenmaschine by courtesy of the Gottfried Wilhelm Leibniz Bibliothek – Niedersächsische Landesbibliothek Hannover
Layout	Wolfgang Karl, TU Graz / Universitätsbibliothek Christina Fraueneder, TU Graz / Büro des Rektorates
Printed	by TU Graz / Büroservice

Verlag der Technischen Universität Graz
www.ub.tugraz.at/Verlag

Print:

ISBN: 978-3-85125-418-1

E-Book:

ISBN: 978-3-85125-419-8

DOI: 10.3217/978-3-85125-418-1

http://creativecommons.org/licenses/by-nc-nd/3.0/at/

Abstract

This work deals with domain decomposition solvers, more precisely the finite element tearing and interconnecting (FETI) approach, to simulate the elastic behavior of cardiovascular tissues, such as the myocardium or the artery. These biological materials are characterized by anisotropic and nonlinear material properties due to preferential orientations of collagen and muscle fibers in the tissue. The high complexity of the underlying nonlinear equations as well as fine geometrical structures of the cardiovascular components demand fast solving algorithms, where FETI is an efficient choice. This approach shows high performance and enables a natural parallelization to solve the nonlinear elasticity problem.

The strategy of the FETI method is to decompose the computational domain into a finite number of non-overlapping subdomains. Therein the corresponding local problems can be handled efficiently by direct solvers. The reduced global system, that is related to discrete Lagrange multipliers on the interface of the subdomains, is then solved with a parallel Krylov space method to compute the desired solution. This is, in the case of elasticity, the stress and subsequently, in a postprocessing step, we deduce the displacement locally. For the global iterative method suitable preconditioning is a substantial factor. Besides a simple lumped preconditioner and an optimal Dirichlet preconditioner a novel BEM based preconditioner, formed by local hypersingular boundary integral operators, is considered. The idea behind this preconditioner is the approximation of Steklov–Poincaré operators, the basis for the optimal Dirichlet preconditioning, by computationally less expensive hypersingular operators.

Another innovative aspect is the usage of all-floating FETI, a variant of classical FETI, for nonlinear soft tissue mechanics. This approach, where the Dirichlet boundary acts as a part of the interface, shows significant advantages in the implementation and in the convergence of the global iterative method which is evidenced by numerical examples. As realistic and clinically relevant applications we present passive inflation experiments, comparable to stenting or angioplasty procedures, using anatomically detailed geometries of arteries and the myocardium.

Zusammenfassung

Die vorliegende Arbeit beschäftigt sich mit Gebietszerlegungsmethoden, genauer gesagt mit der „Finite Element Tearing and Interconnecting“– Methode (FETI), zur Simulation des elastischen Verhaltens von kardiovaskulärem Gewebe. Beispiele hierfür sind der Herzmuskel oder die Arterie. Diese biologischen Materialien zeichnen sich durch anisotrope und nichtlineare Materialeigenschaften aus, die durch eine bevorzugte Orientierung von Kollagen- und Muskelfasern im Gewebe verursacht werden. Die dadurch entstehende hohe Komplexität der zugrunde liegenden nichtlinearen Gleichungen, sowie die feinen Strukturen der Herz–Kreislauf–Komponenten erfordern schnelle und effiziente Lösungsalgorithmen. Eine Möglichkeit hierfür ist die oben genannte FETI–Methode. Dieser Ansatz ermöglicht eine natürliche Parallelisierung des nichtlinearen Elastizitätsproblems, wobei der Kommunikationsaufwand zwischen den einzelnen Prozessen relativ gering gehalten wird.

Die Grundidee der FETI–Methode ist es, das Rechengebiet in eine endliche Anzahl von nicht-überlappenden Teilgebieten zu zerlegen. In diesen Teilgebieten können die kleineren lokalen Probleme effizient durch direkte Löser behandelt werden. Die globale Lösung, im Falle der Elastizität die globale Verschiebung, wird durch ein reduziertes globales System, das mit einem parallelen Krylovraum–Verfahren gelöst wird, rekonstruiert. Für das globale Krylovraum–Verfahren werden geeignete Vorkonditionierungsstrategien benötigt. In dieser Arbeit betrachten wir in diesem Zusammenhang den einfachen „lumped“–Vorkonditionierer, den optimalen Dirichlet–Vorkonditionierer und einen, in dieser Anwendung neuen, auf Randelementverfahren basierenden BEM–Vorkonditionierer. Dieser wird mit dem aus Randelementverfahren bekannten hypersingulären Integraloperator gebildet. Diese Art der Vorkonditionierung funktioniert aufgrund der Spektraläquivalenz der lokalen hypersingulären Operatoren mit den lokalen Steklov–Poincaré–Operatoren. Diese bilden die Grundlage für den optimalen Dirichlet–Vorkonditionierer.

Eine Variante des klassischen FETI-Ansatzes ist „Allfloating“–FETI, wo im Gegensatz zur klassischen Formulierung der Dirichlet–Rand als Teil des Koppelrandes betrachtet wird. Das in der Simulation von nichtlinearen orthotropen biologischen Materialien erstmals angewendete „Allfloating“–FETI Verfahren vereinfacht die Implementierung und verbessert in vielen Fällen die Konvergenz der globalen iterativen Methode. Dies wird durch eine große Anzahl an numerischen Beispiele belegt, wo wir die klassische Formulierung mit dem „Allfloating“–Ansatz und die verschiedenen Vorkonditionierungstechniken vergleichen. Als klinisch relevante Anwendung präsentieren wir Druckexperimente, wie sie vergleichbar bei der Angioplastie oder bei der Stenting Methode auftreten, unter Verwendung von anatomisch realistischen hochdetailierten Geometrien von Arterien und eines Herzmuskels.

CONTENTS

1 INTRODUCTION

Motivation

According to a recent report, published by the World Health Organization (WHO) in 2011, cardiovascular diseases, such as atherosclerosis or heart diseases, "are the leading causes of death and disability in the world" [123]. Hence, the understanding of the underlying pathological processes is a very important topic in many different fields of science.

In the areas of applied mathematics the interest lies, e.g., in the simulation of electrochemical processes in the heart, in the modeling of the blood flow through the human body, resulting in fluid structure interaction problems, and many others. In this work the mechanical behavior of the organs involved in the cardiovascular system, such as arteries or the myocardium of the heart is investigated. *In silico* simulations of arterial tissues which are exposed to boundary forces, may help to improve surgical methods such as angioplasty or artery stenting. The elastomechanical modeling of the myocardium and especially the modeling of the coupling of the mechanics with electrochemical processes in the heart is still in its infancy. Nonetheless, work in this field will give the possibility to study cardiac diseases without open surgery and maybe comprehend activities in the cardiovascular system that are not yet understood.

Partial Differential Equations and Finite Element Methods

The basis for the numerical simulation of biological tissues are *partial differential equations* (PDEs) that appear throughout in the modeling of the physics of natural processes. As cardiovascular tissues are regarded as elastic materials the main PDE to consider in this work are the *stationary equilibrium equations*

$$\operatorname{div} \boldsymbol{\sigma}(\mathbf{u}, \mathbf{x}) + \mathbf{f}(\mathbf{x}) = \mathbf{0} \quad \text{for } \mathbf{x} \in \Omega,$$

with the stress tensor $\boldsymbol{\sigma}$ that depends on the unknown displacement field $\mathbf{u}$, the source term $\mathbf{f}$ and the computational domain $\Omega \subset \mathbb{R}^3$. In order to formulate boundary conditions, the boundary $\Gamma = \partial\Omega$ is decomposed into disjoint parts so that $\Gamma = \overline{\Gamma}_{\mathrm{D}} \cup \overline{\Gamma}_{\mathrm{N}}$. To embed forces that act on the boundary of the domain, like tension, traction or pressure, Neumann boundary conditions $\boldsymbol{\sigma}(\mathbf{u}, \mathbf{x})\mathbf{n}(\mathbf{x}) = \mathbf{g}_{\mathrm{N}}(\mathbf{x})$ are set on Γ_{N}, with

$\mathbf{n}(\mathbf{x})$ the exterior normal vector. Dirichlet boundary conditions $\mathbf{u}(\mathbf{x}) = \mathbf{g}_{\mathrm{D}}(\mathbf{x})$ on Γ_{D} correspond to a prescribed displacement field, that is enforced component-by-component.

The modeling of different elastic materials is realized by using a so-called *strain-energy function* Ψ to formulate a constitutive equation for the stress tensor

$$\boldsymbol{\sigma} = 2\det(\mathbf{F})^{-1}\mathbf{F}\frac{\partial\Psi(\mathbf{C})}{\partial\mathbf{C}}\mathbf{F}^{\top},$$

where $\mathbf{F}$ is the deformation gradient and $\mathbf{C} = \mathbf{F}^{\top}\mathbf{F}$ is the right Cauchy–Green tensor. For a comprehensive overview and mathematical theory on elastic deformations, compare Ciarlet [38], Holzapfel [80], and Ogden [139]. A well established model for arterial tissues is discussed by Holzapfel et al. [82]. An adequate model for the myocardium can be found in a recent publication of Holzapfel and Ogden [85].

In almost every practical application, an analytical solution of the PDE is not possible. The *finite element method* (FEM) provides a powerful numerical tool to find an approximate solution of the equilibrium equations. The analytical framework for the finite element method is discussed in an overwhelming amount of books including the classic works by Ciarlet [39] and Zienkiewicz [192] and more recent by Brenner and Scott [29] and Braess [25]. In addition, for explanations on the solvability of the governing equations, especially for (non)linear elasticity problems, see [38, 43].

Due to preferential orientations of fibers such as collagen, the modeling of biological tissues leads to an anisotropic and highly nonlinear material model. In order to apply the FEM to this problem, Galerkin methods are used to discretize the variational form of the equilibrium equation and a Newton–Raphson's scheme is applied to linearize the problem [81]. This leads to a series of linearized systems of equations that need to be solved by elaborate direct or iterative solution techniques.

Domain Decomposition Methods

Anatomically highly detailed models of cardiovascular organs, where high spatial resolution is necessary to resolve geometric details, result in systems of equations with a vast amount of of degrees of freedom (DOF). Together with the high complexity of the underlying partial differential equations this demands fast solving algorithms and, conforming to up-to-date computer hardware architectures, parallel methods. One possibility to achieve these specifications are *domain decomposition* (DD) methods. The first reference to these numerical techniques was the alternating Schwarz method, already mentioned in the early work of Schwarz [166]. In the last three decades several overlapping as well as non-overlapping DD methods were developed. They all work according to the same principle: the domain Ω is subdivided into a set

of (overlapping or non-overlapping) subdomains Ω_i. The idea of DD algorithms is to decompose the large global system into a set of smaller local subproblems on the subdomains. This yields a natural parallelization of the underlying problem. In addition to well established standard DD methods, other examples for more advanced domain decomposition methods are hybrid methods [177], mortar methods [21, 118, 186] and *tearing and interconnecting* methods. The latter include the FETI method introduced by Farhat and Roux [55] for the finite element approach and the BETI method, see Langer and Steinbach [114], for boundary elements. Commendable compendia on domain decomposition methods are the works of Quarteroni and Valli [145] and Toselli and Widlund [178].

In the following, the emphasis is on the FETI approach and its application to the nonlinear equilibrium equations for elasticity. A modification of the classical finite element tearing and interconnecting method, the dual-primal FETI (FETI–DP) method [53, 110], was already applied to model arterial tissues, see, for example, Klawonn and Rheinbach [106, 147], Brands et al. [27, 28], Balzani et al. [16, 17] and Brinkhues et al. [31]. In contrast to that, this work focuses on the alternative *all-floating tearing and interconnecting method* (AF–FETI), which was introduced independently for the boundary element method by Of and Steinbach [136–138] and as the Total–FETI (TFETI) method for finite elements by Dostál et al. [51]. In Augustin et al. [7, 8], we show the great performance of AF–FETI for nonlinear elasticity problems including passive inflation experiment with cardiovascular tissues as a clinical relevant application. A mathematical analysis of FETI methods with convergence proofs for the classical one-level FETI method is given in [107, 110, 119]. The underlying principle of all FETI methods is a non-overlapping domain decomposition

$$\overline{\Omega} = \bigcup_{i=1}^{p} \overline{\Omega}_i \quad \text{with } \Omega_i \cap \Omega_j = \emptyset \quad \text{for } i \neq j, \quad \Gamma_i = \partial\Omega_i$$

and $\Gamma_{ij} := \Gamma_i \cap \Gamma_j$ defines the local interfaces. The global coupling boundary Γ_{C} is the union of all these local interfaces. Instead of the global problem, local subproblems are considered to find the restrictions $\mathbf{u}_i = \mathbf{u}_{|\Omega_i}$ satisfying the stationary equilibrium equations

$$\operatorname{div}(\boldsymbol{\sigma}(\mathbf{u}_i, \mathbf{x})) + \mathbf{f}(\mathbf{x}) = \mathbf{0} \quad \text{for } \mathbf{x} \in \Omega_i$$

locally. Additionally, Dirichlet and Neumann boundary conditions

$$\mathbf{u}_i = \mathbf{u}_{\mathrm{D}} \text{ on } \Gamma_{\mathrm{D}} \cap \Gamma_i, \quad \boldsymbol{\sigma}(\mathbf{u}_i)\,\mathbf{n}_i = \mathbf{g}_{\mathrm{N}} \text{ on } \Gamma_{\mathrm{N}} \cap \Gamma_i,$$

and the transmission conditions

$$\mathbf{u}_i = \mathbf{u}_j, \quad \mathbf{t}_i + \mathbf{t}_j = \mathbf{0} \quad \text{on } \Gamma_{ij},$$

are imposed, where $\mathbf{t}_i = \boldsymbol{\sigma}(\mathbf{u}_i)\mathbf{n}_i$ is the local boundary stress and $\mathbf{n}_i$ is the exterior

normal vector of the local subdomain boundary $\Gamma_i = \partial\Omega_i$. After discretization the FETI approach leads to a reduced global system of equations that is related to discrete Lagrange multipliers on the coupling boundary Γ_C. This global system is then solved with a parallel Krylov space method with suitable preconditioning. A computationally efficient form of preconditioning, the *lumped preconditioner*, was already discussed by Farhat and Roux [55] and a few years later an optimal, so-called *Dirichlet preconditioner* was introduced [54]. In addition to that, we motivate a novel *BEM based preconditioner*, formed by local hypersingular boundary integral operators. The idea of this preconditioner is the approximation of Steklov–Poincaré operators, the basis for the optimal Dirichlet preconditioning, by computationally less expensive hypersingular operators. Especially for large subdomains the BEM based preconditioner is an excellent alternative since the Steklov–Poincaré operator requires the formation of an additional inverse matrix. On the other hand, given the approximation properties of the hypersingular operator, the BEM preconditioner yields better condition numbers than the computationally more efficient lumped preconditioner. For a comprehensive introduction to boundary integral equation methods see [89, 122, 176].

Solving the local systems of equations is a great challenge, since in so-called *floating subdomains*, which have no contribution to the Dirichlet boundary, this corresponds to a local Neumann problem. The kernel of the local operator is non-trivial and in the case of 3D elasticity the solution is only unique up to the six rigid body modes. In the case of a known kernel the sought-after generalized inverse matrix may be realized using direct solvers with a sparsity preserving stabilization [32] or stabilized iterative methods. Nevertheless, the identification of the kernel is a delicate matter for classical FETI where "semi-floating" subdomains, with only a single edge or a single point on the Dirichlet boundary, may occur. One possibility to overcome this problem is the before mentioned FETI–DP method where some specific *primal* degrees of freedom are fixed. This yields solvable systems for all subdomains, but choosing the primal DOF remains a sophisticated task. For linear elasticity this issue is discussed in Klawonn and Widlund [109, 111]. For our method of choice all-floating FETI the Dirichlet boundary acts as a part of the coupling boundary and all subdomains are considered as "floating". The displacement conditions are incorporated in the system using discrete Lagrange multipliers and the identification of the kernels of the local operators is trivial and equal to the six rigid body modes for all subdomains. This eases the implementation a lot and, due to mapping properties of the local operators, also improves the convergence of the global iterative method. These advantages of AF–FETI compared to classical FETI are shown in the numerical examples section and were also documented in our publications [7, 8]. As an additional advantage the local systems resulting from AF–FETI are typically better conditioned than those arising in the FETI–DP approach [32].

Outline of Contents

Subsequent to this introduction, a short overview on the histology of biological materials is given in the second chapter. The mechanical properties of arteries as well as the myocardium are discussed. Worth mentioning in this context is the layered structure of the tissue and its composition of elastin and reinforced collagen and muscle fibers. This complex structure leads to a highly nonlinear, anisotropic and nearly incompressible material behavior.

The third chapter starts with a general overview to continuum mechanics. Here, we explain two central concepts, the reference and the current configuration, and transformations from one to the other. The main tensors needed to formulate material models such as the deformation gradient or the right and the left Cauchy–Green deformation tensor, are introduced. Subsequently, we set up the main equations using the fundamental *Cauchy stress theorem* which results in PDEs for quasi-stationary elasticity problems. Specific models ranging from simple linear elastic to general nonlinear elastic materials are discussed and we formulate constitutive equations using so-called strain-energy functions. To conclude this chapter we outline the construction of nonlinear material models for the artery and the myocardium. We show the specific representation of the strain-energy function and, using this functional, calculate the tensors and derivatives needed for the implementation of the numerical methods.

In the forth chapter the variational formulation for linear and nonlinear elasticity problems is presented. This formulation is the basis for the finite element approach which is discussed in the following chapter. Nonlinear problems demand the use of linearization techniques, such as the well-known *Newton method* in Banach spaces. We discuss basic ideas of this scheme for the particular case of nonlinear elasticity and outline the main steps that lead to a linearized version of the variational formulation. Numerical challenges which must be taken into account for (nearly) incompressible elastic materials are so-called *locking effects*. A possibility to overcome this worry is the formulation as a *saddle point problem* or the *mean dilatation technique*, which are both based on a decoupled formulation of the weak form. Furthermore, we show unique solvability of linear elasticity problems (*Korn's inequalities*) and we discuss the existence theorems for nonlinear elastic materials. In this context, we introduce a variety of convexity concepts for general nonlinear elasticity, which includes the artery and the myocardium model.

Subsequently, we focus on discretized variational formulations in the fifth chapter. To find an approximate solution of the classical boundary value problem the *finite element method* is used and basic ideas of this concept are outlined. In the case of discretized nonlinear problems *inexact Newton methods* are applied and we give a short overview and a convergence analysis of this linearization procedure. In great detail

the assembling of the involved stiffness matrices and vectors is described. Moreover, we discuss different types of solvers for the system of linear(ized) equations, that arises from the finite element method. Some direct solver packages are presented and we outline the main iterative methods, including the conjugate gradient (CG) and the generalized minimal residual (GMRES) method. At last, we give a short overview to time and load stepping schemes.

The sixth chapter comprises a general introduction to domain decomposition methods. We start with a short historical review and present the basic concepts that are suitable for all DD methods. Subsequently, we concentrate on the finite element tearing and interconnecting approach. The main steps from the general finite element to the FETI formulation are given. This results in a split-up of the global problem in particular local subproblems, which may be solved in parallel, and a global iterative solver. Diverse preconditioning techniques for this global iterative method are presented, including the well known Dirichlet and lumped preconditioners as well as a novel *BEM-based preconditioner* using hypersingular boundary integral operators. We also present a modification of classical FETI, the *all-floating* FETI approach which shows advantages in implementation and convergence of the global solver. This chapter is concluded with an overview on the implementation, including the construction of the main operators and the generalized inverse matrices.

In the seventh chapter we present numerical examples where all-floating FETI and classical FETI are compared and all discussed preconditioners are tested. First the correctness of the FETI implementation is shown for linear elasticity problems where exact solutions are prescribed. Consequently, the FETI methods are applied to the realistic application of a passive inflation experiment using nonlinear elastic materials, in particular the anisotropic artery and the orthotropic myocardium model. Anatomically detailed models of an aorta, a two-layered carotid artery and the myocardium of a rabbit heart are used. We compare different preconditioning techniques and show differences between the AF–FETI and the classical FETI approach concerning convergence of the global iterative method and computational time.

We conclude with a short overview and an outlook to upcoming perspectives and open questions in the last chapter.

2 HISTOLOGY OF BIOLOGICAL MATERIALS

In this chapter, we give a general introduction to the histology and the mechanical properties of biological tissues, where we concentrate on arteries and the cardiac muscle, i.e. the myocardium, in particular. These elastic materials will later be described by material models (Chapter 3) and simulated by in silico experiments (Chapter 7). For more information on the histology of cardiovascular tissues see, e.g., Humphrey [91, 93] for arteries and LeGrice et al. [116, 117], Young et al. [191] and Sands et al. [158] for the heart.

2.1 Histology of Arteries

Arteries are vessels that transport blood from the heart to the organs. In vivo the artery is a prestretched elastic material under an internal pressure load. In this work, we concentrate on the in vitro passive behavior of healthy arteries. Hence, in vivo effects such as the vasa vasorum[1] and others are neglected. In general, arteries are subdivided into two types: *elastic* and *muscular* arteries. The elastic type is characterized by a large diameter and its proximity to the heart. One example for such a proximal artery with elastic behavior is the aorta. On the other hand, muscular vessels are located within the periphery of the body and are also called distral arteries. These vessels, which include for example the small cerebral arteries in the brain, show a pronounced viscoelastic behavior with hysteresis. However, some arteries exhibit morphological structures of both types. Healthy arterial walls consist of three primary layers: the intima, the media and the adventitia. For a diagrammatic model of the major components of a healthy elastic artery see Figure 2.1.

The *intima* is the innermost layer of an artery. It consists solely of a single layer of endothelial cells which serve as an interface between elastic material and blood.

The middle layer of an artery is called *media*. In contrast to the intima it is a complex 3D network of muscle cells, elastin and collagen fibers. The media shows a high ability to resist loads in both the longitudinal and circumferential direction. In healthy arteries it is the most significant layer from the mechanical perspective [82].

[1] Network of small blood vessels that supply the outer tissues of larger ones (e.g. the aorta).

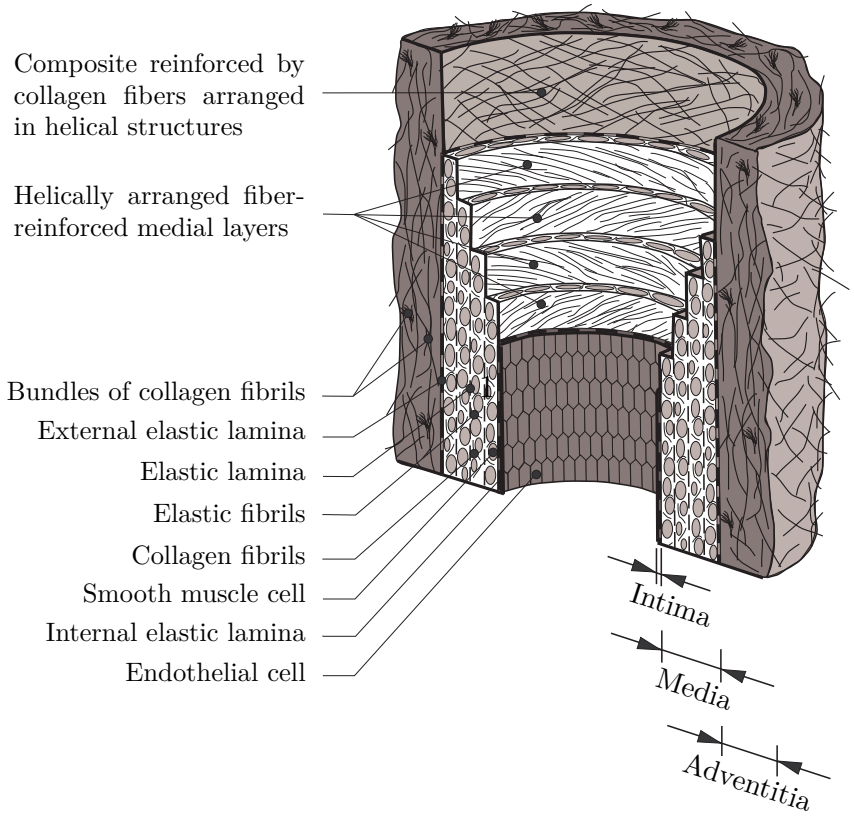

Figure 2.1: Diagrammatic model of the major components of a healthy elastic artery, from Holzapfel et al. [82].

At last the outermost layer of an artery is the so-called *adventitia*. It consists of histological ground substance and thick bundles of collagen fibers. At higher levels of pressure the adventitia behaves like a stiff "jacket-like" tube [165].

2.2 Typical Mechanical Behavior of Arterial Walls

As mentioned before, proximal arteries can be modeled as an elastic material, while distral arteries behave rather like a viscoelastic or pseudo-elastic material. Healthy arteries are highly deformable composite structures and show a nonlinear stress-strain response with a typical stiffening effect at higher pressures. Reasons for this are the embedded collagen fibers which lead to an *anisotropic*, in particular an *orthotropic*, mechanical behavior of arterial walls, see Figure 2.2. In this context anisotropy is the general term for a directionally dependent material property. Orthotropic materials, which are characterized by three orthogonal axes of rotational symmetry,

and transversely isotropic materials, which are symmetric about one axis that is normal to a plane of isotropy, are special cases of fully anisotropic solids.

An important observation is that arteries do not change their volume within the physiological range of deformation [82]. Thus, they are most commonly treated as nearly incompressible materials. Another property is the existence of certain in vivo prestretches in longitudinal direction, the consequence being that a segment of a vessel shortens on removal from the body. In circumferential direction a load-free arterial ring contains residual stresses. So it will spring open when one cuts it in a radial direction. More information on the histology of arterial walls can be found in the works of Humphrey [91, 93], Holzapfel et al. [78, 82] or Rodin [156]. Nice illustrations of the prestretches and residual stresses one can find in Holzapfel et al. [87], the modeling of such a problem is discussed in Holzapfel and Ogden [86] and Bustamante and Holzapfel [33].

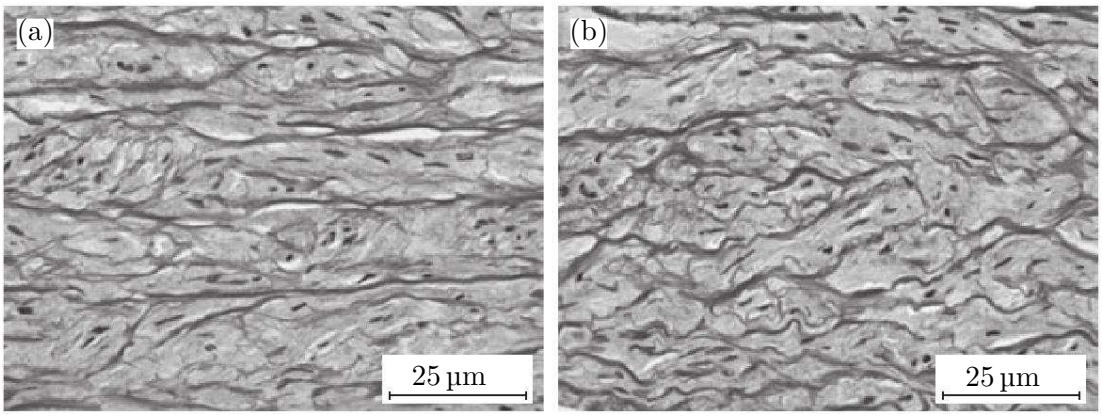

Figure 2.2: Histological images of collagen in the media of a human aorta: (a) stretched and (b) unstretched sample, from Holzapfel [78].

2.3 Histology of the Human Heart

The heart consists of four chambers, the right and the left atrium and the right and the left ventricle. Here, the ventricles serve to pump blood around the body while the atria are the receiving chambers of the heart. The wall thickness varies a lot over these different parts and as well over the different phases of a cardiac cycle.

Like the arterial wall the heart wall consists of different layers. The inner layer is called the *endocardium*, which serves as an interface between elastic media and blood. The *epicardium*, the outermost layer, serves as a protective membrane. Comparable

to the endocardium it is just a thin layer with an approximate wall thickness of 100 µm [85].

The *myocardium* is the middle layer and the functional tissue of the heart wall with a complex orthotropic structure [85]. In this work, we emphasize on passive myocardial tissue of the left ventricle which consists of myocardiocyteal muscle cells and is the most significant part for the modeling of the elastic behavior of the heart wall. The cardiac myocytes[2] are arranged in parallel in different sheets and are the predominant fiber type within the myocardium, while collagen is arranged in a spatial network that connects the muscle fibers. Characteristic for the myocytes is a layered organization which can be described by a right-handed orthonormal set of basis vectors (Figure 2.3). This set consists of a vector field $\mathbf{f}_0$ that coincides with the main direction of the muscle fibers which is referred to as the *fiber axis*. The second basis vector is the so-called *sheet axis* $\mathbf{s}_0$ which is defined to be perpendicular to $\mathbf{f}_0$ in the plane of the layer. This direction coincides with the collagen fiber orientation (Figure 3.4). The orthonormal set is completed by the *sheet-normal axis* $\mathbf{n}_0$.

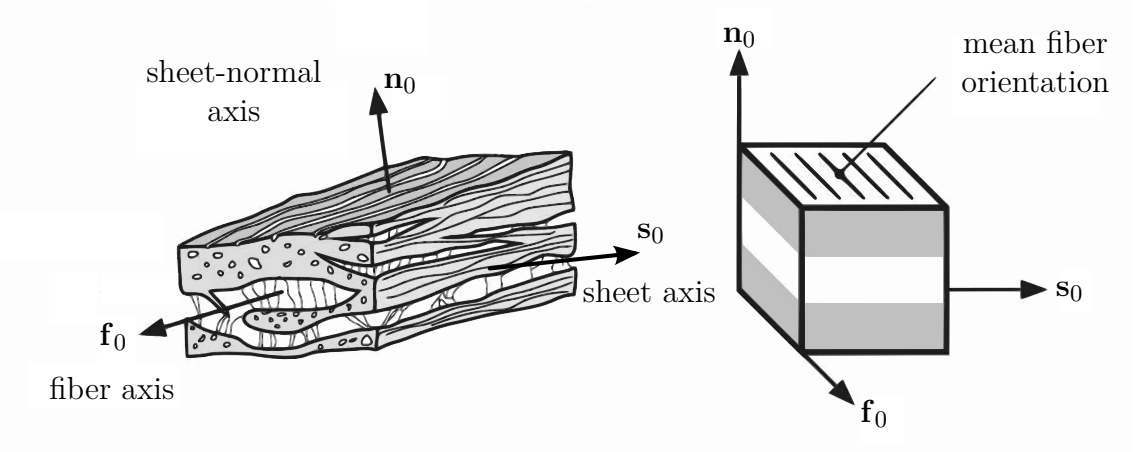

Figure 2.3: Indication of the layered organization of the muscle fibers within the myocardium with a right-handed orthonormal coordinate system where $\mathbf{f}_0$ is the fiber axis, $\mathbf{s}_0$ is the sheet axis and $\mathbf{n}_0$ is the sheet-normal axis. This schematic of the layered tissue serves as a basis for the constitutive model, from Holzapfel and Ogden [85].

2.4 Mechanical Behavior of Heart Walls

As arterial walls and many other biological tissues the myocardium is generally treated as a nearly incompressible material [184]. It shows a highly nonlinear and,

[2] in this context muscle fibers

due to the myocytes and collagen, an orthotropic behavior. The muscle fibers are arranged in a layered organization with an orthogonal basis, which was shown in experiments by Dokos et al. [50]. In this publication the authors also perform shear tests on a cube of myocardial specimen in the direction of the three different orthogonal planes. From these experiments it was observed that the ventricular myocardium is most resistant to shear deformations in the plane built by the vector fields $\mathbf{f}_0$ and $\mathbf{s}_0$ (fs-plane). High resistance was also shown in the fn-plane. In all other directions the resistance to simple shear deformations was considerably smaller. More details concerning the mechanical properties of the myocardium can be found in Holzapfel and Ogden [85] and references therein.

3 MODELING THE NONLINEAR BEHAVIOR OF BIOLOGICAL TISSUES

The aim of this chapter is to describe the highly nonlinear material properties of biological tissues by an anisotropic model that is capable of large elastic deformations. The following is related to the descriptions in the monographs of Holzapfel [80], Ogden [139] and Ciarlet [38]. The mathematical model for arterial walls is discussed in detail in the papers of Holzapfel et al. [82, 84] and the myocardium in the studies of Holzapfel and Ogden [85] and Eriksson et al. [52].

3.1 Preliminaries

A *body* $\mathcal{B}$ is a set with elements that correspond to points of a Lipschitz domain[1] Ω in the three-dimensional Euclidean space. The elements of $\mathcal{B}$ are called *particles* and Ω is the *configuration* of $\mathcal{B}$. If the body moves then this configuration changes with time $t \in \mathbb{R}^+$. For each t a unique configuration Ω_t is associated. For $t = 0$ the body $\mathcal{B}$ occupies an arbitrary but fixed configuration Ω_0 which is called the *reference* or *undeformed configuration*. Here, each particle x of the body may be specified by its position vector $\mathbf{X}$ in Ω_0 relative to some origin. For an arbitrary time t the body occupies the configuration Ω_t which we identify as the *current* or *deformed configuration*. Let $\mathbf{x}$ be the position vector of the particle x in the current configuration. The vector $\mathbf{X}$ describes the *material* or *referential* coordinates of a point, while $\mathbf{x}$ describes the *spatial* or *current* coordinates. Since both Ω_0 and Ω_t are configurations of $\mathcal{B}$ there exists a bijective mapping $\boldsymbol{\chi} : \Omega_0 \mapsto \Omega_t$ such that

$$\mathbf{x} = \boldsymbol{\chi}(\mathbf{X}, t) \quad \text{for all } \mathbf{X} \in \Omega_0,\ t \in \mathbb{R}^+.$$

The mapping $\boldsymbol{\chi}$ is called the *motion* or *deformation* of the body $\mathcal{B}$ from Ω_0 to Ω_t. We assume that $\boldsymbol{\chi}(\mathbf{X}, t)$ is twice continuously differentiable with respect to position and time. Its inverse $\boldsymbol{\chi}^{-1}(\mathbf{x}, t)$ is uniquely defined as

$$\mathbf{X} = \boldsymbol{\chi}^{-1}(\mathbf{x}, t) \quad \text{for all } \mathbf{x} \in \Omega_t,\ t \in \mathbb{R}^+.$$

The terminologies *Lagrangian* and *Eulerian description* are also used with respect to Ω_0 and Ω_t respectively.

[1] a domain whose boundary is "sufficiently regular"

The vector fields $\mathbf{u}(\mathbf{x},t) = \mathbf{x} - \mathbf{X}(\mathbf{x},t)$ and $\mathbf{U}(\mathbf{X},t) = \mathbf{x}(\mathbf{X},t) - \mathbf{X}$ represent the *displacement field* of a particle. One can easily show that

$$\mathbf{u}(\mathbf{x},t) = \mathbf{u}(\boldsymbol{\chi}(\mathbf{X},t)) = \mathbf{U}(\mathbf{X},t). \tag{3.1}$$

In the following we adopt *Einstein's summation convention* which implies a summation over the range of every index that is repeated within the same term.

Definition 3.1 (Material and spatial gradient)**.** *The* material gradient *of a sufficiently smooth material field* $\Phi(\mathbf{X},t)$ *is defined as*

$$\operatorname{Grad}\Phi(\mathbf{X},t) := \nabla_{\mathbf{X}}\Phi(\mathbf{X},t) = \frac{\partial}{\partial X_i}\Phi(\mathbf{X},t)\,\mathbf{e}_i.$$

The spatial gradient *of a sufficiently smooth spatial field* $\phi(\mathbf{x},t)$ *is defined as*

$$\operatorname{grad}\phi(\mathbf{x},t) := \nabla_{\mathbf{x}}\phi(\mathbf{x},t) = \frac{\partial}{\partial x_i}\phi(\mathbf{x},t)\,\mathbf{e}_i.$$

In the case of vector-valued functions $\mathbf{W}$ *and* $\mathbf{w}$ *we define the gradients as*

$$\operatorname{Grad}\mathbf{W}(\mathbf{X},t) := \nabla_{\mathbf{X}} \otimes \mathbf{W}(\mathbf{X},t) = \frac{\partial}{\partial X_j}\mathbf{W}(\mathbf{X},t) \otimes \mathbf{e}_j = \frac{\partial}{\partial X_j}W_i(\mathbf{X},t)\,\mathbf{e}_i \otimes \mathbf{e}_j,$$
$$\operatorname{grad}\mathbf{w}(\mathbf{x},t) := \nabla_{\mathbf{x}} \otimes \mathbf{w}(\mathbf{x},t) = \frac{\partial}{\partial x_j}\mathbf{w}(\mathbf{x},t) \otimes \mathbf{e}_j = \frac{\partial}{\partial x_j}w_i(\mathbf{x},t)\,\mathbf{e}_i \otimes \mathbf{e}_j.$$

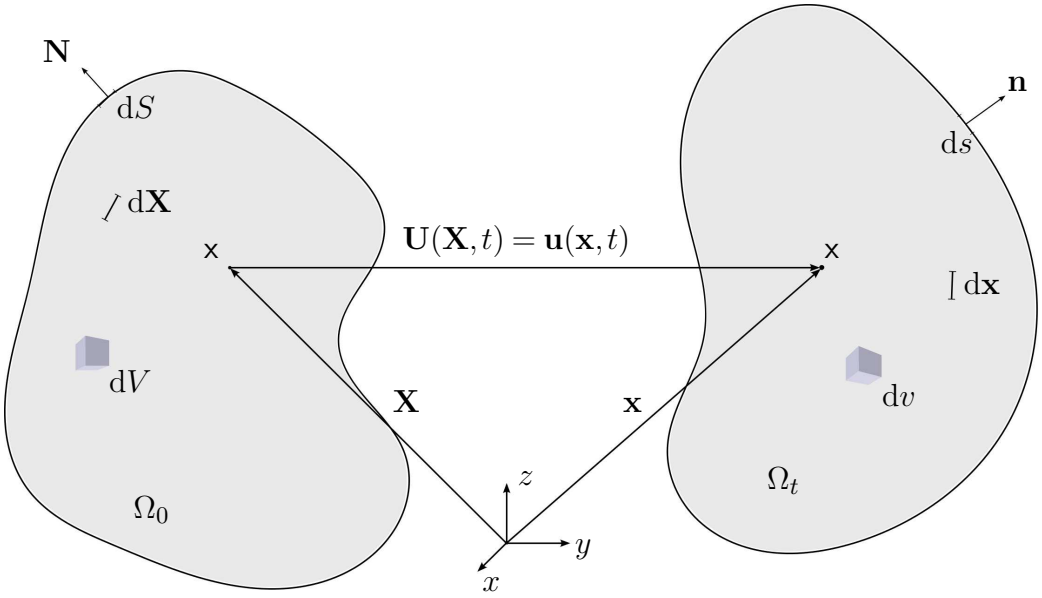

Figure 3.1: Deformation of an elastic body $\mathcal{B}$ from the reference configuration Ω_0 to the current configuration Ω_t.

Definition 3.2 (Material and spatial divergence)**.** *The* material divergence *of a sufficiently smooth vector-valued material field* $\mathbf{W}(\mathbf{X},t)$ *is defined as*

$$\operatorname{Div}\mathbf{W}(\mathbf{X},t) := \nabla_{\mathbf{X}}\cdot\mathbf{W}(\mathbf{X},t) = \frac{\partial}{\partial X_i}W_i(\mathbf{X},t).$$

The spatial gradient *of a sufficiently smooth spatial field* $\mathbf{w}(\mathbf{x},t)$ *is defined as*

$$\operatorname{div}\mathbf{w}(\mathbf{x},t) := \nabla_{\mathbf{x}}\cdot\mathbf{w}(\mathbf{x},t) = \frac{\partial}{\partial x_i}w_i(\mathbf{x},t).$$

In the case of tensor-valued functions $\mathbf{A}$ *and* $\mathbf{a}$ *we define the material and the spatial divergence as*

$$\operatorname{Div}\mathbf{A}(\mathbf{X},t) := \frac{\partial}{\partial X_i}A_{ij}(\mathbf{X},t)\,\mathbf{e}_j,$$
$$\operatorname{div}\mathbf{a}(\mathbf{x},t) := \frac{\partial}{\partial x_i}a_{ij}(\mathbf{x},t)\,\mathbf{e}_j.$$

Definition 3.3 (Deformation gradient)**.** *We define the* deformation gradient $\mathbf{F}$ *by*

$$\mathbf{F}(\mathbf{X},t) := \frac{\partial\boldsymbol{\chi}(\mathbf{X},t)}{\partial\mathbf{X}} = \operatorname{Grad}\boldsymbol{\chi}(\mathbf{X},t) = \operatorname{Grad}\mathbf{x}(\mathbf{X},t).$$

With the definition of the displacement field $\mathbf{U}$ *this can be written as*

$$\mathbf{F}(\mathbf{X},t) = \mathbf{I} + \operatorname{Grad}\mathbf{U}(\mathbf{X},t), \tag{3.2}$$

with $\mathbf{I}$ *being the identity.*

Remark 3.1.1. *From the bijective mapping* $\boldsymbol{\chi}$ *it follows that the deformation gradient* $\mathbf{F}$ *is non-singular. This fits with the observation that* $\mathbf{F}\,\mathrm{d}\mathbf{X}\neq 0$ *if* $\mathrm{d}\mathbf{X}\neq 0$ *which means that a line element cannot be annihilated by the deformation process.*

Definition 3.4 (Right and left Cauchy–Green deformation tensors)**.** *We define the* right *and* left Cauchy–Green deformation tensors *as*

$$\mathbf{C} := \mathbf{F}^{\top}\mathbf{F} \quad \textit{and} \quad \mathbf{B} := \mathbf{F}\mathbf{F}^{\top}, \tag{3.3}$$

which are both symmetric and positive definite.

Remark 3.1.2. *Let* $\mathrm{d}\mathbf{x}$ *and* $\mathrm{d}\mathbf{X}$ *be the infinitesimal line elements in the current and reference configuration, respectively. It holds*

$$\mathrm{d}\mathbf{x} = \mathbf{F}(\mathbf{X},t)\,\mathrm{d}\mathbf{X} \quad \textit{and} \quad \mathrm{d}\mathbf{X} = \mathbf{F}^{-1}(\mathbf{x},t)\,\mathrm{d}\mathbf{x}. \tag{3.4}$$

Let $\mathrm{d}v$ *and* $\mathrm{d}V$ *be the infinitesimal volume elements in the current and reference*

configuration respectively. Then

$$\mathrm{d}v = \det(\mathbf{F}(\mathbf{X},t))\,\mathrm{d}V. \tag{3.5}$$

Definition 3.5 (Jacobian determinant)**.** *We denote* $J(\mathbf{X},t) := \det(\mathbf{F}(\mathbf{X},t))$ *as the* Jacobian determinant *which is also known as volume ratio. It describes the change of volume under the deformation. Since* $\mathbf{F}(\mathbf{X},t)$ *is non-singular and by the convention that volume elements have positive measure it can be stated that*

$$J(\mathbf{X},t) \equiv \det(\mathbf{F}(\mathbf{X},t)) > 0.$$

If we have a deformation without any change of volume then this deformation is called isochoric *and*

$$J(\mathbf{X},t) \equiv \det(\mathbf{F}(\mathbf{X},t)) = 1. \tag{3.6}$$

An incompressible material *is a material for which* (3.6) *holds for all deformations.*

In the following, we omit the arguments of the quantities to enhance readability.

Theorem 3.6 (Nanson's formula)**.** *Let* $\mathrm{d}s$ *and* $\mathrm{d}S$ *be infinitesimal surface elements on the current and reference configuration respectively. Then it holds that*

$$\mathbf{n}\,\mathrm{d}s = J\mathbf{F}^{-\top}\mathbf{N}\,\mathrm{d}S, \tag{3.7}$$

with $\mathbf{F}$ *the deformation gradient,* $J = \det\mathbf{F}$ *and* $\mathbf{n}$ *and* $\mathbf{N}$ *the normal vectors in the current and reference configuration.*

Remark 3.1.3. *For a scalar functions* ϕ, Φ, *vector-valued functions* $\mathbf{w}$, $\mathbf{W}$ *and tensor-valued functions* $\mathbf{a}$, $\mathbf{A}$ *we get by the chain rule the following relations*

$$\mathrm{Grad}\,\Phi = \mathbf{F}^{\top}\,\mathrm{grad}\,\phi,\ \mathrm{Grad}\,\mathbf{W} = (\mathrm{grad}\,\mathbf{w})\,\mathbf{F},\ \mathrm{Grad}\,\mathbf{A} = (\mathrm{grad}\,\mathbf{a})\,\mathbf{F},\ \mathrm{div}\,\mathbf{a} = \mathrm{Grad}\,\mathbf{A} : \mathbf{F}^{-\top}.$$

Remark 3.1.4 (Polar decomposition)**.** *Let* $\mathbf{F}$ *be a second-order tensor with* $\det\mathbf{F} > 0$. *Then there exist unique, positive definite, symmetric tensors,* $\mathbf{U}$ *and* $\mathbf{V}$*, and a unique orthogonal tensor* $\mathbf{R}$ *such that*

$$\mathbf{F} = \mathbf{RU} = \mathbf{VR}.$$

$\mathbf{U}$ *and* $\mathbf{V}$ *are called the right and left stretch tensor,* $\mathbf{R}$ *represents a rotation.*

For the right and the left stretch tensor it holds that

$$\mathbf{U}^2 = \mathbf{F}^{\top}\mathbf{F} = \mathbf{C} \quad \text{and} \quad \mathbf{V}^2 = \mathbf{F}\mathbf{F}^{\top} = \mathbf{B},$$

which is a result of linear algebra and the *square-root theorem* [68].

3.2 Stretch and Strain

Strain is measured locally by changes in the lengths of line elements. In contrast a material is said to be *unstrained* if no line element changes length, i.e.

$$|\mathrm{d}\mathbf{x}|^2 - |\mathrm{d}\mathbf{X}|^2 = 0.$$

Let $\hat{\mathbf{X}}$ and $\hat{\mathbf{x}}$ be the unit vectors along $\mathrm{d}\mathbf{X}$ and $\mathrm{d}\mathbf{x}$ in the reference and current configuration respectively. Then we can write $\mathrm{d}\mathbf{X} = \hat{\mathbf{X}}\,|\mathrm{d}\mathbf{X}|$ and $\mathrm{d}\mathbf{x} = \hat{\mathbf{x}}\,|\mathrm{d}\mathbf{x}|$. With (3.4) we get $\hat{\mathbf{x}}\,|\mathrm{d}\mathbf{x}| = \mathbf{F}\hat{\mathbf{X}}\,|\mathrm{d}\mathbf{X}|$ and

$$|\mathrm{d}\mathbf{x}|^2 = (\mathbf{F}\hat{\mathbf{X}}) \cdot (\mathbf{F}\hat{\mathbf{X}})\,|\mathrm{d}\mathbf{X}|^2 = \left(\mathbf{F}^\top \mathbf{F}\hat{\mathbf{X}}\right) \cdot \hat{\mathbf{X}}\,|\mathrm{d}\mathbf{X}|^2. \tag{3.8}$$

Hence,

$$\frac{|\mathrm{d}\mathbf{x}|}{|\mathrm{d}\mathbf{X}|} = \left[\hat{\mathbf{X}} \cdot (\mathbf{F}^\top \mathbf{F}\hat{\mathbf{X}})\right]^{1/2} =: \lambda(\hat{\mathbf{X}}). \tag{3.9}$$

The value $\lambda(\hat{\mathbf{X}})$ has the physical interpretation of the *stretch* in direction of $\hat{\mathbf{X}}$ at $\mathbf{X}$ and we can easily see that $0 < \lambda(\hat{\mathbf{X}}) < \infty$ for all unit vectors $\hat{\mathbf{X}}$. The equation (3.9) motivates the names stretch tensors for $\mathbf{U}$ and $\mathbf{V}$, introduced in Remark 3.1.4, since $\mathbf{U}^2 = \mathbf{F}^\top \mathbf{F}$ and $\mathbf{V}^2 = \mathbf{F}\mathbf{F}^\top$.

From (3.8) the change in length of a line element from the reference to the current configuration can be described by

$$|\mathrm{d}\mathbf{x}|^2 - |\mathrm{d}\mathbf{X}|^2 = \mathrm{d}\mathbf{X} \cdot \left(\mathbf{F}^\top \mathbf{F} - \mathbf{I}\right) \mathrm{d}\mathbf{X}, \tag{3.10}$$

which is, as mentioned earlier, a measure of strain. Consequently, we define the so-called *Green strain tensor* as

$$\mathbf{E} := \frac{1}{2}\left(\mathbf{F}^\top \mathbf{F} - \mathbf{I}\right) = \frac{1}{2}\left(\mathbf{C} - \mathbf{I}\right)$$

One can see from (3.10) that $\mathbf{E} = 0$ coincides with no change of the line length and thus with no strain.

From the definition of the deformation gradient we can express the Green strain tensor in terms of the gradient as

$$\mathbf{E}(\mathbf{U}) = \frac{1}{2}\left(\mathrm{Grad}\,\mathbf{U} + \mathrm{Grad}^\top \mathbf{U} + \mathrm{Grad}^\top \mathbf{U}\,\mathrm{Grad}\,\mathbf{U}\right).$$

The strain tensors $\mathbf{C}$ and $\mathbf{E}$ are typically for descriptions in the reference configuration while the left Cauchy–Green tensor $\mathbf{B}$ is commonly used in the current configuration.

3.3 The Concept of Stress

To introduce the theory of stress we consider a continuous and deformable body $\mathcal{B}$ which occupies the region Ω at time t. The boundary of this body is denoted as $\partial\Omega$. The forces which act on the boundary surface are called *external* or *contact forces*, where examples are pressure or friction. Those forces which act on the particles of the body are often referred to as *internal* or *body forces*. The latter may arise due to gravity or thermal fields, for example. The body force is denoted by $\mathbf{b}$. For a mathematical description of the contact forces we rely on *Cauchy's stress principle*. This axiom states that the action over a closed surface $\partial\Omega$ is represented by a vector field $\mathbf{t}(t, \mathbf{x}, \mathbf{n})$, defined on $\partial\Omega$. This vector is called *stress vector* and its physical interpretation is the force measured per unit area. With these definitions we may formulate the following fundamental theorem, see, e.g., Ogden [139].

Theorem 3.7 (Cauchy's stress theorem)**.** *Let* $\mathbf{b}$ *and* $\mathbf{t}(t, \mathbf{x}, \mathbf{n})$ *be the body and contact forces for a body* $\mathcal{B}$ *during a motion. Then there exists a unique and symmetric second-order tensor field* $\boldsymbol{\sigma}$*, such that for each unit vector* $\mathbf{n}$

$$\mathbf{t}(t, \mathbf{x}, \mathbf{n}) = \boldsymbol{\sigma}^\top(\mathbf{x})\mathbf{n}, \tag{3.11}$$

where $\boldsymbol{\sigma}$ *is independent of* $\mathbf{n}$ *and satisfies*

$$\boldsymbol{\sigma}^\top = \boldsymbol{\sigma}.$$

Furthermore, $\boldsymbol{\sigma}$ *satisfies Cauchy's equation of motion*

$$\rho \frac{D^2}{Dt^2}\mathbf{u} - \operatorname{div}\boldsymbol{\sigma} = \rho\mathbf{b}, \tag{3.12}$$

where ρ *is the mass density of the material composing* $\mathcal{B}$ *and*

$$\frac{D(\bullet)}{Dt} = \frac{\partial(\bullet)}{\partial t} + \frac{\partial(\bullet)}{\partial x_i}\frac{\partial x_i}{t}$$

the time derivative of a spatial field. $\boldsymbol{\sigma}$ *is called* Cauchy's stress tensor*.*

From (3.11) we get with Nanson's formula (3.7)

$$\mathbf{t}\,\mathrm{d}s = \boldsymbol{\sigma}\mathbf{n}\,\mathrm{d}s = J\boldsymbol{\sigma}\mathbf{F}^{-\top}\mathbf{N}\,\mathrm{d}S,$$

where we define the so-called *first Piola–Kirchhoff stress tensor* by

$$\mathbf{P} := J\boldsymbol{\sigma}\mathbf{F}^{-\top}. \tag{3.13}$$

$\mathbf{P}$ is the applied force divided by the reference area while $\boldsymbol{\sigma}$ measures the force per unit deformed area. Note that in general $\mathbf{P}$ is not symmetric. To provide a symmetric stress tensor in the reference configuration as well, we define the *second Piola–Kirchhoff stress tensor* by

$$\mathbf{S} := \mathbf{F}^{-1}\mathbf{P} = J\mathbf{F}^{-1}\boldsymbol{\sigma}\mathbf{F}^{-\top}. \tag{3.14}$$

Remark 3.3.1 (Piola transformation)**.** $\mathbf{S}$ *is the so-called* Piola transformation *of* $\boldsymbol{\sigma}$*. With this transformation a correspondence between quantities defined over the current and reference configuration is established.*

Corollary 3.1. *An equivalent version of Cauchy's equation of motion in the reference configuration can be re-casted in terms of* $\mathbf{S}$ *by*

$$\rho_0 \frac{\partial^2}{\partial t^2}\mathbf{U} - \operatorname{Div}(\mathbf{FS}) = \rho_0 \mathbf{b}_0 \tag{3.15}$$

with ρ_0 *the mass density and* $\mathbf{b}_0$ *the body force, each in the reference configuration. It holds* $\rho = J^{-1}\rho_0$*.*

For more details and the derivation of Corollary 3.1 compare to Ogden [139, Section 3.4].

3.4 General Problem Formulation

We want to find the displacement field $\mathbf{u}(\mathbf{x},t)$ that satisfies Cauchy's equation of motion (3.11), i.e.

$$\rho(\mathbf{x},t)\frac{D^2}{Dt^2}\mathbf{u}(\mathbf{x},t) - \operatorname{div}\boldsymbol{\sigma}(\mathbf{x},t) = \rho(\mathbf{x},t)\mathbf{b}(\mathbf{x},t) \quad \text{for all } \mathbf{x}\in\Omega,\ t\geq 0.$$

$\mathbf{b}$, the body force per unit volume, acts on a particle of the region Ω and it is considered to be a prescribed (given) force. The inertia force per unit volume is characterized by $\rho D^2\mathbf{u}/Dt^2$, with ρ the spatial mass density of the material.

In order to formulate boundary conditions, $\partial\Omega$ is decomposed into disjoint parts so that

$$\partial\Omega = \overline{\Gamma}_{\mathrm{D}} \cup \overline{\Gamma}_{\mathrm{N}} \qquad \text{with} \qquad \Gamma_{\mathrm{D}} \cap \Gamma_{\mathrm{N}} = \emptyset.$$

Dirichlet boundary conditions on Γ_{D} correspond to a given displacement field $\mathbf{u} = \mathbf{u}_{\mathrm{D}}$, which is enforced component-wise. Neumann boundary conditions on Γ_{N} are identified physically with a given surface traction $\boldsymbol{\sigma}(\mathbf{x},t)\mathbf{n}(\mathbf{x}) = \mathbf{t}_{\mathrm{N}}(\mathbf{x},t)$.

Finally, we require initial conditions. The displacement field and the velocity field at initial time $t = 0$ are specified as

$$\mathbf{u}(\mathbf{x},t)|_{t=0} = \mathbf{u}_0(\mathbf{X}), \qquad \dot{\mathbf{u}}(\mathbf{x},t)|_{t=0} := \frac{D}{Dt}\mathbf{u}(\mathbf{x},t)|_{t=0} = \mathbf{u}_1(\mathbf{X}).$$

If we consider a stress-free reference configuration Ω_0 at time $t = 0$ the initial values are assumed to be zero.

Combining the above-mentioned relations, this leads to the following classical formulation of the boundary value problem of interest:
let Ω be a bounded domain with a sufficiently smooth boundary $\Gamma = \partial\Omega$. We have a disjunct decomposition of the boundary of the form $\Gamma = \overline{\Gamma}_{\mathrm{D}} \cup \overline{\Gamma}_{\mathrm{N}}$. Given a continuous body force $\mathbf{b}$, boundary and initial conditions, the density $\rho > 0$, find the displacement field $\mathbf{u}$ such that

$$\begin{aligned}
\rho(\mathbf{x},t)\frac{D^2}{Dt^2}\mathbf{u}(\mathbf{x},t) - \operatorname{div}\boldsymbol{\sigma}(\mathbf{u},\mathbf{x},t) &= \rho(\mathbf{x},t)\,\mathbf{b}(\mathbf{x},t) && \text{in } \Omega, \quad t > 0,\\
\mathbf{u}(\mathbf{x},t) &= \mathbf{u}_{\mathrm{D}}(\mathbf{x},t) && \text{on } \Gamma_{\mathrm{D}},\ t > 0,\\
\boldsymbol{\sigma}(\mathbf{u},\mathbf{x},t)\,\mathbf{n}(\mathbf{x}) &= \mathbf{t}_{\mathrm{N}}(\mathbf{x},t) && \text{on } \Gamma_{\mathrm{N}},\ t > 0,\\
\mathbf{u}(\mathbf{x},t) &= \mathbf{u}_0(\mathbf{X}) && \text{in } \Omega, \quad t = 0,\\
\dot{\mathbf{u}}(\mathbf{x},t) &= \mathbf{u}_1(\mathbf{X}) && \text{in } \Omega, \quad t = 0.
\end{aligned}$$

For the modeling of biological tissues the second time derivative on the left hand side is of practically negligible order [185]. Additionally we set the body force to zero. Thus, we concentrate on the simplified problem: find $\mathbf{u}$ such that

$$\begin{aligned}
-\operatorname{div}\boldsymbol{\sigma}(\mathbf{u},\mathbf{x},t) &= \mathbf{0} && \text{in } \Omega, \quad t > 0,\\
\mathbf{u}(\mathbf{x},t) &= \mathbf{u}_{\mathrm{D}}(\mathbf{x},t) && \text{on } \Gamma_{\mathrm{D}},\ t > 0,\\
\boldsymbol{\sigma}(\mathbf{u},\mathbf{x},t)\,\mathbf{n}(\mathbf{x}) &= \mathbf{t}_{\mathrm{N}}(\mathbf{x},t) && \text{on } \Gamma_{\mathrm{N}},\ t > 0,
\end{aligned} \tag{3.16}$$

with initial conditions. For a time-stepping scheme this leads to a quasi-stationary approach, as proposed in Holzapfel [81] for biological tissues.

To specify a similar form of this boundary value problem in terms of the reference configuration we use (3.15). With this we get for the stationary boundary value problem in the reference configuration

$$\begin{aligned}
-\operatorname{Div}[\mathbf{FS}(\mathbf{U},\mathbf{X})] &= \mathbf{0} && \text{in } \Omega_0,\\
\mathbf{U}(\mathbf{X}) &= \mathbf{U}_{\mathrm{D}}(\mathbf{X}) && \text{on } \Gamma_{\mathrm{D}},\\
\mathbf{FS}(\mathbf{U},\mathbf{X})\mathbf{N}(\mathbf{X}) &= \mathbf{t}_{\mathrm{N}}(\mathbf{X}) && \text{on } \Gamma_{\mathrm{N}}.
\end{aligned} \tag{3.17}$$

In this case it is important to take a closer look at the embedding of the traction

forces, i.e. the Neumann boundary conditions. If the applied surface force $\mathbf{t}_{\mathrm{N}}(\mathbf{X})$ in the reference configuration is independent of the deformation gradient $\mathbf{F}$ then we consider a *dead load*. This case is a simplification and is seldom usable to model actual applied forces. For the modeling of biological tissue we need to apply *pressure loads* on the boundary of the domain; for example the pressure loads applied to the myocardium in the ventricles of the heart. In the current configuration an applied surface force is a pressure load if it is of the form

$$\mathbf{t}_{\mathrm{N}}(\mathbf{x}) = -\mathcal{p}\mathbf{n}(\mathbf{x}), \tag{3.18}$$

with $\mathcal{p}$ the pressure.

In the reference configuration the surface load then depends on the deformation and is of the form

$$t_{\mathrm{N}}(\mathbf{X}) = \hat{t}_{\mathrm{N}}(\mathbf{U},\mathbf{X}) = -\mathcal{p}J\mathbf{F}^{-\top}\mathbf{N}(\mathbf{X}). \tag{3.19}$$

For a more detailed discussion on displacement dependent pressure loads cf. Ciarlet [38, Sections 2.6 and 5.1] or Schweizerhof and Ramm [167].

3.5 Linear Elasticity

For *small deformations* it is justified not to distinguish between the Eulerian and Lagrangian description and to replace the strain tensor $\mathbf{E}$ by the linearized strain tensor $\boldsymbol{\varepsilon}(\mathbf{u})$, defined by

$$\varepsilon_{ij}(\mathbf{u}) = \frac{1}{2}\left(\frac{\partial u_j}{\partial x_i} + \frac{\partial u_i}{\partial x_j}\right),\ \varepsilon(\mathbf{u}) = \frac{1}{2}\left(\operatorname{grad}\mathbf{u} + \operatorname{grad}^{\top}\mathbf{u}\right) := \operatorname{sym}(\operatorname{grad}\mathbf{u}). \tag{3.20}$$

A material is called linear elastic if it can be modeled using *Hooke's Law* which describes a linear relationship between stress and strain. It states

$$\boldsymbol{\sigma} = \mathbb{C} : \boldsymbol{\varepsilon}, \quad \sigma_{ij} = C_{ijkl}\varepsilon_{kl}, \tag{3.21}$$

using $(\mathrm{A}.5)_1$ and Einstein's summation convention. The *elasticity tensor* $\mathbb{C}$ is formed by so-called elastic coefficients and it satisfies the symmetry conditions

$$C_{ijkl} = C_{klij} \quad \text{and} \quad C_{ijkl} = C_{jikl} = C_{jilk}.$$

An important special case are homogeneous, isotropic linear elastic materials which are called *linear St. Venant–Kirchhoff materials*. In this case

$$\boldsymbol{\sigma} = \frac{E\nu}{(1+\nu)(1-2\nu)}\operatorname{tr}(\boldsymbol{\varepsilon})\mathbf{I} + \frac{E}{(1+\nu)}\boldsymbol{\varepsilon}$$

with Young's modulus $E > 0$, measured normally in Gigapascal (GPa), and Poisson's ratio $\nu \in (0, 0.5)$. E quantifies the stiffness of an elastic material. The range of Young's modulus is from $E = 0.01\,\mathrm{GPa}$, e.g. for some types of rubber, to values around $1000\,\mathrm{GPa}$, e.g. for diamond we have $E = 1220\,\mathrm{GPa}$. ν is a dimensionless parameter and a measure of compressibility. For the incompressible limit we have $\nu = 0.5$, e.g., rubber; for very compressible materials like cork ν is very near to zero. Since biological tissues are considered as rubber-like materials we have Young's modulus around $1\,\mathrm{GPa}$ and a Poisson's ratio close to 0.5. This is consistent with the assumption of nearly incompressibility.

We define the so-called Lamé coefficients λ and μ as

$$\lambda := \frac{E\nu}{(1+\nu)(1-2\nu)}, \quad \mu := \frac{E}{2(1+\nu)}. \tag{3.22}$$

Lamé's second parameter $\mu > 0$ is also known as the shear modulus. It spans between $0\,\mathrm{GPa}$ for rubber and $478\,\mathrm{GPa}$ for diamond. Lamé's first parameter λ has no physical interpretation and is also measured in Gigapascal. With these two constants we can write the elasticity tensor for a linear St. Venant–Kirchhoff material as

$$C_{ijkl} = \lambda\delta_{ij}\delta_{kl} + \mu(\delta_{ik}\delta_{jl} + \delta_{il}\delta_{jk}).$$

For the incompressible limit we have

$$\nu \to 0.5 \quad \text{or} \quad \lambda \to \infty.$$

In the classical literature there exist many treatments of the theory of linear elastic materials. Amongst others see the works of Gurtin [69] or Nečas and Hlaváček [133]. Matters of solvability of the boundary value problem and uniqueness of an eventual solution are discussed in Section 4.3.

3.6 Constitutive Equations for Nonlinear Elasticity

Considering the study of the hyper-elastic properties of biological tissues we have to deal with a nonlinear relationship between stress and strain and with large deformations. Since a linear elasticity model is not adequate to treat such a complex behavior we have to take a look at the more general concept of nonlinear elasticity. Here we model the nonlinear stress-strain response via a constitutive equation that links the stress to a derivative of a so-called *strain-energy function*. This scalar-valued function $W(\mathbf{F})$ represents the elastic stored energy per unit reference volume. It takes one tensor variable $\mathbf{F}$ as argument and we assume it to be continuous. Note that strain-energy functions can also be formulated for linear elasticity.

The *total strain energy* (or the *internal potential energy*) can be described as the integral of $W(\mathbf{F})$ over the domain Ω_0.

In this work we will concentrate on *perfectly elastic materials*. These are by definition materials which produce locally no entropy and thus the internal dissipation[2] equals zero. In other words we exclude plastic deformations as well as damaging or viscous mechanisms.

Theorem 3.8 (Constitutive equation)**.** *Given a strain-energy function W, the first Piola–Kirchhoff stress tensor $\mathbf{P}$ and the deformation gradient $\mathbf{F}$ are linked by the constitutive equation*

$$\mathbf{P} = \frac{\partial W(\mathbf{F})}{\partial \mathbf{F}}. \tag{3.23}$$

Proof. Ciarlet [38] or Ogden [139, Ogden (1997)]. □

Remark 3.6.1. *$W(\mathbf{F})$ is also referred to as the* Helmholtz free-energy function*.*

Remark 3.6.2. *It is important to note that we use the convention*

$$\left(\frac{\partial W(\mathbf{F})}{\partial \mathbf{F}}\right)_{ij} := \frac{\partial W(\mathbf{F})}{\partial F_{ij}},$$

as in the books of Holzapfel [80] and Ciarlet [38]. In the literature the definition

$$\left(\frac{\partial W(\mathbf{F})}{\partial \mathbf{F}}\right)_{ij} := \frac{\partial W(\mathbf{F})}{\partial F_{ji}}.$$

is also common, e.g. in Ogden [139]. In this case the constitutive equation above holds for $\mathbf{P}^\top$.

In the following, we denote the strain-energy function as $W(\mathbf{F})$ if it depends on the deformation gradient $\mathbf{F}$. In case it depends on the right Cauchy–Green tensor $\mathbf{C}$ we denote it as $\Psi(\mathbf{C})$.

Since both functions describe the same behavior of a considered material we can write

$$W(\mathbf{F}) = \Psi(\mathbf{C}) = \Psi(\mathbf{E}). \tag{3.24}$$

Remark 3.6.3 (Frame indifference)**.** *The strain-energy is invariant under rigid body motion. Hence, $W(\mathbf{QF}) = W(\mathbf{F})$ must hold for all proper orthogonal rotations $\mathbf{Q}$.*

[2] Dissipative system: a dynamical system loses energy over time due to a conversion into thermal energy; processes in such a system are irreversible and the entropy in it rises.

Remark 3.6.4 (Normalization conditions)**.** *For convenience we require that W and Ψ vanish in the reference configuration Ω_0. So we get the following so-called normalization conditions*

$$W(\mathbf{I}) = 0, \quad \Psi(\mathbf{I}) = 0. \tag{3.25}$$

Moreover, from a physical observation we require that the strain-energy function increases with a deformation, that it is finite for a finite deformation and that it tends to infinity if the displacement $\mathbf{u}$ tends to infinity, i.e.

$$W(\mathsf{F}) \geq 0, \quad W(\mathsf{F}) < \infty \;\; \textit{if} \;\; |\mathbf{u}| < \infty \quad \textit{and} \lim_{|\mathbf{u}| \to \infty} W(\mathsf{F}(\mathbf{u})) = \infty.$$

These requirements hold for $\Psi(\mathsf{C})$ as well.

Lemma 3.9. *For the different representations of the strain-energy functions $W(\mathsf{F})$ and $\Psi(\mathsf{C})$ it holds:*

$$\left(\frac{\partial W(\mathsf{F})}{\partial \mathsf{F}}\right)^{\top} = 2\frac{\partial \Psi(\mathsf{C})}{\partial \mathsf{C}}\mathsf{F}^{\top},$$

with the deformation gradient F and the right Cauchy–Green tensor C.

Proof. The proof follows from (3.24) and the chain rule. □

Corollary 3.2 (Constitutive equations)**.** *The first Piola–Kirchhoff stress tensor may be expressed in terms of the deformation gradient and a strain-energy function as*

$$\mathsf{P} = \frac{\partial W(\mathsf{F})}{\partial \mathsf{F}} = 2\mathsf{F}\frac{\partial \Psi(\mathsf{C})}{\partial \mathsf{C}}.$$

For the second Piola–Kirchhoff stress tensor we get

$$\mathsf{S} = \mathsf{F}^{-1}\frac{\partial W(\mathsf{F})}{\partial \mathsf{F}} = 2\frac{\partial \Psi(\mathsf{C})}{\partial \mathsf{C}},$$

and for the Cauchy stress tensor the constitutive equations

$$\boldsymbol{\sigma} = J^{-1}\mathsf{F}\left(\frac{\partial W(\mathsf{F})}{\partial \mathsf{F}}\right)^{\top} = 2J^{-1}\mathsf{F}\frac{\partial \Psi(\mathsf{C})}{\partial \mathsf{C}}\mathsf{F}^{\top}$$

hold.

Proof. The different constitutive equations follow immediately from the constitutive equation for P in Theorem 3.8, the Piola transformations (3.13) and (3.14), Lemma 3.9 and the symmetry of $\boldsymbol{\sigma}$ and S. □

3.7 Modeling of Nearly Incompressible Elastic Materials

As mentioned in Chapter 2 we treat biological tissues as nearly incompressible elastic materials [184]. To get a realistic model for such materials, where $J = \det(\mathbf{F})$ gets very close to 1, we have to adapt the constitutive equations slightly.

In this section we will need the derivatives

$$\frac{\partial J}{\partial \mathbf{C}} = \frac{J}{2}\mathbf{C}^{-1} \quad , \quad \frac{\partial J^{-2/3}}{\partial \mathbf{C}} = -\frac{1}{3}J^{-2/3}\mathbf{C}^{-1}, \tag{3.26}$$

see [80]. Additionally, to simplify matters, we introduce the deviatoric operators:

Definition 3.10. *We define the deviatoric operator in the current configuration as*

$$\operatorname{dev}(\bullet) = (\bullet) - \frac{1}{3}\operatorname{tr}(\bullet)\mathbf{I}.$$

The deviatoric operator in the Lagrangian description reads

$$\operatorname{Dev}(\bullet) = (\bullet) - \frac{1}{3}\left[(\bullet) : \mathbf{C}\right]\mathbf{C}^{-1}, \tag{3.27}$$

with the right Cauchy–Green tensor $\mathbf{C} = \mathbf{F}^{\top}\mathbf{F}$.

3.7.1 Decoupling of the Deformation and Saddle Point Formulation

An approach to handle nearly incompressible materials, with $J = \det \mathbf{F}$ close to 1, is the decoupling of the deformation into a *volumetric* (i.e. volume changing) and an *isochoric* (i.e. volume preserving) part. This method was already considered in Flory [57] and it is proposed for the artery model in the papers by Holzapfel et al. [81, 82]. Eriksson et al. [52] suggest this approach for the myocardium model as well.

A multiplicative factorization of the deformation gradient $\mathbf{F}$ is performed by

$$\mathbf{F} = (J^{1/3}\mathbf{I})\,\overline{\mathbf{F}} \qquad \text{with} \qquad \det \overline{\mathbf{F}} = 1, \tag{3.28}$$

where $\mathbf{I}$ denotes the second-order unit tensor. This is motivated by the property of the determinant such that

$$\det(J^{1/3}\overline{\mathbf{F}}) = J\det(\overline{\mathbf{F}}) = J = \det(\mathbf{F}).$$

Hence, with (3.3) we obtain an analogous multiplicative factorization for the left and the right Cauchy–Green strain tensor:

$$\mathbf{C} = J^{2/3}\overline{\mathbf{C}} \quad \text{and} \quad \mathbf{B} = J^{2/3}\overline{\mathbf{B}}.$$

Using this we can postulate a unique decoupled form of the strain-energy function $\Psi(\mathbf{C})$ with the specific representation

$$\Psi(\mathbf{C}) = U(J) + \overline{\Psi}(\overline{\mathbf{C}}), \tag{3.29}$$

where $U(J)$, the so-called *volumetric elastic response*, is a strictly convex function with the unique minimum at $J = 1$. $\overline{\Psi}(\overline{\mathbf{C}})$ is called the *isochoric elastic response*.

We require

$$\begin{aligned} U(J) &= 0, \quad \text{if and only if } J = 1, \\ \overline{\Psi}(\overline{\mathbf{C}}) &= 0, \quad \text{if and only if } \overline{\mathbf{C}} = \mathbf{I} \end{aligned}$$

to fulfill the normalization conditions (3.25).

Definition 3.11 (Volumetric response)**.** *In this work, the volumetric response will be of the form*

$$U(J) := \kappa\,\phi_{\text{vol}}(J), \tag{3.30}$$

with $\kappa > 0$ being the bulk modulus and ϕ_{vol} one of the following three choices

$$\begin{aligned} \phi_{\text{vol},1}(J) &= \frac{1}{2}(J-1)^2, \\ \phi_{\text{vol},2}(J) &= \frac{1}{2}\ln(J)^2, \\ \phi_{\text{vol},3}(J) &= J\ln(J) - J + 1. \end{aligned}$$

With the bulk modulus κ we are now able to penalize a volume change, i.e. $J \neq 1$, and hence we can control the compressibility of the material. Note that for an increasing κ we go towards incompressibility.

Remark 3.7.1. *For a linear elastic material the bulk modulus κ may be expressed in terms of Lamé's coefficients λ and μ ((3.22)) and the elasticity module E and Poisson's ratio ν respectively, as*

$$\kappa = \lambda + \frac{2\mu}{3} = \frac{E}{3(1-2\nu)}.$$

Definition 3.12 (Hydrostatic pressure)**.** *We define the hydrostatic pressure as*

$$p := \frac{\mathrm{d}U(J)}{\mathrm{d}J}. \tag{3.31}$$

Theorem 3.13 (Decoupling of the Cauchy stress tensor)**.** *A decomposition of the energy function* $\Psi(\mathbf{C})$ *into a volumetric and an isochoric part*

$$\Psi(\mathbf{C}) = U(J) + \overline{\Psi}(\overline{\mathbf{C}}) \tag{3.32}$$

yields

$$\boldsymbol{\sigma} = \boldsymbol{\sigma}_{vol} + \boldsymbol{\sigma}_{\mathrm{isc}} \tag{3.33}$$

with

$$\boldsymbol{\sigma}_{\mathrm{vol}} = p\mathbf{I}, \quad \textit{and} \quad \boldsymbol{\sigma}_{\mathrm{isc}} = 2J^{-1}\,\mathrm{dev}\left(\overline{\mathbf{F}}\frac{\partial\overline{\Psi}(\overline{\mathbf{C}})}{\partial\overline{\mathbf{C}}}\overline{\mathbf{F}}^{\top}\right). \tag{3.34}$$

Proof. The main ingredients of the proof are (3.26), Theorem 3.8 and the chain rule [80]. □

In an analogous way a decomposition for the stress tensor in the Lagrangian description $\mathbf{S}$ may be derived.

Corollary 3.3 (Decoupling of the second Piola–Kirchhoff stress tensor)**.** *A decomposition of the energy function* $\Psi(\mathbf{C})$ *as in* (3.32) *yields*

$$\mathbf{S} = \mathbf{S}_{vol} + \mathbf{S}_{\mathrm{isc}} \tag{3.35}$$

with

$$\mathbf{S}_{vol} = Jp\mathbf{C}^{-1}, \quad \textit{and} \quad \mathbf{S}_{\mathrm{isc}} = 2J^{-2/3}\,\mathrm{Dev}\left(\frac{\partial\overline{\Psi}(\overline{\mathbf{C}})}{\partial\overline{\mathbf{C}}}\right). \tag{3.36}$$

A decoupling of the stress tensors together with the definition of the hydrostatic pressure p (3.31) and a volumetric strain-energy function of the form (3.30) leads to the following stationary saddle point problem: find $(\mathbf{u}, p)$ such that

$$\begin{aligned} -\operatorname{div}[\boldsymbol{\sigma}_{\mathrm{isc}}(\mathbf{u},\mathbf{x}) + \boldsymbol{\sigma}_{\mathrm{vol}}(p,\mathbf{x})] &= \mathbf{0} \quad \text{in } \Omega, \\ \kappa\,\phi_{\mathrm{vol}}(\mathbf{u},\mathbf{x}) \; - p(\mathbf{x}) \qquad\quad &= 0 \quad \text{in } \Omega, \end{aligned}$$

with additional Neumann and Dirichlet Boundary conditions. The corresponding version in the reference configuration is: find $(\mathbf{U}, P)$ such that

$$\begin{aligned} -\operatorname{Div}[\mathbf{F}\mathbf{S}_{\mathrm{isc}}(\mathbf{U},\mathbf{X}) \; + \mathbf{F}\mathbf{S}_{\mathrm{vol}}(\mathbf{U},P,\mathbf{X})] &= \mathbf{0} \quad \text{in } \Omega_0, \\ \kappa\,\phi_{\mathrm{vol}}(\mathbf{U},\mathbf{X}) \; - P(\mathbf{X}) \qquad\quad &= 0 \quad \text{in } \Omega_0. \end{aligned} \tag{3.37}$$

Note that the pairs $(\mathbf{u}, p)$ and $(\mathbf{U}, P)$ are identical due to (3.1).

3.8 Elasticity Tensor

We postulate the existence of an energy function $\Psi(\mathbf{C})$.

Definition 3.14 (Elasticity tensor)**.** *The elasticity tensor* $\mathbb{C}$ *in the reference configuration is defined as the gradient of the nonlinear tensor-valued stress tensor* $\mathbf{S}$ *as*

$$\mathbb{C} := 2\frac{\partial \mathbf{S}(\mathbf{C})}{\partial \mathbf{C}} = 4\frac{\partial^2 \Psi(\mathbf{C})}{\partial \mathbf{C}^2}.$$

It measures the change in stress which is evoked through a change of strain. The elasticity tensor in the spatial description, denoted by $\mathbb{c}$ *is defined as the push-forward operation of* $\mathbb{C}$ *times a factor of* J^{-1}

$$c_{ijkl} = J^{-1} F_{ia} F_{jb} F_{kc} F_{ld} C_{abcd}.$$

Remark 3.8.1 (Symmetry properties)**.** *The elasticity tensor* $\mathbb{C}$ *possesses* minor symmetries *in the following way*

$$C_{abcd} = C_{bacd} = C_{abdc}.$$

Following from its definition we can show the major symmetries

$$C_{abcd} = C_{cdab}.$$

This property holds for the elasticity tensor $\mathbb{c}$ *in Eulerian description as well [80, Section 6.6].*

Remark 3.8.2 (Voigt notation)**.** *A forth-order tensor* $\mathbb{C}$*, with the entries* C_{abcd} *for* $a, b, c, d = 1, 2, 3$*, satisfying minor symmetries may be represented as a* 6×6 *matrix* $\mathcal{C}$ *with* 36 *distinctive components. If additionally* $\mathbb{C}$ *is satisfying major symmetries then* $\mathcal{C}$ *is symmetric and has* 21 *distinctive components. It is written as*

$$\mathcal{C} = \begin{pmatrix} C_{1111} & C_{1122} & C_{1133} & C_{1112} & C_{1123} & C_{1113} \\ . & C_{2222} & C_{2233} & C_{2212} & C_{2223} & C_{2213} \\ . & . & C_{3333} & C_{3312} & C_{3323} & C_{3313} \\ . & . & . & C_{1212} & C_{1223} & C_{1213} \\ . & sym. & . & . & C_{2323} & C_{2313} \\ . & . & . & . & . & C_{1313} \end{pmatrix}. \tag{3.38}$$

Remark 3.8.3 (Positive definiteness)**.** *For strict local convex strain-energy functions* Ψ*, see Section 4.4.8, the elasticity tensor* $\mathbb{C}$ *and its representation in Voigt notation* $\mathcal{C}$ (3.38) *are positive definite [139, Section 6.2.3]. This is a fundamental physical requirement that prevents material instabilities.*

In decoupled form the elasticity tensor is written as

$$\mathbb{C} = \mathbb{C}_{\text{vol}} + \mathbb{C}_{\text{isc}} \tag{3.39}$$

with the volumetric and the isochoric part

$$\mathbb{C}_{\text{vol}} = 2\frac{\partial \mathbf{S}_{\text{vol}}(\mathbf{C})}{\partial \mathbf{C}} \quad \text{and} \quad \mathbb{C}_{\text{isc}} = 2\frac{\partial \mathbf{S}_{\text{isc}}(\mathbf{C})}{\partial \mathbf{C}},$$

compare to (3.35). A more specific introduction to elasticity tensors one may find in Marsden and Hughes [121, Chapter 3] or [127, 128].

3.9 The Strain-Energy Function in Terms of Invariants

In the following, we discuss the structure of the strain-energy function. We introduce the concept of invariants and then express the strain-energy function in terms of the principal invariants of its tensor-valued argument. For a compendium on the theory of invariants see Spencer [174].

Definition 3.15 (Principle scalar invariants of a tensor)**.** *Let* $\mathbf{A}$ *be a given* 3×3 *second-order tensor. Then the* characteristic polynomial *of* $\mathbf{A}$ *is given by*

$$p(\lambda) = \det(\mathbf{A} - \lambda \mathbf{I}) = (\lambda_1 - \lambda)(\lambda_2 - \lambda)(\lambda_3 - \lambda) = -\lambda^3 + I_1\lambda^2 - I_2\lambda + I_3.$$

Here λ_i *are the eigenvalues and* $I_i, i = 1,2,3$ *are the so-called* principal scalar invariants *of* $\mathbf{A}$.

From this definition we can easily derive the following corollary:

Corollary 3.4. *The invariants of a* 3×3 *second-order tensor* $\mathbf{A}$ *are*

$$\begin{aligned} I_1(\mathbf{A}) &= \operatorname{tr}(\mathbf{A}) = \lambda_1 + \lambda_2 + \lambda_3, \\ I_2(\mathbf{A}) &= \frac{1}{2}\left(\operatorname{tr}(\mathbf{A})^2 - \operatorname{tr}(\mathbf{A}^2)\right) = \lambda_1\lambda_2 + \lambda_1\lambda_3 + \lambda_2\lambda_3, \\ I_3(\mathbf{A}) &= \det(\mathbf{A}) = \lambda_1\lambda_2\lambda_3. \end{aligned}$$

In the theory of mechanics the eigenvalues of the left and right stretch tensors $\mathbf{U}$ and $\mathbf{V}$, introduced in Remark 3.1.4, may be regarded as stretches in the principal directions. This is due to the coherence described in (3.9). They have the following property:

Corollary 3.5. $\mathbf{U}$ *and* $\mathbf{V}$ *have the same eigenvalues* $\lambda_i > 0$. λ_i *are called the principal stretches.*

As we consider the definition of the invariants in Corollary 3.4 we can state that $I_1(\mathbf{U})$ and $I_2(\mathbf{U})$ can be interpreted as a measure of stretch while $I_3(\mathbf{U})$ is a measure of volume change.

Consequently, if we consider an incompressible material the deformation gradient must satisfy the internal constraint

$$J \equiv \det(\mathbf{F}) = \det(\mathbf{U}) = I_3(\mathbf{U}) = 1. \tag{3.40}$$

If we have no stretch, i.e. $\lambda_i = 1$ for $i = 1,2,3$, then

$$I_1(\mathbf{U}) = I_2(\mathbf{U}) = 3. \tag{3.41}$$

For the two Cauchy–Green deformation tensors $\mathbf{C} = U^2$ and $\mathbf{B} = V^2$ the eigenvalues of both are the squares of the principal stretches. Thus we have for the invariants

$$\begin{aligned} I_1(\mathbf{C}) &= I_1(\mathbf{B}) = \lambda_1^2 + \lambda_2^2 + \lambda_3^2, \\ I_2(\mathbf{C}) &= I_2(\mathbf{B}) = \lambda_1^2\lambda_2^2 + \lambda_1^2\lambda_3^2 + \lambda_2^2\lambda_3^2, \\ I_3(\mathbf{C}) &= I_3(\mathbf{B}) = \lambda_1^2\lambda_2^2\lambda_3^2. \end{aligned}$$

Hence, the same constraints (3.40) and (3.41) are valid for these tensors. Thus we can state that if we have no deformation, i.e. $\mathbf{C} = \mathbf{I}$ then there is consequently no strain, stretch, stress or volume change of the body involved. This fits perfectly well with the physical understanding of elastic materials.

Theorem 3.16 (Representation theorem for invariants)**.** *Let $f(\mathbf{A})$ be a scalar-valued tensor function. If f is invariant under rotations, it may be expressed in terms of the principal invariants of its argument $\mathbf{A}$:*

$$f(\mathbf{A}) = f[I_1(\mathbf{A}), I_2(\mathbf{A}), I_3(\mathbf{A})].$$

Proof. Cf. [68, p. 231] and [180, Chapter 10]. □

In the literature this theorem is also referred to as the *Rivlin–Ericksen representation theorem*. For an extension to anisotropic materials see Raoult [146].

3.10 Strain-Energy Functions for Elastic Materials

3.10.1 Isotropic Materials

In the following, we restrict the structure of the strain-energy function of interest by the property that the material is *isotropic*, i.e. homogeneous in all directions. If that is the case then the strain-energy function is invariant with respect to rotations. Thus

$$\Psi(\mathbf{C}) = \Psi(\mathbf{R}\mathbf{C}\mathbf{R}^\top)$$

holds for all symmetric tensors $\mathbf{C}$ and orthogonal rotation tensors $\mathbf{R}$. For a more detailed discussion see, for example, [80, Section 6.2] or [38, Section 3.6]. Since $\Psi(\mathbf{C})$ fulfills the requirements of Theorem 3.16 we may write

$$\Psi(\mathbf{C}) = \Psi[I_1(\mathbf{C}), I_2(\mathbf{C}), I_3(\mathbf{C})], \tag{3.42}$$

where the principal invariants of the right Cauchy–Green tensor $\mathbf{C}$ are (cf. Corollary 3.4)

$$\begin{aligned} I_1(\mathbf{C}) &= \mathrm{tr}\mathbf{C}, \\ I_2(\mathbf{C}) &= \frac{1}{2}[(\mathrm{tr}\mathbf{C})^2 - \mathrm{tr}(\mathbf{C}^2)], \\ I_3(\mathbf{C}) &= \det\mathbf{C}. \end{aligned}$$

For the stress-free reference configuration $\mathbf{C} = \mathbf{I}$, the strain-energy function (3.42) must satisfy the normalization condition $\Psi(\mathbf{I}) = 0$, i.e. $\Psi = 0$ for $I_1 = I_2 = 3$ and $I_3 = 1$.

Subject to the regularity assumption that Ψ is infinitely many times continuously differentiable with respect to I_1, I_2, I_3, Ogden [139, Chapter 4] proposed the following series representation for a strain-energy function

$$\Psi(I_1, I_2, I_3) = \sum_{p,q,r=0}^{\infty} c_{pqr}(I_1 - 3)^p (I_2 - 3)^q (I_3 - 1)^r, \tag{3.43}$$

with $c_{000} = 0$ and $c_{100} + 2c_{010} + c_{001} = 0$ to satisfy the normalization condition.

If we set $I_3 = 1$, which would be valid for an incompressible material, then we obtain

$$\Psi(I_1, I_2) = \sum_{p,q=0}^{\infty} c_{pq}(I_1 - 3)^p (I_2 - 3)^q$$

with $c_{00} = 0$.

To simplify this expression we make note of the special case

$$\Psi(I_1, I_2) = c_{10}(I_1 - 3) + c_{01}(I_2 - 3), \tag{3.44}$$

which is referred to as the *Mooney–Rivlin* strain-energy function. This important model to cover the behavior of an isotropic elastic material was proposed independently by Melvin Mooney [129] and Ronald Rivlin [150–152].

Finally, with $c_{01} = 0$ and $c_{10} = \mu/2$ this reduces to the *neo–Hookean* model

$$\Psi(I_1) = \frac{\mu}{2}(I_1 - 3), \tag{3.45}$$

where $\mu > 0$ is a stress-like material parameter which may be interpreted as the shear modulus.

Another way to motivate the strain-energy function (3.45) is through *statistical theory*; see [80, Section 7.2] for a brief discussion.

(3.45) just relies on one parameter and offers a simple way to describe the nonlinear deformation behavior of isotropic rubber-like materials. This model may be seen as the nonlinear counterpart of Hooke's law (cf. Sect 3.5) and goes back to Rivlin [149].

Another candidate for a response function, and indeed a very famous one, was proposed independently by Adhémar Jean Claude Barré de Saint Venant in 1844 and Gustav Robert Kirchhoff in 1852 and is thus named after these two physicists:

Definition 3.17 (St. Venant–Kirchhoff material)**.** *The strain-energy function associated with the St. Venant–Kirchhoff model is defined by*

$$\Psi(\mathbf{E}) = \frac{\lambda}{2}(\operatorname{tr} \mathbf{E})^2 + \mu \operatorname{tr}(\mathbf{E}^2), \tag{3.46}$$

where the constants $\lambda > 0, \mu > 0$ are the Lamé parameters.

Although this kind of a function is not polyconvex, cf. Section 4.4.6, existence results were shown in Dacorogna [43]. However, this kind of models brings some other drawbacks. These are, for example, so-called eversion problems, which means that large strains are possible although the stress is small [4, 181]. Another disadvantage is that $J = \det(\mathbf{F})$ could possibly approach zero or even become negative. More details to these drawbacks and other shortcomings of the St. Venant–Kirchhoff model are described in [38, Section 3.9].

3.10.2 Almost Incompressible Isotropic Materials

In Section 3.10.1 we already mentioned some possibilities to model isotropic materials. In this section we consider nearly incompressible materials, like most of the biological tissues. Hence, a unique decoupled representation of the energy function is proposed as in Section 3.7.1.

We formulate the decoupled version of the strain-energy function for isotropic materials as

$$\Psi(\mathbf{C}) = U(J) + \overline{\Psi}(\overline{\mathbf{C}}),$$

where the function $U(J)$ is motivated mathematically and serves as a penalty function within the numerical analysis. It denotes Lagrange multiplier terms which vanish for the incompressible limit.

The function $\overline{\Psi}(\overline{\mathbf{C}})$ can also be written in terms of the invariants of $\overline{\mathbf{C}}$

$$\overline{\Psi}(\overline{\mathbf{C}}) = \overline{\Psi}[\overline{I}_1(\overline{\mathbf{C}}), \overline{I}_2(\overline{\mathbf{C}}), \overline{I}_3(\overline{\mathbf{C}})]$$

as already discussed in (3.42). Since $\overline{I}_3(\overline{\mathbf{C}}) = \det(\overline{\mathbf{C}}) = 1$ we can neglect this invariant and write

$$\overline{\Psi}(\overline{\mathbf{C}}) = \overline{\Psi}[\overline{I}_1(\overline{\mathbf{C}}), \overline{I}_2(\overline{\mathbf{C}})].$$

We formulate the decoupled version of (3.45) in the following definition:

Definition 3.18 (Almost incompressible neo–Hooke material)**.** *The strain-energy function to model nearly incompressible neo–Hookean materials is defined by*

$$\Psi(J, \overline{I}_1) = U(J) + \frac{\mu}{2}(\overline{I}_1 - 3), \tag{3.47}$$

with the material parameter $\mu > 0$.

Analogous we obtain for the decoupled version of (3.44):

Definition 3.19 (Mooney–Rivlin material)**.** *An elastic material is a Mooney–Rivlin material if its strain-energy function is of the form*

$$\Psi(J, \overline{I}_1, \overline{I}_2) = U(J) + c_1(\overline{I}_1 - 3) + c_2(\overline{I}_2 - 3),$$

with material constants $c_1, c_2 > 0$.

In the following, we will concentrate on the neo–Hookean and the Mooney–Rivlin model. Nonetheless, one can formulate similar decoupled strain-energy functions for all Ogden-type materials as given in (3.43).

3.10.3 First Steps to an Anisotropic Material Model

As mentioned in Chapter 2, many biological tissues consist of an isotropic ground substance, in the case of arteries elastin, and collagen fibers which lead to an anisotropic behavior of these materials. The modeling of such a complex structure goes back to Fung [59] where the author proposed a very influential constitutive model. From experiments he observed a linear relation between stiffness, i.e. the ratio of stress and strain, and stress, as seen in Figure 3.2. Denoting by P_{11} the uniaxial component of the first Piola-Kirchhoff stress tensor $\mathbf{P}$ (3.13) and by λ_1 the associated axial stretch ratio, this linear relation can be written as

$$\frac{\mathrm{d}P_{11}}{\mathrm{d}\lambda_1} = k_1 + k_2 P_{11}. \tag{3.48}$$

Here, $k_1 > 0$ is a stress-like and $k_2 > 0$ is a dimensionless parameter. λ_1 is the stretch ratio in the direction of the applied load, i.e. the deformed length over the reference length or simply the strain. By solving the differential equation (3.48) we obtain

$$P_{11} = c\exp(k_2\lambda_1) - \frac{k_1}{k_2}.$$

If $\lambda_1 = 1$, i.e. there is no strain, one has consequently that the stress is zero: $P_{11} = 0$. From this normalization condition the stress-like constant c may be determined and we conclude the following exponential constitutive relation

$$P_{11} = \frac{k_1}{k_2}\left\{\exp[k_2(\lambda_1 - 1)] - 1\right\}, \tag{3.49}$$

known as the 'Fung-Elastic' material model. This exponential function is widely used in the field of biomechanics to model soft tissues. Holzapfel et al. [82] combined the neo–Hookean response function for the isotropic ground substance with Fung's proposal for the collagen fibers and suggest a strain-energy function to model a fiber-reinforced material according to

$$\Psi = \frac{\mu}{2}(I_1 - 3) + \frac{k_1}{k_2}\left\{\exp[k_2(I_4 - 1)^2] - 1\right\}. \tag{3.50}$$

Here the parameters μ, k_1 and k_2 come from the neo–Hookean model (3.47) and the Fung model (3.49), respectively. To guarantee a stiffening in fiber direction, as observed in the histology of the arterial wall, we set $k_1 > 0$ and $k_2 > 0$. The shear modulus μ is positive by definition, cf. (3.47). $I_4 > 1$ is an invariant and can be seen as the stretch in fiber direction. This proposal gives rise to the well known artery model of Holzapfel et al. [82] which will be treated in the next section.

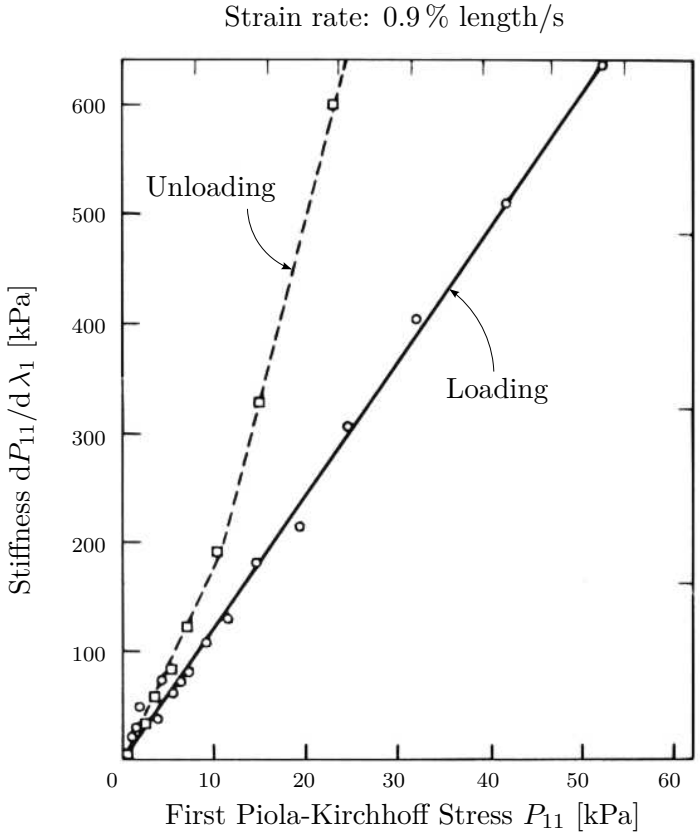

Figure 3.2: Linear relationship between stiffness $dP_{11}/d\lambda_1$ and stress P_{11}; in a modication from [60, 92].

3.11 A Multi-Layer Model for Arterial Walls

In this section a potential is discussed that models each layer of the artery as a fiber-reinforced composite. The anisotropic model was first proposed by Holzapfel et al. [82]. For a more detailed discussion of arterial models the reader is also referred to [83, 84]. Recent issues like modeling with respect to residual stresses is neglected in this work but is discussed in Holzapfel and Ogden [86].

Since the artery is a nearly incompressible tissue the strain-energy function is decoupled into a purely volumetric and a purely isochoric contribution

$$\Psi(\mathbf{C},\mathbf{A}_1,\ldots,\mathbf{A}_n) = \underbrace{U(J)}_{\text{volumetric}} + \underbrace{\overline{\Psi}(\overline{\mathbf{C}},\mathbf{A}_1,\ldots,\mathbf{A}_n)}_{\text{isochoric}},$$

with $\mathbf{C} = J^{-2/3}\overline{\mathbf{C}}$, $\det(\overline{\mathbf{C}}) = 1$ and the Jacobian $J = \det(\mathbf{F})$, see Section 3.1.

The set $\{\mathbf{A}_\alpha \mid \alpha = 1, \ldots, n\}$ of second order tensors is employed to describe the hyperelastic stress response of anisotropic biological tissues. In case of arterial walls, where we have an anisotropy due to collagen bundles with two main directions $\mathbf{a}_{01}, \mathbf{a}_{02}$, two such structure tensors are incorporated. These are defined as the cross product of the two reference direction vectors

$$\mathbf{A}_i := \mathbf{a}_{0i} \otimes \mathbf{a}_{0i}, \quad \text{with } |\mathbf{a}_{0i}| = 1 \text{ for } i = 1, 2.$$

From this definition it is clear that $\mathbf{A}_1$ and $\mathbf{A}_2$ are both symmetric.

A second split of the isochoric strain-energy function $\overline{\Psi}$ into an isotropic part $\overline{\Psi}_{\text{iso}}$ and an anisotropic part $\overline{\Psi}_{\text{aniso}}$ leads to the following response function

$$\overline{\Psi}(\overline{\mathbf{C}}, \mathbf{A}_1, \mathbf{A}_2) = \overline{\Psi}_{\text{iso}}(\overline{\mathbf{C}}) + \overline{\Psi}_{\text{aniso}}(\overline{\mathbf{C}}, \mathbf{A}_1, \mathbf{A}_2). \tag{3.51}$$

A two-term potential of that type was already proposed in the paper of Holzapfel and Weizsäcker [88]. In formula (3.51) the isotropic part is associated with the non-collagenous ground substance elastin and $\overline{\Psi}_{\text{aniso}}$ is associated with anisotropic deformations arising from the collagen fibers.

To formulate the strain-energy function in terms of invariants we need the *integrity basis* of $\overline{\mathbf{C}}, \mathbf{A_1}, \mathbf{A_2}$ which consists of the following nine invariants [82, 173]

$$\begin{aligned}
&\overline{I}_1(\overline{\mathbf{C}}) = \operatorname{tr} \overline{\mathbf{C}}, && \overline{I}_2(\overline{\mathbf{C}}) = \frac{1}{2}\left((\operatorname{tr} \overline{\mathbf{C}})^2 - \operatorname{tr} \overline{\mathbf{C}}^2\right), && \overline{I}_3(\overline{\mathbf{C}}) = \det \overline{\mathbf{C}} = 1, \\
&\overline{I}_4(\overline{\mathbf{C}}, \mathbf{A}_1) = \overline{\mathbf{C}} : \mathbf{A}_1, && \overline{I}_5(\overline{\mathbf{C}}, \mathbf{A}_1) = \overline{\mathbf{C}}^2 : \mathbf{A}_1, && \overline{I}_6(\overline{\mathbf{C}}, \mathbf{A}_2) = \overline{\mathbf{C}} : \mathbf{A}_2, \\
&\overline{I}_7(\overline{\mathbf{C}}, \mathbf{A}_2) = \overline{\mathbf{C}}^2 : \mathbf{A}_2, && \overline{I}_8(\overline{\mathbf{C}}, \mathbf{A}_1, \mathbf{A}_2) = \mathbf{a}_{01}^\top \mathbf{a}_{02}\, \mathbf{a}_{01}^\top \overline{\mathbf{C}} \mathbf{a}_{02}, && \overline{I}_9(\overline{\mathbf{C}}, \mathbf{A}_1, \mathbf{A}_2) = (\mathbf{a}_{01} \cdot \mathbf{a}_{02})^2.
\end{aligned}$$

The invariants $\overline{I}_3$ and $\overline{I}_9$ are omitted since they are constants. The invariants $\overline{I}_4$ and $\overline{I}_6$ have a clear physical interpretation: they are the squares of the stretches in the directions of $\mathbf{a}_{01}$ and $\mathbf{a}_{02}$ respectively, so that they are stretch measures for the two families of fibers.

To ease the fitting to experimental data, the number of material parameters should be reduced. When using the classical neo–Hookean model for the isotropic response we can leave the second invariant $\overline{I}_2$ out:

$$\overline{\Psi}_{\text{iso}}(\overline{I}_1) = \frac{c}{2}(\overline{I}_1 - 3), \tag{3.52}$$

where $c > 0$ is a stress-like material parameter, see Section 3.10.1. $\overline{I}_5$ and $\overline{I}_7$ are a linear combination of $\overline{I}_1$, $\overline{I}_2$, $\overline{I}_4$ and $\overline{I}_6$ (Cayley–Hamilton theorem) and describe a similar physical properties as $\overline{I}_4$ and $\overline{I}_6$. Hence, these two invariants are omitted. Moreover, interactions ($\overline{I}_8$) between the two fiber families are neglected which gives

the reduced model

$$\overline{\Psi}(\overline{\mathbf{C}}) = \overline{\Psi}_{\text{iso}}(\overline{I}_1) + \overline{\Psi}_{\text{aniso}}(\overline{I}_4, \overline{I}_6).$$

Holzapfel et al. [82] propose for the anisotropic part of this strain-energy function

$$\overline{\Psi}_{\text{aniso}}(\overline{I}_4, \overline{I}_6) = \frac{k_1}{2k_2} \sum_{i=4,6} \left\{ \exp[k_2(\overline{I}_i - 1)^2] - 1 \right\}. \tag{3.53}$$

In summary, we have the following strain-energy function to model the anisotropic behavior of arterial walls

$$\Psi(\mathbf{C}) = \Psi(J, \overline{I}_1, \overline{I}_4, \overline{I}_6) = U(J) + \frac{c}{2}(\overline{I}_1 - 3) + \frac{k_1}{2k_2} \sum_{i=4,6} \left\{ \exp[k_2(\overline{I}_i - 1)^2] - 1 \right\}, \tag{3.54}$$

where

$$\overline{I}_1(\overline{\mathbf{C}}) = \operatorname{tr} \overline{\mathbf{C}}, \quad \overline{I}_4(\overline{\mathbf{C}}, \mathbf{a}_{01}) = \overline{\mathbf{C}} : \mathbf{A}_1, \quad \overline{I}_6(\overline{\mathbf{C}}, \mathbf{a}_{02}) = \overline{\mathbf{C}} : \mathbf{A}_2,$$

and all material parameters c, k_1 and k_2 are positive, see (3.50). To obtain these parameters they are fitted to the experimentally observed response of the arterial layers, i.e. they are to be determined from mechanical tests of the tissue.

An important condition in dealing with this model is that the anisotropic response $\overline{\Psi}_{\text{aniso}}$ only contributes if

$$\overline{I}_i > 1 \text{ for } i = 4, 6, \tag{3.55}$$

i.e. if there is a stretch in a fiber direction. This condition is explained with the wavy structure of the collagen fibers, see Figure 2.2, which are hence regarded as not being able to support compressive stresses. Thus the fibers are assumed to be active in extension ($\overline{I}_i > 1$) and inactive in compression ($\overline{I}_i < 1$). This assumption is not only based on physical reasons but it is also essential for reasons of stability [83].

Another consequence of the wavy structure of the collagen fibers is that they are not active at low pressures and if the material behaves isotropic. At high pressures the collagen fibers straighten and then they govern the resistance to stretch of the material. This behavior of collagen was already discussed by Roach and Burton [154] and is fully covered by the artery model (3.54). The described strong stiffening effect at higher pressures also motivates the use of the exponential function in the anisotropic response of the strain-energy function Ψ.

3.11.1 The Artery Modeled as a Two-Layer Thick-Walled Tube

As already mentioned in Section 2.1, arteries are composed of three layers, the intima, the media and the adventitia. For the case of an healthy young artery the innermost layer, the intima, is not of mechanical interest. We model each of the remaining layers with a separate strain-energy function. We assume that the media as well as the adventitia respond with similar mechanical characteristics and therefore we use the same form of strain-energy functions. To capture the specifics of each layer we use different sets of material parameters.

Hence, we write the energy functions for the two-layer problem using the Holzapfel artery model (3.54) as

$$\overline{\Psi}_{\mathrm{med}}(\overline{I}_1,\overline{I}_{4\mathrm{M}},\overline{I}_{6\mathrm{M}}) = \frac{c_{\mathrm{M}}}{2}(\overline{I}_1-3)+\frac{k_{1\mathrm{M}}}{2k_{2\mathrm{M}}}\sum_{i=4,6}\Big\{\exp[k_{2\mathrm{M}}(\overline{I}_{i\mathrm{M}}-1)^2]-1\Big\},$$

$$\overline{\Psi}_{\mathrm{adv}}(\overline{I}_1,\overline{I}_{4\mathrm{A}},\overline{I}_{6\mathrm{A}}) = \frac{c_{\mathrm{A}}}{2}(\overline{I}_1-3)+\frac{k_{1\mathrm{A}}}{2k_{2\mathrm{A}}}\sum_{i=4,6}\Big\{\exp[k_{2\mathrm{A}}(\overline{I}_{i\mathrm{A}}-1)^2]-1\Big\}$$

for the media and adventitia, respectively.

The invariants used in this formulation are defined by

$$\overline{I}_{4\,j} = \mathbf{A}_{1j} : \overline{\mathbf{C}}, \quad \overline{I}_{6\,j} = \mathbf{A}_{2j} : \overline{\mathbf{C}}, \quad j = \mathrm{M},\mathrm{A},$$

with

$$\mathbf{A}_{1j} = \mathbf{a}_{01\,j} \otimes \mathbf{a}_{01\,j}, \quad \mathbf{A}_{2j} = \mathbf{a}_{02\,j} \otimes \mathbf{a}_{02\,j}.$$

If we regard the simplified configuration of an artery as a tube we can describe the components of the direction vectors in cylindrical polar coordinates. Hence, the vectors $\mathbf{a}_{01\,j}$ and $\mathbf{a}_{02\,j}$ have, in matrix notation, the forms

$$[\mathbf{a}_{01\,j}] = \begin{pmatrix} 0 \\ \cos\beta_j \\ \sin\beta_j \end{pmatrix}, \quad [\mathbf{a}_{02\,j}] = \begin{pmatrix} 0 \\ \cos\beta_j \\ -\sin\beta_j \end{pmatrix}, \quad j = \mathrm{M},\mathrm{A},$$

where β_j are the angles between the collagen fibers and the circumferential direction for $j = \mathrm{M},\mathrm{A}$. This angle is indicated in Figure 3.3. There one can find exemplary values for the material and geometrical data for a carotid artery from a rabbit as well.

More experimental data and material and geometrical parameters fitted to the human aorta one may find in Holzapfel [79].

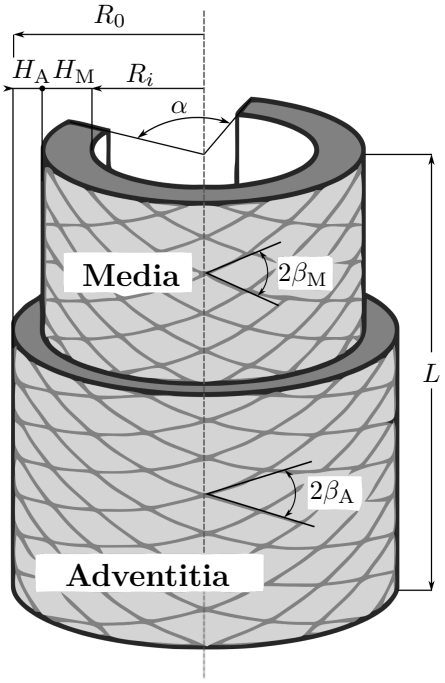

$R_i = 0.71\,\text{mm}$ for $\alpha = 0.0°$
$R_i = 1.43\,\text{mm}$ for $\alpha = 160.0°$

	Material	Geometry
Media	$c_M = 3.0000\,\text{kPa}$ $k_{1M} = 2.3632\,\text{kPa}$ $k_{2M} = 0.8393\,[-]$	$H_M = 0.26\,\text{mm}$ $\beta_M = 29.0°$
Adventitia	$c_A = 0.3000\,\text{kPa}$ $k_{1A} = 0.5620\,\text{kPa}$ $k_{2A} = 0.7112\,[-]$	$H_A = 0.13\,\text{mm}$ $\beta_A = 62.0°$

Figure 3.3: Material parameters for a segment of a carotid artery from a rabbit [37, 82].

3.11.2 Modeling with Respect to Fiber Dispersion

In Section 3.11.1 the existing dispersion of the collagen fibers is ignored. Nonetheless, this model works well for the media, where the collagen fibers are arranged in two helically distributed families with a small pitch and very little dispersion in their orientation. By contrast, in the adventitial and intimal layers the orientation of the collagen fibers is dispersed. Thus an additional measure of the dispersion of collagen fibers is proposed in [62, 78]. Both approaches are concerned with an extension of the model (3.53) to incorporate an isotropic behavior as a special case. In [78] the authors suggest a multiplication of the anisotropic function $\exp[c_2(\overline{I}_i - 1)^2]$ with the isotropic function $\exp[c_1(\overline{I}_1 - 3)^2]$, where c_1, c_2 are two constants. This leads to

$$\overline{\Psi}_{\text{aniso}}(\overline{I}_1, \overline{I}_4, \overline{I}_6) = \frac{k_1}{2k_2} \sum_{i=4,6} \Big(\exp\{k_2[(1-\rho)(\overline{I}_1 - 3)^2 + \rho(\overline{I}_i - 1)^2]\} - 1 \Big) \tag{3.56}$$

with the dimensionless and stress-like parameters $k_2, k_1 > 0$ and a weighting factor $\rho \in [0,1]$. For the limit $\rho = 1$ we get the anisotropic model (3.53), and for $\rho = 0$ an isotropic response is obtained, very similar to Demiray [47].

Another approach was proposed by Gasser et al. [62] where an additional structure

parameter ρ^* is introduced that characterizes the dispersed collagen orientation. As the first dispersion model (3.56) this is an extension to the anisotropic model (3.53):

$$\overline{\Psi}_{\text{aniso}}(\overline{I}_1, \overline{I}_4, \overline{I}_6) = \frac{k_1}{2k_2} \sum_{i=4,6} \left\{ \exp[k_2(\overline{I}_i^* - 1)^2] - 1 \right\},$$

with $\overline{I}_i^* = \rho^* \overline{I}_1 + (1 - 3\rho^*)\overline{I}_i$. This modification of the forth and the sixth invariants enables the representation of the dispersion of the collagen fibers through the dispersion parameter $\rho^* \in [0, 1/3]$. For $\rho^* = 0$ the anisotropic model without dispersion (3.53) is obtained, the choice $\rho^* = 1/3$ leads to an isotropic distribution very similar to that proposed by Demiray [47].

A more detailed overview concerning models with respect to fiber dispersion can be found in [78].

3.12 Modeling of Passive Myocardium

The model of the myocardium that is discussed in this section was introduced by Holzapfel and Ogden [85]. In the derivation of a form for the strain-energy function Ψ for the cardiac tissue we mainly stick to the descriptions of this paper. Nonetheless, there exist a vast amount of other constitutive models for the myocardium. The interested reader is referred to the early works of Humphrey and Yin [95, 189]. Other widely used strain-energy functions were proposed by Guccione et al. [67], Costa et al. [40] and Schmid et al. [162, 163].

As discussed in Section 2.4 we have a layered organization of the muscle fibers within the myocardium which can be described by a right-handed orthonormal set of basis vectors $\mathbf{f}_0$, $\mathbf{s}_0$ and $\mathbf{n}_0$. Hence, we can write the strain-energy function as

$$\Psi = \Psi(\mathbf{C}, \mathbf{A}_f, \mathbf{A}_s, \mathbf{A}_n).$$

We will use a similar decomposition in a volumetric and an isochoric part, see Section 3.11 and [52], such that

$$\Psi = U(J) + \overline{\Psi}(\overline{\mathbf{C}}, \mathbf{A}_f, \mathbf{A}_s, \mathbf{A}_n).$$

As for arterial tissue (Section 3.11) we need the integrity basis of the involved four tensors to formulate the strain-energy function in terms of invariants. In the following only the most important invariants are mentioned, see Spencer [173] for more details. For the isotropic part of the strain-energy function we have the invariants as described in Corollary 3.4. The invariants associated with the fiber, sheet and sheet-normal

direction are defined as

$$\overline{I}_{4\mathrm{f}} := \mathbf{f}_0 \cdot (\overline{\mathbf{C}}\mathbf{f}_0), \quad \overline{I}_{4\mathrm{s}} := \mathbf{s}_0 \cdot (\overline{\mathbf{C}}\mathbf{s}_0) \ \text{ and } \ \overline{I}_{4\mathrm{n}} := \mathbf{n}_0 \cdot (\overline{\mathbf{C}}\mathbf{n}_0).$$

Due to the fact that the three direction vectors are orthonormal, we can state

$$\sum_{i=\mathrm{f,s,n}} \overline{I}_{4i} = \overline{\mathbf{C}} : (\mathbf{f}_0 \otimes \mathbf{f}_0 + \mathbf{s}_0 \otimes \mathbf{s}_0 + \mathbf{n}_0 \otimes \mathbf{n}_0) = \overline{\mathbf{C}} : \mathbf{I} = \overline{I}_1,$$

hence only three of these four invariants are independent.

Next, we mention coupling invariants associated with the pairs of directions

$$\overline{I}_{8\mathrm{fs}} = \overline{I}_{8\mathrm{sf}} := \mathbf{f}_0 \cdot (\overline{\mathbf{C}}\mathbf{s}_0), \ \overline{I}_{8\mathrm{fn}} = \overline{I}_{8\mathrm{nf}} := \mathbf{f}_0 \cdot (\overline{\mathbf{C}}\mathbf{n}_0), \ \overline{I}_{8\mathrm{sn}} = \overline{I}_{8\mathrm{ns}} := \mathbf{s}_0 \cdot (\overline{\mathbf{C}}\mathbf{n}_0).$$

The invariants

$$\overline{I}_{5\mathrm{f}} := \mathbf{f}_0 \cdot (\overline{\mathbf{C}}^2\mathbf{f}_0), \quad \overline{I}_{5\mathrm{s}} := \mathbf{s}_0 \cdot (\overline{\mathbf{C}}^2\mathbf{s}_0) \ \text{ and } \ \overline{I}_{5\mathrm{n}} := \mathbf{n}_0 \cdot (\overline{\mathbf{C}}^2\mathbf{n}_0)$$

can be represented in terms of the other invariants and the orthogonality reduces the number by an additional one [85].

In total we end up with seven independent invariants and we can write the most general form of the isochoric part of the free energy function as

$$\overline{\Psi} = \overline{\Psi}(\overline{I}_1, \ \overline{I}_3, \ \overline{I}_{4\mathrm{f}}, \ \overline{I}_{4\mathrm{s}}, \ \overline{I}_{8\mathrm{fn}}, \ \overline{I}_{8\mathrm{fs}}, \ \overline{I}_{8\mathrm{sn}})$$

for a compressible material. For an incompressible material we can state that $\overline{I}_3 = 1$ and hence we have only six independent invariants.

To reduce the number of invariants and hence the number of material parameters we discuss the interpretations of the invariants. To model the isotropic response of the underlying matrix-material we could use the neo–Hookean model (3.52) as in the case of arteries. Holzapfel and Ogden [85] proposed in the case of the myocardium the exponential model introduced by Demiray [47]

$$\overline{\Psi}_{\mathrm{iso}}(\overline{I}_1) = \frac{a}{2b}\left\{\exp\left[b(\overline{I}_1 - 3)\right] - 1\right\}, \tag{3.57}$$

where $a > 0$ is a stress-like and b a dimensionless material parameter. To guarantee that the stress response increases exponentially in the corresponding stretch we have to set $b > 0$. The requirement of a positive parameter a follows from the analysis of the strain-energy function, see Lemma 4.26 for more details.

To model the transversely isotropic behavior and the stiffening effect in the muscle fiber direction $\mathbf{f}_0$ and in the collagen fiber direction $\mathbf{s}_0$ the same proposal with an

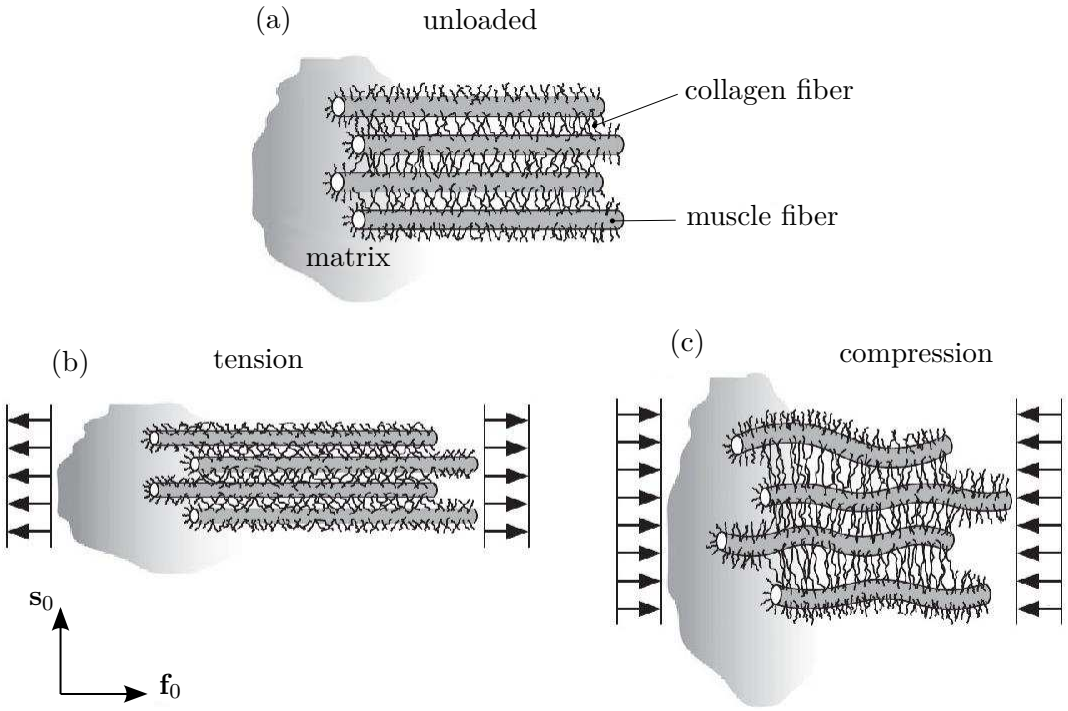

Figure 3.4: Muscle and collagen fibers under tension and compression; $\mathbf{f}_0$ is the muscle fiber axis, $\mathbf{s}_0$ the sheet axis which corresponds to the direction of the collagen fibers. (a) unloaded configuration; (b) structure under tension in direction of $\mathbf{f}_0$ which results in a stretch of the muscle fibers; (c) compression is applied to the fiber network; this leads to a lateral extension of the collagen fibers while the myocytes are buckled. Figure courtesy of Holzapfel and Ogden [85].

exponential function as for the case of arterial walls is used; cf. (3.53). Thus we obtain for this part of the constitutive equation

$$\overline{\Psi}_{\text{trans}}(\overline{I}_{4\text{f}}) = \frac{a_{\text{f}}}{2b_{\text{f}}}\left\{\exp[b_{\text{f}}(\overline{I}_{4\text{f}}-1)^2]-1\right\}, \tag{3.58}$$

$$\overline{\Psi}_{\text{trans}}(\overline{I}_{4\text{s}}) = \frac{a_{\text{s}}}{2b_{\text{s}}}\left\{\exp[b_{\text{s}}(\overline{I}_{4\text{s}}-1)^2]-1\right\}, \tag{3.59}$$

where again this part only contributes if $\overline{I}_{4\text{f}} > 1$ or $\overline{I}_{4\text{s}} > 1$, i.e. we have a stretch in one of the fiber directions, cf. Figure 3.4. All material parameters, the stress like a_i as well as the dimensionless b_i for $i = \text{f},\text{s}$ are supposed to be positive. Using this setting of the parameters we guarantee a stiffening in fiber and sheet direction as observed in the histology of the myocardium.

Finally, the shear behavior as described by Dokos et al. [50] and Section 2.4 is taken into consideration. Since the highest resistance was observed in the fs-plane and since it showed an exponential trend, Holzapfel and Ogden [85] proposed to model

this orthotropic part of the characterization in terms of the invariant $\overline{I}_{8\mathrm{fs}}$ by

$$\overline{\Psi}_{\mathrm{ortho}}(\overline{I}_{8\mathrm{fs}}) = \frac{a_{\mathrm{fs}}}{2b_{\mathrm{fs}}} \left\{ \exp[b_{\mathrm{fs}} \overline{I}^2_{8\mathrm{fs}}] - 1 \right\}, \tag{3.60}$$

with $a_{\mathrm{fs}} > 0$ a stress-like and $b_{\mathrm{fs}} > 0$ a dimensionless material constant.

Summing up, we get the following orthotropic strain-energy function to model the passive myocardium

$$\begin{aligned} \Psi(\mathbf{C}) = U(J) + \frac{a}{2b} \left\{ \exp\left[b(\overline{I}_1 - 3) \right] - 1 \right\} \\ + \sum_{i=\mathrm{f,s}} \frac{a_i}{2b_i} \left\{ \exp[b_i(\overline{I}_{4i} - 1)^2] - 1 \right\} + \frac{a_{\mathrm{fs}}}{2b_{\mathrm{fs}}} \left\{ \exp[b_{\mathrm{fs}} \overline{I}^2_{8\mathrm{fs}}] - 1 \right\}. \end{aligned} \tag{3.61}$$

As discussed before, all of the eight material parameters are supposed to be positive and the transversely isotropic parts only contribute if $\overline{I}_{4\mathrm{f}} > 1$ or $\overline{I}_{4\mathrm{s}} > 1$, respectively.

3.13 Computation of Stress and Elasticity Tensors

In this section, we provide an explicit symbolic expression of the stress and elasticity tensors for the materials discussed in the previous sections. This will be used to calculate a linearized form of the constitutive equation needed for the application of Newton's method, see Section 4.4.1 ff., and the implementation of the material models in the computer code.

Recall Corollary 3.2 and Definition 3.14 for the constitutive equations

$$\mathbf{S} = 2\frac{\partial \Psi(\mathbf{C})}{\partial \mathbf{C}}, \quad \mathbb{C} = 2\frac{\partial \mathbf{S}(\mathbf{C})}{\partial \mathbf{C}} = 4\frac{\partial^2 \Psi(\mathbf{C})}{\partial \mathbf{C}^2}$$

in the reference configuration and the push-forward operations in the current configuration

$$\sigma_{ij} = J^{-1} F_{ia} F_{jb} S_{ab}, \quad c_{ijkl} = J^{-1} F_{ia} F_{jb} F_{kc} F_{ld} C_{abcd}, \tag{3.62}$$

for $i,j,k,l,a,b,c,d = 1,\dots,3$. As an example, the the stress tensor and the elasticity tensor for the St. Venant–Kirchhoff material (3.46) may easily be computed

$$\begin{aligned}
\mathbf{S}_{\mathrm{VK}} &= 2\frac{\partial \Psi_{\mathrm{VK}}(\mathbf{C})}{\partial \mathbf{C}} = \frac{\partial \Psi_{\mathrm{VK}}(\mathbf{E})}{\partial \mathbf{E}} = \lambda \operatorname{tr}(\mathbf{E})\mathbf{I} + 2\mu\mathbf{E}, \\
\mathbb{C}_{\mathrm{VK}} &= 2\frac{\partial \mathbf{S}_{\mathrm{VK}}(\mathbf{C})}{\partial \mathbf{C}} = \frac{\partial \mathbf{S}_{\mathrm{VK}}(\mathbf{E})}{\partial \mathbf{E}} = \lambda \mathbf{I} \otimes \mathbf{I} + 2\mu\mathbb{S},
\end{aligned}$$

using Corollaries A.1, A.3 and A.5.

For more complex nearly incompressible materials our starting point is the decoupled version of the strain-energy function

$$\Psi(\mathbf{C}) = U(J) + \overline{\Psi}(\overline{\mathbf{C}}),$$

see (3.29) and a chain rule of the form

$$\frac{\partial \Psi(\mathbf{C})}{\partial \mathbf{C}} = \frac{\partial U(J)}{\partial \mathbf{C}} + \frac{\partial \overline{\Psi}(\overline{I}_1, \overline{I}_2, \dots)}{\partial \mathbf{C}} = \frac{\partial U(J)}{\partial J}\frac{\partial J}{\partial \mathbf{C}} + \overline{\psi}_1 \frac{\partial \overline{I}_1}{\partial \mathbf{C}} + \overline{\psi}_2 \frac{\partial \overline{I}_2}{\partial \mathbf{C}} + \dots, \tag{3.63}$$

where

$$\overline{\psi}_i = \frac{\partial \overline{\Psi}}{\partial \overline{I}_i}, \quad i = 1,2,\dots.$$

Note that the decoupled formulation leads to an additive split of the stress and elasticity tensors in volumetric and isochoric parts, see (3.33), (3.35) and (3.39),

$$\boldsymbol{\sigma} = \boldsymbol{\sigma}_{\mathrm{vol}} + \boldsymbol{\sigma}_{\mathrm{isc}}, \ \mathbf{S} = \mathbf{S}_{\mathrm{vol}} + \mathbf{S}_{\mathrm{isc}}, \ \mathbb{c} = \mathbb{c}_{\mathrm{vol}} + \mathbb{c}_{\mathrm{isc}}, \ \mathbb{C} = \mathbb{C}_{\mathrm{vol}} + \mathbb{C}_{\mathrm{isc}}.$$

3.13.1 Volumetric Part

We start with the *volumetric part* of the strain-energy function $U(J)$ and compute the volumetric contribution of the stress tensors and the elasticity tensors in each the Lagrangian and the Eulerian configuration. With the definition of the hydrostatic pressure (3.31) and (3.26) we get

$$\mathbf{S}_{\text{vol}} = 2\frac{\partial U(J)}{\partial \mathbf{C}} = 2\frac{\partial U(J)}{\partial J}\frac{\partial J}{\partial \mathbf{C}} = Jp\mathbf{C}^{-1} \tag{3.64}$$

for the volumetric part of the second Piola–Kirchhoff stress tensor.

The elasticity tensor in the Lagrangian configuration is calculated due to

$$\mathbb{C}_{\text{vol}} = 2\frac{\partial \mathbf{S}_{\text{vol}}}{\partial \mathbf{C}} = 2\frac{\partial Jp\mathbf{C}^{-1}}{\partial \mathbf{C}} = 2\mathbf{C}^{-1} \otimes \frac{\partial Jp}{\mathbf{C}} + 2Jp\frac{\partial \mathbf{C}^{-1}}{\partial \mathbf{C}}.$$

This is using Corollary A.4

$$\mathbb{C}_{\text{vol}} = J\left(p + J\frac{\partial p}{\partial J}\right)\mathbf{C}^{-1} \otimes \mathbf{C}^{-1} - 2Jp\ \mathbf{C}^{-1} \odot \mathbf{C}^{-1}.$$

With push-forward operations as described in (3.62) we get

$$\boldsymbol{\sigma}_{\text{vol}} = p\mathbf{I}, \quad \mathbb{c}_{\text{vol}} = \left(p + J\frac{\partial p}{\partial J}\right)\mathbf{I} \otimes \mathbf{I} - 2p\ \mathbb{S}. \tag{3.65}$$

for the elasticity tensor in the Eulerian configuration.

3.13.2 Isochoric Part

Definition 3.20. *We define the* fictitious stress tensors $\overline{\mathbf{S}}$ *in the Lagrangian configuration and* $\overline{\boldsymbol{\sigma}}$ *in the Eulerian configuration as*

$$\overline{\mathbf{S}} := 2\frac{\partial \overline{\Psi}(\overline{\mathbf{C}})}{\partial \overline{\mathbf{C}}}, \quad J\overline{\boldsymbol{\sigma}} := 2\overline{\mathbf{F}}\frac{\partial \overline{\Psi}(\overline{\mathbf{C}})}{\partial \overline{\mathbf{C}}}\overline{\mathbf{F}}^{\top}.$$

The chain rule (3.63) *yields*

$$\overline{\mathbf{S}} = 2\frac{\partial \overline{\Psi}}{\partial \overline{I}_i}\frac{\partial \overline{I}_i}{\partial \overline{\mathbf{C}}}, \quad J\overline{\boldsymbol{\sigma}} = 2\frac{\partial \overline{\Psi}}{\partial \overline{I}_i}\overline{\mathbf{F}}\frac{\partial \overline{I}_i}{\partial \overline{\mathbf{C}}}\overline{\mathbf{F}}^{\top}, \quad i = 1, 2, \dots$$

Definition 3.21. *We define the* fictitious elasticity tensors $\overline{\mathbb{C}}$ *and* $\overline{\mathbb{c}}$ *as*

$$\overline{\mathbb{C}} := 4\frac{\partial^2\overline{\Psi}(\overline{\mathbf{C}})}{\partial\overline{\mathbf{C}}\partial\overline{\mathbf{C}}}$$

in the Lagrangian configuration and the corresponding tensor $\overline{\mathbb{c}}$*, obtained by a push-forward operation of the form* $(3.62)_2$*, in the Eulerian configuration.*

The chain rule (3.63) *yields with a summation over* $i = 1, 2, \ldots$*, and* $[\overline{\mathbb{B}}]_{ijkl} = [\overline{\mathbf{F}}]_{ik}[\overline{\mathbf{F}}]_{jl}$

$$\begin{aligned}\overline{\mathbb{C}} &= 4\left(\frac{\partial\overline{I}_i}{\partial\overline{\mathbf{C}}}\otimes\frac{\partial^2\overline{\Psi}}{\partial\overline{I}_i^2}\frac{\partial\overline{I}_i}{\partial\overline{\mathbf{C}}}+\frac{\partial\overline{\Psi}}{\partial\overline{I}_i}\frac{\partial^2\overline{I}_i}{\partial\overline{\mathbf{C}}^2}\right)\\ J\overline{\mathbb{c}} &= 4\left(\frac{\partial^2\overline{\Psi}}{\partial\overline{I}_i^2}(\overline{\mathbf{F}}\frac{\partial\overline{I}_i}{\partial\overline{\mathbf{C}}}\overline{\mathbf{F}}^\top)\otimes(\overline{\mathbf{F}}\frac{\partial\overline{I}_i}{\partial\overline{\mathbf{C}}}\overline{\mathbf{F}}^\top)+\overline{\mathbb{B}}\frac{\partial\overline{\Psi}}{\partial\overline{I}_i}\frac{\partial^2\overline{I}_i}{\partial\overline{\mathbf{C}}^2}\overline{\mathbb{B}}^\top\right).\end{aligned}$$

Recall from (3.34) and (3.36) and Corollary A.7 the isochoric stress tensors

$$\mathbf{S}_{\text{isc}} = \operatorname{Dev}(\overline{\mathbf{S}}) = \mathbb{P} : \overline{\mathbf{S}}, \quad \boldsymbol{\sigma}_{\text{isc}} = \operatorname{dev}(\overline{\boldsymbol{\sigma}}) = \mathbb{p} : \overline{\boldsymbol{\sigma}}. \tag{3.66}$$

The elasticity tensor is calculated using (3.27) and (A.25)

$$\begin{aligned}\mathbb{C}_{\text{isc}} &= 2\frac{\partial\mathbf{S}_{\text{isc}}}{\partial\mathbf{C}} = 4\frac{\partial\operatorname{Dev}(\overline{\mathbf{S}})}{\partial\mathbf{C}} = 4\frac{\partial}{\partial\mathbf{C}}\left[J^{-2/3}\operatorname{Dev}\left(\frac{\partial\overline{\Psi}(\overline{\mathbf{C}})}{\partial\overline{\mathbf{C}}}\right)\right]\\ &= 4\operatorname{Dev}\left(\frac{\partial\Psi_{\text{iso}}(\overline{\mathbf{C}})}{\partial\overline{\mathbf{C}}}\right)\otimes\frac{\partial J^{-2/3}}{\partial\mathbf{C}}+4J^{-2/3}\frac{\partial}{\partial\mathbf{C}}\operatorname{Dev}\left(\frac{\partial\overline{\Psi}(\overline{\mathbf{C}})}{\partial\overline{\mathbf{C}}}\right).\end{aligned}$$

With $(3.26)_2$, $(3.66)_1$ and (A.25) we get

$$\begin{aligned}\mathbb{C}_{\text{isc}} &= -\frac{4}{3}\operatorname{Dev}\left(\frac{\partial\overline{\Psi}(\overline{\mathbf{C}})}{\partial\overline{\mathbf{C}}}\right)\otimes J^{-2/3}\mathbf{C}^{-1}+4J^{-2/3}\frac{\partial}{\partial\mathbf{C}}\left[\frac{\partial\overline{\Psi}(\overline{\mathbf{C}})}{\partial\overline{\mathbf{C}}}\right]\\ &\quad-\frac{4}{3}J^{-2/3}\frac{\partial}{\partial\mathbf{C}}\left[\operatorname{tr}\left(\mathbf{C}\frac{\partial\overline{\Psi}(\overline{\mathbf{C}})}{\partial\overline{\mathbf{C}}}\right)\mathbf{C}^{-1}\right]\\ &= -\frac{2}{3}\mathbf{S}_{\text{iso}}\otimes\mathbf{C}^{-1}+4J^{-4/3}\frac{\partial^2\overline{\Psi}(\overline{\mathbf{C}})}{\partial\overline{\mathbf{C}}\partial\overline{\mathbf{C}}}\,\mathbb{P}^\top-\frac{4}{3}J^{-2/3}\mathbf{C}^{-1}\otimes\frac{\partial}{\partial\mathbf{C}}\operatorname{tr}\left(\mathbf{C}\frac{\partial\overline{\Psi}(\overline{\mathbf{C}})}{\partial\overline{\mathbf{C}}}\right)\\ &\quad-\frac{4}{3}J^{-2/3}\operatorname{tr}\left(\mathbf{C}\frac{\partial\overline{\Psi}(\overline{\mathbf{C}})}{\partial\overline{\mathbf{C}}}\right)\frac{\partial\mathbf{C}^{-1}}{\partial\mathbf{C}}\end{aligned}$$

Now, Definition 3.21, the chain rule (A.26) and Corollary A.4 yield

$$\mathbb{C}_{\text{isc}} = -\frac{2}{3}\mathbf{S}_{\text{iso}}\otimes\mathbf{C}^{-1}+J^{-4/3}\overline{\mathbb{C}}\mathbb{P}^\top-\frac{4}{3}J^{-2/3}\mathbf{C}^{-1}\otimes\left[\mathbf{C}:\frac{\partial}{\partial\mathbf{C}}\left(\frac{\partial\overline{\Psi}(\overline{\mathbf{C}})}{\partial\overline{\mathbf{C}}}\right)+\frac{\partial\overline{\Psi}(\overline{\mathbf{C}})}{\partial\overline{\mathbf{C}}}:\frac{\partial\mathbf{C}}{\partial\mathbf{C}}\right]$$

$$
\begin{aligned}
&+ J^{-2/3}\frac{2}{3}\operatorname{tr}\left(\mathbf{C}\,\overline{\mathbf{S}}\right)(\mathbf{C}^{-1}\odot\mathbf{C}^{-1}) \\
&= -\frac{2}{3}\mathbf{S}_{\text{iso}}\otimes\mathbf{C}^{-1} + J^{-4/3}\overline{\mathbb{C}}\,\mathbb{P}^{\top} - \frac{4}{3}J^{-2/3}\,\mathbf{C}^{-1}\otimes\frac{\partial\overline{\Psi}(\overline{\mathbf{C}})}{\partial\overline{\mathbf{C}}} \\
&\quad - \frac{4}{3}J^{-4/3}\,(\mathbf{C}^{-1}\otimes\mathbf{C})\,\frac{\partial^2\overline{\Psi}(\overline{\mathbf{C}})}{\partial\overline{\mathbf{C}}\partial\overline{\mathbf{C}}}\,\mathbb{P}^{\top} + J^{-2/3}\frac{2}{3}\operatorname{tr}\left(\mathbf{C}\,\overline{\mathbf{S}}\right)(\mathbf{C}^{-1}\odot\mathbf{C}^{-1}).
\end{aligned}
$$

We obtain

$$
\begin{aligned}
\mathbb{C}_{\text{isc}} = &-\frac{2}{3}\mathbf{S}_{\text{iso}}\otimes\mathbf{C}^{-1} + J^{-4/3}\mathbb{P}\,\overline{\mathbb{C}}\,\mathbb{P}^{\top} - \frac{4}{3}J^{-2/3}\,\mathbf{C}^{-1}\otimes\frac{\partial\overline{\Psi}(\overline{\mathbf{C}})}{\partial\overline{\mathbf{C}}} \\
&+ J^{-2/3}\frac{2}{3}\operatorname{tr}\left(\mathbf{C}\,\overline{\mathbf{S}}\right)(\mathbf{C}^{-1}\odot\mathbf{C}^{-1}),
\end{aligned}
$$

using Definition 3.21 and the definition of the projection tensor, see Corollary A.7. With

$$
\mathbf{C}^{-1}\otimes\frac{\partial\overline{\Psi}(\overline{\mathbf{C}})}{\partial\overline{\mathbf{C}}} = \mathbf{C}^{-1}\otimes\operatorname{Dev}\left(\frac{\partial\overline{\Psi}(\overline{\mathbf{C}})}{\partial\overline{\mathbf{C}}}\right) - \mathbf{C}^{-1}\otimes\left[\frac{1}{3}\operatorname{tr}\left(\frac{\partial\overline{\Psi}(\overline{\mathbf{C}})}{\partial\overline{\mathbf{C}}}\right)\mathbf{C}^{-1}\right]
$$

we finally get

$$
\begin{aligned}
\mathbb{C}_{\text{isc}} = &\; J^{-4/3}\mathbb{P}\,\overline{\mathbb{C}}\,\mathbb{P}^{\top} + J^{-2/3}\frac{2}{3}\operatorname{tr}\left(\mathbf{C}\,\overline{\mathbf{S}}\right)(\mathbf{C}^{-1}\odot\mathbf{C}^{-1} - \frac{1}{3}\mathbf{C}^{-1}\otimes\mathbf{C}^{-1}) \\
&- \frac{2}{3}(\mathbf{S}_{\text{iso}}\otimes\mathbf{C}^{-1} + \mathbf{C}^{-1}\otimes\mathbf{S}_{\text{iso}}).
\end{aligned}
\tag{3.67}
$$

Push-forward operations, see Definition 3.14, lead to the elasticity tensor in the Eulerian configuration

$$
\mathbb{c}_{\text{isc}} = \mathbb{P}\,\overline{\mathbb{C}}\,\mathbb{P} + \frac{2}{3}\operatorname{tr}(\overline{\boldsymbol{\sigma}})\,\mathbb{P} - \frac{2}{3}(\boldsymbol{\sigma}_{\text{iso}}\otimes\mathbf{I} + \mathbf{I}\otimes\boldsymbol{\sigma}_{\text{iso}}). \tag{3.68}
$$

3.13.3 Specific Stress and Elasticity Tensors

For the different material models we have to compute the fictitious stress and elasticity tensors given in Definition 3.20 and Definition 3.21.

Neo–Hookean model, (3.52)**:** the considered isochoric strain-energy function is

$$\overline{\Psi}(\overline{\mathbf{C}}) = \frac{c}{2}(\overline{I}_1 - 3),\ \overline{I}_1 = \mathrm{tr}(\overline{\mathbf{C}}).$$

With $\overline{\mathbf{B}} = \overline{\mathbf{F}}\overline{\mathbf{F}}^{\top}$ the left Cauchy–Green tensor, the stress tensors are computed as

$$\overline{\mathbf{S}} = c\mathbf{I}, \quad J\overline{\boldsymbol{\sigma}} = c\overline{\mathbf{B}},$$

and the elasticity tensors are computed as

$$\overline{\mathbb{C}} = \mathbb{O}, \quad J\overline{\mathbb{C}} = \mathbb{O}.$$

Here, $\mathbb{O}$ denotes the forth-order null matrix.

Demiray model, (3.57)**:** the considered isochoric strain-energy function is

$$\overline{\Psi}(\overline{\mathbf{C}}) = \frac{a}{2b}\left\{\exp\left[b(\overline{I}_1 - 3)\right] - 1\right\},\ \overline{I}_1 = \mathrm{tr}(\overline{\mathbf{C}}).$$

With $\overline{\mathbf{B}} = \overline{\mathbf{F}}\overline{\mathbf{F}}^{\top}$ the left Cauchy–Green tensor, the stress tensors are computed as

$$\overline{\mathbf{S}} = a\exp\left[b(\overline{I}_1 - 3)\right]\mathbf{I}, \quad J\overline{\boldsymbol{\sigma}} = a\exp\left[b(\overline{I}_1 - 3)\right]\overline{\mathbf{B}},$$

and the elasticity tensors as

$$\overline{\mathbb{C}} = 2ab\,\exp\left[b(\overline{I}_1 - 3)\right]\mathbf{I}\otimes\mathbf{I}, \quad J\overline{\mathbb{C}} = 2ab\,\exp\left[b(\overline{I}_1 - 3)\right]\overline{\mathbf{B}}\otimes\overline{\mathbf{B}}.$$

Mooney–Rivlin model, (3.44)**:** the considered isochoric strain-energy function is

$$\overline{\Psi}(\overline{\mathbf{C}}) = c_1(\overline{I}_1 - 3) + c_2(\overline{I}_2 - 3),\ \text{with } \overline{I}_1 = \mathrm{tr}(\overline{\mathbf{C}}),\ \overline{I}_2 = \frac{1}{2}[(\mathrm{tr}\,\overline{\mathbf{C}})^2 - \mathrm{tr}(\overline{\mathbf{C}}^2)].$$

With $\overline{\mathbf{B}} = \overline{\mathbf{F}}\overline{\mathbf{F}}^{\top}$ the left Cauchy–Green tensor, the stress tensors are computed as

$$\overline{\mathbf{S}} = 2c_1\mathbf{I} + 2c_2(\mathrm{tr}(\overline{\mathbf{C}})\mathbf{I} - \overline{\mathbf{C}}), \quad J\overline{\boldsymbol{\sigma}} = 2c_1\overline{\mathbf{B}} + 2c_2(\mathrm{tr}(\overline{\mathbf{B}})\overline{\mathbf{B}} - \overline{\mathbf{B}}^2).$$

The elasticity tensors are computed as

$$\overline{\mathbb{C}} = 4c_2(\mathbf{I}\otimes\mathbf{I} - \mathbb{S}), \quad J\overline{\mathbb{C}} = 4c_2(\overline{\mathbf{B}}\otimes\overline{\mathbf{B}} - \overline{\mathbf{B}}\odot\overline{\mathbf{B}}).$$

Fiber, transversely isotropic model , see (3.53), (3.58) and (3.59), with a fiber direction $\mathbf{f}_0$. The considered isochoric strain-energy function is

$$\overline{\Psi}(\overline{\mathbf{C}}) = \frac{a_\mathrm{f}}{2b_\mathrm{f}}\left\{\exp\left[b_\mathrm{f}(\overline{I}_\mathrm{f}-1)^2\right]-1\right\}, \text{ with } \overline{I}_\mathrm{f} = \mathbf{f}_0\cdot\overline{\mathbf{C}}\mathbf{f}_0 = \overline{\mathbf{F}}\mathbf{f}_0\cdot\overline{\mathbf{F}}\mathbf{f}_0.$$

The stress tensors are computed as

$$\overline{\mathbf{S}} = 2a_\mathrm{f}(\overline{I}_\mathrm{f}-1)\exp\left[b_\mathrm{f}(\overline{I}_\mathrm{f}-1)^2\right]\mathbf{A}_0, \quad J\overline{\boldsymbol{\sigma}} = 2a_\mathrm{f}(\overline{I}_\mathrm{f}-1)\exp\left[b_\mathrm{f}(\overline{I}_\mathrm{f}-1)^2\right]\overline{\mathbf{A}},$$

with $\mathbf{A}_0 = \mathbf{f}_0\otimes\mathbf{f}_0$ and $\overline{\mathbf{A}} = \overline{\mathbf{F}}\mathbf{f}_0\otimes\overline{\mathbf{F}}\mathbf{f}_0$ and the elasticity tensors are computed as

$$\begin{aligned}\overline{\mathbb{C}} &= 4a_\mathrm{f}\exp\left[b_\mathrm{f}(\overline{I}_\mathrm{f}-1)^2\right](2b_\mathrm{f}(\overline{I}_\mathrm{f}-1)^2+1)\,\mathbf{A}_0\otimes\mathbf{A}_0,\\ J\overline{\mathbb{C}} &= 4a_\mathrm{f}\exp\left[b_\mathrm{f}(\overline{I}_\mathrm{f}-1)^2\right](2b_\mathrm{f}(\overline{I}_\mathrm{f}-1)^2+1)\,\overline{\mathbf{A}}\otimes\overline{\mathbf{A}}.\end{aligned}$$

Interaction, orthotropic model, (3.60) with a fiber direction $\mathbf{f}_0$ and a sheet direction $\mathbf{s}_0$. The considered isochoric strain-energy function is

$$\overline{\Psi}(\overline{\mathbf{C}}) = \frac{a_\mathrm{fs}}{2b_\mathrm{fs}}\left\{\exp\left[b_\mathrm{fs}\overline{I}_\mathrm{fs}^2\right]-1\right\},$$

with $\overline{I}_\mathrm{fs} = \mathbf{f}_0\cdot\overline{\mathbf{C}}\mathbf{s}_0$. Using $\mathbf{M}_0 = \frac{1}{2}(\mathbf{f}_0\otimes\mathbf{s}_0+\mathbf{s}_0\otimes\mathbf{f}_0)$ and $\overline{\mathbf{M}} = \frac{1}{2}(\overline{\mathbf{F}}\mathbf{f}_0\otimes\overline{\mathbf{F}}\mathbf{s}_0+\overline{\mathbf{F}}\mathbf{s}_0\otimes\overline{\mathbf{F}}\mathbf{f}_0)$ we have the representations

$$\overline{\mathbf{S}} = 2a_\mathrm{fs}\,\overline{I}_\mathrm{fs}\exp\left[b_\mathrm{fs}\overline{I}_\mathrm{fs}^2\right]\mathbf{M}_0, \quad J\overline{\boldsymbol{\sigma}} = 2a_\mathrm{fs}\,\overline{I}_\mathrm{fs}\exp\left[b_\mathrm{fs}\overline{I}_\mathrm{fs}^2\right]\overline{\mathbf{M}},$$

for the stress tensors and

$$\begin{aligned}\overline{\mathbb{C}} &= 4a_\mathrm{fs}\exp\left[b_\mathrm{fs}\overline{I}_\mathrm{fs}^2\right](2b_\mathrm{fs}\overline{I}_\mathrm{fs}^2+1)\,\mathbf{M}_0\otimes\mathbf{M}_0,\\ J\overline{\mathbb{C}} &= 4a_\mathrm{fs}\exp\left[b_\mathrm{fs}\overline{I}_\mathrm{fs}^2\right](2b_\mathrm{fs}\overline{I}_\mathrm{fs}^2+1)\,\overline{\mathbf{M}}\otimes\overline{\mathbf{M}},\end{aligned}$$

for the elasticity tensors.

4 VARIATIONAL FORMULATION

The variational formulation of the mixed boundary value problem as described in Section 3.4 is the basis for discretization techniques (Chapter 5) and in particular the finite element method (FEM), see Section 5.1. General principles of variational approaches as well as the specific weak formulation for elasticity problems are discussed in this chapter. In addition, solvability conditions for linear and nonlinear elasticity models as introduced in Chapter 3 are in the focus. For linear elasticity problems not only the existence but also the uniqueness of a solution can be proven. In contrast to this, it is not possible to give a similar statement for general nonlinear elasticity problems. Although there are conditions that give evidence about solvability, no cogent arguments are known that show uniqueness. For more information on this topic see the books by Braess [25], Ciarlet [38] and Dacorogna [43].

For nonlinear problems, as for instance the tissue models discussed in Section 3.11 and Section 3.12 Newton's method is applied. This requires a linearization of the underlying variational formulation, cf. Section 4.4.2. A comprehensive monograph on Newton methods is Deuflhard [49].

4.1 Preliminaries

In this section, we present basic definitions and theorems that allow us to set up the theory of variational formulations. Definitions and tools to discuss the solvability of an abstract operator equation $Au = f$ are given. Finally, we introduce concepts for derivatives in Banach spaces, which will be used for the linearization of the nonlinear weak formulations.

Let X be a Hilbert space with the scalar product $\langle \cdot, \cdot \rangle_X$ and the corresponding induced norm $\|\cdot\|_X = \sqrt{\langle \cdot, \cdot \rangle_X}$. We denote by X' the dual space of X with the duality product $\langle \cdot, \cdot \rangle$ and with the norm

$$\|f\|_{X'} = \sup_{0 \neq v \in X} \frac{|\langle f, v \rangle|}{\|v\|_X} \quad \text{for all } f \in X'.$$

In the linear case we want to find the solution $u \in X$ of the *linear operator equation*

$$Au = f \tag{4.1}$$

with $A : X \mapsto X'$ and $f \in X'$.

Equivalent to this operator equation is the *variational formulation* to find $u \in X$, such that

$$\langle Au, v\rangle = \langle f, v\rangle \quad \text{for all } v \in X. \tag{4.2}$$

One can easily show that a solution of the variational formulation (4.2) is as well a solution of the operator equation (4.1), and vice versa.

The *bilinear form*

$$a(\cdot,\cdot) : X \times X \mapsto \mathbb{R}$$

is induced by the operator $A : X \mapsto X'$ through

$$a(u, v) := \langle Au, v\rangle \quad \text{for all } u, v \in X.$$

Definition 4.1 (Boundedness)**.** *The operator $A : X \mapsto X'$ is called* bounded *if*

$$\|Av\|_{X'} \le c_2^A \|v\|_X \quad \textit{for all } v \in X$$

with a constant $c_2^A > 0$.

Definition 4.2 (X–ellipticity)**.** *The operator A is called X–*elliptic *if*

$$\langle Av, v\rangle \ge c_1^A \|v\|_X^2 \quad \textit{for all } v \in X$$

with a constant $c_1^A > 0$.

Definition 4.3 (Self-adjointness)**.** *The operator A is called* self-adjoint *if*

$$\langle Au, v\rangle = \langle Av, u\rangle \quad \textit{for all } u, v \in X.$$

Theorem 4.4 (Lax–Milgram theorem)**.** *Let the operator $A : X \mapsto X'$ be bounded and X–elliptic. Then the operator equation $Au = f$ is uniquely solvable for every $f \in X'$. For the solution $u \in X$ it holds*

$$\|u\|_X \le \frac{1}{c_1^A} \|f\|_{X'}.$$

Proof. See, for example, Steinbach [176] or Yosida [190]. □

Proposition 4.5 (Poincaré–Friedrich's inequality)**.** *Let Ω be a subset of a cube in $\mathbb{R}^3$ with edge length c_F. Then*

$$\|v\|_{L_2(\Omega)} \le c_F |v|_{H^1(\Omega)} \quad \textit{for all } v \in H_0^1(\Omega) := \left\{ v \in H^1(\Omega) : v = 0 \text{ on } \partial\Omega \right\}.$$

Proof. Cf. Braess [25]. □

From Proposition 4.5 it follows immediately that

$$\|\mathbf{v}\|^2_{[H^1(\Omega)]^3} \leq (1+c_F^2)|\mathbf{v}|^2_{[H^1(\Omega)]^3}\ , \quad \text{for all } \mathbf{v} \in [H_0^1(\Omega)]^3. \tag{4.3}$$

In the nonlinear case, we write in analogy to (4.1) the *nonlinear operator equation*

$$A(u) = f$$

with the equivalent variational formulation

$$\langle A(u), v\rangle = \langle f, v\rangle \quad \text{for all } v \in X.$$

For the linearization of the nonlinear variational formulation and the discussion of existence theorems, we need the following two definitions of derivatives in Banach spaces:

Definition 4.6 (Fréchet derivative)**.** *Let X and Y be Banach spaces and G be an open subset of X. A function $f : G \subset X \mapsto Y$ is called differentiable at $\xi \in G$, if there is a bounded linear operator $\Lambda : X \mapsto Y$, such that for all $h \in X$*

$$f(\xi+h) - f(\xi) = \Lambda h + r(h) \quad \textit{with} \quad \lim_{h\to 0} \frac{r(h)}{\|h\|_X} = 0.$$

If the limit exists, then the uniquely defined operator Λ is called the Fréchet derivative of f at ξ and we denote it as $f'(\xi)$; e.g., cf. Heuser [75].

Definition 4.7 (Gâteaux derivative)**.** *Let X and Y be Banach spaces and G be an open subset of X. A function $f : X \mapsto Y$ is called differentiable at $\xi \in G$ in the direction $h \in X$, if there is a bounded and linear operator $\Lambda : X \mapsto Y$, such that*

$$\Lambda = \lim_{t\to 0} \frac{f(\xi+th) - f(\xi)}{t}$$

If the limit exists for every $h \in X$, then the operator Λ is called the Gâteaux derivative of f at ξ, and we denote it as $\Lambda = Df(\xi).h = f'_G(\xi)$; e.g., cf. Tröltzsch [179].

Remark 4.1.1. *Every Fréchet differentiable function is Gâteaux differentiable and it holds*

$$f'(\xi) = f'_G(\xi).$$

With this we can calculate the particular Fréchet derivative using the definition of the Gâteaux derivative; e.g., cf. Tröltzsch [179].

Remark 4.1.2 (Chain rule)**.** *Let X,Y and Z be Banach spaces and $f : X \mapsto Y$ and $g : V \mapsto Z$ be Fréchet differentiable at ξ and $f(\xi)$, respectively, then*

$$e(\xi) = g(f(\xi))$$

is also Fréchet differentiable at ξ and

$$e'(\xi) = g'(f(\xi)) \circ f'(\xi);$$

e.g. cf. Ioffe and Tihomirov [96].

Lemma 4.8 (Frobenius matrix norm)**.** *Let $\mathbf{A}, \mathbf{B} \in \mathbb{R}^{3\times 3}$. Then*

$$\langle \mathbf{A}, \mathbf{B} \rangle_{\mathrm{F}} := \operatorname{tr}(\mathbf{A}\mathbf{B}^{\top})$$

defines a scalar product on $\mathbb{R}^{3\times 3}$ with the induced Frobenius matrix norm

$$\|\mathbf{A}\|_{\mathrm{F}} = \langle \mathbf{A}, \mathbf{A} \rangle_{\mathrm{F}}.$$

In the following sections, we consider the domain in the current configuration $\Omega_t \subset \mathbb{R}^3$ and the domain in the reference configuration $\Omega_0 \subset \mathbb{R}^3$ to be open and bounded domains with Lipschitz-continuous boundaries $\partial\Omega_t = \Gamma_t$ and $\partial\Omega_0 = \Gamma_0$, respectively.

4.2 Variational Formulation for Elasticity Problems

First, we consider the classical formulation of the boundary value problem (3.16): given sufficiently smooth and continuous input data, find the displacement $\mathbf{u}$ such that

$$-\operatorname{div} \boldsymbol{\sigma}(\mathbf{u}, \mathbf{x}) = \mathbf{0} \quad \text{in } \Omega_t,$$

with the Dirichlet boundary conditions

$$\mathbf{u}(\mathbf{x}) = \mathbf{u}_{\mathrm{D}}(\mathbf{x}) \quad \text{on } \Gamma_{t,\mathrm{D}},$$

and with the Neumann boundary conditions

$$\boldsymbol{\sigma}(\mathbf{u}, \mathbf{x})\mathbf{n}(\mathbf{x}) = \mathbf{t}_{\mathrm{N}}(\mathbf{x}) \quad \text{on } \Gamma_{t,\mathrm{N}}.$$

Let $\mathbf{u}$ be from some suitable space X with $\mathbf{u} = \mathbf{u}_{\mathrm{D}}$ on $\Gamma_{t,\mathrm{D}}$. Integration over Ω_t and multiplying component-wise with a test-function $\mathbf{v} \in X$ with $\mathbf{v} = \mathbf{0}$ on the Dirichlet boundary $\Gamma_{t,\mathrm{D}}$ leads to

$$\int_{\Omega_t} -\operatorname{div} \boldsymbol{\sigma}(\mathbf{u}, \mathbf{x}) \cdot \mathbf{v}(\mathbf{x}) \, \mathrm{d}\mathbf{x} = 0. \tag{4.4}$$

By using the identity, implied by the product rule,

$$\operatorname{div} \boldsymbol{\sigma} \cdot \mathbf{v} = \operatorname{div}(\boldsymbol{\sigma}\mathbf{v}) - \boldsymbol{\sigma} : \operatorname{grad} \mathbf{v},$$

and the following formulation of the Gauss' divergence theorem

$$\int_{\Omega_t} \operatorname{div}(\boldsymbol{\sigma}\mathbf{v})\,\mathrm{d}\mathbf{x} = \int_{\Gamma_t} \mathbf{v}\cdot\boldsymbol{\sigma}\mathbf{n}\,\mathrm{d}s_{\mathbf{x}},$$

equation (4.4) may be written as

$$\int_{\Omega_t} \boldsymbol{\sigma}(\mathbf{u},\mathbf{x}) : \operatorname{grad}\mathbf{v}(\mathbf{x})\,\mathrm{d}\mathbf{x} - \int_{\Gamma_t} \mathbf{v}(\mathbf{x})\cdot\boldsymbol{\sigma}\mathbf{n}(\mathbf{x})\,\mathrm{d}s_{\mathbf{x}} = 0.$$

The symmetry of $\boldsymbol{\sigma}$ implies that

$$\boldsymbol{\sigma} : \operatorname{grad}\mathbf{v} = \boldsymbol{\sigma} : \frac{1}{2}\left(\operatorname{grad}\mathbf{v} + (\operatorname{grad}\mathbf{v})^{\top}\right) = \boldsymbol{\sigma} : \boldsymbol{\varepsilon}(\mathbf{v}).$$

With this and the fact that $\mathbf{v}$ vanishes on the part $\Gamma_{t,\mathrm{D}}$ of the boundary we may formulate the *weak form* of the *boundary-value problem* as

$$\int_{\Omega_t} \boldsymbol{\sigma}(\mathbf{u},\mathbf{x}) : \boldsymbol{\varepsilon}(\mathbf{v},\mathbf{x})\,\mathrm{d}\mathbf{x} - \int_{\Gamma_{t,\mathrm{N}}} \mathbf{t}_{\mathrm{N}}(\mathbf{x})\cdot\mathbf{v}(\mathbf{x})\,\mathrm{d}s_{\mathbf{x}} = 0.$$

Hence, the boundary value problem (3.16) is formally equivalent to the variational equations

$$\langle A_t(\mathbf{u}),\mathbf{v}\rangle_{\Omega_t} := \int_{\Omega_t} \boldsymbol{\sigma}(\mathbf{u},\mathbf{x}) : \boldsymbol{\varepsilon}(\mathbf{v},\mathbf{x})\,\mathrm{d}\mathbf{x} = \int_{\Gamma_{t,\mathrm{N}}} \mathbf{t}_{\mathrm{N}}(\mathbf{x})\cdot\mathbf{v}(\mathbf{x})\,\mathrm{d}s_{\mathbf{x}} =: \langle\mathcal{F},\mathbf{v}\rangle_{\Omega_t}, \tag{4.5}$$

valid for a smooth enough tensor field $\boldsymbol{\sigma}(\mathbf{u}) : \overline{\Omega}_t \mapsto \mathbb{R}^{3\times 3}$ and all smooth enough vector fields $\mathbf{v} : \overline{\Omega}_t \mapsto \mathbb{R}^3$, which vanish on $\Gamma_{t,\mathrm{D}}$, see, e.g., [38, Theorem 2.4-1] and [15].

In terms of the reference configuration, the boundary value problem (3.17) is formally equivalent to the variational equations

$$\langle A_0(\mathbf{U}),\mathbf{V}\rangle_{\Omega_0} := \int_{\Omega_0} (\mathbf{FS})(\mathbf{U},\mathbf{X}) : \operatorname{Grad}\mathbf{V}(\mathbf{X})\,\mathrm{d}\mathbf{X} = \int_{\Gamma_{0,\mathrm{N}}} \mathbf{t}_{\mathrm{N}}(\mathbf{X})\cdot\mathbf{V}(\mathbf{X})\,\mathrm{d}S_{\mathbf{X}} =: \langle\mathcal{F}_0,\mathbf{V}\rangle_{\Omega_0}, \tag{4.6}$$

valid for a smooth enough tensor field $\mathbf{S}(\mathbf{U}) : \overline{\Omega}_0 \mapsto \mathbb{R}^{3\times 3}$ and all smooth enough vector fields $\mathbf{V} : \overline{\Omega}_0 \mapsto \mathbb{R}^3$ with $\mathbf{V} = \mathbf{0}$ on $\Gamma_{0,\mathrm{D}}$, see, e.g., [38, Theorem 2.6-1]. Note that the tensor $\mathbf{FS}$ is not necessarily symmetric.

The variational formulation (4.6) can be rewritten using the directional derivative of

the Green-Lagrange strain tensor $\mathbf{E}$

$$\boldsymbol{\Sigma}(\mathbf{U},\mathbf{V}) := \frac{1}{2}\left(\operatorname{Grad}^\top \mathbf{V}\mathbf{F}(\mathbf{U}) + \mathbf{F}^\top(\mathbf{U})\operatorname{Grad}\mathbf{V}\right) = \operatorname{sym}\left(\mathbf{F}^\top(\mathbf{U})\operatorname{Grad}\mathbf{V}\right) \tag{4.7}$$

as

$$\langle A_0(\mathbf{U}),\mathbf{V}\rangle_{\Omega_0} = \int_{\Omega_0} \mathbf{S}(\mathbf{U},\mathbf{X}) : \boldsymbol{\Sigma}(\mathbf{U},\mathbf{V})\,\mathrm{d}\mathbf{X} = \langle \mathcal{F}_0,\mathbf{V}\rangle_{\Omega_0}. \tag{4.8}$$

Remark 4.2.1. *The weak forms of the right hand sides for pressure loads, see* (3.18) *and* (3.19)*, are computed by*

$$\langle \mathcal{F}(\mathbf{u}),\mathbf{v}\rangle_{\Omega_t} = -\int_{\Gamma_{t,\mathrm{N}}} \mathcal{p}\mathbf{n}(\mathbf{x})\cdot\mathbf{v}(\mathbf{x})\,\mathrm{d}s_{\mathbf{x}},$$
$$\langle \mathcal{F}_0(\mathbf{U}),\mathbf{V}\rangle_{\Omega_0} = -\int_{\Gamma_{0,\mathrm{N}}} \mathcal{p}J\mathbf{F}^{-\top}(\mathbf{U})\mathbf{N}(\mathbf{X})\cdot\mathbf{V}(\mathbf{X})\,\mathrm{d}S_{\mathbf{X}}.$$

Remark 4.2.2. *For a Neumann boundary value problem, i.e.* $\Gamma = \Gamma_\mathrm{N}$*, we assume the following condition of solvability*

$$\int_\Omega \mathbf{r}_k(\mathbf{x})^\top \mathbf{f}(\mathbf{x})\,\mathrm{d}\mathbf{x} + \int_\Gamma \mathbf{r}_k(\mathbf{x})^\top \mathbf{t}_\mathrm{N}(\mathbf{x})\,\mathrm{d}s_{\mathbf{x}} = 0 \quad \textit{for all } \mathbf{r}_k \in \mathcal{R}, \tag{4.9}$$

where $\mathbf{r}_k \in \mathcal{R}$ *are the rigid body modes. In 3D we have*

$$\mathcal{R} = \operatorname{span}\left\{ \begin{pmatrix}1\\0\\0\end{pmatrix}, \begin{pmatrix}0\\1\\0\end{pmatrix}, \begin{pmatrix}0\\0\\1\end{pmatrix}, \begin{pmatrix}-x_2\\x_1\\0\end{pmatrix}, \begin{pmatrix}0\\-x_3\\x_2\end{pmatrix}, \begin{pmatrix}x_3\\0\\-x_1\end{pmatrix} \right\},$$

which describe rotations and translations of a rigid body.

4.3 Linear Elasticity

As mentioned before in Section 3.5, in the case of linear elasticity it is justified not to distinguish between the current and the reference configuration, since we are only considering small deformations. With Hooke's Law (3.21)

$$\boldsymbol{\sigma} = \mathbb{C} : \boldsymbol{\varepsilon}, \quad \sigma_{ij} = \sum_{kl} C_{ijkl}\varepsilon_{kl}, \quad C_{ijkl} = \lambda\delta_{ij}\delta_{kl} + \mu(\delta_{ik}\delta_{jl} + \delta_{il}\delta_{jk}),$$

we get the specific variational formulation for linear elasticity, see, e.g. [38, Chapter 6]: find $\mathbf{u} \in [H^1(\Omega)]^3$, $\mathbf{u} = \mathbf{u}_\mathrm{D}$ on Γ_D such that

$$\int_\Omega \boldsymbol{\varepsilon}(\mathbf{u},\mathbf{x}) : \mathbb{C} : \boldsymbol{\varepsilon}(\mathbf{v},\mathbf{x})\,\mathrm{d}\mathbf{x} - \int_{\Gamma_\mathrm{N}} \mathbf{t}_\mathrm{N}(\mathbf{x}) \cdot \mathbf{v}(\mathbf{x})\,\mathrm{d}s_\mathbf{x} = 0 \tag{4.10}$$

holds for all $\mathbf{v} \in [H^1_0(\Omega,\Gamma_\mathrm{D})]^3$. We write for the bilinear form

$$a(\mathbf{u},\mathbf{v}) = \int_\Omega \sum_{i,j,k,l=1}^{3} C_{ijkl}\,\varepsilon_{kl}(\mathbf{u},\mathbf{x})\varepsilon_{ij}(\mathbf{v},\mathbf{x})\,\mathrm{d}\mathbf{x} = \int_\Omega \mathcal{C}\,\boldsymbol{\varepsilon}(\mathbf{u},\mathbf{x}) : \boldsymbol{\varepsilon}(\mathbf{v},\mathbf{x})\,\mathrm{d}\mathbf{x}, \tag{4.11}$$

with $\mathcal{C}$ the constant elasticity tensor in Voigt notation.

To satisfy the conditions in the Lax–Milgram theorem 4.4 we need the famous Korn inequalities which were first formulated and named after Arthur Korn [112].

Lemma 4.9 (First Korn inequality)**.** *For* $\mathbf{v} \in [H^1_0(\Omega,\Gamma_\mathrm{D})]^3$

$$\int_\Omega \sum_{i,j=1}^{3} [\varepsilon_{ij}(\mathbf{v},\mathbf{x})]^2\,\mathrm{d}\mathbf{x} \geq \frac{1}{2}|\mathbf{v}|^2_{[H^1(\Omega)]^3}.$$

Lemma 4.10 (Second Korn Inequality)**.** *There exists a constant* $c = c(\Omega) > 0$ *such that*

$$\int_\Omega \sum_{i,j=1}^{3} [\varepsilon_{ij}(\mathbf{v},\mathbf{x})]^2\,\mathrm{d}\mathbf{x} + \|\mathbf{v}\|^2_{[L_2(\Omega)]^3} \geq c\|\mathbf{v}\|^2_{[H^1(\Omega)]^3}, \quad \textit{for all } \mathbf{v} \in [H^1(\Omega)]^3.$$

Proof. For proofs of these inequalities compare Hlaváček and Nečas [76, 77], Nitsche [135], and Steinbach [176]. □

To fulfill the conditions of Theorem 4.4 (Lax–Milgram) the boundedness of the bilinear form (4.11) has to be shown. This is done via the following lemma:

Lemma 4.11 (Boundedness of the bilinear form)**.** *For all* $\mathbf{u},\mathbf{v} \in [H^1(\Omega)]^3$ *it holds*

$$|a(\mathbf{u},\mathbf{v})| \leq \lambda_{max}(\mathcal{C})\,|\mathbf{u}|_{[H^1(\Omega)]^3}|\mathbf{v}|_{[H^1(\Omega)]^3}.$$

Proof. See, for example, Steinbach [176]. □

To show $[H^1_0(\Omega,\Gamma_{\mathrm{D}})]^3$–ellipticity of the bilinear form (4.11) in the case that $\Gamma = \Gamma_{\mathrm{D}}$ the first Korn inequality (Lemma 4.9) is used. For all $\mathbf{v} \in [H^1_0(\Omega,\Gamma_{\mathrm{D}})]^3$ it holds

$$\begin{aligned} a(\mathbf{v},\mathbf{v}) &= \int_\Omega \mathcal{C}\,\varepsilon(\mathbf{v}.\mathbf{x}) : \varepsilon(\mathbf{v},\mathbf{x})\,\mathrm{d}\mathbf{x} \geq \lambda_{\min}(\mathcal{C}) \int_\Omega \sum_{i,j=1}^{3} [\varepsilon_{ij}(\mathbf{v},\mathbf{x})]^2\,\mathrm{d}\mathbf{x} \\ &\geq \lambda_{\min}(\mathcal{C})\frac{1}{2}|\mathbf{v}|^2_{[H^1(\Omega)]^3} \geq \lambda_{\min}(\mathcal{C})\frac{1}{2(1+c_F^2)}\|\mathbf{v}\|^2_{[H^1(\Omega)]^3}, \end{aligned}$$

where c_F denotes the constant from the Poincaré–Friedrich's inequality (4.3).

$[H^1_0(\Omega,\Gamma_{\mathrm{D}})]^3$–ellipticity for the mixed boundary value problem is proven using the second Korn inequality (Lemma 4.10), cf. Steinbach [176].

We have shown boundedness and $[H^1_0(\Omega)]^3$–ellipticity for the Dirichlet and the mixed boundary value problem. With Theorem 4.4 the unique solvability of the linear elasticity problem follows.

For the Neumann boundary value problem with $\Gamma = \Gamma_{\mathrm{N}}$ we assume the solvability conditions (4.9) and note that the solution is only unique up to the rigid body modes. These can be fixed using suitable scaling conditions. With the space

$$[H^1_*(\Omega)]^3 := \left\{ \mathbf{v} \in [H^1(\Omega)]^3 : \int_\Omega \mathbf{r}_k(\mathbf{x})^\top \mathbf{v}(\mathbf{x})\,\mathrm{d}x = 0 \text{ for all } \mathbf{r}_k \in \mathcal{R} \right\}$$

we can show $[H^1_*(\Omega)]^3$–ellipticity and hence unique solvability in $[H^1_*(\Omega)]^3$, see, e.g., Steinbach [176].

4.3.1 Almost Incompressible Linear Materials

For almost incompressible materials it can happen that so-called *locking effects* occur. This means that the problem becomes very ill-conditioned and the calculated displacement field $\mathbf{u}$ is smaller than expected. For a more detailed exposition of locking effects the reader is referred to the works of Arnold [5], Babuška and Suri [11] and Braess [25, Chapter VI, § 4]. How to overcome these numerical difficulties is discussed in this section.

Without any loss of generality we can focus on homogeneous boundary conditions $\mathbf{u}_\mathrm{D} = \mathbf{0}$. Furthermore, we introduce the spaces

$$\mathcal{X} := [H_0^1(\Omega, \Gamma_\mathrm{D})]^3, \quad \mathcal{M} := L_2(\Omega). \tag{4.12}$$

A possibility to prevent locking phenomena and to receive a better conditioned problem for almost incompressible linear elastic materials is a saddle point formulation of the boundary value problem. This yields a variational formulation that is similar to a Stokes problem. The main idea is to bring in a pressure term p which serves as a Lagrangian multiplier. A drawback of this method will be an increased number of degrees of freedom in the numerical simulation.

We start from the variational formulation for linear elasticity problems (4.10), which can be written, using the Lamé coefficients (3.22), as

$$2\mu \int_\Omega \boldsymbol{\varepsilon}(\mathbf{u}) : \boldsymbol{\varepsilon}(\mathbf{v}) \,\mathrm{d}\mathbf{x} + \lambda \int_\Omega \operatorname{div}(\mathbf{u}) \operatorname{div}(\mathbf{v}) \,\mathrm{d}\mathbf{x} - \int_{\Gamma_\mathrm{N}} \mathbf{t}_\mathrm{N}(\mathbf{x}) \cdot \mathbf{v}(\mathbf{x}) \,\mathrm{d}s_\mathbf{x} = 0. \tag{4.13}$$

We introduce the penalty variable p as

$$p = \lambda \operatorname{div} \mathbf{u}. \tag{4.14}$$

Note that for the (academic) case of an incompressible material λ goes to infinity.

From (4.13) and the weak form of (4.14), we get the following saddle point problem: find $(\mathbf{u}, p) \in \mathcal{X} \times \mathcal{M}$, such that

$$\begin{aligned} a_0(\mathbf{u}, \mathbf{v}) \; + \quad & b(\mathbf{v}, p) = \langle \mathcal{F}, \mathbf{v} \rangle, \\ b(\mathbf{u}, q) \; - \; \lambda^{-1} \; & c(p, q) = 0, \end{aligned} \tag{4.15}$$

for all test functions $v \in \mathcal{X}$ and $q \in \mathcal{M}$ and

$$\begin{aligned} a_0(\mathbf{u}, \mathbf{v}) &= \int_\Omega 2\mu \boldsymbol{\varepsilon}(\mathbf{u}, \mathbf{x}) : \boldsymbol{\varepsilon}(\mathbf{v}, \mathbf{x}) \,\mathrm{d}x, \\ b(\mathbf{v}, q) &= \int_\Omega q \operatorname{div} \mathbf{v} \,\mathrm{d}\mathbf{x} = -\int_\Omega \mathbf{v} \cdot \operatorname{grad} q \,\mathrm{d}\mathbf{x}, \\ c(p, q) &= \int_\Omega pq \,\mathrm{d}\mathbf{x} \end{aligned}$$

The right-hand-side for elastostatics reads, disregarding body forces,

$$\langle \mathcal{F}, \mathbf{v} \rangle = \int_{\Gamma_\mathrm{N}} \mathbf{t}_\mathrm{N}(\mathbf{x}) \cdot \mathbf{v}(\mathbf{x}) \,\mathrm{d}s_\mathbf{x}.$$

For the limiting case $\lambda \to \infty$, i.e. for the rather academic incompressible linear elastic material, we obtain: find $(\mathbf{u}, p) \in \mathcal{X} \times \mathcal{M}$ such that

$$\begin{aligned} a_0(\mathbf{u}, \mathbf{v}) \; + \; b(\mathbf{v}, p) &= \langle \mathcal{F}, \mathbf{v} \rangle, \\ b(\mathbf{u}, q) \qquad\qquad &= 0, \end{aligned} \tag{4.16}$$

for all test functions $(\mathbf{v}, q) \in \mathcal{X} \times \mathcal{M}$ and with the definitions from above.

Remark 4.3.1. *The saddle point problems* (4.15) *and* (4.16) *are uniquely solvable, e.g., cf. [25, Chapter 6, §4].*

Remark 4.3.2. *For the case of a pure Dirichlet problem, i.e.* $\Gamma = \Gamma_{\mathrm{D}}$*, we replace the ansatz space for the pressure* p*,* $\mathcal{M} = L_2(\Omega)$ *in* (4.12)*, by* $L_2(\Omega)/\mathbb{R}$*. This issue is also known for the Stokes problem, e.g., cf. [25, Chapter 3].*

4.4 Nonlinear Elasticity

In this section, we derive a variational formulation for nonlinear elasticity models. We present a Newton method suitable for the linearization of the considered problem and show the linearization procedure for an arbitrary elastic material that is modeled using a stress in the form (3.23). Here, we follow the descriptions of Holzapfel in [80, Section 8.4] and [81]. As proposed in these works we will perform the linearization in the reference configuration, since there we can interchange differentiation and integration. To get a linearized version of the constitutive equation in the current configuration we use tools that can be found in Section 3.1. We will also present the mean dilatation method that is used to treat nearly incompressible nonlinear materials. In the last part of this section we discuss existence theorems for nonlinear elasticity problems, following the results of Ball in the late 1970s [13, 14].

4.4.1 Newton's Method

To obtain solutions of a nonlinear boundary value problem, iterative solution techniques of Newton type are often applied. This leads to a sequence of linearized problems. A great compendium on Newton's method is the book of Deuflhard [49]. We start with the nonlinear operator equation

$$F(x) = 0,$$

where $F : D \subset X \mapsto Y$ for the Banach spaces X and Y. Given a starting guess x_0 for the unknown solution x^*, we obtain, using the technique of successive linearization, the general Newton method

$$F'(x^k)\Delta x^k = -F(x^k),\ x^{k+1} = x^k + \Delta x^k,\ k = 0, 1, \dots \tag{4.17}$$

Here, F' is a derivative defined in Banach spaces, i.e. the Fréchet (Definition 4.6) or the Gâteaux derivative (Definition 4.7). For the convergence analysis we give the fundamental Newton–Kantorovich theorem.

Theorem 4.12. *Let X and Y be Banach spaces and $D \subset X$ open and convex. Let $F : D \mapsto Y$ be a continuously Fréchet differentiable operator and let $x^0 \in D$ be a starting point such that $F'(x^0)$ is invertible. Given that*

$$\|F'(x^0)^{-1}F(x^0)\| \leq \alpha \text{ and } \|F'(x^0)^{-1}(F'(y) - F'(\mathbf{x}))\| \leq \overline{\omega}_0\|y - x\|,$$

the sequence $\{x^k\}$, obtained from Newton's method (4.17) is well-defined and converges to a x^* with $F(x^*) = 0$. The convergence is quadratic for $h_0 := \alpha\overline{\omega}_0 < \frac{1}{2}$ and the sequence $\{x^k\}$ stays in the sphere $S(x^0, (1 - \sqrt{1 - 2h_0})/\overline{\omega}_0) \subset D$.

Proof. Cf. Deuflhard [49] and the classical work of Kantorovich [101]. □

For more information on convergence of the Newton method in Banach spaces, see [49, Section 2.1]. Later we will discuss *inexact Newton methods* for discretized problems, see Section 5.2.

4.4.2 Linearization of the Standard Variational Formulation

In this section, we linearize the variational formulation (4.6). As mentioned before, this is done in the reference configuration since there the integration domain Ω_0 is not dependent on the deformation $\mathbf{U}$ and hence we can interchange differentiation and integration. At first, the loads are considered as independent of the deformation of the continuum body. Thus, the linearization only affects the term

$$\langle A_0(\mathbf{U}), \mathbf{V}\rangle_{\Omega_0} := \int_{\Omega_0} (\mathbf{FS})(\mathbf{U}) : \mathrm{Grad}(\mathbf{V})\,\mathrm{d}\mathbf{X}.$$

Hence, to apply Newton's method (4.17), we use the scheme

$$\langle \Delta\mathbf{U}, A_0'(\mathbf{U}^k)\mathbf{V}\rangle_{\Omega_0} = \langle \mathcal{F}_0, \mathbf{V}\rangle_{\Omega_0} - \langle A_0(\mathbf{U}^k), \mathbf{V}\rangle_{\Omega_0}, \quad \mathbf{U}^{k+1} = \mathbf{U}^k + \Delta\mathbf{U},\ k = 0, 1, \ldots.$$

with the Fréchet derivative $A_0'(\mathbf{U}^k)$. To simplify matters, we make use of Remark 4.1.1 and compute $A_0'(\mathbf{U}^k)$ as the Gâteaux derivative in direction of the increment $\Delta\mathbf{U}$. For better readability we omit the dependencies on the deformation $\mathbf{U}^k$ and denote by $(\bullet)' := D(\bullet).\Delta\mathbf{U}$ the Gâteaux derivatives. By interchanging differentiation and integration we obtain

$$\begin{aligned}\langle \Delta\mathbf{U}, A_0'(\mathbf{U}^k)\mathbf{V}\rangle_{\Omega_0} &= \int_{\Omega_0} (\mathbf{FS})' : \mathrm{Grad}\,\mathbf{V}\,\mathrm{d}\mathbf{X} \\ &= \int_{\Omega_0} (\mathbf{F})'\mathbf{S} : \mathrm{Grad}\,\mathbf{V}\,\mathrm{d}\mathbf{X} + \int_{\Omega_0} \mathbf{F}(\mathbf{S})' : \mathrm{Grad}\,\mathbf{V}\,\mathrm{d}\mathbf{X}.\end{aligned}$$

Using the chain rule we may write for the Gâteaux derivative of the stress tensor $\mathbf{S}$

$$(\mathbf{S})' = \frac{\partial \mathbf{S}}{\partial \mathbf{C}} : (\mathbf{C})' = 2\frac{\partial \mathbf{S}}{\partial \mathbf{C}} : \frac{1}{2}(\mathbf{C})' = \mathbb{C} : \frac{1}{2}(\mathbf{C})',$$

with $\mathbb{C}$ the elasticity tensor in the reference configuration and the tensor product (A.5). For the Gâteaux derivative of the deformation gradient $\mathbf{F}$ we obtain with

definitions (4.7) and (3.2)

$$D\mathbf{F}(\mathbf{U}).\Delta\mathbf{U} = \lim_{\tau\to\infty} \frac{\mathbf{I} + \operatorname{Grad}(\mathbf{U}+\tau\Delta\mathbf{U}) - \mathbf{I} - \operatorname{Grad}(\mathbf{U})}{\tau}.$$

Due to the linearity of the gradient we get

$$D\mathbf{F}(\mathbf{U}).\Delta\mathbf{U} = \lim_{\tau\to\infty} \frac{\tau \operatorname{Grad}(\Delta\mathbf{U})}{\tau} = \operatorname{Grad}(\Delta\mathbf{U}). \tag{4.18}$$

For the Gâteaux derivative of the left Cauchy–Green tensor it holds

$$\mathbf{C}' = (\mathbf{F}^\top\mathbf{F})' = (\mathbf{F}^\top)'\mathbf{F} + \mathbf{F}^\top\mathbf{F}' = (\operatorname{Grad}\Delta\mathbf{U})^\top\mathbf{F} + \mathbf{F}^\top\operatorname{Grad}\Delta\mathbf{U} = 2\boldsymbol{\Sigma}(\mathbf{U},\Delta\mathbf{U}), \tag{4.19}$$

where $\boldsymbol{\Sigma}$ was defined in (4.7).

Hence, the tangent is calculated by

$$\begin{aligned}\langle\Delta\mathbf{U}, A_0'(\mathbf{U}^k)\mathbf{V}\rangle_{\Omega_0} &= \int_{\Omega_0} \mathbf{S}(\mathbf{U}^k) : \boldsymbol{\Sigma}(\Delta\mathbf{U},\mathbf{V})\,\mathrm{d}\mathbf{X} \\ &\quad + \int_{\Omega_0} \boldsymbol{\Sigma}(\mathbf{U}^k,\Delta\mathbf{U}) : \mathbb{C}(\mathbf{U}^k) : \boldsymbol{\Sigma}(\mathbf{U}^k,\mathbf{V})\,\mathrm{d}\mathbf{X}. \\ &= \int_{\Omega_0} \operatorname{Grad}(\Delta\mathbf{U})\,\mathbf{S}(\mathbf{U}^k) : \operatorname{Grad}\mathbf{V}\,\mathrm{d}\mathbf{X} \\ &\quad + \int_{\Omega_0} \mathbf{F}^\top(\mathbf{U}^k)\operatorname{Grad}(\Delta\mathbf{U}) : \mathbb{C}(\mathbf{U}^k) : \mathbf{F}^\top(\mathbf{U}^k)\operatorname{Grad}\mathbf{V}\,\mathrm{d}\mathbf{X},\end{aligned} \tag{4.20}$$

using (A.13) and symmetry properties of $\mathbb{C}$, see Remark 3.8.1.

We define the bilinear and the linear form

$$a_0'(\Delta\mathbf{U},\mathbf{V}) := \langle\Delta\mathbf{U}, A_0'(\mathbf{U}^k)\,\mathbf{V}\rangle_{\Omega_0}, \quad \langle\mathcal{R}_0,\mathbf{V}\rangle := \langle\mathcal{F}_0,\mathbf{V}\rangle_{\Omega_0} - \langle A_0(\mathbf{U}^k),\mathbf{V}\rangle_{\Omega_0}. \tag{4.21}$$

In each Newton step we have to solve the linearized system:
find $\Delta\mathbf{U} \in [H_0^1(\Omega_0,\Gamma_{0,\mathrm{D}})]^3$ such that

$$a_0'(\Delta\mathbf{U},\mathbf{V}) = \langle\mathcal{R}_0,\mathbf{V}\rangle \tag{4.22}$$

holds for all $\mathbf{V} \in [H_0^1(\Omega_0,\Gamma_{0,\mathrm{D}})]^3$.

To gain the formulation of the tangent in spatial quantities we use the properties

$$\mathrm{d}\mathbf{x} = J\,\mathrm{d}X, \quad \operatorname{Grad}(\bullet) = \operatorname{grad}(\bullet)\,\mathbf{F} \tag{4.23}$$

and the identity of all appearing vector valued variables in current and reference configuration, as mentioned in Section 3.1. So we get for the first part of (4.20)

$$\begin{aligned}\int_{\Omega_0} \operatorname{Grad}(\Delta\mathbf{U})\,\mathbf{S}(\mathbf{U}^k) : \operatorname{Grad}\mathbf{V}\,\mathrm{d}\mathbf{X} &= \int_{\Omega_t} \operatorname{grad}(\Delta\mathbf{u})\,\mathbf{F}\,\mathbf{S}(\mathbf{u}^k) : \operatorname{grad}(\mathbf{v})\,\mathbf{F}J^{-1}\,\mathrm{d}\mathbf{x} \\ &= \int_{\Omega_t} \operatorname{grad}(\Delta\mathbf{u})\,(J^{-1}\mathbf{F}\mathbf{S}\mathbf{F}^\top)(\mathbf{u}^k) : \operatorname{grad}\mathbf{v}\,\mathrm{d}\mathbf{x} \\ &= \int_{\Omega_t} \operatorname{grad}(\Delta\mathbf{u})\,\boldsymbol{\sigma}(\mathbf{u}^k) : \operatorname{grad}\mathbf{v}\,\mathrm{d}\mathbf{x}.\end{aligned}$$

The second part yields

$$\int_{\Omega_0} \mathbf{F}^\top \operatorname{Grad}(\Delta\mathbf{U}) : \mathbb{C}(\mathbf{U}^k) : \mathbf{F}^\top \operatorname{Grad}\mathbf{V}\,\mathrm{d}\mathbf{X} = \int_{\Omega_t} \operatorname{grad}(\Delta\mathbf{u}) : \mathbb{c}(\mathbf{u}^k) : \operatorname{grad}\mathbf{v}\,\mathrm{d}\mathbf{x}.$$

Here, we use the definition of the forth-order spatial elasticity tensor $\mathbb{c}$, see Definition 3.14, and its major and minor symmetry properties, see Remark 3.8.1.

In total, the tangent in current configuration is

$$\langle \Delta\mathbf{u}, A'(\mathbf{u}^k)\,\mathbf{v}\rangle_{\Omega_t} = \int_{\Omega_t} \operatorname{grad}(\Delta\mathbf{u})\,\boldsymbol{\sigma}(\mathbf{u}^k) : \operatorname{grad}\mathbf{v}\,\mathrm{d}\mathbf{x} + \int_{\Omega_t} \operatorname{grad}(\Delta\mathbf{u}) : \mathbb{c}(\mathbf{u}^k) : \operatorname{grad}\mathbf{v}\,\mathrm{d}\mathbf{x}.$$

Due to the symmetry properties of $\mathbb{c}$ this is equivalent to

$$\langle \Delta\mathbf{u}, A'(\mathbf{u}^k)\,\mathbf{v}\rangle_{\Omega_t} = \int_{\Omega_t} \operatorname{grad}(\Delta\mathbf{u})\,\boldsymbol{\sigma}(\mathbf{u}^k) : \operatorname{grad}\mathbf{v}\,\mathrm{d}\mathbf{x} + \int_{\Omega_t} \boldsymbol{\varepsilon}(\Delta\mathbf{u}) : \mathbb{c}(\mathbf{u}^k) : \boldsymbol{\varepsilon}(\mathbf{v})\,\mathrm{d}\mathbf{x}. \quad (4.24)$$

We define the bilinear and the linear form in the current configuration as

$$a'(\Delta\mathbf{u}, \mathbf{v}) := \langle \Delta\mathbf{u}, A'(\mathbf{u}^k)\,\mathbf{v}\rangle_{\Omega_t}, \quad \langle \mathcal{R}, \mathbf{v}\rangle := \langle \mathcal{F}, \mathbf{v}\rangle_{\Omega_t} - \langle A(\mathbf{u}^k), \mathbf{v}\rangle_{\Omega_t}. \quad (4.25)$$

In each Newton step we have to solve the linearized system: find $\Delta\mathbf{u} \in [H_0^1(\Omega_t, \Gamma_{t,\mathrm{D}})]^3$ such that

$$a'(\Delta\mathbf{u}, \mathbf{v}) = \langle \mathcal{R}, \mathbf{v}\rangle \quad (4.26)$$

holds for all $\mathbf{v} \in [H_0^1(\Omega_t, \Gamma_{t,\mathrm{D}})]^3$.

4.4.3 Linearization of Pressure Loads

Since pressure loads, see (3.18), (3.19) and Remark 4.2.1, are dependent on the deformation, they have to be considered in the linearization of the variational formulation. One possibility is the direct linearization of the formulation in the reference configuration (3.19):

$$\begin{aligned}\langle \Delta\mathbf{U}, \mathcal{F}_0'(\mathbf{U})\mathbf{V}\rangle_{\Omega_0} &:= D\langle \mathcal{F}_0(\mathbf{U}), \mathbf{V}\rangle_{\Omega_0}.\Delta\mathbf{U} = -\int_{\Gamma_{0,\mathrm{N}}} \mathcal{P}[D(J\mathbf{F}^{-\top}).\Delta\mathbf{U}]\,\mathbf{N}\cdot\mathbf{V}\,\mathrm{d}S_{\mathbf{X}} \\ &= -\int_{\Gamma_{0,\mathrm{N}}} \mathcal{P}[D(J).\Delta\mathbf{U}]\mathbf{F}^{-\top}\mathbf{N}\cdot\mathbf{V}\,\mathrm{d}S_{\mathbf{X}} - \int_{\Gamma_{0,\mathrm{N}}} \mathcal{P}J[D(\mathbf{F}^{-\top}).\Delta\mathbf{U}]\,\mathbf{N}\cdot\mathbf{V}\,\mathrm{d}S_{\mathbf{X}}\end{aligned}$$

Using Corollary A.2, (A.23) and (4.18) we get

$$D(J).\Delta\mathbf{U} = \frac{\partial J}{\partial \mathbf{F}} : D\mathbf{F}.\Delta\mathbf{U} = J\mathbf{F}^{-\top} : \mathrm{Grad}\,\Delta\mathbf{U}$$

and with (A.24) it holds

$$D(\mathbf{F}^{-\top}).\Delta\mathbf{U} = \frac{\partial \mathbf{F}^{-\top}}{\partial \mathbf{F}^{\top}} : D\mathbf{F}^{\top}.\Delta\mathbf{U} = \frac{\partial \mathbf{F}^{-\top}}{\partial \mathbf{F}^{\top}} : \mathrm{Grad}^{\top}\Delta\mathbf{U}.$$

Corollary A.4 and $(\mathrm{A}.5)_1$ yield

$$\left[\frac{\partial \mathbf{F}^{-\top}}{\partial \mathbf{F}^{\top}} : \mathrm{Grad}^{\top}\Delta\mathbf{U}\right]_{ijkl} = -F^{-\top}_{ik}F^{-\top}_{lj}\left[\mathrm{Grad}^{\top}\Delta\mathbf{U}\right]_{kl} = -\left[\mathbf{F}^{-\top}\,\mathrm{Grad}^{\top}\Delta\mathbf{U}\;\mathbf{F}^{-\top}\right]_{ijkl}$$

and consequently

$$\langle \Delta\mathbf{U}, \mathcal{F}_0'(\mathbf{U})\mathbf{V}\rangle_{\Omega_0} = \int_{\Gamma_{0,\mathrm{N}}} \mathcal{P}J\left[\mathbf{F}^{-\top}\,\mathrm{Grad}^{\top}\Delta\mathbf{U} - (\mathbf{F}^{-\top} : \mathrm{Grad}\,\Delta\mathbf{U})\,\mathbf{I}\right]\mathbf{F}^{-\top}\mathbf{N}\cdot\mathbf{V}\,\mathrm{d}S_{\mathbf{X}}.$$

To avoid assembling this rather complicated integral an alternative approach is a a parametrization of the boundary surface in the current configuration $\Gamma_{t,\mathrm{N}}$ by the plane $\Gamma_{\boldsymbol{\xi}}$, $\mathbf{x} = \boldsymbol{\gamma}(\xi_1, \xi_2)$, see Figure 4.1, [24, Section 6.5.2] and [187, Section 3.5]. Then, the outward unit normal in the current configuration and the infinitesimal surface element can be expressed as the cross product of two tangential vectors, i.e.,

$$\mathbf{n} = \frac{\frac{\partial\boldsymbol{\gamma}}{\partial\xi_1}\times\frac{\partial\boldsymbol{\gamma}}{\partial\xi_2}}{\left|\frac{\partial\boldsymbol{\gamma}}{\partial\xi_1}\times\frac{\partial\boldsymbol{\gamma}}{\partial\xi_2}\right|}, \quad \mathrm{d}s_{\mathbf{x}} = \left|\frac{\partial\boldsymbol{\gamma}}{\partial\xi_1}\times\frac{\partial\boldsymbol{\gamma}}{\partial\xi_2}\right|\mathrm{d}\xi_1\,\mathrm{d}\xi_2.$$

Hence, we get for the equations in Remark 4.2.1

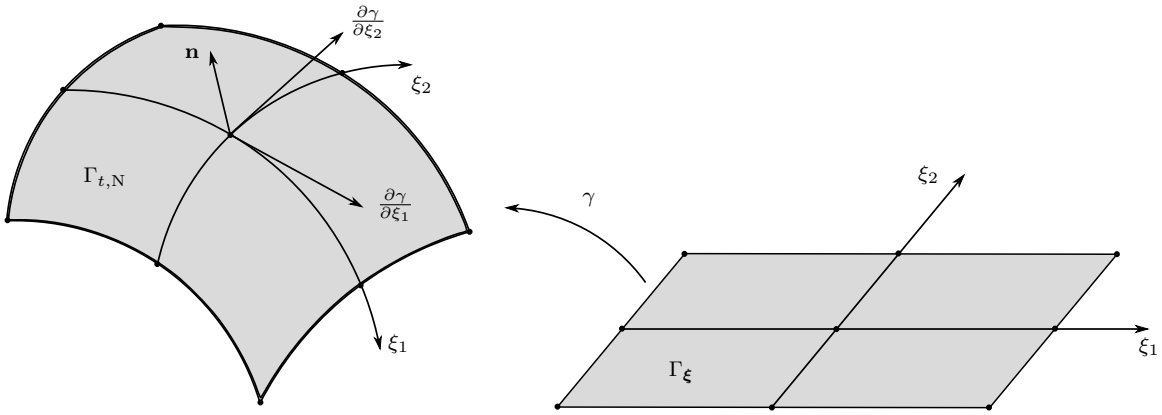

Figure 4.1: Parametrization of the boundary surface in the current configuration $\Gamma_{t,\mathrm{N}}$ for deformation dependent loads.

$$\langle \mathcal{F}(\mathbf{u}), \mathbf{v} \rangle_{\Omega_t} = -\int_{\Gamma_{\boldsymbol{\xi}}} \mathcal{P}\left(\frac{\partial \boldsymbol{\gamma}}{\partial \xi_1} \times \frac{\partial \boldsymbol{\gamma}}{\partial \xi_2}\right) \cdot \mathbf{v}\, \mathrm{d}\xi_1\, \mathrm{d}\xi_2. \tag{4.27}$$

$\Gamma_{\boldsymbol{\xi}}$ is independent of the deformation and we compute the the Gâteaux derivative with respect to the update $\Delta\mathbf{u}$

$$\begin{aligned} \langle \Delta\mathbf{u}, \mathcal{F}'(\mathbf{u})\mathbf{v} \rangle_{\Omega_t} &:= D\langle \mathcal{F}(\mathbf{u}), \mathbf{v} \rangle_{\Omega_t}.\Delta\mathbf{u} \\ &= -\int_{\Gamma_{\boldsymbol{\xi}}} \mathcal{P}\left(\frac{\partial \Delta\mathbf{u}}{\partial \xi_1} \times \frac{\partial \boldsymbol{\gamma}}{\partial \xi_2} + \frac{\partial \boldsymbol{\gamma}}{\partial \xi_1} \times \frac{\partial \Delta\mathbf{u}}{\partial \xi_2}\right) \cdot \mathbf{v}\, \mathrm{d}\xi_1\, \mathrm{d}\xi_2, \end{aligned} \tag{4.28}$$

using $\boldsymbol{\gamma} = \mathbf{x} = \mathbf{X} + \mathbf{u}$ and thus $D\boldsymbol{\gamma}.\Delta\mathbf{u} = \Delta\mathbf{u}$.

Due to (3.1) we get the same result

$$\begin{aligned} \langle \Delta\mathbf{U}, \mathcal{F}_0'(\mathbf{U})\mathbf{V} \rangle_{\Omega_0} &:= D\langle \mathcal{F}_0(\mathbf{U}), \mathbf{V} \rangle_{\Omega_0}.\Delta\mathbf{U} \\ &= -\int_{\Gamma_{\boldsymbol{\xi}}} \mathcal{P}\left(\frac{\partial \Delta\mathbf{U}}{\partial \xi_1} \times \frac{\partial \boldsymbol{\gamma}}{\partial \xi_2} + \frac{\partial \boldsymbol{\gamma}}{\partial \xi_1} \times \frac{\partial \Delta\mathbf{U}}{\partial \xi_2}\right) \cdot \mathbf{V}\, \mathrm{d}\xi_1\, \mathrm{d}\xi_2. \end{aligned} \tag{4.29}$$

in the reference configuration. It is obvious that neither (4.28) nor (4.29) give rise to self-adjoint operators in the sense of Definition 4.3. Hence, the discretization of these terms would lead to a non-symmetric matrix. For the special case of closed boundary conditions a self-adjoint expression for pressure loads can be constructed, see Bonet and Wood [24].

4.4.4 Linearization of the Saddlepoint Formulation

For nearly incompressible materials we compute the linearization of the variational formulation of the saddle point problem (3.37). Let $\mathcal{X}$ and $\mathcal{M}$ be the spaces defined in (4.12). Then, we want to find $(\mathbf{U}, P) \in \mathcal{X} \times \mathcal{M}$, such that

$$\langle A_{0,\mathrm{isc}}(\mathbf{U}), \mathbf{V}\rangle_{\Omega_0} + \langle A_{0,\mathrm{vol}}(\mathbf{U}, P), \mathbf{V}\rangle_{\Omega_0} = \langle \mathcal{F}_0, \mathbf{V}\rangle_{\Omega_0}, \tag{4.30}$$

$$\langle B_0(\mathbf{U}), Q\rangle_{\Omega_0} - \kappa^{-1} \langle C_0(P), Q\rangle_{\Omega_0} = 0, \tag{4.31}$$

holds for all test functions $(\mathbf{V}, Q) \in \mathcal{X} \times \mathcal{M}$. The specific expressions in (4.30–4.31) are

$$\langle A_{0,\mathrm{isc}}(\mathbf{U}), \mathbf{V}\rangle_{\Omega_0} = \int_{\Omega_0} \mathbf{FS}_{\mathrm{isc}}(\mathbf{U}) : \mathrm{Grad}(\mathbf{V})\, \mathrm{d}\mathbf{X}, \tag{4.32}$$

$$\langle A_{0,\mathrm{vol}}(\mathbf{U}, P), \mathbf{V}\rangle_{\Omega_0} = \int_{\Omega_0} \mathbf{FS}_{\mathrm{vol}}(\mathbf{U}, P)(\mathbf{U}) : \mathrm{Grad}(\mathbf{V})\, \mathrm{d}\mathbf{X}, \tag{4.33}$$

$$\langle B_0(\mathbf{U}), Q\rangle_{\Omega_0} = \int_{\Omega_0} \frac{\partial \phi_{\mathrm{vol}}(J(\mathbf{U}))}{\partial J}\, Q\, \mathrm{d}\mathbf{X}, \tag{4.34}$$

$$\langle C_0(P), Q\rangle_{\Omega_0} = \langle P, Q\rangle_{\Omega_0} = \int_{\Omega_0} PQ\, \mathrm{d}\mathbf{X}, \tag{4.35}$$

$$\langle \mathcal{F}_0, \mathbf{V}\rangle_{\Omega_0} = \int_{\Gamma_{0,\mathrm{N}}} \mathbf{t}_{\mathrm{N}}(\mathbf{X}) \cdot \mathbf{V}(\mathbf{X})\, \mathrm{d}S_{\mathbf{X}}. \tag{4.36}$$

and κ is the bulk modulus, see Definition 3.11.

For the linearization we have to perform the Gâteaux derivative of these terms with respect to $\Delta\mathbf{U}$ and ΔP to get the Newton scheme

$$\begin{aligned} \langle \Delta\mathbf{U}, A_0'(\mathbf{U}^k, P^k)\,\mathbf{V}\rangle_{\Omega_0} + \langle \Delta P, B_0'(\mathbf{U}^k)\,\mathbf{V}\rangle_{\Omega_0} &= \langle \mathcal{F}_0, \mathbf{V}\rangle_{\Omega_0} - \langle A_0(\mathbf{U}^k, P^k), \mathbf{V}\rangle_{\Omega_0}, \\ \langle \Delta\mathbf{U}, B_0'(\mathbf{U}^k)\,Q\rangle_{\Omega_0} - \kappa^{-1} \langle \Delta P, Q\rangle_{\Omega_0} &= \langle P^k, Q\rangle_{\Omega_0} - \langle B_0(\mathbf{U}^k), Q\rangle_{\Omega_0}, \end{aligned}$$

with the updates $\mathbf{U}^{k+1} = \mathbf{U}^k + \Delta\mathbf{U}$ and $P^{k+1} = P^k + \Delta P$. The first tangential term is the Gâteaux derivative of (4.32) and (4.33) with respect to $\Delta\mathbf{U}$. This is done analogous to Section 4.4.2 and we get the result

$$\begin{aligned} \langle \Delta\mathbf{U}, A_0'(\mathbf{U}^k, P^k)\mathbf{V}\rangle_{\Omega_0} = &\int_{\Omega_0} \mathrm{Grad}(\Delta\mathbf{U}) \left(\mathbf{S}_{\mathrm{isc}}(\mathbf{U}^k) + \mathbf{S}_{\mathrm{vol}}(\mathbf{U}^k, P^k)\right) : \mathrm{Grad}\,\mathbf{V}\, \mathrm{d}\mathbf{X} \\ &+ \int_{\Omega_0} \mathbf{F}^{\top}(\mathbf{U}^k)\,\mathrm{Grad}(\Delta\mathbf{U}) : \left(\mathbb{C}_{\mathrm{isc}}(\mathbf{U}^k) + \mathbb{C}_{\mathrm{vol}}(\mathbf{U}^k, P^k)\right) : \mathbf{F}^{\top}(\mathbf{U}^k)\,\mathrm{Grad}\,\mathbf{V}\, \mathrm{d}\mathbf{X}. \end{aligned}$$

Next, we compute the Gâteaux derivative of (4.32) and (4.33) with respect to ΔP. This is, using the formulation (4.8) and $\mathbf{S}_{\mathrm{vol}}(\mathbf{U},P) = P(J\mathbf{C}^{-1})(\mathbf{U})$, see (3.64),

$$\langle \Delta P, B_0'(\mathbf{U}^k)\,\mathbf{V}\rangle_{\Omega_0} = D\langle A_{0,\mathrm{vol}}(\mathbf{U},P),\mathbf{V}\rangle_{\Omega_0}.\Delta P = \int_{\Omega_0} \Delta P\,(J\mathbf{C}^{-1})(\mathbf{U}^k) : \mathbf{\Sigma}(\mathbf{U}^k,\mathbf{V})\,\mathrm{d}\mathbf{X}.$$

The Gâteaux derivative of (4.34) with respect to $\Delta\mathbf{U}$ is

$$\begin{aligned}
\langle \Delta\mathbf{U}, B_0'(\mathbf{U}^k)\,Q\rangle_{\Omega_0} &= \int_{\Omega_0} Q\,D\,\frac{\partial\phi_{\mathrm{vol}}(J(\mathbf{U}^k))}{\partial J}.\Delta\mathbf{U}\,\mathrm{d}\mathbf{X} = \int_{\Omega_0} Q\,D\,\phi_{\mathrm{vol}}'(\mathbf{U}^k).\Delta\mathbf{U}\,\mathrm{d}\mathbf{X}\\
&= \int_{\Omega_0} Q\,\frac{\partial\phi_{\mathrm{vol}}'(\mathbf{U}^k)}{\partial\mathbf{C}} : D\mathbf{C}.\Delta\mathbf{U}\,\mathrm{d}\mathbf{X}\\
&= \int_{\Omega_0} Q\,\frac{\partial\phi_{\mathrm{vol}}'(\mathbf{U}^k)}{\partial\mathbf{C}} : 2\mathbf{\Sigma}(\mathbf{U}^k,\Delta\mathbf{U})\,\mathrm{d}\mathbf{X}\\
&= \int_{\Omega_0} Q\,\frac{\partial\phi_{\mathrm{vol}}'(\mathbf{U}^k)}{\partial J}\frac{\partial J}{\partial\mathbf{C}} : 2\mathbf{\Sigma}(\mathbf{U}^k,\Delta\mathbf{U})\,\mathrm{d}\mathbf{X}\\
&= \int_{\Omega_0} Q\,\frac{\partial\phi_{\mathrm{vol}}'(\mathbf{U}^k)}{\partial J}(J\mathbf{C}^{-1})(\mathbf{U}^k) : \mathbf{\Sigma}(\mathbf{U}^k,\Delta\mathbf{U}^k)\,\mathrm{d}\mathbf{X}\\
&= \int_{\Omega_0} Q\,\frac{\partial^2\phi_{\mathrm{vol}}(J(\mathbf{U}^k))}{\partial J^2}(J\mathbf{C}^{-1})(\mathbf{U}^k) : \mathbf{\Sigma}(\mathbf{U}^k,\Delta\mathbf{U}^k)\,\mathrm{d}\mathbf{X},
\end{aligned}$$

using (4.19), $(3.26)_1$, the chain rule and the definition $\phi_{\mathrm{vol}}' := \partial\phi_{\mathrm{vol}}/\partial J$.

For the choice $\phi_{\mathrm{vol}}(J) = \frac{1}{2}(J-1)^2$ we have

$$\langle \Delta\mathbf{U}, B_0'(\mathbf{U}^k)\,Q\rangle_{\Omega_0} = \int_{\Omega_0} Q\,(J\mathbf{C}^{-1})(\mathbf{U}^k) : \mathbf{\Sigma}(\mathbf{U}^k,\Delta\mathbf{U})\,\mathrm{d}\mathbf{X},$$

see Definition 3.11.

Finally, we compute the contribution of (4.35)

$$\langle \Delta P, Q\rangle_{\Omega_0} = \int_{\Omega_0} \Delta P\,Q\,\mathrm{d}\mathbf{X}.$$

Using the push-forward properties (3.14, 4.23) and the defintion of the elasticity tensor (Definition 3.14) , we obtain the corresponding scheme in the current config-

uration:

$$\begin{aligned} \langle \Delta\mathbf{u}, A'(\mathbf{u}^k,p^k)\,\mathbf{v}\rangle_{\Omega_t} + \langle \Delta p, B'(\mathbf{u}^k)\,\mathbf{v}\rangle_{\Omega_t} &= \langle \mathcal{F},\mathbf{v}\rangle_{\Omega_t} - \langle A(\mathbf{u}^k,p^k),\mathbf{v}\rangle_{\Omega_t} \\ \langle \Delta\mathbf{u}, B'(\mathbf{u}^k)\,q\rangle_{\Omega_t} - \kappa^{-1}\langle \Delta p, q\rangle_{\Omega_t} &= \langle p^k,q\rangle_{\Omega_t} - \langle B(\mathbf{u}^k),q\rangle_{\Omega_t}, \end{aligned} \tag{4.37}$$

with the updates $\mathbf{u}^{k+1} = \mathbf{u}^k + \Delta\mathbf{u}$ and $p^{k+1} = p^k + \Delta p$.

The specific terms in (4.37) are

$$\begin{aligned} \langle \Delta\mathbf{u}, A'(\mathbf{u}^k,p^k)\,\mathbf{v}\rangle_{\Omega_t} &= \int_{\Omega_t} \operatorname{grad}(\Delta\mathbf{u}) \left(\boldsymbol{\sigma}_{\mathrm{isc}}(\mathbf{u}^k) + \boldsymbol{\sigma}_{\mathrm{vol}}(p^k)\right) : \operatorname{grad}\mathbf{v}\,\mathrm{d}\mathbf{x} \\ &\quad + \int_{\Omega_t} \operatorname{grad}(\Delta\mathbf{u}) : \left(\mathbb{C}_{\mathrm{isc}}(\mathbf{u}^k) + \mathbb{C}_{\mathrm{vol}}(p^k)\right) : \operatorname{grad}\mathbf{v}\,\mathrm{d}\mathbf{x}, \\ \langle \Delta p, B'(\mathbf{u}^k)\,\mathbf{v}\rangle_{\Omega_t} &= \int_{\Omega_t} \Delta p\,\mathbf{I} : \boldsymbol{\varepsilon}(\mathbf{v})\,\mathrm{d}\mathbf{x}, \\ \langle \Delta\mathbf{u}, B'(\mathbf{u}^k)\,q\rangle_{\Omega_t} &= \int_{\Omega_t} q\mathbf{I} : \boldsymbol{\varepsilon}(\Delta\mathbf{u})\,\mathrm{d}\mathbf{x}, \\ \langle \Delta p, q\rangle_{\Omega_t} &= \int_{\Omega_t} \Delta p\, q\,\mathrm{d}\mathbf{x}. \end{aligned}$$

For pressure loads we have additional terms according to Section 4.4.3.

Remark 4.4.1. *It is obvious that we can find a starting point* $\mathbf{u}_0$ *that satisfies the requirements of Theorem 4.12 for the derivative of the variational formulations in Sections 4.4.2 and 4.4.4. This is due to the properties of the strain-energy function described in Remark 3.6.4 (Normalization Conditions). A possible choice would be the solution of the linear elasticity problem.*

4.4.5 On the Solvability of the Linearized Equations

In this section we analyze the solvability of the linearized variational formulations as described in Section 4.4.2 and Section 4.4.4.

Remark 4.4.2 (Self-adjointness)**.** *The operators* $A_0'(\mathbf{U}^k)$ *and* $A'(\mathbf{u}^k)$ *in Eqs.* (4.20) *and* (4.24) *are self-adjoint. This is due to the symmetry properties of the elasticity tensor, compare to Remark 3.8.1, and the symmetry of the stress tensors* $\mathbf{S}$ *and* $\boldsymbol{\sigma}$*.*

In the following, we show boundedness and ellipticity of the bilinear form $a'(\Delta\mathbf{u},\mathbf{v})$, defined in (4.25). Since the formulations in the reference and the current configuration are equivalent, similar estimates also hold for $a_0'(\Delta\mathbf{U},\mathbf{V})$, defined in (4.21).

Lemma 4.13 (Boundedness of the bilinear form)**.** *For a sufficiently regular domain* Ω *and for sufficiently smooth* $\Delta\mathbf{u}, \mathbf{v} \in [H^1(\Omega)]^3$ *it holds*

$$|a'(\Delta\mathbf{u}, \mathbf{v})| \leq (c_2^g + c_2^m)\, |\Delta\mathbf{u}|_{[H^1(\Omega)]^3} |\mathbf{v}|_{[H^1(\Omega)]^3},$$

with positive constants c_2^g *and* c_2^m*.*

Proof. We show the boundedness of (4.24)

$$a'(\Delta\mathbf{u}, \mathbf{v}) = \int_\Omega \operatorname{grad}(\Delta\mathbf{u})\, \boldsymbol{\sigma}(\mathbf{u}^k) : \operatorname{grad}\mathbf{v}\, \mathrm{d}\mathbf{x} + \int_\Omega \boldsymbol{\varepsilon}(\Delta\mathbf{u}) : \mathbb{C}(\mathbf{u}^k) : \boldsymbol{\varepsilon}(\mathbf{v})\, \mathrm{d}\mathbf{x}.$$

For a sufficiently regular domain Ω and sufficiently smooth $\mathbf{u}^k$ the values $\boldsymbol{\sigma}(\mathbf{u}^k)$ and $\mathbb{C}(\mathbf{u}^k)$ may be treated as finite-valued constants within a Newton step. Hence, with the boundedness of the bilinear form of linear elasticity, cf. Lemma 4.11, and the boundedness of the vectorial potential equation [176], it follows

$$\begin{aligned} |a'(\Delta\mathbf{u}, \mathbf{v})| &\leq \left| \int_\Omega \operatorname{grad}(\Delta\mathbf{u})\, \boldsymbol{\sigma}(\mathbf{u}^k) : \operatorname{grad}\mathbf{v}\, \mathrm{d}\mathbf{x} \right| + \left| \int_\Omega \boldsymbol{\varepsilon}(\Delta\mathbf{u}) : \mathbb{C}(\mathbf{u}^k) : \boldsymbol{\varepsilon}(\mathbf{v})\, \mathrm{d}\mathbf{x} \right| \\ &\leq 3\|\boldsymbol{\sigma}\|_{L_\infty} |\Delta\mathbf{u}|_{[H^1(\Omega)]^3} |\mathbf{v}|_{[H^1(\Omega)]^3} + |\lambda_{\max}(\mathcal{C})| |\Delta\mathbf{u}|_{[H^1(\Omega)]^3} |\mathbf{v}|_{[H^1(\Omega)]^3}, \end{aligned}$$

where $\|\boldsymbol{\sigma}\|_{L_\infty} := \max_{i,j=1,2,3} |\sigma_{ij}(\mathbf{u}^k)|$ and $\lambda_{\max}(\mathcal{C})$ is the largest eigenvalue of $\mathcal{C}(\mathbf{u}^k)$ which is the elasticity tensor $\mathbb{C}(\mathbf{u}^k)$ in Voigt notation.

Due to the equivalence of the standard and the decoupled formulation, we get the same result for the decoupled formulation with $\boldsymbol{\sigma} = p\mathbf{I} + \boldsymbol{\sigma}_{\text{isc}}$ and $\mathbb{C} = \mathbb{C}_{\text{vol}} + \mathbb{C}_{\text{isc}}$. □

Note that the regularity conditions of the previous Lemma could be very restrictive, see also [38, 182].

We know that the stress tensor $\boldsymbol{\sigma}$ and the elasticity tensor $\mathcal{C}$ in Voigt notation, cf. Remark 3.8.2, are both symmetric.

Remark 4.4.3. *The eigenvalues of* $\boldsymbol{\sigma}$ *are called* principal stresses *and may be calculated by*

$$\sigma_i = J^{-1} \lambda_i \frac{\partial \Psi}{\partial \lambda_i}, \quad \textit{for } i = 1, 2, 3,$$

with $\Psi(\mathbf{C}) = \Psi(\lambda_1, \lambda_2, \lambda_3)$ *the strain energy function and* $\lambda_i > 0$ *the principal stretches, cf. Cor. 3.5.*

Then we get, using results of Section 4.3, for all $\mathbf{v} \in [H_0^1(\Omega)]^3$

$$\begin{aligned} a'(\mathbf{v},\mathbf{v}) &\geq \lambda_{\min}(\boldsymbol{\sigma}(\mathbf{u}^k)) \sum_{i,j=1}^{3} \int_\Omega \left[\frac{\partial}{\partial x_j} v_i(\mathbf{x})\right]^2 \mathrm{d}\mathbf{x} + \lambda_{\min}(\mathcal{C}) \frac{1}{2(1+c_F^2)} \|\mathbf{v}\|^2_{[H^1(\Omega)]^3} \\ &= \lambda_{\min}(\boldsymbol{\sigma}(\mathbf{u}^k)) |\mathbf{v}|^2_{[H^1(\Omega)]^3} + \lambda_{\min}(\mathcal{C}) \frac{1}{2(1+c_F^2)} \|\mathbf{v}\|^2_{[H^1(\Omega)]^3} \\ &\geq \frac{1}{2(1+c_F^2)} (2\lambda_{\min}(\boldsymbol{\sigma}(\mathbf{u}^k)) + \lambda_{\min}(\mathcal{C})) \|\mathbf{v}\|^2_{[H^1(\Omega)]^3} \\ &= \frac{1}{2(1+c_F^2)} (2 \min_{i=1,2,3}(\sigma_i)) + \lambda_{\min}(\mathcal{C})) \|\mathbf{v}\|^2_{[H^1(\Omega)]^3} \end{aligned}$$

where c_F denotes the constant from the Poincaré–Friedrich's inequality (4.3) and σ_i are the principal stresses of $\boldsymbol{\sigma}(\mathbf{u}^k)$. With the normalization conditions for the strain-energy function, cf. Remark 3.6.4, and the positive definiteness of the elasticity tensor, cf. Remark 3.8.3, we can state that $\lambda_{\min}(\mathcal{C}) > 0$ and

$$a'(\mathbf{v},\mathbf{v}) \geq \frac{1}{2(1+c_F^2)} (2 \min_{i=1,2,3}(\sigma_i)) \|\mathbf{v}\|^2_{[H^1(\Omega)]^3} = c\|\mathbf{v}\|^2_{[H^1(\Omega)]^3}.$$

Given that $c > 0$, i.e. $\sigma_{\min} := \min_{i=1,2,3}(\sigma_i) > 0$, we obtain $[H_0^1(\Omega, \Gamma_{\mathrm{D}})]^3$–ellipticity of the bilinear form for the Dirichlet and the mixed boundary value problem, given the strain-energy function fulfills the normalization conditions and is convex, cf. Section 4.4.8.

Note that $\sigma_{\min} > 0$ is only fulfilled for specific classes of (convex) strain-energy functions and deformations, see 4.4.6 and Remark 4.4.3. See also the books [38, 182].

Similar to Section 4.3, we can show $[H_*^1(\Omega)]^3$–ellipticity for the Neumann case.

With these ellipticity results and Lemma 4.13 the unique solvability of the linearized elasticity equations in the appropriate spaces follows.

4.4.6 Convexity concepts

In the following, we will introduce convexity concepts for vector valued functions.

Definition 4.14. *Let $f : \mathbb{R}^{m\times n} \mapsto \mathbb{R}$ a function.*

1. *The function f is said to be convex if*

$$f(\lambda \mathbf{A} + (1-\lambda)\mathbf{B}) \leq \lambda f(\mathbf{A}) + (1-\lambda) f(\mathbf{B})$$

for all $\mathbf{A}, \mathbf{B} \in \mathbb{R}^{m\times n},\ \lambda \in [0,1]$.

2. *The function f is said to be polyconvex if there exists $F : \mathbb{R}^{\tau(n,m)} \mapsto \mathbb{R}$ convex, such that*

$$f(\mathbf{A}) = F(T(\mathbf{A})).$$

Here, $T : \mathbb{R}^{m\times n} \mapsto \mathbb{R}^{\tau(n,m)}$ is defined such that

$$T(\mathbf{A}) = (\mathbf{A}, \operatorname{adj}_2 \mathbf{A}, \ldots, \operatorname{adj}_{\min\{m,n\}} \mathbf{A})$$

where $\operatorname{adj}_s \mathbf{A}$, $2 \le s \le \min\{n,m\}$, is the matrix of all $s \times s$ minors of the matrix $\mathbf{A}$. Furthermore

$$\tau(n,m) = \sum_{s=1}^{\min\{n,m\}} \binom{m}{s}\binom{n}{s}.$$

3. *The function f is said to be quasiconvex if it is Borel measurable and locally bounded and satisfies*

$$f(\mathbf{A}) \le \frac{1}{\operatorname{meas} D} \int_D f(\mathbf{A} + \nabla\varphi(\mathbf{x}))\,\mathrm{d}\mathbf{x}$$

for all open and bounded sets $D \subset \mathbb{R}^n$, for all $\mathbf{A} \in \mathbb{R}^{m\times n}$ and for all $\varphi \in W_0^{1,\infty}(D;\mathbb{R}^m)$.

4. *The function f is said to be rank-one convex if*

$$f(\lambda\mathbf{A} + (1-\lambda)\mathbf{B}) \le \lambda f(\mathbf{A}) + (1-\lambda) f(\mathbf{B})$$

for every $\lambda \in [0,1]$, $\mathbf{A}, \mathbf{B} \in \mathbb{R}^{m\times n}$ with $\operatorname{rank}(\mathbf{A}-\mathbf{B}) \le 1$.

Theorem 4.15 (Connection of the convexity concepts)**.** *Let $f : \mathbb{R}^{m\times n} \mapsto \mathbb{R}$ be a function.*

1. *The convexity concepts are linked by the implications*

$$f \text{ convex} \Rightarrow f \text{ polyconvex} \Rightarrow f \text{ quasiconvex} \Rightarrow f \text{rank-one convex}$$

The converse implications are in general not true.

2. *If $\min\{m,n\} = 1$, then all of the convexity concepts are equivalent.*

3. *If $f \in \mathcal{C}^2(\mathbb{R}^{m\times n})$, then rank one convexity is equivalent to the following state-*

ment, often called ellipticity *or* Legendre–Hadamard condition

$$\sum_{i,j=1}^{m}\sum_{\alpha,\beta}^{n}\frac{\partial^2 f(\mathbf{A})}{\partial A_{i,\alpha}\partial A_{j,\beta}}\lambda_i\lambda_j\mu_\alpha\mu_\beta \geq 0$$

for all $\underline{\lambda}\in\mathbb{R}^m$, $\underline{\mu}\in\mathbb{R}^n$ *and* $\mathbf{A}\in\mathbb{R}^{m\times n}$.

Proof. Cf. [43, Theorem 5.3]. □

Example 4.1. *Examples to illustrate the convexity prinicples:*

1. *Let* $\mathbf{A}\in\mathbb{R}^{2\times 2}$. *Then the function* $\det(\mathbf{A})$ *is polyconvex, but not convex.*
2. *Let* $\mathbf{M}\in\mathbb{R}^{m\times m}$ *be symmetric,* $\mathbf{A}\in\mathbb{R}^{m\times n}$ *and* $\langle .,.\rangle_{\mathrm{F}}$ *denote the Frobenius inner product. Then, the function*

$$f(\mathbf{A}) = \langle \mathbf{MA}, \mathbf{A}\rangle_{\mathrm{F}}.$$

is convex if and only if $f(\mathbf{A})\geq 0$ *for every* $\mathbf{A}\in\mathbb{R}^{m\times n}$, *and* f *is rank one convex if and only if* $f(\mathbf{a}\otimes\mathbf{b})\geq 0$ *for every* $\mathbf{a}\in\mathbb{R}^m, \mathbf{b}\in\mathbb{R}^n$.

Subsequently, we denote by $D_{\mathbf{A}}f(\cdot).\mathbf{H}$ the Gâteaux derivative with respect to $\mathbf{A}$ in the direction of $\mathbf{H}$.

Lemma 4.16. *Let* K *be a convex set and let* $f: K\mapsto\mathbb{R}$ *be two times differentiable. Then the following statements are equivalent.*

$$\begin{aligned} &(i)\ f \text{ is convex}\\ &(ii)\ D^2_{\mathbf{A}}f(\mathbf{A}).(\mathbf{H},\mathbf{H})\geq 0 \quad \text{for all } \mathbf{A}\in K \text{ and for all } \mathbf{H}\in \mathrm{span}(K), \end{aligned}$$

where $\mathrm{span}(K)$ *is the linear span (also called the linear hull) of* K.

Proof. See [155, p. 27]. □

It is easy to see, using the definition of the derivative of a second-order tensor valued function (A.20), that the condition in Lemma 4.16 implies Legendre Hadamard ellipticity (see Theorem 4.15_3), cf. [18, p. 6067].

In the following, we denote by $P\mathbb{S}\mathrm{ym}(3)$ the set of all real, positive definite and symmetric 3×3 matrices. Likewise is $P\mathbb{S}\mathrm{ym}_0(3)$ the set of all real, positive semi-definite and symmetric 3×3 matrices.

Remark 4.4.4. *Let K be a convex set. To show that $\Psi(\mathbf{C}) : K \mapsto \mathbb{R}$ is convex it is not sufficient to assume*

$$D^2_{\mathbf{C}}\Psi(\mathbf{C}).(\mathbf{H},\mathbf{H}) \geq 0 \quad \textit{for all } \mathbf{C} \in K \textit{ and for all } \mathbf{H} \in K.$$

A counterexample is $\Psi : P\mathbb{S}\mathrm{ym}(3) \mapsto \mathbb{R}, \Psi(\mathbf{C}) = \det(\mathbf{C})$ with the convex cone $K = P\mathbb{S}\mathrm{ym}(3)$ where

$$D^2_{\mathbf{C}}\Psi(\mathbf{C}).(\mathbf{H},\mathbf{H}) = 2\langle \mathbf{C}, \det(\mathbf{H})\mathbf{H}^{-1}\rangle \geq 0 \quad \textit{for all } \mathbf{C},\mathbf{H} \in P\mathbb{S}\mathrm{ym},$$

albeit that $\Psi(\mathbf{C})$ is not convex as a function of $\mathbf{C}$.

Proof. Follows from the series expansion

$$\det(\mathbf{C}+\mathbf{H}) = \det(\mathbf{C}) + \det(\mathbf{C})\,\mathrm{tr}(\mathbf{H}\mathbf{C}^{-1}) + \det(\mathbf{H})\,\mathrm{tr}(\mathbf{H}^{-1}\mathbf{C}) + \det(\mathbf{H})$$

and basic properties of positive definite matrices, see, e.g., [134, Chapter 11]. For the non-convexity of $\det(\mathbf{C})$ see Example 4.1. □

Lemma 4.17 (Convexity in $\mathbb{R}^{3\times3}$ and $P\mathbb{S}\mathrm{ym}(3)$)**.** *Let $\mathbf{C} \in \mathbb{R}^{3\times3}$ be positive definite and symmetric, i.e. $\mathbf{C} \in P\mathbb{S}\mathrm{ym}(3)$ and $\Psi : P\mathbb{S}\mathrm{ym}(3) \mapsto \mathbb{R}$. Let*

$$D^2_{\mathbf{C}}\Psi(\mathbf{C}).(\mathbf{H},\mathbf{H}) \geq 0 \quad \textit{and} \tag{4.38}$$

be for all $\mathbf{H} \in \mathbb{S}\mathrm{ym}(3)$. Then the function

$$W : \mathbb{R}^{3\times3} \mapsto \mathbb{R}, \quad W(\mathbf{F}) := \Psi(\mathbf{F}^{\top}\mathbf{F}) = \Psi(\mathbf{C})$$

is locally convex*. If additionally*

$$D_{\mathbf{C}}\Psi(\mathbf{C}) = \frac{\partial\Psi(\mathbf{C})}{\partial\mathbf{C}} \in P\mathbb{S}\mathrm{ym}_0(3), \tag{4.39}$$

then the function W is convex*.*

Proof. Note that the right Cauchy–Green tensor $\mathbf{C}$ is positive definite, see (3.3). The proof follows from $\mathrm{span}(P\mathbb{S}\mathrm{ym}) = \mathbb{S}\mathrm{ym}$ and basic properties of the scalar product, e.g., see Schröder and Neff [164]. □

Lemma 4.18. *Let W be strongly elliptic, i.e. strongly rank-one convex. Then the* Baker–Ericksen inequalities *are satisfied. These conditions guarantee a plausible physical behavior of the material. For more information see Baker and Ericksen [12] and Marsden and Hughes [121].*

4.4.7 Existence Theorems in Nonlinear Elasticity

In this section we will give existence theorems for nonlinear elasticity problems using convexity concepts. Here, we follow the fundamental results of Ball [13, 14] and the monographs of Ciarlet [38] and Dacorogna [42, 43].

To prove the existence of a solution for nonlinear elasticity problems we first have to introduce some tools from variational calculus.

Definition 4.19 (Lower semicontinuity)**.** *A functional $\mathcal{I} : X \mapsto \mathbb{R} \cup \{\infty\}$ is said to be lower semicontinuous in a Banach space X, if for every sequence $u_n \to u^*$ in X it holds that*

$$\liminf_{n\to\infty} \mathcal{I}(u_n) \geq \mathcal{I}(u^*).$$

Definition 4.20 (Weak lower semicontinuity)**.** *A functional $\mathcal{I} : X \mapsto \mathbb{R} \cup \{\infty\}$ is said to be weakly lower semicontinuous in a Banach space X, if for every sequence $u_n \rightharpoonup u^*$ in X it holds that*

$$\liminf_{n\to\infty} \mathcal{I}(u_n) \geq \mathcal{I}(u^*).$$

Definition 4.21 (Coercivity)**.** *A functional $\mathcal{I} : X \mapsto \mathbb{R} \cup \{\infty\}$ is called coercive in a Banach space X, if for every sequence $u_n \subset X$ with $\|u_n\|_X \to \infty$ it holds that $\mathcal{I}(u_n) \to \infty$.*

With these definitions we can state the fundamental theorem:

Theorem 4.22. *Let X be a reflexive Banach space and let the functional $\mathcal{I} : X \mapsto \mathbb{R} \cup \{\infty\}$ be weakly lower semicontinuous and coercive over X. Assume that there exists $\tilde{u} \in X$ with $\mathcal{I}(\tilde{u}) < \infty$, then the minimization problem*

$$\mathcal{I}(u) = \inf\{\mathcal{I}(v) : v \in X\}$$

has at least one solution $u^* \in X$.

Proof. This theorem is due to Meyers [126] and Morrey [130, 131]. For the proof and more information, e.g., see [43, Chapter 8]. □

This theorem allows us to show the existence of a solution for minimization problems if we have weakly lower semicontinuous functionals $\mathcal{I}$. Since this rather abstract concept is hard to show for concrete examples, we will give a proposition which links the convexity principle, see Section 4.4.6, with weak lower semicontinuity:

Proposition 4.23. *Let $\Omega \subset \mathbb{R}^3$ be a bounded open set and let $f : \mathbb{R}^{3\times 3} \mapsto [0,\infty]$ be quasiconvex and satisfying the following growth condition*

$$-\alpha(1+|\boldsymbol{\xi}|) \leq f(\boldsymbol{\xi}) \leq \alpha(1+|\boldsymbol{\xi}|^2) \text{ for every } \boldsymbol{\xi} \in \mathbb{R}^{3\times 3}$$

with $\alpha \geq 0$. Then

$$\mathcal{I}(\mathbf{u}) := \int_\Omega f(\nabla \mathbf{u})\,\mathrm{d}\mathbf{x}$$

is weakly lower semicontinuous in $[H^1(\Omega)]^3$.

Proof. See, e.g., [43, Theorems 8.4 and 8.11]. □

To apply the above mentioned theorems to the case of nonlinear elasticity we have to reformulate the equilibrium equations as a minimization problem.

Let $\Omega_0 \subset \mathbb{R}^3$ be a domain with a Lipschitz boundary $\partial\Omega_0 = \overline{\Gamma}_{0,\mathrm{D}} \cup \overline{\Gamma}_{0,\mathrm{N}}$ as considered in Section 3.4. In the following, we restrict ourselves to the case of vanishing body forces $\mathbf{b} = \mathbf{0}$. Note that the existence results also hold for sufficiently regular $\mathbf{b} \neq \mathbf{0}$.

We define the functional

$$\mathcal{I}(\mathbf{U},\mathbf{X}) := \int_{\Omega_0} W(\mathbf{F},\mathbf{X})\,\mathrm{d}\mathbf{X} - \int_{\Gamma_{0,\mathrm{N}}} \mathbf{t}_\mathrm{N}(\mathbf{U},\mathbf{X})\,\mathrm{d}S_\mathbf{X}, \tag{4.40}$$

where $W(\mathbf{F},\mathbf{X})$ is a strain-energy function and $\mathbf{t}_\mathrm{N}(\mathbf{X})$ is a surface traction on $\Gamma_{0,\mathrm{N}}$. Now we consider the minimization problem

$$\inf\{\mathcal{I}(\mathbf{U}) : \mathbf{U} \in \mathcal{H}(\Omega_0)\}, \tag{4.41}$$

with the space

$$\mathcal{H}(\Omega_0) = [H^1_{\mathbf{U}_\mathrm{D}}(\Omega_0)]^3 := \left\{\mathbf{U} \in H^1(\Omega_0,\mathbb{R}^3) : \mathbf{U}(\mathbf{X}) = \mathbf{U}_\mathrm{D}(\mathbf{X}) \text{ on } \Gamma_{0,\mathrm{D}}\right\}.$$

Note that we have $\det \mathbf{F} > 0$ for the considered elasticity problems, see Chapter 3.

Proposition 4.24. *Let $\mathbf{U}^*$ be sufficiently regular and a solution of* (4.41)*. Let the strain-energy function W be twice continuously differentiable, then $\mathbf{U}^*$ satisfies the weak system of the equilibrium equations* (4.6)

$$\int_{\Omega_0} \mathbf{FS}(\mathbf{U}^*,\mathbf{X}) : \operatorname{Grad}\mathbf{V}(\mathbf{X})\,\mathrm{d}\mathbf{X} - \int_{\Gamma_{0,\mathrm{N}}} \mathbf{t}_\mathrm{N}(\mathbf{U}^*,\mathbf{X}) \cdot \mathbf{V}(\mathbf{X})\,\mathrm{d}S_\mathbf{X} = 0,$$

for all $\mathbf{V}(\mathbf{X}) \in [H^1_0(\Omega_0)]^3$.

Proof. We show the equivalence of the minimization problem and the weak system of the equilibrium equations by using the first variation of $\mathcal{I}(\mathbf{U})$, i.e.

$$\phi(s) := \mathcal{I}(\mathbf{U}^* + s\mathbf{V})$$

for an arbitrary $\mathbf{V} \in [H_0^1(\Omega_0)]^3$. $\mathcal{I}(\mathbf{U}^*) = 0$ is fulfilled if $\phi(s)$ has a local extremal value at $s = 0$. Hence, we calculate the stationary point of the first variation, which yields

$$\nabla_s \mathcal{I}(\mathbf{U}^* + s\mathbf{V})|_{s=0} \stackrel{!}{=} 0. \tag{4.42}$$

The chain rule yields

$$\begin{aligned}\nabla_s \mathcal{I}(\mathbf{U}^* + s\mathbf{V}) = &\int_{\Omega_0} \frac{\partial W(\mathbf{F})}{\partial \mathbf{F}}(\mathbf{U}^* + s\mathbf{V}) : \frac{\partial \mathbf{F}(\mathbf{U}^* + s\mathbf{V})}{\partial s}\,\mathrm{d}\mathbf{X} \\ &- \int_{\Gamma_{0,\mathrm{N}}} \mathbf{t}_\mathrm{N}(\mathbf{U}^* + s\mathbf{V}) \cdot \mathbf{V}\,\mathrm{d}S_\mathbf{X}.\end{aligned}$$

Due to the linearity of the gradient we get

$$\nabla_s \mathcal{I}(\mathbf{U}^* + s\mathbf{V})|_{s=0} = \int_{\Omega_0} \frac{\partial W(\mathbf{F})}{\partial \mathbf{F}}(\mathbf{U}^*) : \mathrm{Grad}\,\mathbf{V}\,\mathrm{d}\mathbf{X} - \int_{\Gamma_{0,\mathrm{N}}} \mathbf{t}_\mathrm{N}(\mathbf{U}^*) \cdot \mathbf{V}\,\mathrm{d}S_\mathbf{X},$$

With (4.42), Theorem 3.8 and (3.14) we get the desired result. □

Remark 4.4.5. *Since the formulation of the weak form of the equilibrium equations in the reference and the current configuration are equivalent, a similar result to Proposition 4.24 is also valid for*

$$\int_{\Omega_t} \boldsymbol{\sigma}(\mathbf{u}^*, \mathbf{x}) : \boldsymbol{\varepsilon}(\mathbf{v}, \mathbf{x})\,\mathrm{d}\mathbf{x} - \int_{\Gamma_{t,\mathrm{N}}} \mathbf{t}_\mathrm{N}(\mathbf{x}) \cdot \mathbf{v}(\mathbf{x})\,\mathrm{d}s_\mathbf{x} = 0,$$

with $\mathbf{u}^* \in \mathcal{H}(\Omega_t)$ *and* $\mathbf{v} \in [H_0^1(\Omega_t)]^3$.

Remark 4.4.6. *A similar result to Proposition 4.24 holds also for incompressible and nearly incompressible elasticity models as described in Section 3.7 and Section 5.1.4, cf. [42, Section A.1.2].*

Hence, we have to show the polyconvexity of the strain-energy function $W(\mathbf{F})$, which is used to model the elastic material. Polyconvex $W(\mathbf{F})$ yield a weakly lower semi-continuous functional $\mathcal{I}(\mathbf{U})$, see Proposition 4.23 and Eq. (4.40). The minimization problem to find the infimum of $\mathcal{I}(\mathbf{U})$ with $\mathbf{U} \in \mathcal{H}$ is equivalent to the weak form of the equilibrium equations, cf. Proposition 4.24. With Theorem 4.22 we get the

existence of a solution. To summarize we fomulate the following theorem, known as John Ball's existence result.

Theorem 4.25 (John Ball's Existence Result)**.** *Let $\Omega \subset \mathbb{R}^3$ be a bounded Lipschitz domain. Let the strain energy function $W : \mathbb{R}^{3\times 3} \mapsto [0, \infty]$ be polyconvex, coercive and*

$$\lim_{\det \mathbf{F} \to 0} W(\mathbf{F}, \mathbf{x}) = +\infty.$$

Let the traction force $\mathbf{t}_{\mathrm{N}}(\mathbf{x})$ be such that the linear form $\langle \mathbf{f}, \mathbf{v} \rangle$ is well defined and continuous. Let the Dirichlet boundary conditions $\mathbf{u}_{\mathrm{D}}(\mathbf{x}) : \Gamma_0 \mapsto \mathbb{R}^3$ be a measurable function on $\Gamma_{\mathrm{D}} \neq \emptyset$ such that

$$\mathcal{H} = \left\{ \mathbf{u} \in H^1(\Omega, \mathbb{R}^3) : \mathbf{u}(\mathbf{x}) = \mathbf{u}_{\mathrm{D}}(\mathbf{x}) \text{ on } \Gamma_{\mathrm{D}} \text{ and } \det \mathbf{F} > 0 \right\} \neq \emptyset.$$

Let there exist $\tilde{\mathbf{u}} \in \mathcal{H}$ such that $\mathcal{I}(\tilde{\mathbf{u}}) < \infty$, with

$$\mathcal{I}(\mathbf{u}) = \int_{\Omega} W(\mathbf{F}, \mathbf{x}) \, \mathrm{d}\mathbf{x} - \int_{\Gamma_{\mathrm{N}}} \mathbf{t}_{\mathrm{N}}(\mathbf{u}, \mathbf{x}) \, \mathrm{d}s_{\mathbf{x}}.$$

Then there exists at least one $\mathbf{u}^* \in \mathcal{H}$ which satisfies

$$\mathcal{I}(\mathbf{u}^*) \leq \mathcal{I}(\mathbf{u}) \quad \text{for all } \mathbf{u} \in \mathcal{H}$$

and hence solves the equilibrium equations.

Proof. Following [13, Theorems 7.3 and 7.6]. For the full proof see , e.g., [38, Section 7.7] and [42, Section A.1]. □

Remark 4.4.7. *The coercivity and the assumption $W(\mathbf{F}, \mathbf{x}) \to +\infty$ for $\det \mathbf{F} \to 0$ reflect the property that large deformations must accompany large strains.*

Remark 4.4.8. *The linear form $\langle \mathbf{f}, \mathbf{v} \rangle$ is well defined and continuous for a traction force $\mathbf{t}_{\mathrm{N}} \in H^{-1/2}(\Gamma_{\mathrm{N}})$ and $\mathbf{v} \in [H_0^1(\Omega)]^3$.*

Remark 4.4.9. *It is worth to mention that the solution is not necessarily unique. Physical examples of non-uniqueness one may find, e.g., in [38, Section 5.8].*

4.4.8 Convexity of the Specific Nonlinear Elasticity Models

A large class of materials are the so-called *Ogden materials*, see Section 3.10.1. A subclass of Ogden materials are *Mooney–Rivlin* (3.44) and *neo–Hookean materials* (3.45).

Remark 4.4.10. *Ogden material models give rise to a* polyconvex *stored energy function W and in the case of neo–Hookean materials this function is even* convex *[43].*

Lemma 4.26. *The strain-energy function for the artery model*

$$\Psi(\mathbf{C}) = \frac{c}{2}(I_1 - 3) + \frac{k_1}{2k_2} \sum_{i=4,6} \Big\{ \exp[k_2(I_i - 1)^2] - 1 \Big\},$$

see Section 3.11 is convex *if all involved constants are positive and $I_4, I_6 > 1$. The strain-energy function for the myocardium model*

$$\Psi(\mathbf{C}) = \frac{a}{2b} \exp\left[b(I_1 - 3)\right] + \sum_{i=f,s} \frac{a_i}{2b_i} \Big\{ \exp[b_i(I_{4i} - 1)^2] - 1 \Big\} + \frac{a_{\mathrm{fs}}}{2b_{\mathrm{fs}}} \Big[\exp(b_{\mathrm{fs}} I_{8\mathrm{fs}}^2) - 1 \Big],$$

see Section 3.12, is locally convex *if all involved constants are positive and $I_{4\mathrm{f}}, I_{4\mathrm{s}} > 1$.*

Proof. The convexity of the strain-energy function follows if we can show the requirements of Lemma 4.17. Since the sum of convex functions remains convex, we show the two constraints (4.38) and (4.39) for each summand in the strain-energy function $\Psi(\mathbf{C})$. As one can easily see later, a strict inequality cannot be achived as $\mathbf{H}$ is arbitrary. For the convexity of the isotropic part of the artery model, which is nothing else than the neo–Hooke model, cf. 4.4.10. For the isotropic part of the myocardium model we have, using the chain rule, the first Fréchet derivative

$$D_{\mathbf{C}} \left(\frac{a}{2b} \exp[b(I_1(\mathbf{C}) - 3)] \right) = \frac{a}{2} \exp[b(I_1(\mathbf{C}) - 3)] \, D_{\mathbf{C}} I_1(\mathbf{C}), \tag{4.43}$$

with

$$D_{\mathbf{C}} I_1(\mathbf{C}) = D_{\mathbf{C}} \operatorname{tr}(\mathbf{C}) = \mathbf{I}.$$

Hence, the requirement (4.39) in Lemma 4.17 holds for $a \geq 0$. The second Gâteaux derivative is, using (4.43)

$$D_{\mathbf{C}}^2 \left(\frac{a}{2b} \exp[b(I_1(\mathbf{C}) - 3)] \right).(\mathbf{H}, \mathbf{H}) = \frac{ab}{2} \exp[b(I_1(\mathbf{C}) - 3)] (D_{\mathbf{C}} I_1(\mathbf{C}).\mathbf{H})^2.$$

With $I_1(\mathbf{C}) = \mathrm{tr}(\mathbf{C})$ and the definition of the Gâteaux derivative 4.7 we get

$$D^2_{\mathbf{C}}\left(\frac{a}{2b}\exp[b(I_1(\mathbf{C})-3)]\right).(\mathbf{H},\mathbf{H}) = \frac{ab}{2}\exp[b(I_1(\mathbf{C})-3)](\mathrm{tr}\,\mathbf{H})^2$$

which has to hold for all $\mathbf{H}$. Hence, we require that $a \geq 0$ and $b \geq 0$. Note that this holds by definition, see (3.57).

The terms corresponding to stretches in fiber directions have the structure

$$\psi(\mathbf{C}) := \frac{c_1}{2c_2}\left\{\exp[c_2(I(\mathbf{C},\mathbf{a})-1)^2]-1\right\},$$

where c_1, c_2 are constants and $\mathbf{a} \in \mathbb{R}^3$ is a constant vector, i.e a fiber direction. The first Fréchet derivative of this exponential function yields

$$D_{\mathbf{C}}\,\psi(\mathbf{C}) = c_1\exp[c_2(I(\mathbf{C},\mathbf{a})-1)^2]\,(I(\mathbf{C},\mathbf{a})-1)\,D_{\mathbf{C}}I(\mathbf{C},\mathbf{a}). \tag{4.44}$$

With Lemma A.2 we can write the invariants I_4, I_6, $I_{4\mathrm{s}}$ and $I_{4\mathrm{f}}$ in the form $I(\mathbf{C},\mathbf{a}) = \mathrm{tr}(\mathbf{C}(\mathbf{a}\otimes\mathbf{a}))$ and we obtain, using (A.15), (A.26) and Corollary A.1,

$$D_{\mathbf{C}}I(\mathbf{C},\mathbf{a}) = \mathbf{a}\otimes\mathbf{a}$$

which is a symmetric and positive semi-definite 3×3 matrix. Hence, we require that $c_1 > 0$ and $I(\mathbf{C},\mathbf{a}) \geq 1$ to fulfill (4.39). The latter holds since the anisotropic parts only contribute given a stretch in fiber direction, i.e. the corresponding invariants are larger than one; cf. Eqs. (3.55), (3.58) and (3.59). Using (4.44) we get for the second Gâteaux derivative

$$\begin{aligned} D^2_{\mathbf{C}}\,\psi(\mathbf{C}).(\mathbf{H},\mathbf{H}) = c_1\exp[c_2(I(\mathbf{C},\mathbf{a})-1)^2]\Big\{&2c_2(I(\mathbf{C},\mathbf{a})-1)^2\,(D_{\mathbf{C}}I(\mathbf{C},\mathbf{a}).\mathbf{H})^2 \\ &+(D_{\mathbf{C}}I(\mathbf{C},\mathbf{a}).\mathbf{H})^2\Big\}. \end{aligned}$$

Thus, (4.38) holds for $c_1 \geq 0$ and $c_2 \geq 0$. The requirement that all constants, i.e. k_1, k_2, a_{f}, b_{f}, a_{s} and b_{s}, are positive, fits with the histology of the biological materials, cf. Eqs. (3.50), (3.58) and (3.59). Hence, we have shown convexity of the strain-energy function for the artery model.

To show local convexity of the myocardium model we first compute the Fréchet derivative of the orthotropic part is using $I_{8\mathrm{fs}} = I_{8\mathrm{fs}}(\mathbf{C},\mathbf{f}_0,\mathbf{s}_0)$

$$D_{\mathbf{C}}\,\frac{a_{\mathrm{fs}}}{2b_{\mathrm{fs}}}\left\{\exp(b_{\mathrm{fs}}I^2_{8\mathrm{fs}})-1\right\} = a_{\mathrm{fs}}\exp(b_{\mathrm{fs}}I^2_{8\mathrm{fs}})\,I_{8\mathrm{fs}}\,D_{\mathbf{C}}I_{8\mathrm{fs}} \tag{4.45}$$

$$= a_{\mathrm{fs}}\exp(b_{\mathrm{fs}}I^2_{8\mathrm{fs}})\,I_{8\mathrm{fs}}\,\frac{1}{2}(\mathbf{f}_0\otimes\mathbf{s}_0+\mathbf{f}_0\otimes\mathbf{s}_0). \tag{4.46}$$

Note that this term is not necessarily positive definite and thus does not fulfill the constraint (4.39). This means that we cannot show convexity of the orthotropic part. Using (4.45) we get for the second Gâteaux derivative

$$D^2_{\mathbf{C}}\left(\frac{a_{\mathrm{fs}}}{2b_{\mathrm{fs}}}\left\{\exp(b_{\mathrm{fs}}I^2_{8\mathrm{fs}})-1\right\}\right).(\mathbf{H},\mathbf{H}) = a_{\mathrm{fs}}\exp(b_{\mathrm{fs}}I^2_{8\mathrm{fs}})\left(2b_{\mathrm{fs}}I^2_{8\mathrm{fs}}(D_{\mathbf{C}}I_{8\mathrm{fs}}.\mathbf{H})^2 + (D_{\mathbf{C}}I_{8\mathrm{fs}}.\mathbf{H})^2\right),$$

which is positive for $a_{\mathrm{fs}} \geq 0$ and $b_{\mathrm{fs}} \geq 0$. So we can at least show (4.39) which gives us the local convexity of the strain-energy of the myocardium model. □

Lemma 4.27. *For nearly incompressible materials a decomposition in a volume deserving and a volume dilating part, see Section 3.7.1, is used. Given that the strain-energy function $\overline{W}(\mathbf{F})$ is polyconvex we can state that the decomposed strain-energy function*

$$W(\mathbf{F}) = \overline{W}\left(\frac{\mathbf{F}}{\det(\mathbf{F})^{1/3}}\right) + U(\det(\mathbf{F}))$$

is polyconvex for all models considered in this work.

Proof. See Charrier et al. [36] or Hartmann and Neff [73]. □

It is easy to see that for $\mathbf{U} = \mathbf{0}$ it holds that $\mathbf{C} = \mathbf{I}$ and hence $\Psi(\mathbf{I}) < \infty$. Using Definition 4.40 we get $\mathcal{I}(\mathbf{0}) < \infty$ for a bounded Lipschitz domain Ω. Thus, we fulfill the requirements of Theorem 4.25 and obtain the existence of a solution for the system of equations arising from the considered isotropic models and the artery. With Remark 4.4.6 and 4.27 we have the same for the incompressible and nearly incompressible case.

For the myocardium model we have a loss of convexity and ellipticity in the sense of Lemma 4.18. This loss can cause instabilities and failure modes, e.g., fiber debonding, weak surface discontinuities and fiber kinking or splitting, see Merodio and Ogden [124, 125]. Note that these failures might be physically correct (for extreme displacements) and within a physiological range of deformation the ellipticity condition may even hold. Nonetheless, ellipticity for a reasonable range of deformation is not enough to establish an existence theorem for the myocardium model.

5 DISCRETIZATION

In almost every practical application an exact solution of the variational formulations discussed in Chapter 4 is not possible. Hence, we use discretization techniques, in particular the finite element method (FEM), see Section 5.1, as powerful numerical tools to find an approximate solution of the equilibrium equations.

To apply an inexact Newton method, see Section 5.2, we take a closer look at the discretization of the linearized variational formulations arising from nonlinear elasticity and the assembling of the corresponding stiffness matrices, see Section 5.3.

The resulting series of linear systems of equations may contain, especially for practical applications, a very high number of degrees of freedom. Hence, we need elaborate algorithms to solve such a system. In Section 5.6 we outline the most common direct and iterative solution methods.

5.1 Galerkin Discretizations and Finite Element Method

We consider the bounded and nonlinear operator $A(\mathbf{u})$, satisfying the variational formulation (4.5):

$$\mathbf{u} \in X: \quad \langle A(\mathbf{u}), \mathbf{v} \rangle = \langle \mathbf{f}, \mathbf{v} \rangle \quad \text{for all } \mathbf{v} \in X.$$

For $M \in \mathbb{N}$ let

$$X_M := \operatorname{span} \{\varphi_k\}_{k=1}^{M} \subset X$$

be a conforming ansatz space. With

$$\mathbf{u}_M := \sum_{k=1}^{M} \mathbf{u}_k \varphi_k \in X_M$$

we formulate an approximate solution of the *Galerkin–Bubnov variational formulation* to find

$$\mathbf{u}_M \in X_M: \quad \langle A(\mathbf{u}_M), \mathbf{v}_M \rangle = \langle \mathbf{f}, \mathbf{v}_M \rangle \quad \text{for all } \mathbf{v}_M \in X_M.$$

For stability and error estimates of this approximation we refer to the following *Céa's Lemma* and the *Lemmas of Strang*. For more information see the book of Steinbach [176].

Theorem 5.1 (Céa's Lemma)**.** *Let $a : X \times X' \to \mathbb{R}$ be a bounded and X–elliptic bilinear form. Moreover let f be a bounded linear form in X and $X_h \subset X$ be a finite dimensional ansatz space. Then the discrete version of the variational formulation*

$$a(\mathbf{u}_h, \mathbf{v}_h) = \langle \mathbf{f}, \mathbf{v}_h \rangle \quad \textit{for all } \mathbf{v}_h \in X_h$$

is uniquely solvable. For the discrete solution $u_h \in X_h$ the following stability estimate

$$\|\mathbf{u}_h\|_X \leq \frac{1}{c_1^A} \|\mathbf{f}\|_{X'}$$

and the error estimate

$$\|\mathbf{u} - \mathbf{u}_h\|_X \leq \frac{c_2^A}{c_1^A} \inf_{\mathbf{v}_h \in X_h} \|\mathbf{u} - \mathbf{v}_h\|_X$$

hold.

Proof. See for example [176, Section 8.1]. □

For the nonlinear case we may apply Céa's Lemma to the discrete version of the linearized bilinear form $a'(\delta\mathbf{u}_h, \mathbf{v})$ with $\delta\mathbf{u}_h \in X$ the approximation of $\Delta\mathbf{u}$, see Sections 4.4.5 and 5.2.

To find an approximate solution of the variational problem (4.5), we will use the finite element method (FEM). This numerical technique goes about one hundred years back to Galerkin [61], Ritz [148], and Schellbach [159]. For this we will construct finite-dimensional ansatz spaces V_h, typically containing piecewise polynomial functions of degree k, and then find an approximate solution $\mathbf{u}_h \in V_h$. In the following, the parameter h indicates that we have a finite-dimensional approximation. Under appropriate assumptions, i.e. the regularity of the solution, we can estimate the approximation error by

$$\inf_{\mathbf{v}_h \in V_h} \|\mathbf{u}^* - \mathbf{v}_h\|_{[H^1(\Omega)]^3} \leq c h^k |\mathbf{u}^*|_{[H^{k+1}(\Omega)]^3},$$

with $\mathbf{u}^*$ the unique exact solution of the variational formulation. Using the *Aubin–Nitsche Trick* [176, Section 11.1], this approximation error can be formulated in the L_2 space:

$$\inf_{\mathbf{v}_h \in V_h} \|\mathbf{u}^* - \mathbf{v}_h\|_{[L^2(\Omega)]^3} \leq c h^{k+1} |\mathbf{u}^*|_{[H^{k+1}(\Omega)]^3}.$$

For further information on the finite element method the interested reader is referred to the classical works of Ciarlet [39] and Zienkiewicz [192]. From the almost overwhelming amount of more recent publications we want to mention the monographs by Braess [25], Brenner and Scott [29], Jung and Langer [100], and Steinbach [176].

For the pure displacement problem in elastostatics we have as starting point for the finite element formulation the primal variational problem (4.5). In using Galerkin's principle of discretization we choose an appropriate finite-dimensional subspace $V_h \subset [H^1_{\mathrm{D}}(\Omega, \Gamma_{\mathrm{D}})]^3$. Hence, we want to compute the approximate solution $\mathbf{u}_h \in V_h$ of the finite-dimensional variational problem

$$a(\mathbf{u}_h, \mathbf{v}_h) = \langle \mathcal{F}, \mathbf{v}_h \rangle, \tag{5.1}$$

for the finite-dimensional test functions $\mathbf{v}_h \in V_h^0 \subset [H^1_0(\Omega, \Gamma_{\mathrm{D}})]^3$. In the nonlinear case, see (4.22) and (4.26), we want to solve

$$a'(\delta\mathbf{u}_h, \mathbf{v}_h) = \langle \mathcal{R}, \mathbf{v}_h \rangle$$

in each Newton step for $\delta\mathbf{u}_h \in V_h$ and $\mathbf{v}_h \in V_h^0$.

Inhomogeneous and homogeneous Dirichlet boundary conditions are included using standard homogenization techniques. For more information, e.g., cf. [100, Section 4.5].

5.1.1 Discretization in Finite Elements

Let $\Omega \subset \mathbb{R}^3$ be a bounded domain which is subdivided into N *finite elements* τ_l such that

$$\overline{\Omega}_h = \bigcup_{l=1}^{N} \overline{\tau}_l \ , \quad \text{with } \overline{\Omega}_h \to \ \overline{\Omega} \ , \quad \text{for } h \to 0. \tag{5.2}$$

Our choice for the finite elements in $\mathbb{R}^3$ are polyhedral tetrahedrons and hexahedrons. To approximate the fine structures on the surface of arterial and cardiac tissues a discretization in tetrahedrons shows the best results.

For each finite element τ_l we define the volume Δ_l and the local mesh size h_l as

$$\Delta_l := \int_{\tau_l} \mathrm{d}\mathbf{x} \quad \text{and} \quad h_l := \Delta_l^{1/3}.$$

With this we can define the *global mesh size* as

$$h := \max_{l=1,\cdots,N} h_l.$$

All elements of our discretized mesh can be derived from one specific element the so-called *reference element* τ. In the case of tetrahedrons the reference element is given through

$$\tau = \left\{ \boldsymbol{\xi} \in \mathbb{R}^3 : 0 \leq \xi_1 \leq 1, 0 \leq \xi_2 \leq 1 - \xi_1, 0 \leq \xi_3 \leq 1 - \xi_1 - \xi_2 \right\}.$$

For an arbitrary $\mathbf{x} \in \tau_l$ we then have the following representation

$$\mathbf{x} = \mathbf{x}_{l_1} + \sum_{i=1}^{3} \boldsymbol{\xi}(\mathbf{x}_{l_{i+1}} - \mathbf{x}_{l_1}) = \mathbf{x}_{l_1} + J_l \boldsymbol{\xi} \quad \text{for } \boldsymbol{\xi} \in \tau$$

with the Jacobian matrix

$$J_l = \begin{pmatrix} x_{l_2,1} - x_{l_1,1} & x_{l_3,1} - x_{l_1,1} & x_{l_4,1} - x_{l_1,1} \\ x_{l_2,2} - x_{l_1,2} & x_{l_3,2} - x_{l_1,2} & x_{l_4,2} - x_{l_1,2} \\ x_{l_2,3} - x_{l_1,3} & x_{l_3,3} - x_{l_1,3} & x_{l_4,3} - x_{l_1,3} \end{pmatrix} = \begin{pmatrix} \frac{\partial x_1}{\partial \xi_1} & \frac{\partial x_1}{\partial \xi_2} & \frac{\partial x_1}{\partial \xi_3} \\ \frac{\partial x_2}{\partial \xi_1} & \frac{\partial x_2}{\partial \xi_2} & \frac{\partial x_2}{\partial \xi_3} \\ \frac{\partial x_3}{\partial \xi_1} & \frac{\partial x_3}{\partial \xi_2} & \frac{\partial x_3}{\partial \xi_3} \end{pmatrix}. \tag{5.3}$$

With a simple calculation we get for the volume

$$\Delta_l = \frac{1}{6} |\det J_l| \ .$$

For an arbitrary function $v(\mathbf{x})$ we then have the representation

$$v(\mathbf{x}) = v(\mathbf{x}_{l_1} + J_l \boldsymbol{\xi}) = \tilde{v}_l(\boldsymbol{\xi}) \quad \text{for } \boldsymbol{\xi} \in \tau \ .$$

and for the gradient

$$\nabla_{\mathbf{x}} v(\mathbf{x}) = J_l^{-\top} \nabla_{\boldsymbol{\xi}} \tilde{v}_l(\boldsymbol{\xi}) \ , \quad \nabla_{\boldsymbol{\xi}} \tilde{v}_l(\boldsymbol{\xi}) = J_l^{\top} \nabla_{\mathbf{x}} v(\mathbf{x}).$$

5.1.2 Shape Functions

We now define ansatz spaces for the discretization Ω_h, (5.2). These spaces are constructed by piecewise polynomial functions, called shape functions. They are locally defined on the specific finite elements τ_l.

A simple possibility to discretize the variational formulations described in Section 4.2 are to use piecewise linear shape functions for each component of the displacement field $\mathbf{u}$. Unless otherwise indicated, we will use this kind of shape functions for our numerical simulations. The other type that is used are piecewise quadratic shape functions, which show advantages for the simulation of nearly incompressible materials.

Example 5.1. *For tetrahedrons the* linear shape functions *for the displacement field are given with*

$$\varphi_1^1(\boldsymbol{\xi}) := 1-\xi_1-\xi_2-\xi_3,\ \varphi_2^1(\boldsymbol{\xi}) := \xi_1,\ \varphi_3^1(\boldsymbol{\xi}) := \xi_2,\ \varphi_4^1(\boldsymbol{\xi}) := \xi_3,\ \textit{for } \boldsymbol{\xi} \in \tau.$$

Let τ_l be an arbitrary tetrahedral finite element with the nodes $x_{l_1}, x_{l_2}, x_{l_3}, x_{l_4}$. Then we have for a linear function, given in τ_l, the following representation:

$$v_h(\mathbf{x}) = v_h(\mathbf{x}_{l_1} + J_l\boldsymbol{\xi}) = \sum_{k=1}^{4} v_{l_k}\varphi_k^1(\boldsymbol{\xi}) \quad \textit{for } \mathbf{x} \in \tau_l, \boldsymbol{\xi} \in \tau\ ,$$

with coefficients v_{l_k}.

See Jung and Langer [100] or Braess [25] for higher-order shape functions and shape functions on many different elements.

From the discrete variational formulation (5.1) we get with the basis representation for the wanted solution vector $\mathbf{u}_h = \sum_i \mathbf{u}_i\varphi_i$ the linear system of equations

$$\mathbf{K}_h\underline{u} = \underline{b}, \tag{5.4}$$

where $\underline{u} \in \mathbb{R}^m$ is the vector consisting of the coefficients $\mathbf{u}_i$, $\mathbf{K}_h \in \mathbb{R}^{m\times m}$ the stiffness matrix, $\underline{b} \in \mathbb{R}^m$ the right hand side vector and m the number of degrees of freedom. The entries of the stiffness matrix are determined by $\mathbf{K}_h = [a(\varphi_j, \varphi_i)]_{i,j\in\omega_h}$ with ω_h the node-indices of nodes on $\Omega \cup \Gamma_{\mathrm{N}}$. The right hand side vector by $\underline{b} = [\langle \mathbf{f}, \varphi_i\rangle]_{i\in\omega_h}$. For the nonlinear case see (5.9).

5.1.3 Discretization of the Saddle Point Formulation

In this section we will sketch two possible choices of finite elements that can be used to treat saddle point problems (cf. 4.3.1). For additional information and other finite elements that may be of interest we refer to Braess [25] and Crouzeix and Raviart [41].

Let $\mathcal{X}_h$ and $\mathcal{M}_h$ the discrete version of the spaces defined in (4.12).

$\mathcal{Q}_k - \mathcal{P}_0$ element For this hexahedral element we use ansatz functions of polynomial degree $k \geq 1$ for the displacement $\mathbf{u}$ and piecewise constant functions for the pressure p, i.e.

$$\begin{aligned}\mathcal{X}_h &:= \{\mathbf{v} \in C^0(\overline{\Omega})^3 :\ \mathbf{v}|_\tau \in \mathcal{Q}_k \text{ for } \tau \in \Omega_h, k \geq 1\},\\ \mathcal{M}_h &:= \{q \in L_2(\Omega) :\ q|_\tau \in \mathcal{P}_0 \text{ for } \tau \in \Omega_h\}.\end{aligned}$$

Concerning the saddle point system arising from nearly incompressible linear elasticity this element with $k = 1$ does not fulfill the *inf-sup-condition*, also called the LBB-condition, from Ladyzhenskaya [113], Babuška [10] and Brezzi [30]. Nonetheless, it can be stabilized, see [103, 104].

$\mathcal{P}_k - \mathcal{P}_0$ element: the tetrahedral counterpart of the $\mathcal{Q}_k - \mathcal{P}_0$ element.

For the stability of the $\mathcal{Q}_2 - \mathcal{P}_0$ element and the $\mathcal{P}_2 - \mathcal{P}_0$ element for the Stokes problem and the nearly incompressible linear elasticity problem in 2D compare to Boffi et al. [22, 23]. To the best of our knowledge no stability proofs for nonlinear elasticity are yet known. It is known that linear finite elements are very prone to volumetric locking. Hence, for nearly incompressible materials piecewise quadratic elements ($k = 2$) are a better choice, see Simo [169].

Taylor–Hood element In contrast to the above mentioned $\mathcal{Q}_1 - \mathcal{P}_0$ element, the Taylor–Hood element fulfills the inf-sup-condition for the case of almost incompressible linear elasticity and is therefore considered as stable. Furthermore, it shows better approximation properties than the $\mathcal{P}_2 - \mathcal{P}_0$ element. We use quadratic ansatz functions for the displacement $\mathbf{u}$ and linear ansatz functions for the pressure p, i.e.

$$\begin{aligned} \mathcal{X}_h &:= \{\mathbf{v}_h \in C(\overline{\Omega})^3 \cap H_0^1(\Omega)^3 : \ \mathbf{v}_h|_\tau \in \mathcal{P}_2 \text{ for } \tau \in \Omega_h\}, \\ \mathcal{M}_h &:= \{q_h \in C(\Omega) \cap L_2(\Omega) : q_h|_\tau \in \mathcal{P}_1 \text{ for } \tau \in \Omega_h\}. \end{aligned}$$

For the proof of the inf-sup-condition compare to Girault and Raviart [64] and Verfürth [183].

In the case of domain decomposition approaches, the usage of Taylor–Hood elements is not straightforward and the continuity of the pressure across the interface imposes difficulties especially concerning preconditioning and the scalability of the parallel algorithms [20, 34, 171]. Thus, the emphasis is on standard finite elements ($\mathcal{P}_k$) and $\mathcal{P}_k - \mathcal{P}_0$ elements in the following. We show no results for hexahedral elements as they are comparable to tetrahedral elements [35] and, in addition, meshes for practical applications were provided with tetrahedral elements.

The difference in the order of the displacement and the pressure in all introduced elements is motivated by the differential operators that appear. For the displacement we have derivatives up to second order, while for the pressure we have to compute the gradient of p, hence first order.

5.1.4 Static Condensation and Mean Dilatation Technique

While the deformation $\mathbf{u}$ is continuous over the whole domain Ω, the volumetric variables can be modeled to be discontinuous across element boundaries, e.g. as piecewise constants, in the finite element formulation. Hence, the hydrostatic pressure $p(\mathbf{u})$, see (3.31), can be eliminated at the element level, a procedure which is known as *static condensation*. This results in a nonlinear problem in the unknown displacement field $\mathbf{u}$, that is solved using a Newton scheme.

The related mean dilatation technique goes back to Nagtegaal et al. [132] and it has shown that it prevents locking effects when we deal with almost incompressible materials like biological tissue. For more information on this approach see the works of Holzapfel [81], Hughes [90], Simo [169], and Simo et al. [170].

Here, we have an additional variational formulation for the volumetric variables J and p. Since we have defined the hydrostatic pressure p in Eq. (3.31) such that $p = \mathrm{d}U(J)/\mathrm{d}J$ it is sufficient to concentrate on the Jacobian J. Let $\overline{J}$ be a scalar variable that satisfies $\overline{J} = J$ in a weak sense, i.e.

$$\int_{\Omega_0} \left(\overline{J} - J(\mathbf{U}, \mathbf{X})\right) q(\mathbf{X}) \, \mathrm{d}\mathbf{X} = 0, \quad \text{for all } q \in L_2(\Omega_0). \tag{5.5}$$

The idea of the mean dilatation method is to eliminate this volumetric variable element-wise (static condensation) using using discontinuous ansatz functions, where we will concentrate on piecewise constants. Let $\tau_0 \subset \Omega_0$ be an arbitrary finite element. We choose q_h, such that it is constant over the element domain τ_0 and zero elsewhere. Hence, the discretized version of (5.5) in the element domain τ_0 reads

$$\int_{\tau_0} \left(\overline{J}_h - J(\mathbf{U}, \mathbf{X})\right) \mathrm{d}\mathbf{X} = 0.$$

Since the element-wise constant $\overline{J}_h$ does not depend on $\mathbf{X}$ in τ_0, we obtain

$$\overline{J}_h \int_{\tau_0} \mathrm{d}\mathbf{X} - \int_{\tau_0} J(\mathbf{U}, \mathbf{X}) \, \mathrm{d}\mathbf{X} = 0.$$

Let $\mathrm{vol}(\tau_0)$ and $\mathrm{vol}(\tau)$ be the volumes of the domain τ_0 in the reference configuration and in the current configuration, respectively. Using (3.5) we get

$$\overline{J}_h = \frac{\mathrm{vol}(\tau)}{\mathrm{vol}(\tau_0)}.$$

With this we may calculate the discretized version $\overline{p}_h$ of the hydrostatic pressure p using (3.31). In the arbitrary domain τ_0, where both volumetric functions are

constant, we can state

$$\overline{p}_h = \left.\frac{\mathrm{d}U(\overline{J}_h)}{\mathrm{d}\overline{J}_h}\right|_{\overline{J}_h=\frac{\mathrm{vol}(\tau)}{\mathrm{vol}(\tau_0)}},$$

with the scalar variable $\overline{p}$, such that $\overline{p} = p$ is satisfied in a weak sense.

Example 5.2. *With a function $U(J)$ as defined in* (3.30) *we get for the hydrostatic pressure in an arbitrary element τ_0*

$$\overline{p}_h = \kappa\left(\frac{\mathrm{vol}(\tau)}{\mathrm{vol}(\tau_0)} - 1\right).$$

These piecewise constant volumetric variables are incorporated in the discrete version of the decoupled variational formulation, see Section 5.3. This leads, as in the pure static condensation case, to a $\mathcal{Q}_k - \mathcal{P}_0$ element for hexahedrons and a $\mathcal{P}_k - \mathcal{P}_0$ element for tetrahedrons, where k is the order of the base functions for the displacement field. Due to considerations in Section 5.1.3 we choose piecewise quadratic elements ($k = 2$) for nearly incompressible The resulting $\mathcal{P}_2 - \mathcal{P}_0$ element was also the choice to model nearly incompressible arterial materials in the papers of Augustin et al. [7, 8], Balzani et al. [16, 17], Brands et al. [27, 28], and Klawonn and Rheinbach [106].

5.2 Inexact Newton Methods

In the case of the numerical solution of nonlinear elasticity problems we have to take function and derivative approximations into account. Hence, we have to study inexact Newton methods of the kind

$$F'(x^k)\delta x^k = -F(x^k) + r^k, \quad x^{k+1} = x^k + \delta x^k,$$

with the inexact Newton corrections δx^k. Equivalently, using (4.17), this can be written as

$$F'(x^k)(\delta x^k - \Delta x^k) = r^k, \quad x^{k+1} = x^k + \delta x^k,$$

where Δx^k are the exact Newton corrections. In this work we use Galerkin methods as a dicretization technique. Thus, we focus on *Newton-Galerkin methods* [49] as described in the following. For $x^k \in H^1(\Omega)$ we have the scheme

$$x^{k+1} = x^k + \delta x^k,$$

where the inexact Newton corrections δx^k have to satisfy

$$\langle x^k, F'(x^k)(\delta x^k - \Delta x^k)\rangle = \langle \delta x^k, r^k\rangle \ . \tag{5.6}$$

As a theoretical framework to the convergence properties of the above Newton–Galerkin method we formulate the following Newton–Mysovskikh type theorem.

Theorem 5.2 (Newton–Mysovskikh)**.** *Let $D \subset H^1(\Omega)$ be an open and convex subset equipped with the norm $\|\bullet\|_{\mathrm{D}}$. Let $f : D \to \mathbb{R}$ be a twice continuously differentiable functional which is minimized over D. Let $F'(x) = f''(x)$ such that it is strictly positive and fulfills the affine conjugate Lipschitz condition*

$$\|F'(z)^{-1/2}(F'(y) - F'(x))v\|_{\mathrm{D}} \le \omega \|F'(x)^{-1/2}(y-x)\|_{\mathrm{D}} \dot{\|} F'(x)^{1/2} v\|_{\mathrm{D}},$$

with $0 \le \omega < \infty$ and collinear $x, y, z \in D$. We consider a Newton–Galerkin method satisfying (5.6) *with*

$$\delta_k := \frac{\|F'(x^k)^{1/2}(\delta x^k - \Delta x^k)\|_{\mathrm{D}}}{\|F'(x^k)^{1/2}\delta x^k\|_{\mathrm{D}}}$$

the approximation errors. Define the so-called Kantorovich quantities

$$\eta_k := \omega \|F'(x^k)^{1/2}\Delta x^k\|_{\mathrm{D}}, \quad \eta_k^\delta := \omega \|F'(x^k)^{1/2}\delta x^k\|_{\mathrm{D}} = \frac{\eta_k}{\sqrt{1+\delta_k^2}}$$

for any well-defined iterate x^k. Assume that for an initial guess $x^0 \in D$ the level set

$$\mathcal{L} := \left\{ x \in D : f(x) \le f(x^0) \right\} \neq \emptyset$$

is bounded and closed. Then it holds:

1. (Linear convergence) *Let the initial guess x_0 satisfy for a constant $\Theta < 1$*

$$\eta_0 \le 2\Theta < 2 \tag{5.7}$$

and assume that $\delta_{k+1} \ge \delta_k$ for all k. Let the Galerkin approximation be such that

$$\frac{\eta_k^\delta + \delta_k\left(\eta_k^\delta + \sqrt{4 + (\eta_k^\delta)^2}\right)}{2\sqrt{1+\delta_k^2}} \le \Theta.$$

Then we have a minimizing point $x^* \in \mathcal{L}_0$ such that the iterates $x^k \in \mathcal{L}_0$ converge to x^* at least linearly, i.e.

$$\eta_{k+1} \le \Theta\eta_k \ \text{ and } \ \eta_{k+1}^\delta \le \Theta\eta_k^\delta.$$

2. (Quadratic convergence) *Let the initial guess x_0 satisfy for a constant $\theta > 0$*

$$\eta_0 < \frac{2}{1+\theta} \tag{5.8}$$

and let the Galerkin approximation be such that

$$\delta_k \leq \frac{\theta \eta_k^\delta}{\eta_k^\delta + \sqrt{4 + (\eta_k^\delta)^2}}.$$

Then $x^k \in \mathcal{L}_0$ converge quadratically to the minimizing point $x^* \in \mathcal{L}_0$, i.e.

$$\eta_{k+1} \leq \frac{(1+\theta)}{2}(\eta_k)^2 \text{ and } \eta_{k+1}^\delta \leq \frac{(1+\theta)}{2}(\eta_k^\delta)^2.$$

Proof. For more information and the proof see [49, Sections 2.3 and 8.3]. □

In our case the assumptions of Theorem 5.2 are satisfied due to the properties of the strain-energy function, see Remark 3.6.4 (Normalization Conditions), and the equivalence to the minimization problem (4.41). Using Eq. (4.17) we can write η_0 in Eqs. (5.7) and (5.8) as

$$\eta_0 = \omega \| F'(x^0)^{1/2} \Delta x^0 \|_{H^1(\Omega)} = \omega \| F'(x^0)^{-1/2} F(x^0) \|_{H^1(\Omega)}.$$

In the case of nonlinear elasticity we have with the definitions and assumptions in Section 4.4

$$\eta_0 = \| \langle \Delta \mathbf{u}, A'(\mathbf{u}^0)\, \mathbf{v} \rangle_\Omega^{-1/2} (\langle \mathcal{F}, \mathbf{v} \rangle_\Omega - \langle A(\mathbf{u}^0), \mathbf{v} \rangle_\Omega) \|_{[H^1(\Omega)]^3}.$$

Hence, the convergence rate is dependent on the initial solution $\mathbf{u}^0$, on the parameters used in the model and on the inhomogeneous Dirichlet and Neumann boundary conditions which influence $\langle \mathcal{F}, \mathbf{v} \rangle_\Omega$. An appropriate choice for the initial solution $\mathbf{u}^0$ could be the solution of a simplified problem, like the linear elasticity or the Neo-Hooke model, or the solution of a modified nonlinear elasticity problem. The latter comprises the solution of the same nonlinear model with modified parameters, e.g. a reduced bulk modulus κ, or modified boundary conditions, e.g., a reduced pressure on the surface.

We write for the Newton method that we use in our numerical simulations

$$\langle \delta \mathbf{u}_h, A'(\mathbf{u}_h^k)\, \mathbf{v}_h \rangle = \langle \mathcal{F}, \mathbf{v}_h \rangle - \langle A(\mathbf{u}_h^k), \mathbf{v}_h \rangle, \quad \mathbf{u}_h^{k+1} = \mathbf{u}_h^k + \delta \mathbf{u}_h.$$

Using the equivalent linear system of equations we have to solve

$$\mathbf{K}'(\underline{u}^k)\,\delta\underline{u} = \underline{f} - K(\underline{u}^k), \quad \underline{u}^{k+1} = \underline{u}^k + \delta\underline{u} \tag{5.9}$$

with the tangent stiffness matrix

$$\mathbf{K}'(\underline{u}^k)[i,j] := (\varphi_j, A'(\mathbf{u}_h^k)\,\varphi_i)$$

and the right hand sides

$$\underline{f}[i] := \langle \mathbf{f}, \varphi_i \rangle \quad \text{and} \quad \underline{K}(\underline{u}^k)[i] := (A(\mathbf{u}_h^k), \varphi_i).$$

5.3 Assembling of the Stiffness Matrices

In this section we will give a short overview to the assembling of the element stiffness matrices using the discretized and linearized variational equations for the elasticity models. Using standard methods [100, Section 4.5.3], these element stiffness matrix are assembled to global stiffness matrix.

For linear elasticity we have the discretized bilinear form

$$a(\mathbf{u}_h, \mathbf{v}_h) = \int_\Omega \mathbb{C}\,\boldsymbol{\varepsilon}(\mathbf{u}_h, \mathbf{x}) : \boldsymbol{\varepsilon}(\mathbf{v}_h, \mathbf{x})\,\mathrm{d}\mathbf{x},$$

For this we obtain the 3×3 entries in the element stiffness matrix for each degree of freedom by

$$\mathbf{K}_{(\tau)}[i,j] = a'(\varphi_j, \varphi_i) = \int_\tau \mathcal{B}_i^\top\, \mathcal{C}\, \mathcal{B}_j\,\mathrm{d}\mathbf{x} \quad \text{for } i,j = 1,\ldots,\hat{N},$$

with $\mathcal{C} \in \mathbb{R}^{6\times 6}$ the elasticity tensor in Voigt notation. The representation of the matrix

$$\mathcal{B}_i^\top = \begin{pmatrix} \frac{\partial\varphi_i}{\partial x_1} & 0 & 0 & \frac{\partial\varphi_i}{\partial x_2} & 0 & \frac{\partial\varphi_i}{\partial x_3} \\ 0 & \frac{\partial\varphi_i}{\partial x_2} & 0 & \frac{\partial\varphi_i}{\partial x_1} & \frac{\partial\varphi_i}{\partial x_3} & 0 \\ 0 & 0 & \frac{\partial\varphi_i}{\partial x_3} & 0 & \frac{\partial\varphi_i}{\partial x_2} & \frac{\partial\varphi_i}{\partial x_1} \end{pmatrix}. \tag{5.10}$$

follows from the convention

$$\boldsymbol{\varepsilon} = [\varepsilon_{11}, \varepsilon_{22}, \varepsilon_{33}, 2\varepsilon_{12}, 2\varepsilon_{23}, 2\varepsilon_{13}]^\top.$$

In the case of nonlinear elasticity we show the assembling of the stiffness matrices in the current configuration. A similar procedure in the reference configuration is obtained using the corresponding pull-back operations. For the first summand in

Eq. (4.24) we have the discretized form

$$a'_{\text{geo}}(\delta\mathbf{u}_h, \mathbf{v}_h) := \int_\Omega \operatorname{grad}(\delta\mathbf{u}_h)\, \boldsymbol{\sigma}(\mathbf{u}_h^k) : \operatorname{grad}\mathbf{v}_h \, \mathrm{d}\mathbf{x}.$$

Applying the ansatz functions component-wise yields the so-called geometrical part of the tangent element stiffness matrix $\mathbf{K}'^{(\tau)}_{\text{geo}}(\underline{u}^k)$

$$\mathbf{K}'^{(\tau)}_{\text{geo}}[i,j] = a'_{\text{geo}}(\varphi_j, \varphi_i) = \mathbf{I} \int_\tau (\operatorname{grad}\varphi_j)^\top \boldsymbol{\sigma}(\mathbf{u}_h^k) \operatorname{grad}\varphi_i \, \mathrm{d}\mathbf{x} \quad \text{for } i,j = 1,\ldots,\hat{N}.$$

Using static condensation we have for the decoupled representation (3.33) the stress tensor

$$\boldsymbol{\sigma}(\mathbf{u}_h^k) = \overline{p}_h \mathbf{I} + \boldsymbol{\sigma}_{\text{iso}}(\mathbf{u}_h^k),$$

where $\overline{p}_h$ is an element-wise constant volumetric variable , see Example 5.2. Similar to linear elasticity we get for the second summand in Eq. (4.24), the so-called material part of the element tangent stiffness matrix $\mathbf{K}'^{(\tau)}_{\text{mat}}(\underline{u}^k)$

$$\mathbf{K}'^{(\tau)}_{\text{mat}}[i,j] = a'_{\text{mat}}(\varphi_j, \varphi_i) = \int_\tau \mathcal{B}_j^\top \, \mathcal{C}(\mathbf{u}_h^k)\, \mathcal{B}_i \, \mathrm{d}\mathbf{x} \quad \text{for } i,j = 1,\ldots,\hat{N},$$

with $\mathcal{C}(\mathbf{u}_h^k)$ the elasticity tensor in Voigt notation, see (3.38), and $\mathcal{B}$ from Eq. (5.10). In the case of static condensation and the decoupled formulation we write

$$\mathcal{C} = \mathcal{C}_{\text{vol}}(\overline{p}_h) + \mathcal{C}_{\text{iso}}(\mathbf{u}_h^k),$$

with the volumetric and the isochoric parts of the elasticity tensor as disussed in Section 3.13.3 and the element-wise constant hydrostatic pressure $\overline{p}_h$.

The construction of the global tangent stiffness matrix follows the standard assembly procedure of element stiffness matrices

$$\mathbf{K}'(\underline{u}^k) = \sum_{\tau \in \Omega_h} \mathbf{A}_\tau^\top \left(\mathbf{K}'^{(\tau)}_{\text{geo}}(\underline{u}^k) + \mathbf{K}'^{(\tau)}_{\text{mat}}(\underline{u}^k) \right) \mathbf{A}_\tau$$

with $\mathbf{A}_\tau$ connectivity matrices. Due to the self-adjointness (cf. Remark 4.4.2) and the $H^1(\Omega)$–ellipticity (cf. Section 4.4.5) of the operator A', the stiffness matrix $\mathbf{K}'(\underline{u}^k)$ is symmetric and positive definite in the case of the Eulerian formulation. The same holds true for the stiffness matrix derived from the Lagrangian formulation.

5.4 Assembling of Pressure Loads

The following holds true for elements $\tau = \tau_t$ in the current configuration and $\tau = \tau_0$ in the reference configuration. From (4.27) we get the discretized linear form

$$\langle \mathcal{F}, \mathbf{v}_h \rangle := \langle \mathcal{F}(\mathbf{u}_h^k), \mathbf{v}_h \rangle = -\int_{\Gamma_{\boldsymbol{\xi}}} \mathcal{P} \left(\frac{\partial \mathbf{x}}{\partial \xi_1} \times \frac{\partial \mathbf{x}}{\partial \xi_2} \right) \cdot \mathbf{v}_h \, \mathrm{d}\boldsymbol{\xi}.$$

Applying the ansatz functions component-wise with $\mathbf{x} = (x_1, x_2, x_3)^\top$ we obtain

$$\underline{f}[i] = \langle \mathcal{F}, \varphi_i \rangle = -\int_\tau \mathcal{P} \left(\frac{\partial \mathbf{x}}{\partial \xi_1} \times \frac{\partial \mathbf{x}}{\partial \xi_2} \right) \varphi_i \, \mathrm{d}\boldsymbol{\xi} = \int_\tau \mathcal{P} \begin{pmatrix} \frac{\partial x_2}{\partial \xi_1}\frac{\partial x_3}{\partial \xi_2} - \frac{\partial x_3}{\partial \xi_1}\frac{\partial x_2}{\partial \xi_2} \\ \frac{\partial x_3}{\partial \xi_1}\frac{\partial x_1}{\partial \xi_2} - \frac{\partial x_1}{\partial \xi_1}\frac{\partial x_3}{\partial \xi_2} \\ \frac{\partial x_1}{\partial \xi_1}\frac{\partial x_2}{\partial \xi_2} - \frac{\partial x_2}{\partial \xi_1}\frac{\partial x_1}{\partial \xi_2} \end{pmatrix} \varphi_i \, \mathrm{d}\boldsymbol{\xi}$$

Consequentely, we get for the tangent term

$$f'(\delta \mathbf{u}_h, \mathbf{v}_h) := \langle \Delta \mathbf{u}_h, \mathcal{F}'(\mathbf{u}_h^k) \mathbf{v}_h \rangle = -\int_{\Gamma_{\boldsymbol{\xi}}} \mathcal{P} \left(\frac{\partial \delta \mathbf{u}_h}{\partial \xi_1} \times \frac{\partial \mathbf{x}}{\partial \xi_2} + \frac{\partial \mathbf{x}}{\partial \xi_1} \times \frac{\partial \delta \mathbf{u}_h}{\partial \xi_2} \right) \cdot \mathbf{v}_h \, \mathrm{d}\boldsymbol{\xi}.$$

Applying the ansatz functions component-wise yields

$$\mathbf{M}'(\underline{u}^k)[i,j] = f'(\varphi_j, \varphi_i) = -\int_\tau \mathcal{P} \left(\frac{\partial \varphi_j}{\partial \xi_1} \mathcal{N}_2 - \frac{\partial \varphi_j}{\partial \xi_2} \mathcal{N}_1 \right) \varphi_i \, \mathrm{d}\boldsymbol{\xi}, \tag{5.11}$$

where the columns of the matrix $\mathcal{N}_\alpha$ are computed as $\mathbf{e}_i \times \frac{\partial \mathbf{x}}{\partial \xi_\alpha}$, $i = 1,2,3$, $\alpha = 1,2$. Hence, with $\mathbf{x} = (x_1, x_2, x_3)^\top$ we have

$$\mathcal{N}_\alpha = \begin{pmatrix} 0 & \frac{\partial x_3}{\partial \xi_\alpha} & -\frac{\partial x_2}{\partial \xi_\alpha} \\ -\frac{\partial x_3}{\partial \xi_\alpha} & 0 & \frac{\partial x_1}{\partial \xi_\alpha} \\ \frac{\partial x_2}{\partial \xi_\alpha} & -\frac{\partial x_1}{\partial \xi_\alpha} & 0 \end{pmatrix}, \quad \alpha = 1,2.$$

Note that the matrix $\mathbf{M}'$ from (5.11) is not symmetric and thus the total system

$$\left(\mathbf{K}'(\underline{u}^k) + \mathbf{M}'(\underline{u}^k) \right) \delta \underline{u} = \underline{f}(\underline{u}^k) - \underline{K}(\underline{u}^k), \quad \underline{u}^{k+1} = \underline{u}^k + \delta \underline{u}$$

is no longer symmetric for simulations with pressure loads. For an equivalent symmetric version of this system we use

$$\mathbf{M}'(\underline{u}^k)[i,j] = \int_\tau \frac{\mathcal{P}}{2} \left[\left(\frac{\partial \varphi_i}{\partial \xi_1} \varphi_j - \frac{\partial \varphi_j}{\partial \xi_1} \varphi_i \right) \mathcal{N}_2 + \left(\frac{\partial \varphi_j}{\partial \xi_2} \varphi_i - \frac{\partial \varphi_i}{\partial \xi_2} \varphi_j \right) \mathcal{N}_1 \right] \mathrm{d}\boldsymbol{\xi}, \tag{5.12}$$

see [24, Section 7.4.4].

5.5 Time and Load Stepping Schemes

As shown in Section 5.2 the convergence rate of the Newton method is dependent on the initial guess, on the parameters used in the model and on the inhomogeneous Dirichlet and Neumann boundary conditions which influence the right hand side. For example in the case of the simulation of biological tissues very high pressure loads may lead to a system where the Newton method is not converging at all. This problem can be overcome by a time or load stepping scheme.

In such a scheme we use zero for the initial guess, and the result of the k–th time step as initial solution for the next step. The initial guess may also be the solution of a modified nonlinear elasticity problem such as the solution of the same nonlinear model but with modified parameters, e.g., a reduced penalty parameter κ, or modified boundary conditions, e.g., a reduced pressure on the surface. The latter is equivalent to an incremental load stepping scheme with a parameter $\tau \in (0, 1]$, $\tau \to 1$, so that

$$\mathbf{K}'(\underline{u}^k)\,\delta\underline{u} = \tau\,\underline{f} - K(\underline{u}^k), \quad \underline{u}^{k+1} = \underline{u}^k + \delta\underline{u}. \tag{5.13}$$

Augustin et al. [7] and Klawonn and Rheinbach [106] used a load stepping scheme of this kind, for more information on load stepping and global Newton methods, see Wriggers [187] and Deuflhard [49].

Total and updated Lagrangian formulation As we have seen in Section 4.2 we can express the variational formulation in terms of variables in the original and undeformed reference configuration. A term often used in this context are *material variables*. Another way is to express the variables in the current or deformed configuration; such variables are referred to as *spatial variables*.

The *total Lagrangian scheme* is characterized by using the formulation with material variables and the differentiations and integrations are carried out with respect to the domain Ω_0 and the Lagrangian coordinates $\mathbf{X}$.

On the other hand for the *updated Lagrangian scheme* we use spatial variables and the differentiation and integration procedures are carried out within Eulerian coordinates $\mathbf{x}$. With a coordinate transformation one can show that both formulations are equivalent.

Nonetheless the total Lagrangian scheme has the advantage that it is always based on the reference configuration Ω_0. Hence, we do not have to update the coordinates of our underlying mesh. In contrast to that the updated Lagrangian scheme uses an updated reference geometry. In our case, this is the last equilibrium state of the problem, which is the situation at the end of the previous time step. Thus, we have to update our coordinates after each time step and take the resulting configuration

as new reference configuration. For nonlinear problems it is important to mention that the coordinates are not changed within the Newton steps.

The total Lagrangian and the updated Lagrangian time stepping methods are most common within the field of solid mechanics. Another way would be the *Eulerian scheme* which is mainly used in fluid mechanics. The basis of a finite element approach in this scheme is that the finite elements are fixed in space and do not deform as in the case of the two Lagrangian schemes as mentioned above. For more information on this topic see Shabana [168].

5.6 Solving a Linear System of Equations

The finite element method, discussed in Section 5.1, leads to linear systems of equations with – in many cases – a very large number of degrees of freedom. One possibility to solve such systems are direct methods, cf. Section 5.6.1, such as the very well known Gaussian elimination. For many practical applications, for instance modeling biological tissues, direct solvers reach their limits concerning runtime and memory use. Hence for larger systems iterative solvers become important, see Section 5.6.2.

5.6.1 Direct Solvers

The very simplest method to solve a linear system of equations in the form $\mathbf{A}\underline{x} = \underline{f}$ with $\mathbf{A} \in \mathbb{R}^{m \times m}$ is the Gaussian elimination, which needs $\mathcal{O}(m^3)$ operations. To improve this cubic order there are many different approaches and strategies, e.g. a smart re-ordering of the matrix $\mathbf{A}$.

Stiffness matrices arising from the finite element method are generally sparse, since the support of the basis functions of the FE spaces is local. In this case, given optimal orderings, the computational costs may be reduced to $\mathcal{O}(m^{3/2})$ in 2D and $\mathcal{O}(m^2)$ in 3D. The sparsity of the FE stiffness matrices also allows us to reduce memory costs, since only nonzero entries have to be stored.

There are many software packages available to solve linear systems of equations directly. Two of them are MUMPS [1, 2] and UMFPACK [45, 46], which are both available in source code. Another direct solver, which showed some advantages in computational speed but needs a licence and is not available in source code, is PARDISO [160, 161].

5.6.2 Iterative Solvers

We will concentrate on the special case of *Krylov subspace methods* to solve the linear system $\mathbf{A}\underline{x} = \underline{f}$. For a general theory and introduction to iterative solvers see amongst many others the books of Axelsson [9], Greenbaum [66], Hackbusch [71], and Steinbach [176].

Software packages that deal with highly scalable iterative solving on massively parallel computers are for example

- *Hypre* (`http://acts.nersc.gov/hypre/`),
- *PETSc* (`http://www-unix.mcs.anl.gov/petsc/petsc-as/`) and
- *DUNE* (`http://www.dune-project.org/`).

In the case of finite element methods, an elliptic variational problem results in a symmetric and positive definite stiffness matrix. Here we can apply the preconditioned conjugate gradient method.

Preconditioned Conjugate Gradient Method (PCGM). Let $\mathbf{C_A} \in \mathbb{R}^{m\times m}$ be a symmetric and positive definite matrix. Then Algorithm 1 describes the PCG-method to solve the linear system $\mathbf{A}\underline{x} = \underline{f}$.

Algorithm 1 Preconditioned conjugate gradient method (PCGM)

Initialize:
$\underline{r}^0 := \mathbf{A}\underline{x}^0 - f,\ v^0 := \mathbf{C_A}^{-1}\underline{r}^0,\ \underline{p}^0 = \underline{v}_0,\ \rho_0 := \langle \underline{v}^0, \underline{r}^0 \rangle$

Iterate:
for $k = 0, \ldots, m-1$ **do**
  $\underline{s}^k := \mathbf{A}\underline{p}^k,\ \sigma_k := \langle \underline{s}^k, \underline{p}^k \rangle,\ \alpha_k := \rho_k/\sigma_k$
  $\underline{x}^{k+1} := \underline{x}^k - \alpha_k \underline{p}^k,\ \underline{r}^{k+1} := \underline{r}^k - \alpha_k \underline{s}^k$
  $\underline{v}^{k+1} := \mathbf{C_A}^{-1}\underline{r}^{k+1},\ \rho_{k+1} := \langle \underline{v}^{k+1}, \underline{r}^{k+1} \rangle$
  if $\rho_{k+1} < \varepsilon\rho_0$ **then** {breaking condition for given $\varepsilon > 0$}
    break
  else {find new conjugate direction}
    $\beta_k := \rho_{k+1}/\rho_k,\ \underline{p}^{k+1} := \underline{v}^{k+1} + \beta_k \underline{p}^k$
  end if
end for

Proposition 5.3 (Error estimate for the PCGM)**.** *Let $\mathbf{A} \in \mathbb{R}^{m\times m}$ be a symmetric and positive definite matrix and $\underline{x}^* \in \mathbb{R}^m$ be the exact solution of the system of linear equations $\mathbf{A}\underline{x} = \underline{f}$. Then the PCGM (Algorithm 1) converges for every initial value $\underline{u}_0 \in \mathbb{R}^m$ to the exact solution $\underline{x}^*$ and the following error estimate holds*

$$\|\underline{x}^k - \underline{x}^*\|_{\mathbf{A}} \leq \frac{2q}{1+q^{2k}} \|\underline{x}^0 - \underline{x}^*\|_{\mathbf{A}}, \quad \text{with } q = \frac{\sqrt{\kappa(\mathbf{C}_{\mathbf{A}}^{-1}\mathbf{A})}+1}{\sqrt{\kappa(\mathbf{C}_{\mathbf{A}}^{-1}\mathbf{A})}-1},$$

with $\kappa = \lambda_{max}(\mathbf{C}_{\mathbf{A}}^{-1}\mathbf{A})/\lambda_{min}(\mathbf{C}_{\mathbf{A}}^{-1}\mathbf{A})$ the condition number.

Proof. Cf. Hackbusch [71]. □

Preconditioned Conjugate Residual Method (PCG). A generalization of the CG method for symmetric and indefinite problems is the preconditioned conjugate residual method [6, 71]. This method is very closely related to the CG method and has similar convergence properties.

Generalized Minimal Residual Method (GMRES). In the field of elasticity displacement dependent pressure loads (3.17) may lead to a non-symmetric load stiffness matrix, see Section 5.5 and [167], and consequently the CG method is no longer applicable.

One possibility to handle this problem is the Generalized Minimal Residual (GMRES) method [157], where the main idea is the minimization of the residual over some certain Krylov subspace. For error estimates of GMRES we refer to [66, 175].

Remark 5.6.1 (Jacobi preconditioner)**.** *Assuming $A_{ii} \neq 0$ for all i, then one possible choice for the preconditioner $\mathbf{C}_{\mathbf{A}}$ is the so-called Jacobi preconditioner*

$$\mathbf{C}_{\mathbf{A}} = \operatorname{diag}(\mathbf{A}).$$

The Jacobi preconditioner is a very simple form of preconditioning, but shows good results for diagonal dominant matrices $\mathbf{A}$ for non-uniform meshes. More efficient possibilities for preconditioning are multilevel preconditioners such as the BPX-preconditioner [26] or multigrid methods [72]. An algebraic multigrid software package, suitable for efficient preconditioning, is *BoomerAMG* [188] included in the *Hypre* project.

6 DOMAIN DECOMPOSITION METHODS

Fine structured biological tissues and their anisotropic material behavior evoke significant challenges in regard to numerical simulations. The discretization (Section 5.1) of anatomically detailed high-resolution geometries results in very fine meshes and hence in a very large number of degrees of freedom. Moreover, due to the multi-layered character of the considered materials, jumping coefficients, which are changing material parameters over layer interfaces, may be encountered.

For such complex problems the application of direct solvers results in non-optimal efficiency and high memory usage. Typically, these problems cannot be solved sufficiently fast and accurate in serial, i.e. on a single core of a computer. A promising resolution for this problem are iterative solvers in combination with domain decomposition (DD) methods, which are proven to be a very useful and efficient parallel solution strategy. These techniques offer the possibility to distribute the calculations to many compute cores with relatively low communication between the processors. Furthermore, domain decomposition methods provide a natural way to treat jumping coefficients.

The basic principle of DD methods is the decomposition of the original domain into several overlapping or non-overlapping subdomains which dates back to the 19th century when Schwarz [166] introduced the *Alternating Schwarz Method*, see Figure 6.1. For a detailed discussion of domain decomposition methods, including

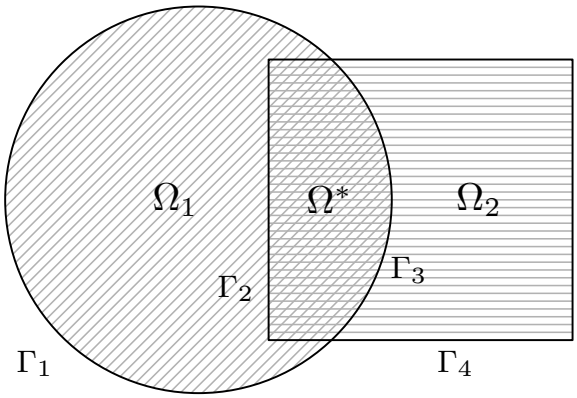

Figure 6.1: Picture, modified from [166], to illustrate the Alternating Schwarz Method. Ω_1 and Ω_2 are the subdomains, Ω^* is the overlap, $\Gamma_i,\ i = 1,2,3,4$ are the different parts of the boundary.

overlapping as well as non-overlapping approaches, the interested reader is referred to the monograph by Toselli and Widlund [178], see also [70, 145, 172].

In the following, we concentrate on non-overlapping domain decompositions and the *finite element tearing and interconnecting* (FETI) method.

6.1 Basic Principles of Domain Decomposition Methods

Let $\Omega \subset \mathbb{R}^3$ be a bounded Lipschitz domain. The underlying principle of DD methods is the partition of Ω into p non-overlapping subdomains

$$\overline{\Omega} = \bigcup_{i=1}^{p} \overline{\Omega}_i \ , \quad \text{with} \quad \Omega_i \cap \Omega_j = \emptyset \text{ for } i \neq j, \tag{6.1}$$

where Ω_i are as well Lipschitz domains, see Figure 6.2. With $\Gamma_i := \partial\Omega_i$ we denote the boundary of one specific subdomain. The local interface is $\Gamma_{ij} := \Gamma_i \cap \Gamma_j$ for all $i < j$, while the global interface Γ_{C} and the skeleton Γ_{S} of the decomposition are

$$\Gamma_{\mathrm{C}} := \bigcup_{i<j} \overline{\Gamma}_{ij}, \quad \Gamma_{\mathrm{S}} := \bigcup_{i=1}^{p} \Gamma_i = \Gamma \cup \Gamma_{\mathrm{C}}.$$

The typical diameter of the subdomains is defined by

$$H := \max_{i \in \mathcal{I}} \{\operatorname{diam} \Omega_i\}, \quad \text{with the index set } \mathcal{I} := \{1, \ldots, p\}; \tag{6.2}$$

bear in mind that the typical diameter of a finite element is h.

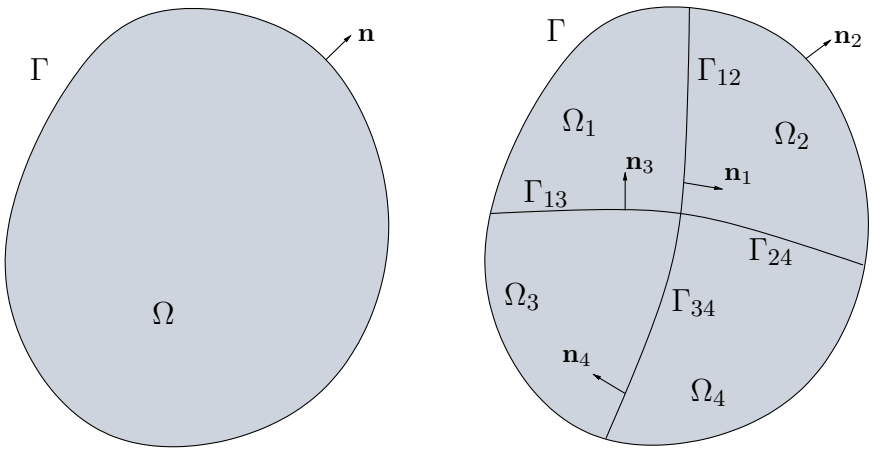

Figure 6.2: Decomposition of a domain Ω into four subdomains Ω_i.

The decomposition of academic test example meshes like cubes or spheres can easily be created by simple algorithms. For general meshes, e.g., high-resolution geometries of cardiovascular tissue, the usage of mesh partitioners, for example, METIS [102] is favorable, see Figure 6.3. Attention should be paid to possibly not admissible decompositions as illustrated in Figure 6.3 (b). For dendritic geometries it can happen that the METIS algorithm produces subdomains that have more than one component. To avoid problems in this regard, we eliminate such situations with a simple check for connectivity. Hence, in the following, we treat each Ω_i as a connected subdomain with Lipschitz boundary.

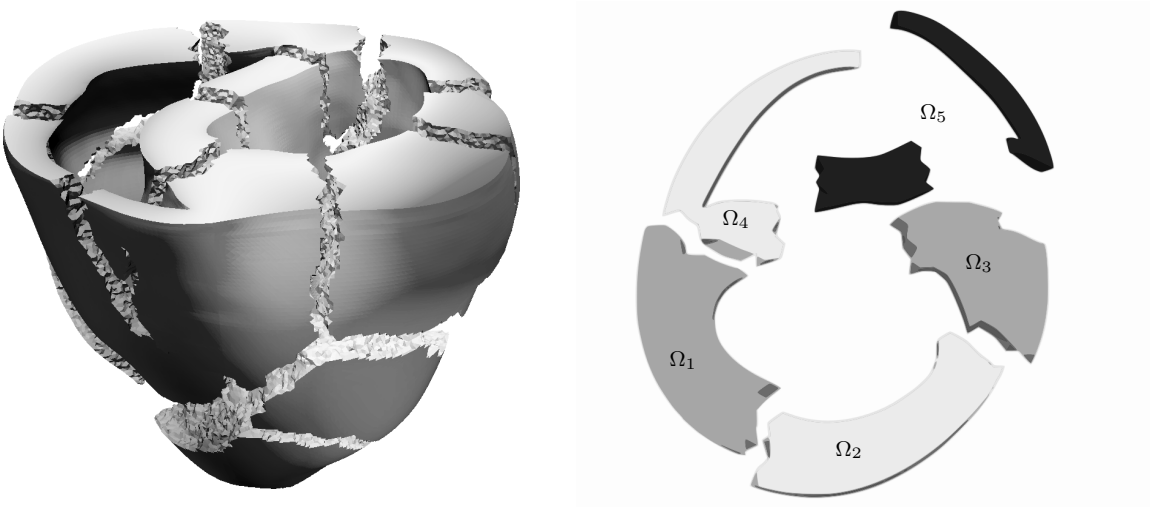

Figure 6.3: Decomposition of the mesh of a rabbit heart in several subdomains via METIS: On the left-hand side there is a decomposition of the myocardium into 16 connected subdomains, where the colors show displacements arising from a passive inflation experiment. To the right we show a decomposition of the cross section of the heart in five subdomains; note that the algorithm generated four connected subdomains and one that has two components (Ω_5); meshes courtesy of Gernot Plank and Anton Prassl, Institute of Biophysics, Medical University of Graz [143].

For matters of simplicity, the domain decomposition formulation of a boundary value problem is first derived for the simple example of the *scalar potential equation*

$$\begin{aligned} -\operatorname{div}[\alpha(\mathbf{x})\nabla u(\mathbf{x})] &= f(\mathbf{x}) \qquad \text{for } \mathbf{x} \in \Omega, \\ \gamma_0^{\text{int}} u(\mathbf{x}) &= g_{\text{D}}(\mathbf{x}) \qquad \text{for } \mathbf{x} \in \Gamma_{\text{D}}, \\ \gamma_1^{\text{int}} u(\mathbf{x}) &= g_{\text{N}}(\mathbf{x}) \qquad \text{for } \mathbf{x} \in \Gamma_{\text{N}}, \end{aligned} \tag{6.3}$$

where γ_0^{int} is the Dirichlet trace operator and γ_1^{int} the Neumann trace operator.

The coefficient $\alpha(\mathbf{x})$ is piecewise constant, i.e.

$$\alpha(\mathbf{x}) = \alpha_i \quad \text{for} \quad \mathbf{x} \in \Omega_i, \quad i = 1, \ldots, p. \tag{6.4}$$

The conforming variational formulation is to find $u \in H^1(\Omega)$, $u = g_\mathrm{D}$ on Γ_D so that

$$\int_\Omega \alpha \nabla u \cdot \nabla v \, \mathrm{d}\mathbf{x} = \int_\Omega f v \, \mathrm{d}\mathbf{x} + \int_{\Gamma_\mathrm{N}} g_\mathrm{N} v \, \mathrm{d}s_\mathbf{x}, \quad \text{for all } v \in H^1_0(\Omega, \Gamma_\mathrm{D}).$$

In accordance with (6.1) and (6.4) we can rewrite this variational formulation for the simple case of two subdomains: find $u \in H^1(\Omega)$ with $u = g_\mathrm{D}$ on Γ_D such that

$$\alpha_1 \int_{\Omega_1} \nabla u \cdot \nabla v \, \mathrm{d}\mathbf{x} + \alpha_2 \int_{\Omega_2} \nabla u \cdot \nabla v \, \mathrm{d}\mathbf{x} = \int_\Omega f v \, \mathrm{d}\mathbf{x} + \int_{\Gamma_\mathrm{N}} g_\mathrm{N} v \, \mathrm{d}s_\mathbf{x},$$

for all test functions $v \in H^1_0(\Omega, \Gamma_\mathrm{D})$. Green's formula leads to

$$\sum_{i=1,2} \left[-\alpha_i \int_{\Omega_i} \Delta u v \, \mathrm{d}\mathbf{x} - \alpha_i \int_{\Gamma_i} (\mathbf{n}_i \cdot \nabla u) v \, \mathrm{d}s_x \right] = \int_\Omega f v \, \mathrm{d}\mathbf{x} + \int_{\Gamma_\mathrm{N}} g_\mathrm{N} v \, \mathrm{d}s_\mathbf{x},$$

for all $v \in H^1_0(\Omega, \Gamma_\mathrm{D})$, where $\mathbf{n}_i$ is the exterior normal vector of Ω_i. Hence,

$$\sum_{i=1,2} \alpha_i \int_{\Omega_i} -\Delta u \; v \, \mathrm{d}\mathbf{x} - \int_{\Gamma_i} \sum_{i=1,2} (\alpha_i \mathbf{n}_i \cdot \nabla u) \, v \, \mathrm{d}s_\mathbf{x} = \int_\Omega f v \, \mathrm{d}\mathbf{x} + \int_{\Gamma_\mathrm{N}} g_\mathrm{N} v \, \mathrm{d}s_\mathbf{x}.$$

With the conormal derivatives

$$t_i := \alpha_i \mathbf{n}_i \cdot \nabla u_i, \quad i = 1, 2$$

and density and extension arguments [145], we may formulate the following boundary value problem which is equivalent to (6.3): find $u_i = u|_{\Omega_i}$, $i = 1, 2$ so that

$$\begin{aligned} -\alpha_i \Delta u_i(\mathbf{x}) &= f(\mathbf{x}) && \text{for } \mathbf{x} \in \Omega_i, \\ u_i(\mathbf{x}) &= g_\mathrm{D} && \text{for } \mathbf{x} \in \Gamma_\mathrm{D} \cap \Gamma_i, \\ \alpha_i \mathbf{n}_i \cdot \nabla u_i(\mathbf{x}) &= g_\mathrm{N} && \text{for } \mathbf{x} \in \Gamma_\mathrm{N} \cap \Gamma_i, \end{aligned}$$

and the so-called *transmission conditions*

$$\begin{aligned} t_1(\mathbf{x}) + t_2(\mathbf{x}) &= 0 \quad \text{for } \mathbf{x} \in \Gamma_{12}, \\ u_1(\mathbf{x}) - u_2(\mathbf{x}) &= 0 \quad \text{for } \mathbf{x} \in \Gamma_{12} \end{aligned}$$

are fulfilled.

The above ideas are valid for any elliptic partial differential equation and thus also hold for the linear elasticity problem (3.16). Generalizing for an arbitrary amount

of p subdomains we can formulate the coupled boundary value problem for linear elasticity: find $\mathbf{u} \in [H^1(\Omega)]^3$ with $\mathbf{u} = \mathbf{u}_\mathrm{D}$ on Γ_D such that

$$\begin{aligned} -\operatorname{div} \boldsymbol{\sigma}(\mathbf{u}_i, \mathbf{x}) &= \mathbf{f}(\mathbf{x}) && \text{for } \mathbf{x} \in \Omega_i, \\ \mathbf{u}_i(\mathbf{x}) &= \mathbf{u}_\mathrm{D}(\mathbf{x}) && \text{for } \mathbf{x} \in \Gamma_\mathrm{D} \cap \Gamma_i, \\ \boldsymbol{\sigma}(\mathbf{u}_i, \mathbf{x})\, \mathbf{n}_i(\mathbf{x}) &= \mathbf{t}_\mathrm{N}(\mathbf{x}) && \text{for } x \in \Gamma_\mathrm{N} \cap \Gamma_i, \\ \mathbf{u}_i(\mathbf{x}) &= \mathbf{u}_j(\mathbf{x}) && \text{for } \mathbf{x} \in \Gamma_{ij}, \\ \mathbf{t}_i(\mathbf{x}) + \mathbf{t}_j(\mathbf{x}) &= \mathbf{0} && \text{for } \mathbf{x} \in \Gamma_{ij}, \end{aligned} \tag{6.5}$$

with $\mathbf{u}_i = \mathbf{u}|_{\Omega_i} \in [H^1(\Omega_i)]^3$. The boundary stresses are defined as

$$\mathbf{t}_i(\mathbf{x}) := \boldsymbol{\sigma}(\mathbf{u}_i, \mathbf{x}) \mathbf{n}_i(\mathbf{x}).$$

In the absence of volume forces, i.e. $\mathbf{f}(\mathbf{x}) = \mathbf{0}$ and using the *Steklov–Poincaré operators* $S_i^{\mathrm{int}} : [H^{1/2}(\Gamma_i)]^3 \to [H^{-1/2}(\Gamma_i)]^3$ we can describe the *Dirichlet to Neumann map*

$$\mathbf{t}_i(\mathbf{x}) = \gamma_1^{\mathrm{int}} \mathbf{u}_i(\mathbf{x}) = (S_i^{\mathrm{int}} \gamma_0^{\mathrm{int}}) \mathbf{u}_i(\mathbf{x}) \quad \text{for } \mathbf{x} \in \Gamma_i, \tag{6.6}$$

e.g., cf. [176, Section 6.6]. In the case of linear elasticity jumping coefficients may arise from $\boldsymbol{\sigma}(\mathbf{u}_i) = \mathbb{C}_i \varepsilon(\mathbf{u}_i)$ with the constant forth-order tensor

$$\mathbb{C}_i = \mathbb{C}|_{\Omega_i}, \quad \text{for all } i \in \mathcal{I}.$$

For sufficiently smooth $\mathbf{u}_i$ and tensor fields $\boldsymbol{\sigma}(\mathbf{u}_i)$ the formulation 6.5 also holds for nonlinear elasticity with the constitutive equation

$$\boldsymbol{\sigma}(\mathbf{u}_i) = 2J^{-1}(\mathbf{u}_i) \mathbf{F}(\mathbf{u}_i) \frac{\partial \Psi_i(\mathbf{C})}{\partial \mathbf{C}} \mathbf{F}^\top(\mathbf{u}_i)$$

where Ψ_i is the strain-energy function in Ω_i. Hence, the stress tensor $\boldsymbol{\sigma}(\mathbf{u}_i)$ is defined locally using Ψ_i, as introduced in Section 3.10, and localized parameter sets and fiber directions.

6.2 Standard One-level FETI Methods

First ideas of this specific domain decomposition method go back to the early work of Glowinski and Wheeler [65], but as the classical one-level FETI method it was introduced by Farhat and Roux [55, 56]. Since then these techniques got very popular and are widely used in the scientific computing community. Our presentation is based on the explanations of Toselli and Widlund [178, Section 6.3] and Langer and Steinbach [114]. Other contributions include the works of Mandel and Tezaur

[119], publishing a first convergence proof of these methods in the non-redundant case, Klawonn and Widlund [107, 108], doing the same for a redundant formulation, and Langer and Steinbach [114, 115] where the authors enhanced the method to boundary element methods and present a coupling of finite and boundary element domain decomposition methods.

We assume that the finite element mesh $\mathcal{T}_N$ matches the domain decomposition (6.1), i.e., we can reorder the degrees of freedom to rewrite the linear system (5.4) as

$$\begin{pmatrix} \mathbf{K}_{11} & & & \mathbf{K}_{1\mathrm{C}}\mathbf{A}_1 \\ & \ddots & & \vdots \\ & & \mathbf{K}_{pp} & \mathbf{K}_{p\mathrm{C}}\mathbf{A}_p \\ \mathbf{A}_1^\top\mathbf{K}_{\mathrm{C}1} & \cdots & \mathbf{A}_p^\top\mathbf{K}_{\mathrm{C}p} & \sum_{i=1}^{p}\mathbf{A}_i^\top\mathbf{K}_{\mathrm{CC},i}\mathbf{A}_i \end{pmatrix} \begin{pmatrix} \underline{u}_{1,I} \\ \vdots \\ \underline{u}_{p,I} \\ \underline{u}_{\mathrm{C}} \end{pmatrix} = \begin{pmatrix} \underline{b}_1 \\ \vdots \\ \underline{b}_p \\ \sum_{i=1}^{p}\mathbf{A}_i^\top\underline{b}_{\mathrm{C},i} \end{pmatrix},$$

and the linearized system of equations (5.9) can be written as

$$\begin{pmatrix} \mathbf{K}'_{11}(\underline{u}_1^k) & & & \mathbf{K}'_{1\mathrm{C}}(\underline{u}_1^k)\mathbf{A}_1 \\ & \ddots & & \vdots \\ & & \mathbf{K}'_{pp}(\underline{u}_p^k) & \mathbf{K}'_{p\mathrm{C}}(\underline{u}_p^k)\mathbf{A}_p \\ \mathbf{A}_1^\top\mathbf{K}'_{\mathrm{C}1}(\underline{u}_1^k) & \cdots & \mathbf{A}_p^\top\mathbf{K}'_{\mathrm{C}p}(\underline{u}_p^k) & \sum_{i=1}^{p}\mathbf{A}_i^\top\mathbf{K}'_{\mathrm{CC},i}(\underline{u}_i^k)\mathbf{A}_i \end{pmatrix} \begin{pmatrix} \delta\underline{u}_{1,I} \\ \vdots \\ \delta\underline{u}_{p,I} \\ \delta\underline{u}_{\mathrm{C}} \end{pmatrix} = \begin{pmatrix} \underline{b}_1(\underline{u}_1^k) \\ \vdots \\ \underline{b}_p(\underline{u}_p^k) \\ \sum_{i=1}^{p}\mathbf{A}_i^\top\underline{b}_{\mathrm{C},i}(\underline{u}_i^k) \end{pmatrix},$$

where $\underline{u}_{i,\mathrm{I}}$ and the increments $\delta\underline{u}_{i,\mathrm{I}}$ correspond to the local degrees of freedom within the subdomain Ω_i, and $\underline{u}_{\mathrm{C}}$ and $\delta\underline{u}_{\mathrm{C}}^k$ are related to all global degrees of freedom on the coupling boundary Γ_{C} and $\underline{b}_i(\underline{u}_i^k) = \underline{f}_i - \underline{K}_i(\underline{u}_i^k)$. $\mathbf{A}_i$ denote simple reordering matrices taking boolean values. Note that the same system of equations can be deduced by applying the finite element method to the DD problem (6.5) [178].

We introduce the tearing for linear elasticity

$$\underline{u}_i = \begin{pmatrix} \underline{u}_{i,\mathrm{I}} \\ \mathbf{A}_i\underline{u}_{\mathrm{C}} \end{pmatrix},\ \mathbf{K}_i = \begin{pmatrix} \mathbf{K}_{ii} & \mathbf{K}_{i\mathrm{C}} \\ \mathbf{K}_{\mathrm{C}i} & \mathbf{K}_{\mathrm{CC},i} \end{pmatrix},\ \underline{f}_i = \begin{pmatrix} \underline{b}_i \\ \underline{b}_{\mathrm{C},i} \end{pmatrix},$$

and for nonlinear elasticity

$$\delta\underline{u}_i = \begin{pmatrix} \delta\underline{u}_{i,\mathrm{I}}^k \\ \mathbf{A}_i\delta\underline{u}_{\mathrm{C}}^k \end{pmatrix},\ \mathbf{K}'_i(\underline{u}_i^k) = \begin{pmatrix} \mathbf{K}'_{ii}(\underline{u}_i^k) & \mathbf{K}'_{i\mathrm{C}}(\underline{u}_i^k) \\ \mathbf{K}'_{\mathrm{C}i}(\underline{u}_i^k) & \mathbf{K}'_{\mathrm{CC},i}(\underline{u}_i^k) \end{pmatrix},\ \underline{f}(\underline{u}_i^k) = \begin{pmatrix} \underline{b}_i(\underline{u}_i^k) \\ \underline{b}_{\mathrm{C},i}(\underline{u}_i^k) \end{pmatrix}.$$

As the unknowns $\underline{u}_i$ and $\underline{u}_i^{k+1} = \underline{u}_i^k + \delta\underline{u}_i$ are typically not continuous over the interfaces we have to ensure the continuity of the solution by the constraints

$$\underline{u}_i = \underline{u}_j \quad \text{and} \quad \delta\underline{u}_i = \delta\underline{u}_j \quad \text{on } \Gamma_{ij},\ i,j \in \mathcal{I}. \tag{6.7}$$

There are two different schemes how to implement constraints for coupling nodes which appear on three or more subdomains: a non-redundant, see Figure 6.4 (a) and [178, Section 6.3.2] and a fully-redundant case, see Figure 6.4 (b) and [178, Section 6.3.3]. In case of elasticity, the constraints have to be fulfilled for each component, i.e. in 3D for all three components. The redundant formulation shows

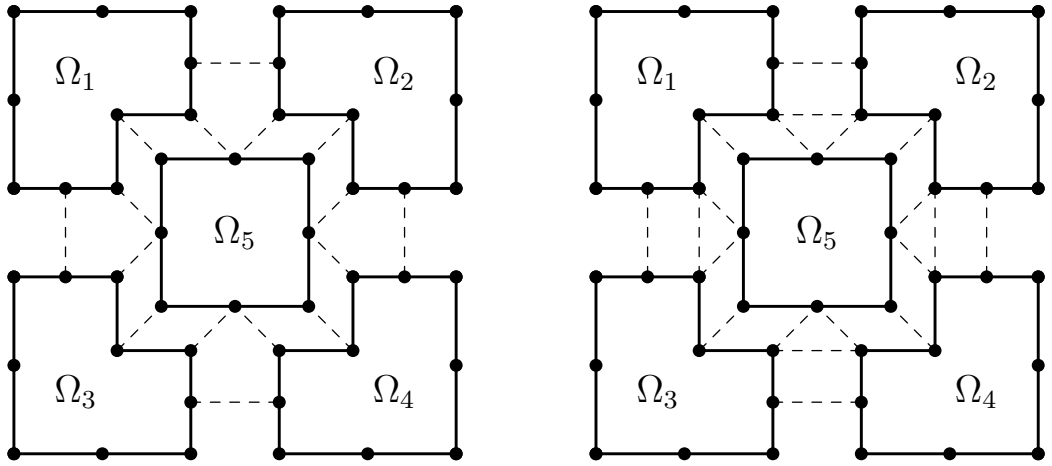

Figure 6.4: For the non-redundant case (left) the number of necessary constraints is minimized, fully-redundant constraints (right) are typically easier to implement.

slight advantages in treating the constraints in a fully symmetric way and is easier to implement. This lets us get over the drawback of a larger amount of Lagrange multipliers compared to the non-redundant formulation.

In compact form, we can write the constraints for linear elasticity as

$$\sum_{i=1}^{p} \mathbf{B}_i \underline{u}_i = \underline{0} \quad \text{or} \quad \mathbf{B}\underline{u} = \underline{0}. \tag{6.8}$$

The so-called *jump operators* $\mathbf{B}_i$ are signed boolean matrices and have a sparse structure since entries are only generated for coupling nodes, i.e. for neighboring subdomains. We denote by m the total number of constraints and by m_i the number of degrees of freedom of a specific domain Ω_i. Then we can state that

$$\mathbf{B}_i \in \mathbb{R}^{m \times m_i} \quad \text{and} \quad \mathbf{B}_i : \mathbb{R}^{m_i} \to \mathbb{R}^m$$

holds for each $i \in \mathcal{I}$. To fulfill the constraints $(6.7)_1$, the jump operators are defined as

$$\left(\mathbf{B}_i \mathbf{u}_i\right)_{jk}(\mathbf{x}) = \begin{cases} \underline{u}_i(\mathbf{x}) & \text{if } i = j \\ -\underline{u}_i(\mathbf{x}) & \text{if } i = k \\ \underline{0} & \text{else} \end{cases}$$

for $\mathbf{x} \in \Gamma_{jk}$ and per definition $j > k$. By construction it holds that

$$\langle \mathbf{B}\underline{u}, \underline{\mu} \rangle = \sum_{i=1}^{p} \langle \mathbf{B}_i \underline{u}_i, \underline{\mu} \rangle \quad \text{for all } \underline{\mu} \in \mathbb{R}^m. \tag{6.9}$$

In a similar way, we define the jump operators for nonlinear elasticity by $(6.7)_2$. To enforce continuity of the solution (6.8) we use (6.9) and introduce the vector of Lagrange multipliers $\underline{\lambda}$ to get the saddle point system: find $(\underline{u}_i, \underline{\lambda}) \in \mathbb{R}^{m_i} \times \mathbb{R}^m$ such that

$$\begin{pmatrix} \mathbf{K}_1 & & & \mathbf{B}_1^\top \\ & \ddots & & \vdots \\ & & \mathbf{K}_p & \mathbf{B}_p^\top \\ \mathbf{B}_1 & \dots & \mathbf{B}_p & \end{pmatrix} \begin{pmatrix} \underline{u}_1 \\ \vdots \\ \underline{u}_p \\ \underline{\lambda} \end{pmatrix} = \begin{pmatrix} \underline{f}_1 \\ \vdots \\ \underline{f}_p \\ \underline{0} \end{pmatrix}. \tag{6.10}$$

Correspondingly, for the nonlinear elasticity case, cf. (5.9), we get the linearized system of equations

$$\begin{pmatrix} \mathbf{K}_1'(\underline{u}_i^k) & & & \mathbf{B}_1^\top \\ & \ddots & & \vdots \\ & & \mathbf{K}_p'(\underline{u}_i^k) & \mathbf{B}_p^\top \\ \mathbf{B}_1 & \dots & \mathbf{B}_p & \end{pmatrix} \begin{pmatrix} \delta\underline{u}_1 \\ \vdots \\ \delta\underline{u}_p \\ \underline{\lambda} \end{pmatrix} = \begin{pmatrix} \widetilde{\underline{f}}_1(\underline{u}_i^k) \\ \vdots \\ \widetilde{\underline{f}}_p(\underline{u}_i^k) \\ \underline{0} \end{pmatrix}. \tag{6.11}$$

An identical representation can be retrieved using the transmission conditions with the Dirichlet to Neumann mapping (6.6). From this derivation of the FETI method we notice that the Lagrange multipliers λ may be interpreted as boundary stresses [141, 153, 178].

Note that the problems (6.10) and (6.11) are uniquely solvable given that

$$\ker \mathbf{K}_i \cap \ker \mathbf{B}_i = \emptyset, \quad \ker \mathbf{K}_i'(\underline{u}_i^k) \cap \ker \mathbf{B}_i = \emptyset \quad \text{for all } i \in \mathcal{I}, \tag{6.12}$$

see Fortin and Brezzi [58]. Condition (6.12) is fulfilled for subdomains Ω_i with a Dirichlet boundary, i.e. $\Gamma_i \cap \Gamma_{\mathrm{D}} \neq \emptyset$ and there it holds that $\ker \mathbf{K}_i = \emptyset$ and $\ker \mathbf{K}_i'(\underline{u}_i^k) = \emptyset$, respectively. For Neumann subdomains, typically referred to as *floating subdomains*, the additional solvability conditions

$$(\underline{f}_i - \mathbf{B}_i^\top \underline{\lambda}, \underline{r}_{k,i}) = 0 \text{ and } (\widetilde{\underline{f}}_i(\underline{u}_i^k) - \mathbf{B}_i^\top \underline{\lambda}, \underline{r}_{k,i}) = 0 \text{ for } k = 1, \dots, 6;\ i \in \mathcal{I}_{\text{floating}}$$

are required, where $\underline{r}_{k,i} \in \ker \mathbf{K}_i'$ correspond to the rigid body modes of elasticity (Remark 4.2.2) and $\mathcal{I}_{\text{floating}}$ is the index set of all floating subdomains. In the following, the focus is on the more general nonlinear elasticity problem and we denote by $\mathbf{K}_i' := \mathbf{K}_i'(\underline{u}_i^k)$ the local tangent stiffness matrices and by $\widetilde{\underline{f}}_i := \widetilde{\underline{f}}_i(\underline{u}_i^k)$ the local right hand sides.

Starting from (6.11), we follow the standard approach of tearing and interconnecting methods in eliminating the local degrees of freedom $\delta\underline{u}_i$. In the case of a floating subdomain Ω_i, i.e. $\Gamma_i \cap \Gamma_D = \emptyset$, the local matrices $\mathbf{K}_i'$ are singular. Hence, a generalized inverse matrix $\mathbf{K}_i^\dagger$ is introduced to represent the local solutions as

$$\delta\underline{u}_i = \mathbf{K}_i^\dagger(\widetilde{\underline{f}}_i - \mathbf{B}_i^\top \underline{\lambda}) + \sum_{k=1}^{6} \gamma_{k,i}\underline{r}_{k,i}, \tag{6.13}$$

where $\gamma_{k,i}$ are unknown constants. In the case of a non-floating subdomain, i.e. $\ker \mathbf{K}_i = \emptyset$, the local stiffness matrices are invertible and $\mathbf{K}_i^\dagger = \mathbf{K}_i^{-1}$. In some circumstances the kernel of $\mathbf{K}_i'$ is non-trivial and its dimension is lower than 6. This is the case if the set $\Gamma_{0,i} \cap \Gamma_{0,D}$ is either a single vertex or a single edge. For classical FETI this requires the implementation of an effective strategy to identify these kernels reliably. Beyond question, this is a key advantage of the all-floating FETI approach, see Section 6.2.1, where all subdomains are treated the same and the kernel of each local operator is known to be $\ker \mathbf{K}_i' = 6$. In consequence, the solution of the local problems to find the generalized inverse $\mathbf{K}_i^\dagger$ can be reduced to sparse systems. As an additional advantage of all-floating FETI, these local problems are typically better conditioned compared to the systems arising from the FETI–DP method, see, e.g., Brzobohatý et al. [32].

In general, we consider the Schur complement of (6.11) to obtain

$$\sum_{i=1}^{p} \mathbf{B}_i \mathbf{K}_i^\dagger \mathbf{B}_i^\top \underline{\lambda} - \sum_{i=1}^{p}\sum_{k=1}^{6} \gamma_{k,i}\mathbf{B}_i \underline{v}_{k,i} = \sum_{i=1}^{p} \mathbf{B}_i \mathbf{K}_i^\dagger \widetilde{\underline{f}}_i, \quad (\widetilde{\underline{f}}_i - \mathbf{B}_i^\top \underline{\lambda}, \underline{r}_{k,i}) = 0,$$

which can be written as

$$\begin{pmatrix} \mathbf{F} & -\mathbf{G} \\ \mathbf{G}^\top & \end{pmatrix} \begin{pmatrix} \underline{\lambda} \\ \underline{\gamma} \end{pmatrix} = \begin{pmatrix} \underline{d} \\ \underline{e} \end{pmatrix}, \tag{6.14}$$

with the denotations

$$\mathbf{F} := \sum_{i=1}^{p} \mathbf{B}_i \mathbf{K}_i^\dagger \mathbf{B}_i^\top,\ \mathbf{G} := \sum_{i=1}^{p}\sum_{k=1}^{6} \mathbf{B}_i \underline{r}_{k,i},\ \underline{d} =: \sum_{i=1}^{p} \mathbf{B}_i \mathbf{K}_i^\dagger \widetilde{\underline{f}}_i,\ e_{k,i} := (\widetilde{\underline{f}}_i, \underline{r}_{k,i}). \tag{6.15}$$

Denote by X the space

$$X := \ker(\mathbf{G}^\top) = \{\underline{\lambda} \in \mathbb{R}^m : \langle \mathbf{B}_i \underline{r}, \underline{\lambda}\rangle = 0 \text{ for all } \underline{r}_{k,i} \in \ker \mathbf{K}_i',\ k = 1,\dots,6;\ i \in \mathcal{I}\}.$$

For the solution of the linear system (6.14) we introduce the projection $\mathbf{P} : \mathbb{R}^m \to X$ as

$$\mathbf{P}^\top := \mathbf{I} - \mathbf{G}\left(\mathbf{G}^\top \mathbf{G}\right)^{-1} \mathbf{G}^\top \tag{6.16}$$

and it remains to consider the projected system

$$\mathbf{P}^\top \mathbf{F} \underline{\lambda} = \mathbf{P}^\top \underline{d}, \quad \underline{\lambda} \in \underline{\lambda}_0 + X, \tag{6.17}$$

which can be solved by using a parallel iterative Krylov subspace method with suitable preconditioning, cf. Section 6.2.2. The initial approximate solution $\underline{\lambda}_0$ has to satisfy the compatibility condition $\mathbf{G}^\top \underline{\lambda}_0 = \underline{e}$ where a possible choice is

$$\underline{\lambda}_0 = \mathbf{G} \left(\mathbf{G}^\top \mathbf{G} \right)^{-1} \underline{e}.$$

In a postprocessing step, we finally recover the vector of constants

$$\underline{\gamma} = \left(\mathbf{G}^\top \mathbf{G} \right)^{-1} \mathbf{G}^\top \left(\mathbf{F} \underline{\lambda} - \underline{d} \right)$$

and subsequently the desired solution by (6.13).

Remark 6.2.1. *Due to the construction of* $\mathbf{F}$*, see* (6.15)*, and the projection* $\mathbf{P}$*, see* (6.16)*, the system* (6.17) *is symmetric given that the local stiffness matrices* $\mathbf{K}_i'$ *are symmetric.*

Remark 6.2.2. *With the positive definiteness of the local tangent stiffness matrices* $\mathbf{K}_i'$ *and the definitions of* $\mathbf{F}$ *and* $\mathbf{P}$ *it holds for all* $\underline{\lambda}$ *in the quotient space* $\underline{\lambda} \in X / \ker \mathbf{B}^\top$ *and* $\underline{\lambda} \neq 0$

$$\langle \mathbf{P}^\top \mathbf{F} \underline{\lambda}, \underline{\lambda} \rangle = \langle \mathbf{F} \underline{\lambda}, \mathbf{P} \underline{\lambda} \rangle = \langle \mathbf{F} \underline{\lambda}, \underline{\lambda} \rangle = \langle \sum_{i=1}^{p} \mathbf{B}_i \mathbf{K}_i^\dagger \mathbf{B}_i^\top \ \underline{\lambda}, \underline{\lambda} \rangle = \sum_{i=1}^{p} \langle \mathbf{K}_i^\dagger \mathbf{B}_i^\top \underline{\lambda}, \mathbf{B}_i^\top \underline{\lambda} \rangle > 0,$$

with $\mathbf{P} \underline{\lambda} = \underline{\lambda}$*, since* $\underline{\lambda} \in X / \ker \mathbf{B}^\top = \left\{ \widetilde{\lambda} + \ker \mathbf{B}^\top : \widetilde{\lambda} \in \ker(\mathbf{G}^\top) \right\}$*. For a detailed proof see [141, Section 2.2.1]. This shows the positive definiteness of the system* (6.17) *on* $X / \ker \mathbf{B}^\top$ *for the considered linear and nonlinear elasticity problems.*

6.2.1 All-floating FETI Methods

The idea of all-floating FETI (AF–FETI) is to treat *all* subdomains as floating subdomains, Figure 6.5. In addition to the standard procedure of gluing the subregions along the auxiliary interfaces, the Lagrange multipliers are likewise used to incorporate Dirichlet boundary conditions. All subdomain stiffness matrices have the same and known kernel, which eases the implementation of the FETI procedure in a software framework significantly. Further to that, some tests (Chapter 7) showed more efficiency than the classical FETI method as the asymptotic behavior improves, which is explained by mapping properties of the Steklov–Poincaré operator, see [138,

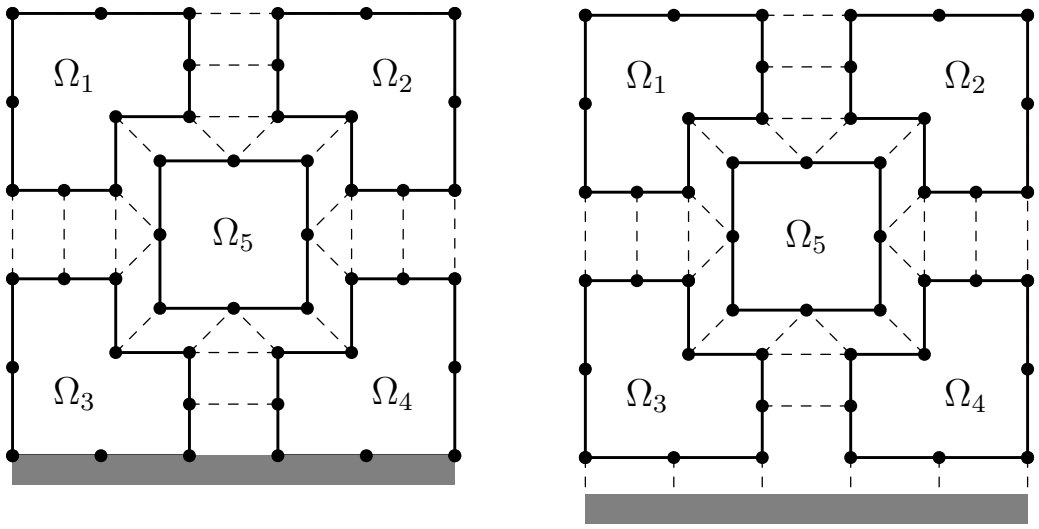

Figure 6.5: To the left a sketch of the classical FETI method and to the right a sketch of the all-floating FETI method. The gray bar depicts Dirichlet boundary conditions.

Remark 1]. The drawback is an increasing number of degrees of freedom and Lagrange multipliers. More information on all-floating FETI one may find in [136, 138] and on the related Total–FETI (TFETI) method in [51].

To incorporate Dirichlet boundary conditions the system of constraints (6.8) is modified in the following way

$$\sum_{i=1}^{p} \tilde{\mathbf{B}}_i \underline{u}_i = \underline{b}, \tag{6.18}$$

where the matrices $\tilde{\mathbf{B}}_i$ and the vector $\underline{b}$ are given such that

$$\left(\tilde{\mathbf{B}}_i \underline{u}_i\right)_{jk}(\mathbf{x}) = \begin{cases} \underline{u}_i(\mathbf{x}) & \text{if } i = j,\ \mathbf{x} \in \Gamma_{jk},\ j > k, \\ -\underline{u}_i(\mathbf{x}) & \text{if } i = k,\ \mathbf{x} \in \Gamma_{jk},\ j > k, \\ \underline{u}_i(\mathbf{x}) & \text{if } \mathbf{x} \in \Gamma_j \cap \Gamma_{\mathrm{D}}, \\ \underline{0} & \text{else} \end{cases} \tag{6.19}$$

and

$$\underline{b}_{jk}(\mathbf{x}) = \begin{cases} \underline{0} & \text{if } \mathbf{x} \in \Gamma_{jk}, \\ \underline{u}_{\mathrm{D}}(\mathbf{x}) & \text{if } \mathbf{x} \in \Gamma_j \cap \Gamma_{\mathrm{D}}. \end{cases}$$

6.2.2 Preconditioning

In order to present suitable preconditioners for the described FETI methods we first introduce a weighting function, known from balancing Neumann-Neumann methods

[178, Section 6.2] and [136, Section 5.5.2],

$$\delta_i^\dagger(\mathbf{x}) := \frac{\alpha_i^\gamma}{\sum_k^n \alpha_k^\gamma}, \quad \mathbf{x} \in \Gamma_i,\ i \in \mathcal{I}$$

with $\gamma \in [0.5, \infty]$, n the number of subdomains which share the coupling node x and α_i a coefficient depending on the material parameters. In the case of linear elasticity we choose $\alpha_i = E_i/(1+\nu_i)$ with Young's modulus E_i and Poisson's ratio ν_i in Ω_i [111]. For the neo–Hooke and the artery model we choose $\alpha_i = c_i/2$ and for the myocardium model $\alpha_i = a_i/2$, $i \in \mathcal{I}$. Using this scaling factor we can define the scaled jump operators $\mathbf{B_D}$ as

$$\mathbf{B}_{\mathbf{D},i} := \mathbf{D}_i \mathbf{B}_i,$$

where $\mathbf{D}_i = \operatorname{diag}(\delta_i^\dagger(\mathbf{x}))$, $\mathbf{x} \in \Gamma_i$. With this denotation all preconditioners for the FETI method can be written as

$$\mathbf{M}^{-1} := \sum_{i=1}^{p} \mathbf{B}_{\mathbf{D},i} \mathbf{Y}_i \mathbf{B}_{\mathbf{D},i}^\top, \tag{6.20}$$

with a matrix $\mathbf{Y}_i \in \mathbb{R}^{m_i \times m_i}$.

Definition 6.1 (Lumped preconditioner)**.** *Following Farhat and Roux [55] we define the* lumped preconditioner *as*

$$\mathbf{M}_{\mathrm{l}}^{-1} := \sum_{i=1}^{p} \mathbf{B}_{\mathbf{D},i} \mathbf{A}_i \mathbf{B}_{\mathbf{D},i}^\top,$$

with $\mathbf{A}_i$ the local stiffness matrix $\mathbf{K}_i$ for linear elasticity or the local tangent stiffness matrix $\mathbf{K}_i'(u_{i,h}^k)$ for nonlinear elasticity, respectively.

Definition 6.2 (Dirichlet preconditioner)**.** *An* optimal *domain decomposition preconditioner is the* Dirichlet preconditioner*, see Farhat et al. [54],*

$$\mathbf{M}_{\mathrm{D}}^{-1} := \sum_{i=1}^{p} \mathbf{B}_i \begin{pmatrix} \mathbf{0} & \mathbf{0} \\ \mathbf{0} & \mathbf{S}_i \end{pmatrix} \mathbf{B}_i^\top,$$

where

$$\mathbf{S}_i = \mathbf{K}_{\mathrm{CC}}'(\underline{u}_i^k) - \mathbf{K}_{\mathrm{C}i}'(\underline{u}_i^k) \mathbf{K}_{ii}'^{-1}(\underline{u}_i^k) \mathbf{K}_{i\mathrm{C}}'(\underline{u}_i^k)$$

is the Schur complement of the local tangent finite element matrices $\mathbf{K}_i'(\underline{u}_{i,h}^k)$ in the case of nonlinear elasticity. For FETI this Schur complement is the discrete version of the Steklov–Poincaré operator $S_i^{int} : [H^{1/2}(\Gamma_i)]^3 \to [H^{-1/2}(\Gamma_i)]^3$ described in (6.6)*.*

The optimality of the Dirichlet preconditioner is highlighted by numerical examples in Chapter 7, where it showed the lowest condition numbers of the FETI system (6.17)

and hence also the lowest number of global Krylov iterations compared to other forms of preconditioning. Nonetheless, the formation of the Dirichlet preconditioner needs the computation of an additional inverse matrix to construct the Schur complement. To avoid local iterative solving in each global Krylov solver step, which would clearly decrease the computational performance for most problems, we use a direct solver package, cf. Section 5.6.1, to compute the needed factorization. On the other hand, this strategy is possibly very time and memory consuming for large subdomains. Hence, the choice of the number of subdomains and thereby the local problem size is a very delicate matter. By experience, this is in fact a question of available (fast) memory where direct solvers are known to be rather costly. Since this factorization is a local operation the burden of more computational complexity and the increased number of FLOPS is not as serious. As evidence, some numerical examples, see Chapter 7, were not solvable due to depleting memory.

In contrast, the lumped preconditioner is more economical and needs no additional storage or computation. Thus, this type of preconditioning outperforms the more sophisticated Dirichlet preconditioner for certain numerical setups. Nevertheless, we encountered experiments where the global Krylov method was not converging within a commensurate number of iterations, see Chapter 7.

Definition 6.3 (Identity preconditioner)**.** *For comparison we define the trivial* identity preconditioner*, where* $\mathbf{Y}_i$ *in* (6.20) *is replaced by the identity matrix.*

Alternatively, we use a novel scaled hypersingular boundary integral operator preconditioner as proposed in in the publication of Langer and Steinbach [114]. Following [176], we introduce the *hypersingular boundary integral operators* $D_i : [H^{1/2}(\Gamma_i)]^3 \to [H^{-1/2}(\Gamma_i)]^3$ as

$$(\mathbf{D}_i \mathbf{u}_i)(\mathbf{x}) = -\gamma_{1,x}^{i,\mathrm{int}} \int_{\Gamma_i} \left(\gamma_{1,y}^{i,\mathrm{int}} \mathbf{U}^*(\mathbf{x},\mathbf{y})\right)^\top \mathbf{u}_i(\mathbf{y}) \, \mathrm{d}s_{\mathbf{y}}, \tag{6.21}$$

with the fundamental solution of linear elasticity, *Kelvin's tensor* $\mathbf{U}^*(\mathbf{x},\mathbf{y})$,

$$U_{kl}^*(\mathbf{x},\mathbf{y}) = \frac{1}{8\pi}\frac{1}{E}\frac{1+\nu}{1-\nu}\left[(3-4\nu)\frac{\delta_{kl}}{|\mathbf{x}-\mathbf{y}|} + \frac{(x_k-y_k)(x_l-y_l)}{|\mathbf{x}-\mathbf{y}|^3}\right], \quad k,l = 1,2,3,$$

and $\gamma_{1,(\bullet)}^{i,\mathrm{int}}$ the Neumann trace operator for $\mathbf{x},\mathbf{y} \in \Gamma_i$.

Definition 6.4 (BETI preconditioner)**.** *On the basis of [114], we define the* BETI preconditioner *for linear and nonlinear elasticity problems as*

$$\mathbf{M}_{\mathrm{BETI}}^{-1} := \sum_{i=1}^{p} \mathbf{B}_i \begin{pmatrix} \mathbf{0} & \mathbf{0} \\ \mathbf{0} & \mathbf{D}_{i,h} \end{pmatrix} \mathbf{B}_i^\top,$$

with $\mathbf{D}_{i,h}$ *the discretized version of the hypersingular boundary integral operator introduced in* (6.21).

Lemma 6.5. *For linear elasticity problems the condition number of the FETI problems with Dirichlet preconditioning is estimated by*

$$\kappa(\mathbf{P}\mathbf{M}_{\mathrm{D}}^{-1}\mathbf{P}^{\top}\mathbf{F}) = c\left(1+\log\left(\frac{H}{h}\right)\right)^2,$$

with the positive constant c *which is independent of* h, H, p *and the values of the coefficients* E_i *and* ν_i.

Proof. For the proof cf. Klawonn and Widlund [110] building on results of Mandel and Tezaur [119] and also [140, Pechstein and Scheichl (2008)]. □

Lemma 6.6. *The condition number of the preconditioned linear elasticity FETI problem with the BETI preconditioner* $\mathbf{M}_{\mathrm{BETI}}^{-1}$ *satisfies*

$$\kappa(\mathbf{P}\mathbf{M}_{\mathrm{BETI}}^{-1}\mathbf{P}^{\top}\mathbf{F}) = c\left(1+\log\left(\frac{H}{h}\right)\right)^2,$$

with the positive constant c *which is independent of* h, H, p *and the values of the coefficients* E_i *and* ν_i.

Proof. This was proved by Langer and Steinbach [114] by showing the spectral equivalence of $\mathbf{M}_{\mathrm{BETI}}^{-1}$ and $\mathbf{M}_{\mathrm{D}}^{-1}$ and using Lemma 6.5. □

6.2.3 Computing the Generalized Inverse Matrix

In order to set up the projected FETI system (6.17) we need to compute the local pseudo inverse matrices $\mathbf{K}_i^{\dagger}$. In this work we will concentrate on local direct solvers, see Section 5.6.1. The alternative, local iterative solving, shows advantages in storage consumption but may have certain drawbacks in the computational performance. This is due to the fact that within every single global Krylov solver iteration we have several local iterations, while in using direct solvers we just have to factorize the local stiffness matrix once and subsequently compute a matrix vector multiplication in each global step. Nevertheless, for large subdomains and problems with storage restrictions an iterative strategy for the local inversion may be advantageous. See also the reflections after Definition 6.2.

As mentioned before, for non-floating subdomains the pseudo-inverse matrix $\mathbf{K}_i^{\dagger}$ is simply the inverse matrix $\mathbf{K}_i^{-1}$. For floating subdomains we need to compute a

generalized inverse matrix such that

$$\mathbf{K}_i \mathbf{K}_i^\dagger \mathbf{K}_i = \mathbf{K}_i, \quad \text{for } i \in \mathcal{I}_{\text{floating}}.$$

Given the local stiffness matrix $\mathbf{K}_i$ and $\underline{u}, \underline{v} \in \mathbb{R}^{m_i}$ this can be achieved as follows. With $k_i = \dim(\ker(\mathbf{K}_i))$ we write

$$(\tilde{\mathbf{K}}_i \underline{u}, \underline{v}) := (\mathbf{K}_i \underline{u}, \underline{v}) + \sum_{j=1}^{k_i} \beta_k \, (\underline{u}, \mathbf{r}_j^{(i)})_{\mathcal{R}_i} \, (\underline{v}, \underline{r}_j^{(i)})_{\mathcal{R}_i},$$

where $(\cdot,\cdot)_{\mathcal{R}_i}$ is a bilinear form that is coercive and bounded on $\ker \mathbf{K}_i$ and $\{\underline{r}_j^{(i)}\}_j$, $j = 1, \ldots, k_i$ is a set of vectors spanning $\ker \mathbf{K}_i$. In the case of elasticity these are the rigid body motions. We set

$$\mathbf{K}_i^\dagger := (\tilde{\mathbf{K}}_i)^{-1}.$$

For $\underline{f} \in \text{range}(\mathbf{K}_i)$ we then have $(\mathbf{K}_i^\dagger \underline{f}, \underline{r}_j^{(i)})_{\mathcal{R}_i} = 0$ for all $j = 1, \ldots, k_i$. This implies

$$\mathbf{K}_i^\dagger \underline{f} \perp_{\mathcal{R}_i} \ker \mathbf{K}_i.$$

Thus $\mathbf{K}_i^\dagger$ is a generalized inverse matrix with respect to a special inner product. In order to preserve the sparsity of the stiffness matrix, a requirement to use a direct solver, we choose the scalar product

$$(\underline{u}, \underline{v})_{\mathcal{R}_i} := \int_{\omega_i} \underline{u} \cdot \underline{w} \, \mathrm{d}X_i,$$

where ω_i is a subset of Ω_i, or a submanifold in Ω_i. This can be a set of points, edges or faces.

For elasticity we choose the scalar product as follows: Let Ω_i be some subdomain with a point set $\mathcal{P}$ containing at least three points $p^{(1)}$, $p^{(2)}$ and $p^{(3)}$ that are not collinear, see Figure 6.6. We then use

$$(\underline{v}, \underline{w})_{\mathcal{R}_i} := \sum_{m=1}^{n_{\text{p}}} \underline{v}(p^{(m)}) \cdot \underline{w}(p^{(m)})$$

where $\underline{v}(p^{(\bullet)})$ and $\underline{w}(p^{(\bullet)})$ are the point evaluations of the vectors $\mathbf{v}$ and $\mathbf{w}$ at the point $p^{(\bullet)}$ and n_{p} is the number of regularization points. The kernel $\ker \mathbf{K}_i$ for linear elasticity and the kernel $\ker \mathbf{K}_i'$ for nonlinear elasticity are spanned by $\mathbf{r}_j^{(i)}$, the rigid body modes. Let k_m^* denote the node index of vertex $p^{(m)}$. All basis functions vanish at the point $p^{(m)}$ except for those associated to it. In addition, just one component of the point realizes as 1 as we apply the basis function. Hence, the regularization

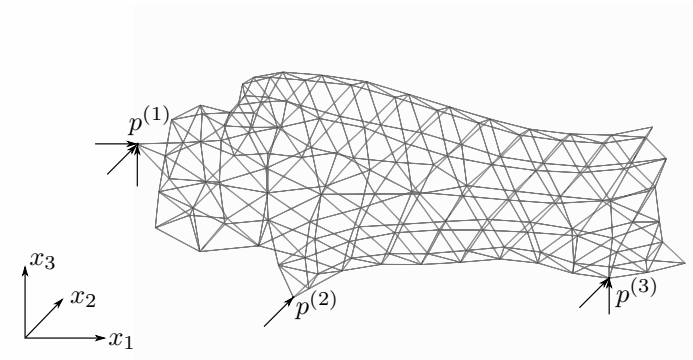

Figure 6.6: One possibility to fix the six rigid body motions of a Neumann subdomain with three non-collinear points; point $p^{(1)}$ is fixed in all three directions, $p^{(2)}$ is fixed in x_2 direction and $p^{(3)}$ is fixed in direction of x_2 and x_3.

with n_{p} points in 3D results in

$$\tilde{\mathbf{K}}_i[j,k] = \mathbf{K}_i[j,k] + \sum_{l=1}^{k_i} \sum_{m=1}^{n_{\mathrm{p}}} \sum_{d=1}^{3} \beta_l \, \delta_{j(3k_m^*+d)} r_l(p^{(m)}) \cdot \delta_{k(3k_m^*+d)} r_l(p^{(m)})$$

For the choice of the constants β_l we take a look at the condition number of the regularized elasticity matrix.

Condition Number of the Regularized Elasticity Matrix Let H be the typical subdomain diameter, see (6.2), and let us assume a quasi-uniform triangulation of Ω with mesh size h. In the following we concentrate on the linear elasticity case but the estimates also hold true for nonlinear elasticity. For $\underline{v}$, $\underline{w} \in \mathbb{R}^{m_i}$ we set

$$(\tilde{\mathbf{K}}\underline{v}, \underline{w}) = (\mathbf{K}\underline{v}, \underline{w}) + \sum_{l=1}^{6} \sum_{m=1}^{n_{\mathrm{p}}} \beta_l \underline{v}(p^{(m)}) \underline{w}(p^{(m)})$$

for a vertex p and $\mathbf{K}$ the stiffness matrix arising from the linear elasticity problem. From the inverse inequality and the usual reference element transformation, we get that

$$\begin{aligned}(\mathbf{K}\underline{v}, \underline{v}) &\leq \frac{2E}{1-2\nu} |\mathbf{v}_h|^2_{[H^1(\Omega_i)]^3} = \frac{2E}{1-2\nu} \|\nabla \mathbf{v}_h\|^2_{[L_2(\Omega_i)]^3} \leq \tilde{C} \, \frac{2E}{1-2\nu} h^{-2} \|\mathbf{v}_h\|^2_{[L_2(\Omega_i)]^3} \\ &\leq \tilde{C} \, \frac{2E}{1-2\nu} h^{-2} h^3 \|\underline{v}\|_2^2 = C \, h \, \|\underline{v}\|_2^2.\end{aligned}$$

Hence, with $\beta_{\max} = \max \beta_l$, $l = 1, \ldots, 6$,

$$(\tilde{\mathbf{K}}\underline{v}, \underline{v}) \leq (C \, h + 6 \, \beta_{\max}) \, \|\underline{v}\|_2^2.$$

For the lower bound we get with $\beta_{\min} = \min \beta_l$, $l = 1, \ldots, 6$,

$$(\tilde{\mathbf{K}}\underline{v}, \underline{v}) \geq |\mathbf{v}_h|^2_{[H^1(\Omega)]^3} + \beta_{\min} \sum_{m=1}^{n_p} |\mathbf{v}(p^{(m)})|^2.$$

We now use the discrete Poincaré–Friedrich inequality, [178, Section 4.6],

$$\|\mathbf{v}_h - \overline{\mathbf{v}}(\epsilon))\|^2_{[L^2(\Omega_i)]^3} \leq C\, H^2\, (H/h) |\mathbf{v}_h|^2_{[H^1(\Omega_i)]^3} \qquad \forall \mathbf{v}_h \in V_h(\Omega_i)\,,$$

for ϵ an edge, a face or a wire basket.

From this inequality and the Cauchy–Schwarz inequality we can conclude that

$$\begin{aligned} \|\mathbf{v}_h\|^2_{[L^2(\Omega_i)]^3} &\leq 2C\, H^2\, (H/h)\, |\mathbf{v}_h|^2_{[H^1(\Omega_i)]^3} + 2\, |\Omega_i|\, |\overline{\mathbf{v}}(\epsilon)|^2 \\ &\leq\ C\, H^2 \max\left(H/h, \frac{|\Omega_i|}{\beta_{\min}\, H^2}\right) (\tilde{\mathbf{K}}\underline{v}, \underline{v}) \end{aligned}$$

Finally, we have

$$\|\mathbf{v}_h\|^2_{[L^2(\Omega_i)]^3} \ \geq\ C\, h^3\, \|\underline{v}\|_2^2.$$

Summarizing, using

$$\kappa(\tilde{\mathbf{K}}) \ \leq\ C\, H^2 \max(h, 6\,\beta_{\max}) \max\left(H/h, \frac{|\Omega_i|}{\beta_{\min}\, H^2}\right)$$

we can estimate the condition number of the regularized stiffness matrix.

This suggests to choose

$$\beta_l \in \left[\frac{|\Omega_i|}{H^2\,(H/h)}, \frac{1}{6\,h}\right], \quad \text{for } l = 1, \ldots, 6,$$

which is satisfied, e.g., for $\beta = 1$. Then,

$$\kappa(\tilde{\mathbf{K}}) = \mathcal{O}((H/h)^2 (H/h)).$$

The extra factor of (H/h) is unavoidable and there is no better choice of β to get a better result than $\kappa(\tilde{\mathbf{K}}) = \mathcal{O}((H/h)^3)$ in comparison to $\kappa(\mathbf{K}) = \mathcal{O}((H/h)^2)$. The only way to improve the condition number is to choose a different inner product $\mathcal{R}_i$ which then affects the sparsity of the regularized stiffness matrix $\tilde{\mathbf{K}}$. Since we are using direct solvers the higher condition number will be negligible: all that is affected by the condition number itself is the rounding error, which means, that we only loose a bit of accuracy.

7 NUMERICAL EXAMPLES

In this chapter we give numerical examples for the finite element tearing and interconnecting approach as described in Chapter 6. In Section 7.1 we test the FETI implementation for the linear elasticity case. Here we are able to compare the computed results to a given exact solution. This enables us to show the correctness of our implementation and to show the convergence rates as predicted from the theory. We compare the different preconditioning techniques and present differences between the classical FETI and the all-floating FETI approach. Following to this in Section 7.2 we apply the FETI approach to nonlinear elasticity problems. We focus on the artery and the myocardium model as described in Chapter 3. As in the linear case we compare the different preconditioning techniques as well as all-floating FETI and the classical FETI method for simple geometries. At the end we present examples using more realistic triangulations. We apply the anisotropic artery model to a geometry of an aorta and a carotid artery consisting of two materials, i.e. the media and the adventitia, and the orthotropic myocardium model to the myocardium of the ventricles of a rabbit heart.

The calculations were done using the *GHOST*-cluster located at the Graz University of Technology and the *VSC2*-cluster (`http://vsc.ac.at/`) in Vienna.

GHOST is a Linux-cluster consisting of two nodes, each with eight Quad-Core AMD Opteron 8356 Barcelona processors and a memory of 252.48 GB RAM. The AMD processors run with a clockrate of 2.3 GHz. The The Linux-cluster *VSC2* features 1314 compute nodes, each with two AMD Opteron Magny Cours 6132HE (8 Cores, 2.2 GHz) processors and 8 x 4 RAM. This yields the total number of 21 024 available processor cores.

The mechanics and the FETI framework was implemented in coorporation with Clemens Pechstein from the Johannes Kepler University in Linz, using the C++ template software package ParMax[1].

As local direct solver we use PARDISO [160, 161], included in Intel's Math Kernel Library (MKL).

[1] `http://www.numa.uni-linz.ac.at/P19255/software.shtml`, Clemens Pechstein and others.

7.1 Linear Elasticity

In this first section of numerical examples we consider linear elasticity problems with the academical example of a unit cube which is decomposed into a certain number of subcubes. Dirichlet boundary conditions are imposed all over the surface $\Gamma_D = \partial\Omega$, see Figure 7.1. The calculated solution is compared to the fundamental solution of linear elastostatics [176]

$$U^*_{1k}(\mathbf{x},\mathbf{x}^*) = \frac{1}{8\pi}\frac{1}{E}\frac{1+\nu}{1-\nu}\left[(3-4\nu)\frac{\delta_{1k}}{|\mathbf{x}-\mathbf{x}^*|} + \frac{(x_1-x_1^*)(x_k-x_k^*)}{|\mathbf{x}-\mathbf{x}^*|^3}\right], \quad k=1,2,3, \quad (7.1)$$

where $\mathbf{x} \in \Omega$, $\mathbf{x}^* \in \mathbb{R}^3$ is an arbitrary point outside of the domain Ω and δ_{ij} is the Kronecker delta. We compare the different strategies of preconditioning and all-floating and classical FETI. As the global iterative method we use the conjugate gradient method with a relative error reduction of 1×10^{-8}.

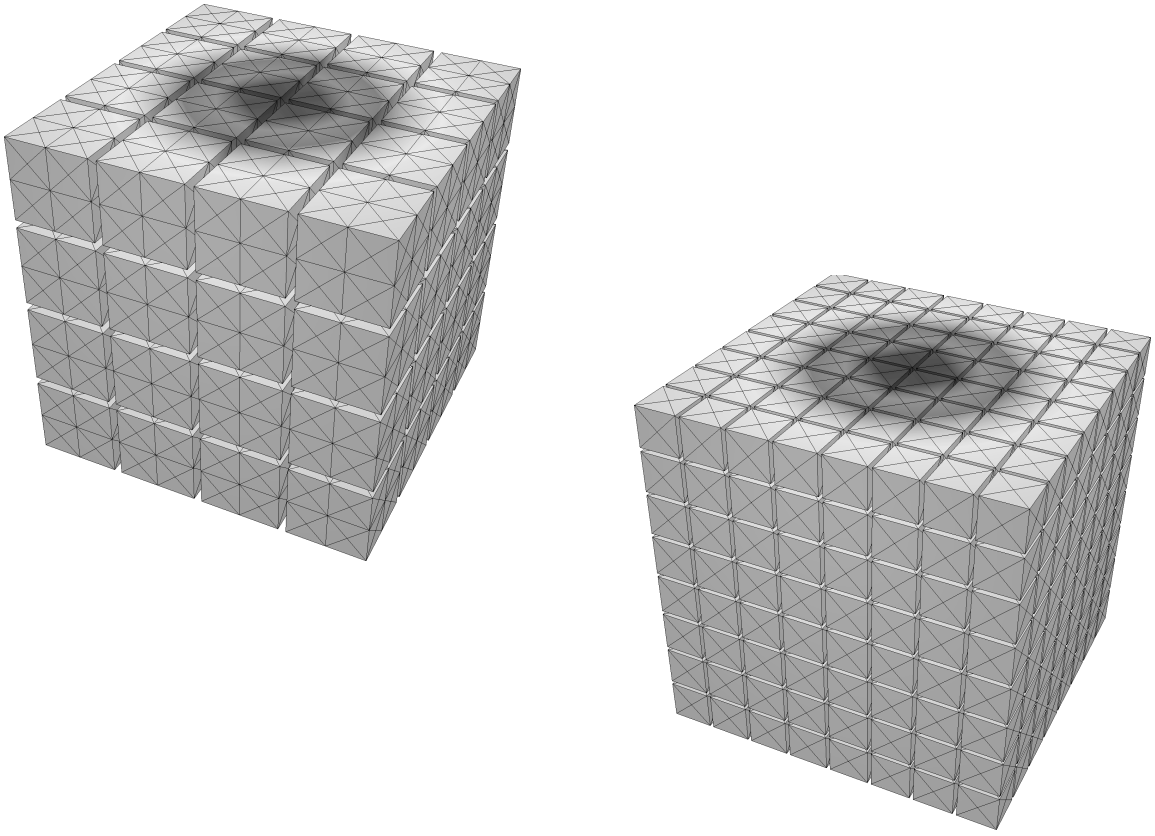

Figure 7.1: Unit cube decomposed in 64 subdomains, level $\ell = 2$ (left) and decomposed in 512 subdomains, level $\ell = 1$ (right). Black and white shadings show fundamental solution (7.1).

7.1.1 Linear Elements

We consider a linear elasticity problem using linear tetrahedral elements ($\mathcal{P}_1$ element) given a cube with 512 subdomains and a cube with 64 subdomains. The parameters are $E = 210\,\text{GPa}$ and $\nu = 0.3$. Note at first that for all examined settings, see Table 7.1 and Table 7.3 the L2 error, i.e.

$$\|\mathbf{u} - \mathbf{u}_h\|_{L_2(\Omega)}, \tag{7.2}$$

where $\mathbf{u}_h$ is the approximate and $\mathbf{u}$ the exact solution, and the estimated order of convergence (eoc)

$$\text{eoc}_\ell = \frac{\ln\|\mathbf{u} - \mathbf{u}_{h,\ell}\|_{L_2(\Omega)} - \ln\|\mathbf{u} - \mathbf{u}_{h,\ell}\|_{L_2(\Omega)}}{\ln 2} \tag{7.3}$$

behave as expected from the theory. For both mesh settings, the cube subdivided into 512 subdomains and the cube subdivided into 64 subdomains, we get similar results if we compare the iteration numbers of the global CG method subject to the preconditioning techniques. We get the least iteration numbers for the optimal Dirichlet preconditioner. Given a large enough size of the subcubes, the application of the BETI preconditioner results in better iteration numbers than the lumped preconditioner and the very simple preconditioning technique, using the identity matrix for $\mathbf{Y}_i$ in (6.20), leads to the most iteration numbers. In fact for all-floating FETI this preconditioning techinique shows almost no reduction of the condition numbers. Since we need no additional time to compute the lumped preconditioner, in contrast to the Dirichlet and the BETI preconditioner, this type of preconditioning yields the best computational time for the problem with the largest amount of DOF (level $\ell = 5$).

	All-floating				**Classical**			
ℓ	DOF	Lagr. mult.	L2 error	eoc	DOF	Lagr. mult.	L2 error	eoc
1	9981	38052	9.60e-05	–	6621	38388	1.01e-04	–
2	62397	84276	2.52e-05	1.98	56349	77700	2.54e-05	1.98
3	480573	238932	6.41e-06	1.98	469149	204708	6.42e-06	1.98
4	3860541	797076	1.62e-06	1.99	3838365	652260	1.62e-06	1.99
5	31116861	2908692	4.08e-07	1.99	31073181	2321508	4.08e-07	1.99

Table 7.1: Number of DOF and Lagrange multipliers for a cube subdivided into 512 subdomains using $\mathcal{P}_1$ elements. ℓ is the level of uniform refinement. For the L2 error, the definition is given in (7.2), whereas for the estimated order of convergence (eoc), the definition is given in (7.3).

All-floating												
ℓ	Identity prec.			Lumped prec.			Dirichlet prec.			BETI prec.		
1	35 it	16.2	23.3 s	16 it	3.9	19.3 s	13 it	3.1	19.7 s	33 it	15.8	20.6 s
2	47 it	28.5	22.1 s	23 it	7.3	19.8 s	18 it	4.7	19.5 s	30 it	11.8	19.9 s
3	61 it	50.2	22.6 s	28 it	10.3	21.1 s	21 it	6.0	21.2 s	32 it	14.3	23.1 s
4	83 it	100.2	33.6 s	43 it	25.3	28.9 s	26 it	8.7	28.1 s	37 it	19.4	46.1 s
5	113 it	199.2	187.8 s	63 it	59.6	143.3 s	31 it	12.0	174.8 s	44 it	26.3	321.7 s
Classical												
ℓ	Identity prec.			Lumped prec.			Dirichlet prec.			BETI prec.		
1	50 it	33.2	6.3 s	23 it	6.3	6.6 s	19 it	4.7	5.9 s	49 it	44.3	6.5 s
2	77 it	78.7	6.8 s	39 it	18.6	7.1 s	28 it	10.0	6.2 s	49 it	44.2	6.7 s
3	104 it	154.8	8.9 s	61 it	49.6	7.4 s	37 it	17.0	8.2 s	57 it	45.8	10.3 s
4	141 it	297.8	18.7 s	90 it	115.4	15.7 s	45 it	25.0	13.9 s	66 it	60.6	37.8 s
5	187 it	576.5	207.7 s	123 it	248.9	158.0 s	52 it	33.5	173.5 s	77 it	79.9	341.8 s

Table 7.2: Iteration numbers (it), condition numbers and computational time (s) for each preconditioning technique using $\mathcal{P}_1$ elements and a linear elastic material. ℓ is the level of uniform refinement and the mesh is a cube with 512 subdomains.

For the numbers in Table 7.1 and Table 7.2 the underlying mesh is a cube with 512 subdomains and we used 512 processing units on the *VSC2* cluster to do our computations. We observe that all-floating FETI yields better condition numbers for all preconditioners and hence as well better convergence rates of the global conjugate gradient method. Although the global iterative method converges in less iterations for the all-floating approach, we achieve lower computational times for the classical FETI method for the first four levels, cf. Table 7.2. This is mainly due to the larger expenditure of time to set up the all-floating FETI system, i.e. set up the jump operators (6.19), the larger coarse system $\mathbf{G}\mathbf{G}^\top$, compare (6.16), and because of the higher amount of Lagrange multipliers. In level 5 the global system gets large enough that all-floating FETI outperforms the classical approach in computational time. That means that the lower amount of iteration numbers overbalances the higher setup times for this case. From level 4, with a maximum of 8 907 local degrees of freedom, to level 5, with a maximum of 66 195 local degrees of freedom, we observe an increase in local assembling and factorization time from approximately 2 seconds up to about 66 seconds for the Dirichlet preconditioner. This is mainly due to the higher memory requirements of the direct solver. To some extend this also explains the higher numbers of the BETI preconditioner, but for sure we need to invest additional time in improving the implementation of the hypersingular operators to be competitive with the sophisticated direct solver packages. For the examples summarized in Table 7.3 and Table 7.4 a cube with 64 subdomains was considered. For the computation we used 32 processing units on *GHOST*. Note that the higher levels of this calculation are inexecutable on the larger *VSC2* cluster, since there each processor has only a

	all-floating				classical			
ℓ	DOF	Lagr. mult.	L2 error	eoc	DOF	Lagr. mult.	L2 error	eoc
1	1733	3876	1.40e-04	–	1049	3780	1.54e-04	–
2	9212	9708	3.95e-05	1.96	7984	7884	3.98e-05	1.96
3	64874	30012	9.95e-06	2.00	62557	21276	9.96e-06	2.00
4	500293	105180	2.51e-06	1.99	495801	68796	2.51e-06	1.99
5	3957756	393756	6.34e-07	1.99	3948912	246780	6.34e-07	1.99
6	31541098	1523868	1.59e-07	1.99	31523549	934524	1.59e-07	1.99

Table 7.3: Number of DOF and Lagrange multipliers for a cube subdivided into 64 subdomains using $\mathcal{P}_1$ elements. ℓ is the level of uniform refinement. For the L2 error, the definition is given in (7.2), whereas for the estimated order of convergence (eoc), the definition is given in (7.3).

limited amount of private memory and there is no global shared memory. That means that the memory consuming factorization of the local stiffness matrices by the direct solver is unfeasible, if the number of local degrees of freedom gets too large. On the other hand on the *GHOST* cluster we have additional global shared memory. Here we have the drawback that the communication between this shared memory and the processing units is comparatively slow. This explains the high computational times for level 6 in Table 7.4. Moreover, the larger memory requirements of the Dirichlet and the BETI preconditioning technique lead to an "out of memory" error for the highest level (i.e. 31 million DOF). We see very clearly, that in this case the FETI method with direct local solving is not really practicable. A possibility to overcome this performance problem would be the usage of fast local iterative solvers, e.g. the CG method with a multigrid or a BPX preconditioner.

As in the previous case with 512 subdomains we observe better iteration numbers for the all-floating FETI method. Again, given large enough local subdomains, the all-floating approach outperforms classical FETI, cf. Table 7.4. Summing up it seems, at least for this example of a unit cube, that all-floating FETI is more feasible for larger subdomains, while classical FETI shows advantages for many smaller subdomains. Moreover the simple lumped preconditioner appears to be favorable for this academical example with very structured subdomains.

All-floating	**Preconditioning**											
ℓ	Identity prec.			Lumped prec.			Dirichlet prec.			BETI prec.		
1	35 it	16.7	0.9 s	15 it	3.8	1.0 s	12 it	2.8	0.9 s	33 it	15.9	3.4 s
2	46 it	28.8	1.2 s	21 it	7.4	0.9 s	17 it	4.5	1.0 s	30 it	12.0	4.4 s
3	59 it	50.8	2.3 s	28 it	10.5	2.3 s	20 it	5.6	2.7 s	31 it	13.7	9.1 s
4	80 it	101.8	35.6 s	42 it	25.5	26.6 s	25 it	8.3	35.6 s	36 it	18.8	80.7 s
5	109 it	202.3	712.2 s	62 it	60.3	516.9 s	30 it	11.5	691.8 s	42 it	25.8	1113 s
6	148 it	399.3	16 123 s	89 it	130.7	11 850 s	out of memory					
Classical	**Preconditioning**											
ℓ	Identity prec.			Lumped prec.			Dirichlet prec.			BETI prec.		
1	44 it	30.4	0.3 s	19 it	6.0	0.2 s	17 it	4.7	0.2 s	44 it	31.6	2.8 s
2	63 it	72.6	0.5 s	33 it	17.0	0.3 s	24 it	9.6	0.5 s	43 it	30.5	3.8 s
3	83 it	143.2	1.6 s	47 it	44.1	1.5 s	31 it	16.2	2.2 s	52 it	43.6	10.3 s
4	113 it	273.3	38.5 s	68 it	101.7	29.7 s	37 it	23.5	38.6 s	59 it	58.7	83.3 s
5	151 it	527.4	799.9 s	95 it	218.4	582.3 s	43 it	31.7	726.7 s	68 it	78.4	1277 s
6	202 it	1032	19 341 s	131 it	452.6	14 496 s	out of memory					

Table 7.4: Iteration numbers (it), condition numbers and computational time (s) for each preconditioning technique using $\mathcal{P}_1$ elements and a linear elastic material. ℓ is the level of uniform refinement and the mesh is a cube with 64 subdomains.

7.1.2 Quadratic Elements

In this section we consider a linear elasticity problem using tetrahedral elements and quadratic ansatz functions, i.e. $\mathcal{P}_2$ elements. The parameters are $E = 210\,\text{GPa}$ and $\nu = 0.49$. Note that for all preconditioning types as well as for all-floating and classical FETI the L2 error compared to the fundamental solution behaves as expected from the theory and hence we get a cubic convergence rate (eoc), see Table 7.6 for the cube decomposed into 512 subdomains. The cubic convergence rates were also achieved for the cube decomposed into 64 subdomains.

First, we look at a cube with 64 subdomains. For reasons of memory limits this example was computed on the *GHOST* cluster. As for the case of linear ansatz functions, see Section 7.1.1, we get the lowest condition numbers of the global system and thus the least iteration numbers of the global CG method using the optimal Dirichlet preconditioner. The highest iteration numbers we observe with the simple identity preconditioning technique, using the identity matrix for $\mathbf{Y}_i$ in (6.20). We did not implement the BETI preconditioner for quadratic ansatz functions. For all-floating FETI we have the very interesting case that the global CG iteration numbers stay almost constant for the lumped preconditioner and even seem to decay for the identity and the Dirichlet preconditioner, if we increase the local degrees of freedom, i.e. increase the level l. For the classical FETI approach the iteration numbers stay

almost constant for the Dirichlet preconditioner and increase slightly for the other two preconditioning techniques, see Table 7.5.

All-floating									
ℓ	Identity preconditioner			Lumped preconditioner			Dirichlet preconditioner		
1	149 it	444.7	23.3 s	73 it	73.7	22.0 s	47 it	36.7	18.7 s
2	129 it	330.8	21.9 s	75 it	74.3	20.8 s	43 it	27.7	19.3 s
3	114 it	210.3	30.3 s	73 it	68.8	27.3 s	36 it	16.6	28.5 s
4	105 it	167.8	99.8 s	69 it	65.2	93.4 s	33 it	14.4	90.2 s
Classical									
ℓ	Identity preconditioner			Lumped preconditioner			Dirichlet preconditioner		
1	120 it	405.0	7.5 s	65 it	48.9	6.9 s	40 it	21.0	6.5 s
2	108 it	302.6	7.5 s	69 it	57.6	6.7 s	41 it	20.6	7.5 s
3	112 it	253.4	12.6 s	91 it	116.2	11.7 s	42 it	21.0	12.3 s
4	136 it	273.1	76.3 s	128 it	262.8	77.3 s	48 it	27.7	79.1 s

Table 7.5: Iteration numbers (it), condition numbers and computational times (s) for each preconditioning technique using $\mathcal{P}_2$ elements and a linear elastic material. ℓ is the level of uniform refinement and the mesh is a cube with 64 subdomains.

Given a high enough number of local degrees of freedom, in this example level $l = 4$, the all-floating FETI method outperforms the classical approach regarding the computational times for all preconditioners. This characteristic was also observed with linear ansatz functions, see Section 7.1.1. In contrast to the formulation with $\mathcal{P}_1$ elements, the optimal Dirichlet preconditioner now shows a noticeable advantage to the other two preconditioners. As in Section 7.1.1, the significantly higher computational times in level 4 compared to level 3 are mainly due to high memory requirements of the direct solver in this case.

In the following we deal with at a cube with 512 subdomains and again use quadratic

	All-floating				**Classical**			
ℓ	DOF	Lagr. mult.	L2 error	eoc	DOF	Lagr. mult.	L2 error	eoc
1	53 181	84 276	1.13e-05	–	47 133	77 700	1.17e-05	–
2	406 845	238 932	1.44e-06	2.97	395 421	204 708	1.46e-06	3.00
3	3 270 717	797 076	1.81e-07	2.99	3 248 541	652 260	1.82e-07	3.01
4	26 398 269	2 908 692	2.26e-08	3.00	26 354 589	2 321 508	2.26e-08	3.01

Table 7.6: Number of DOF and Lagrange multipliers for a cube subdivided into 512 subdomains and the level of uniform refinement ℓ. For the L2 error, the definition is given in (7.2), whereas for the estimated order of convergence (eoc), the definition is given in (7.3).

ansatz functions on tetrahedral elements. Now the computations were done on the *VSC2* cluster. We investigate iteration numbers and computational times depending on Poisson's ratio ν, see Table 7.7. With '– it' and '– s' we indicate that the global conjugate gradient method did not converge within 1000 iterations to reach the relative error reduction of 1e-08. In all the examples where the global CG method converged, the estimated order of convergence behaves as expected, i.e. we get a cubic convergence rate. Again we observe that for almost every case the iteration numbers for all-floating FETI improve with a higher level. This can be seen especially for the simple identity preconditioner and the Dirichlet preconditioner for materials with almost incompressible behavior. Note that the lumped preconditioner does not seem to work very well for quadratic elements and a nearly incompressible material, i.e. $\nu = 0.4999$. This behavior can be explained with the very ill-conditioned local stiffness matrices that result from dealing with almost incompressible materials, see Section 4.3.1. In fact all preconditioners show high iteration numbers for almost incompressible materials and the FETI methods seems to be unstable. A possibility to overcome these locking effects is the usage of $\mathcal{P}_2 - \mathcal{P}_0$ elements, see Section 5.1.3. This case is handled for the more general nonlinear materials in Section 7.2. For numerical examples that examine the behavior of the FETI-DP method given nearly incompressible linear materials see, for instance, Klawonn and Rheinbach [105].

All-floating, iterations									
ℓ	Identity preconditioner			Lumped preconditioner			Dirichlet preconditioner		
1	102 it	199 it	878 it	44 it	148 it	– it	32 it	90 it	796 it
2	89 it	181 it	754 it	47 it	153 it	– it	31 it	80 it	703 it
3	82 it	169 it	662 it	45 it	147 it	– it	27 it	64 it	535 it
4	77 it	160 it	584 it	45 it	138 it	– it	24 it	50 it	404 it
Classical,iterations									
ℓ	Identity preconditioner			Lumped preconditioner			Dirichlet preconditioner		
1	92 it	178 it	672 it	40 it	133 it	– it	27 it	79 it	696 it
2	85 it	181 it	662 it	44 it	140 it	– it	29 it	76 it	663 it
3	88 it	195 it	656 it	64 it	182 it	– it	36 it	73 it	603 it
4	108 it	216 it	716 it	89 it	205 it	– it	42 it	75 it	575 it
All-floating, computational times									
ℓ	Identity preconditioner			Lumped preconditioner			Dirichlet preconditioner		
1	27.9 s	30.2 s	74.9 s	22.5 s	28.4 s	– s	20.6 s	25.8 s	86.2 s
2	25.5 s	30.6 s	74.2 s	22.9 s	30.9 s	– s	21.2 s	26.3 s	77.0 s
3	34.6 s	44.3 s	99.6 s	29.6 s	46.3 s	– s	29.2 s	35.9 s	118.4 s
4	239.0 s	417.8 s	853.9 s	220.3 s	390.5 s	– s	299.4 s	346.0 s	968.4 s
Classical, computational times									
ℓ	Identity preconditioner			Lumped preconditioner			Dirichlet preconditioner		
1	7.7 s	9.6 s	23.9 s	7.9 s	9.1 s	– s	7.6 s	9.6 s	24.3 s
2	8.4 s	10.2 s	27.7 s	7.2 s	10.8 s	– s	6.6 s	8.8 s	29.0 s
3	16.1 s	25.2 s	62.4 s	14.3 s	24.7 s	– s	14.9 s	19.7 s	93.6 s
4	233.1 s	421.4 s	772.2 s	219.4 s	370.9 s	– s	292.0 s	350.2 s	1269.7 s

Table 7.7: Iteration numbers and computational times for the different preconditioning techniques depending on Poisson's ratio ν using $\mathcal{P}_2$ elements and a linear elastic material. Young's modulus was set to $E = 210\,\text{GPa}$ for all experiments. The Poisson's ratio ν was set to 0.3 for each left column, to 0.49 for each middle column and to 0.4999 for each right column. The mesh was a cube decomposed into 512 subdomains and the experiments were computed on *VSC2* with 512 cores. '– it' and '– s' indicate that the global CG method did not converge within 1000 iterations.

7.1.3 Scaling for Linear Elasticity

In this section we analyze our computational framework with respect to strong scaling efficiency, i.e.

$$\text{eff} = \frac{t_{\text{I}}}{P\, t_{\text{P}}}, \tag{7.4}$$

where t_{I} is the amount of time to complete a computation with the initial number of processing units I (in our case $\text{I} = 16$) and t_{P} is the amount of time to complete the same computation with P processing units. In particular, we consider a unit cube that is subdivided into 512 subcubes with inhomogeneous Dirichlet boundary conditions all over the boundary. With linear ansatz functions this leads to a linear elasticity problem with approximately 3.9 million total DOF. We apply the all-floating FETI approach with the lumped preconditioner. The global FETI system has 797 096 Lagrange multipliers and was solved using the CG method with a varying amount of processing units p on the *VSC*-cluster. In all cases the global iterative method converged within 45 iterations and the estimated condition number for the system is 26.86.

As expected the local time, i.e. the assembling of the stiffness matrices and the factorization of the local problems with the direct solver scales almost perfectly. This is not surprising, since we do not need any communication between the processing units for these operations. The efficiency for the solving time of the global conjugate gradient method and the efficiency of the total time is good up to 64 processing units and then decays to 55 % and 38 %. This is due to the communication within the iterative method and within the setup of the FETI method and the realization of the coarse system $(\mathbf{G}^\top \mathbf{G})^{-1}$, see (6.16). Possiblities to overcome this lower scaling with a large amount of processors are perhaps the usage of parallel solver packages as *hypre* and a more efficient assembling of the coarse system. It also needs some tricks with MPI and memory management. It is obvious that a longer lasting assembling procedure effects the scaling in a positive way. Hence, with nonlinear elasticity we expect a better parallel efficiency.

P	Local time	eff	Global CG time	eff	Total time	eff
16	46.00 s	1.000	50.12 s	1.000	179.76 s	1.000
32	23.18 s	0.992	26.42 s	0.949	99.11 s	0.907
64	11.61 s	0.991	14.56 s	0.861	59.40 s	0.757
128	5.84 s	0.985	8.47 s	0.739	37.47 s	0.600
256	2.95 s	0.975	5.65 s	0.554	29.24 s	0.384

Table 7.8: Computational times (s) and efficiency (eff) according to (7.4) for a linear elasticity problem using a varying number of processing units P.

7.2 Nonlinear Elasticity

In this section we will apply the FETI method to nonlinear elasticity problems, i.e. the nonlinear artery model, see Section 3.11, and the nonlinear myocardium model, see Section 3.12. The computations in this chapter are all done using the *VSC2*-cluster.

For most examples in this section, we will apply a rather low pressure to the nonlinear materials to have a converging Newton scheme. Nonetheless, the material model as used is orthotropic. To simulate a higher pressure, an appropriate time stepping scheme has to be used, see Section 7.2.2. However, this does not affect the number of local iterations significantly.

Media	**Adventitia**	**Myocardium**
$c_{\mathrm{M}} = 3.0000\,\mathrm{kPa}$,	$c_{\mathrm{A}} = 0.3000\,\mathrm{kPa}$,	$a = 0.333\,\mathrm{kPa}$,
$k_{1\mathrm{M}} = 2.3632\,\mathrm{kPa}$,	$k_{1\mathrm{A}} = 0.5620\,\mathrm{kPa}$,	$a_{\mathrm{f}} = 18.535\,\mathrm{kPa}$,
$k_{2\mathrm{M}} = 0.8393\,[-]$,	$k_{2\mathrm{A}} = 0.7112\,[-]$,	$a_{\mathrm{s}} = 2.564\,\mathrm{kPa}$,
		$a_{\mathrm{fs}} = 0.417\,\mathrm{kPa}$,
		$b = 9.242\,[-]$,
		$b_{\mathrm{s}} = 10.446\,[-]$,
		$b_{\mathrm{f}} = 15.972\,[-]$,
		$b_{\mathrm{fs}} = 11.602\,[-]$.

Table 7.9: Material parameters for an arterial material [82], see Figure 3.3. Material parameters for the myocardium from [52] where they use an adaptation from [85].

7.2.1 Academic Example

At first, we will do the computations on a simple unit cube that is subdivided in 512 subcubes with a tetrahedral triangulation. We will use the following boundary conditions: one face ($y = 0$) is fixed with homogneous Dirichlet boundary conditions, on one face ($y = 1$) we apply a tensile stress of 1 mmHg, on the other four faces we have homogeneous Neumann boundary conditions. With linear ansatz functions and the FETI approach this yields a system with a total number of approximately 3.9 million DOF and 652260 Lagrange multipliers. This example was calculated on 64 processing units on *VSC2*. We use the myocardium model (3.61) and the parameters as indicated in Table 7.9. The results of these calculations can be found in Table 7.10. The Jacobian $J = \det(\mathbf{F})$, the volume ratio change of the tetrahedral elements, varied within the interval $(1., 1.05)$ for $\kappa = 0.8333\,\mathrm{kPa}$ and within the interval $(0.999\,998, 1.000\,001)$ for $\kappa = 3333\,\mathrm{kPa}$. The Newton scheme needed 3 to 4 Newton steps to reach the stopping criterion. The stopping criterion is an absolute

All-floating								
κ	Identity prec.		Lumped prec.		Dirichlet prec.		BETI prec.	
0.833	80 it	34 s	41 it	30 s	25 it	28 s	36 it	34 s
3.333	114 it	36 s	59 it	33 s	31 it	31 s	53 it	41 s
33.330	276 it	54 s	149 it	39 s	71 it	36 s	173 it	74 s
333.300	734 it	90 s	408 it	64 s	203 it	52 s	– it	– s
3333.000	– it	– s	– it	– s	592 it	101 s	– it	– s
Classical								
κ	Identity prec.		Lumped prec.		Dirichlet prec.		BETI prec.	
0.833	143 it	34 s	91 it	33 s	44 it	27 s	63 it	37 s
3.333	194 it	38 s	127 it	31 s	52 it	28 s	88 it	42 s
33.330	442 it	58 s	301 it	48 s	105 it	36 s	214 it	74 s
333.300	– it	– s	808 it	96 s	293 it	57 s	603 it	169 s
3333.000	– it	– s	– it	– s	867 it	134 s	– it	– s

Table 7.10: Iteration numbers (it) and computational times (s) per Newton step for all-floating and classical FETI with $\mathcal{P}_1$ elements. We compare the performance of the different preconditioners with a varied setting of the bulk modulus κ. '– it' and '– s' indicate that the global CG method did not converge within 1000 iterations.

residual norm of 1e-06, as also used in Brands et al. [27]. We observe that for the proposed setting of $\kappa = 3333\,\text{kPa}$ only the Dirichlet preconditioner yields iteration numbers of the global iterative method below 1000 iterations. This preconditioning technique seems to be a good choice for all other settings as well. In this example all-floating FETI yields better iteration numbers than the classical approach. With the BETI preconditioner we achieve in most cases better iteration numbers than with the lumped preconditioner, although it is built with the hypersingular operators for linear elasticity and we had to fit the nonlinear parameters to it.

Using quadratic ansatz functions we get a system with a total number of 26 488 475 degrees of freedom and 2 420 142 Lagrange multipliers. For the parameter setting as given in Table 7.9, the global iterative method only converged within 1000 iterations using the Dirichlet preconditioner: 506 iterations for the all-floating and 701 iterations for the classical approach. The computational times per Newton step (assembling and solving) was 1275 seconds for all-floating and 1623 seconds for classical FETI.

7.2.2 Arterial Model on a Realistic Mesh Geometry

An application of the FETI approach with a realistic mesh geometry is the inflation of an artery segment. We consider the mesh of an aorta and the mesh of a common carotid artery, see Figures 7.2 and 7.3. The geometries are from AneuriskWeb [3] and Gmsh [63]. The generation of the volume mesh was performed using VMTK and Gmsh, see Marchandise et al. [120].

The fiber directions, see Figure 7.4, were calculated using a method described by Bayer et al. [19] for the myocardium. To adapt this method for the artery we first solved the Laplace equation on the arterial domain Ω with homogeneous Dirichlet boundary conditions on the inner surface and inhomogeneous Dirichlet boundary conditions on the outer wall. The gradient of the solution is used to define the transmural direction $\hat{\mathbf{e}}_2$ in each element. As a second step we repeat this procedure using homogeneous Dirichlet boundary conditions on the inlet surface and inhomogeneous boundary conditions on the outlet surfaces which yields the longitudinal direction $\hat{\mathbf{e}}_1$. The cross product of these two vectors eventually provides the circumferential direction $\hat{\mathbf{e}}_0$. With a rotation we get the two desired fiber directions $\mathbf{a}_{0,1}$ and $\mathbf{a}_{0,2}$ in the media and the adventitia, respectively.

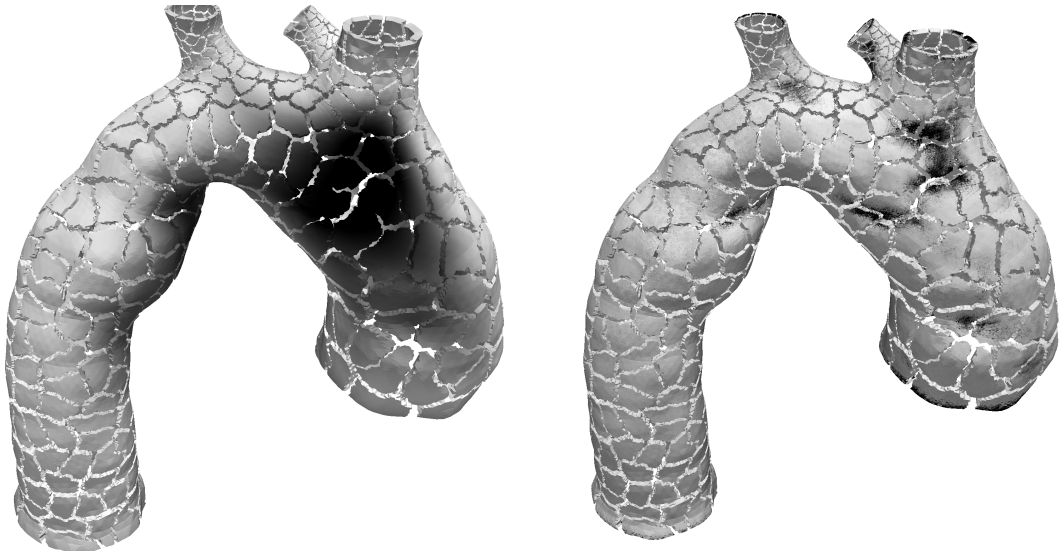

Figure 7.2: Mesh of an aorta consisting of 5 418 594 tetrahedrons and 1 055 901 vertices. Point of view is from above showing the links to the brachiocephalic, the left common carotid and the left subclavian artery. Black and white colors indicate the displacement field (left) and the stress magnitude according to (7.5) (right) generated by applying a pressure to the inner walls of the arteries. Darker gray colors indicate high, lighter gray colors indicate low values. Additionally, the splits show the decomposition of the mesh into 480 subdomains.

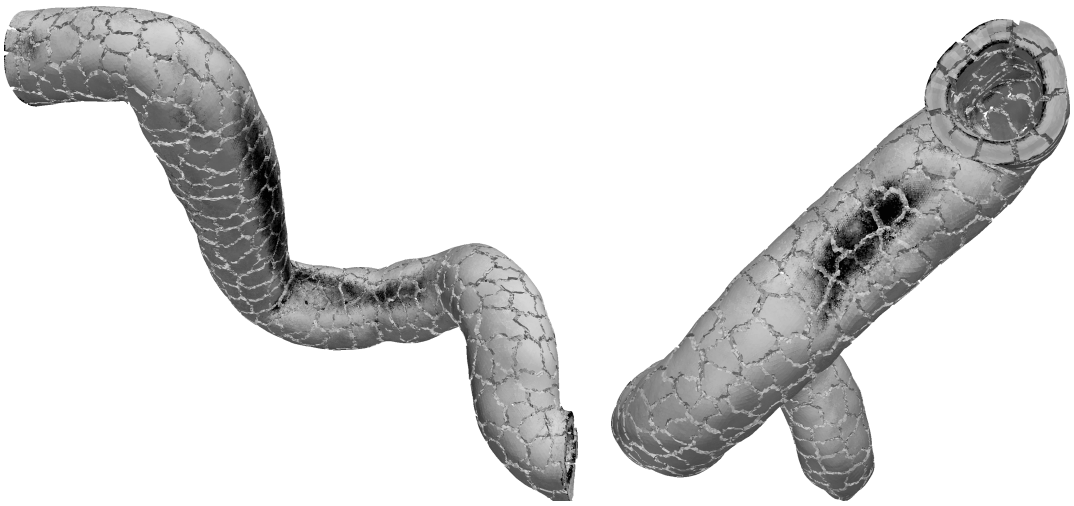

Figure 7.3: Mesh of a segment of a common carotid artery from two different points of view. The mesh consists of 9 195 336 tetrahedrons and 1 621 365 vertices. Black and white colors indicate the stress magnitude field (7.5) generated by applying a pressure to the inner walls of the artery. Darker shadings indicate high, light gray colors indicates low values. Additionally, the splits show the decomposition of the mesh into 512 subdomains.

Thus,

$$\begin{pmatrix} \mathbf{a}_{0,1} & -\mathbf{a}_{0,2} & \hat{\mathbf{e}}_2 \end{pmatrix} = \begin{pmatrix} \hat{\mathbf{e}}_0 & \hat{\mathbf{e}}_1 & \hat{\mathbf{e}}_2 \end{pmatrix} \begin{pmatrix} \cos\alpha & -\sin\alpha & 0 \\ \sin\alpha & \cos\alpha & 0 \\ 0 & 0 & 1 \end{pmatrix} \begin{pmatrix} \hat{\mathbf{e}}_0^\top \\ \hat{\mathbf{e}}_1^\top \\ \hat{\mathbf{e}}_2^\top \end{pmatrix} \begin{pmatrix} \hat{\mathbf{e}}_0 & \hat{\mathbf{e}}_1 & \hat{\mathbf{e}}_2 \end{pmatrix}.$$

The values for the angle α are $\alpha_{\mathrm{M}} = 29°$ for the media and $\alpha_{\mathrm{A}} = 62°$ for the adventitia, taken from [82], see also Figure 3.3. To describe the anisotropic and nonlinear arterial tissue, we use the material model outlined in Section 3.11.1, with the parameters given in Table 7.9 and κ is varied. Dirichlet boundary conditions are imposed on the respective intersection areas. We perform an inflation simulation on the artery segment where the interior wall is exposed to a constant pressure p. This is performed using Neumann boundary conditions. Here, we present the results of one load step applying a rather low pressure of 1 mmHg. This is necessary to have a converging Newton method. Nonetheless, the material model as used is anisotropic. To simulate a higher pressure, an appropriate load stepping scheme, see (5.13), has to be used. However, this does not affect the number of local iterations significantly. We use the CG method as global iterative solver. Experiments with a standard non-symmetric nonlinear elasticity system, see (5.11), and the hence necessary GMRES method as an iterative solver showed similar results as presented in the following with the symmetric system. However, the memory requirements of the GMRES solver are much higher. Hence, a symmetrization of the system, compare (5.12), is favourable.

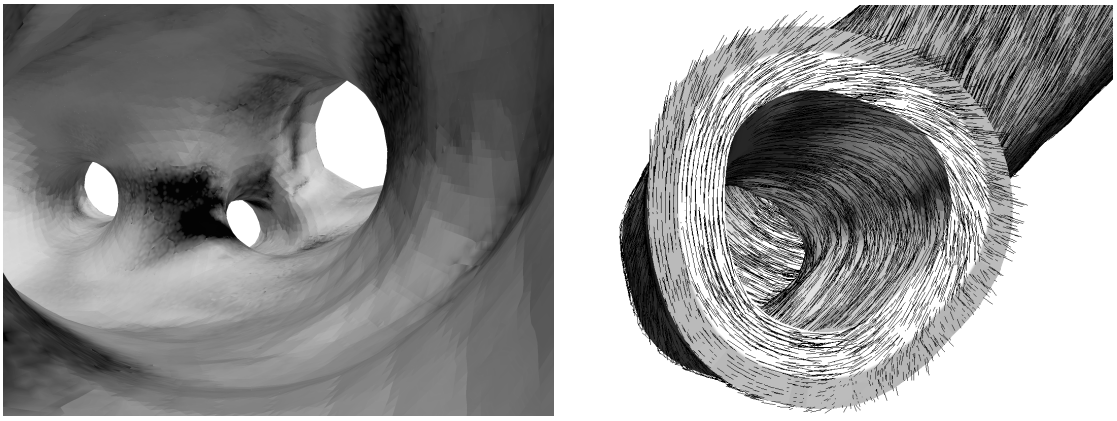

Figure 7.4: Stress magnitude (7.5) looking inside the aorta (left); values of high stress in dark and of low stress in light gray. To the right the fiber directions (black lines) and the two layers (adventitia in darker and media in lighter gray) of the carotis are shown.

The local generalized pseudo–inverse matrices are realized with a sparsity preserving regularization and the direct solver package Pardiso. The global nonlinear finite element system is solved by a Newton scheme, where the FETI approach is used in each Newton step. For the considered examples the Newton scheme needed four to six iterations. Due to the non-uniformity of the subdomains the efficiency of a global preconditioner becomes more important. It can happen that the decomposition of a mesh results in subdomains that have only a few points on the Dirichlet boundary. This negatively affects the convergence of the CG method using classical FETI, but does not affect the global iterative method of the all-floating approach at all. This is a major advantage of all-floating FETI since here all subdomains are treated the same and hence all subdomains are stabilized. This behavior is observed for almost all settings for preconditioners and the penalty parameter κ as well as for linear and quadratic ansatz functions, see Tables 7.11–7.14. For instance, applying all-floating FETI with the Dirichlet preconditioner to the aorta mesh using a penalty parameter

FETI type	Identity prec.		Lumped prec.		Dirichlet prec.	
All-floating	– it	– s	1084 it	100.6 s	497 it	85.5 s
Classical	5130 it	357.0 s	1794 it	200.2 s	588 it	97.7 s

Table 7.11: Iteration numbers (it) per Newton step and computational times (s) per Newton step for the all-floating and the classical FETI approach with *linear* ansatz functions comparing the three considered preconditioners. The penalty parameter κ was set to 1000 kPa. The mesh is the carotis with two layers (adventitia and media) subdivided in 512 subdomains, computed with 512 cores. '– it' and '– s' indicate that the global CG method did not converge within 10 000 iterations.

All-floating						
κ	Identity prec.		Lumped prec.		Dirichlet prec.	
10	1052 it	57.6 s	160 it	31.0 s	56 it	22.8 s
100	1879 it	94.6 s	305 it	29.5 s	85 it	25.4 s
1000	4122 it	177.1 s	681 it	48.8 s	209 it	31.8 s
Classical						
κ	Identity prec.		Lumped prec.		Dirichlet prec.	
10	2056 it	98.7 s	305 it	35.5 s	117 it	27.2 s
100	3711 it	149.8 s	540 it	35.5 s	144 it	28.4 s
1000	8245 it	327.8 s	1190 it	60.9 s	263 it	32.9 s

Table 7.12: Iteration numbers (it) and computational times (s) per Newton step for the all-floating and the classical FETI approach with *linear* ansatz functions comparing the three considered preconditioners. The penalty parameter κ was varied from 10 to 1000 kPa. Mesh: mesh of the aorta subdivided in 480 subdomains, computed with 480 cores.

$\kappa = 1000\,\text{kPa}$ the global CG method converged in considerable less iterations (209) than the CG method using classical FETI (263), see Table 7.12. The advantage of the smaller number of iterations is not so significantly reflected in the computational times since, as for the linear case, we have higher set up times and a larger coarse system $\mathbf{G}\mathbf{G}^\top$. Nonetheless, it shows for the considered examples that all-floating FETI yields lower iterations numbers of the global systems and is also competitive or even advantageous to the classical approach concerning the computational times.

In contrast to the academic example in Section 7.2.1 the more complex Dirichlet preconditioner is the best choice for all considered settings. Especially for $\kappa \gg 1\,\text{kPa}$ the iteration numbers with the lumped and the identity preconditioner escalate. Admittedly, the numbers in Table 7.12 also show that the convergence of the CG method, within all FETI approaches and preconditioner settings, is dependent on the penalty parameter κ.

FETI type	Identity prec.		Lumped prec.		Dirichlet prec.	
All-floating	– it	– s	2163 it	1133.9 s	674 it	994.6 s
Classical	6006 it	2672.6 s	4798 it	2306.8 s	764 it	771.2 s

Table 7.13: Iteration numbers (it) and computational times (s) per Newton step for the all-floating and the classical FETI approach with *quadratic* ansatz functions comparing the three considered preconditioners. The penalty parameter κ was set to 1000 kPa. Mesh: mesh of the carotis with two layers (adventitia and media) subdivided in 1024 subdomains, calculated with 1024 cores. '– it' and '– s' indicate that the global CG method did not converge within 10 000 iterations.

Using quadratic ansatz functions we have a total number of 23 031 620 DOF for the aorta mesh and 36 527 435 DOF for the carotis mesh. In order to not infringe the memory limitations on the *VSC2* cluster we have to use a decomposition into 1024 subdomains for the carotis. For the aorta it was possible to stay with 480 subdomains. The number of Lagrange multipliers then are 1 552 665 (aorta) and 4 585 203 (carotis). Comparing the numbers in Table 7.14 and Table 7.13 show similar results as in the case with linear ansatz functions. The Dirichlet preconditioner is preferable for all test cases and the all-floating approach is competitive to the classical FETI approach. Albeit quadratic ansatz functions resolve the nearly incompressible elastic behavior better than linear ansatz functions we also notice a certain dependence of the global iteration numbers to the penalty parameter κ, see Table 7.14. Nonetheless, the iteration numbers rise not as quickly as for the $\mathcal{P}_1 - \mathcal{P}_0$ element case and the values of $J = \det(\mathbf{F})$ in each element are much closer to 1 for $\mathcal{P}_2 - \mathcal{P}_0$ elements.

All-floating						
κ	Identity prec.		Lumped prec.		Dirichlet prec.	
10	940 it	491.1 s	283 it	209.5 s	71 it	157.3 s
100	1519 it	1186.4 s	523 it	332.0 s	105 it	178.1 s
1000	3371 it	2584.5 s	1372 it	746.0 s	206 it	282.7 s
Classical						
κ	Identity prec.		Lumped prec.		Dirichlet prec.	
10	1319 it	654.2 s	333 it	225.2 s	113 it	188.4 s
100	2362 it	1140.6 s	664 it	402.6 s	110 it	177.5 s
1000	5563 it	4168.3 s	1742 it	943.1 s	204 it	280.1 s

Table 7.14: Iteration numbers (it) per Newton step and computational times (s) per Newton step for the all-floating and the classical FETI approach with *quadratic* ansatz functions comparing the three considered preconditioners. The penalty parameter κ was varied from 10 to 1000 kPa. Mesh: mesh of the aorta subdivided in 480 subdomains, calculated with 480 cores.

Load stepping scheme for the Arterial Model

In this section we analyze the biomechanical behavior of the aorta up to an internal pressure of 300 mmHg. Higher pressures would induce damage and softening behavior which cannot be captured with the arterial model discussed in Section 3.11. For that purpose we consider a coarser version of the mesh of the aorta (see Figure 7.2), which is subdivided into 32 subdomains since for this mesh the all-floating FETI method looks significantly advantageous. The reasons for that are as follows: (i) we have lower iteration numbers for the all-floating FETI approach, as already observed in Section 7.2.2; (ii) the matrix $\mathbf{G}\mathbf{G}^\top$ in (6.16) is small, and hence less time is needed to compute the inverse of this coarse system, especially in comparison to the assembly time and the global solving time of the CG method.

With this mesh we simulate an arterial model with the parameters from Table 7.9 and with $c = 6\,\text{kPa}$ and $\kappa = 1000\,\text{kPa}$ using the Dirichlet preconditioner. The results of a load stepping scheme, where we applied an internal pressure up to 300 mmHg over 572 loading steps, are found in the Figs. 7.5 and 7.6. Note that the average iteration number over one time step increased from 248 to 268 for all-floating FETI and from 340 to 358 for the classical FETI approach for higher pressures, and, consequently, a more anisotropic material behavior. The simulation needed four to five Newton steps and the solving times for all-floating FETI are significantly faster, see Figure 7.6.

In our plots we used a *stress magnitude* $\boldsymbol{\sigma}_{\text{mag}}$ according to

$$\boldsymbol{\sigma}_{\text{mag}} = \sqrt{\sigma_{11}^2 + \sigma_{22}^2 + \sigma_{33}^2 + 2\sigma_{12}^2 + 2\sigma_{13}^2 + 2\sigma_{23}^2}, \tag{7.5}$$

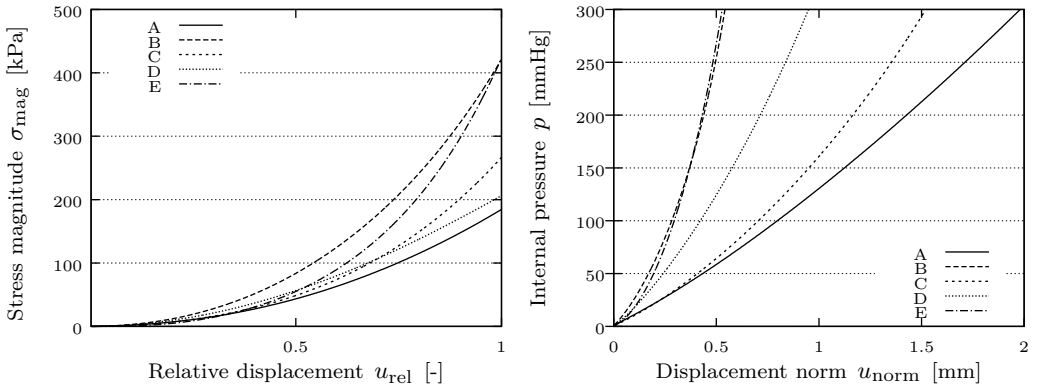

Figure 7.5: Stress magnitude $\boldsymbol{\sigma}_{\text{mag}}$ versus relative displacement u_{rel} (left) and evolution of the displacement norm u_{norm} over the load steps up to an internal pressure p of 300 mmHg (right). The plots were generated using data at the specific points A–E, as shown in Figure 7.2 (right).

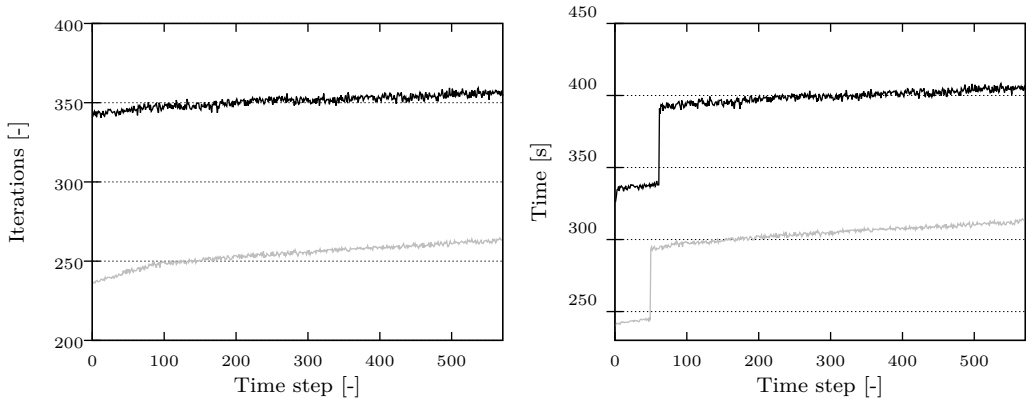

Figure 7.6: Comparison of all-floating FETI (gray) and classical FETI (black) for a time stepping scheme. Average iteration numbers of one time step (left) and solving times in seconds for one time step (right) over 572 load steps.

used as a measure to visualize our data. For advantages and disadvantages of certain stress values concerning the analysis of rupture and failure in aortic tissues, see, e.g., Humphrey and Holzapfel [94]. Other values used in Figure 7.5 are the *displacement norm* u_{norm} and the *relative displacement* u_{rel}, i.e.

$$u_{\text{norm}} = \sqrt{u_1^2 + u_2^2 + u_3^2}, \qquad u_{\text{rel}} = \frac{u_{\text{norm}}}{u_{\max}}, \tag{7.6}$$

for a point with the displacement vector $\mathbf{u} = (u_1, u_2, u_3)$ at the time step t, and $u_{\max}$ is the largest occurring displacement norm for that point over all time steps.

7.2.3 Myocardium Model on a Realistic Mesh Geometry

In this section, we present some examples to show the applicability of the FETI approach for the simulation of the myocardium on a realistic geometry. The mesh was generated using segmented medical image stacks of rabbit ventricles, see [143] and orthotropic tissue properties, i.e. fiber directions, were assigned using a rule-based approach [19]. The mesh is of the left and the right ventricle of a rabbit heart with given myocyte fiber direction $\mathbf{f}_0$ and the sheet direction $\mathbf{s}_0$ (left), which is decomposed into a certain number of subdomains, see Figure 7.7 and Figure 7.8. To describe the anisotropic and nonlinear cardiac tissue, we use the material model (3.61) with the parameters given in Table 7.9. Dirichlet boundary conditions are imposed on the top of the myocardium mesh. The interior wall of the right ventricle is exposed to the pressure of 1 mmHg which is modeled with Neumann boundary conditions. The local generalized inverse matrices are realized with a sparsity preserving regularization and the direct solver package PARDISO. The global nonlinear finite element system with

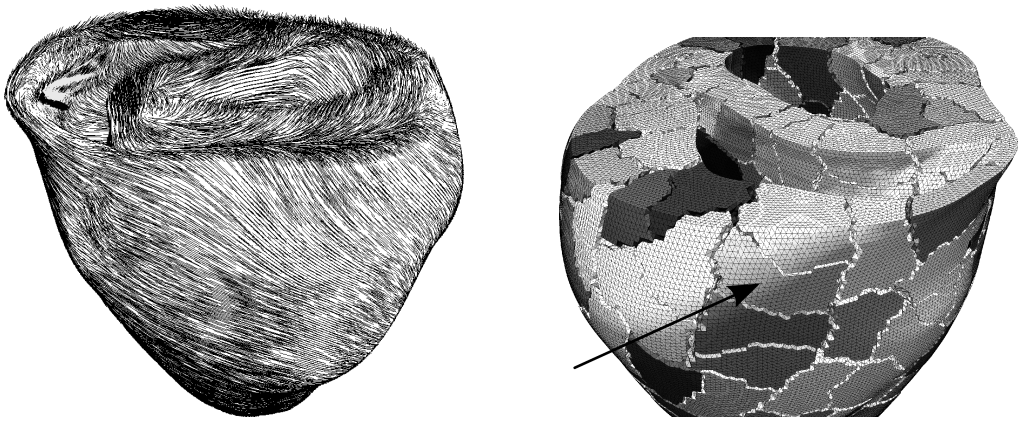

Figure 7.7: Left and right ventricle of the rabbit heart. Mesh consists of 3 073 529 tetrahedrons and 547 680 vertices. Point of view is from above showing the interior of the left and right ventricle. Black lines on the left picture indicate fiber directions $\mathbf{f}_0$. Some decompositions, here into 256 subdomains, (right picture) generate subdomains that have only a few or even only one point on the dirichlet boundary (indicated by the black arrow). This leads to problems with classical FETI.

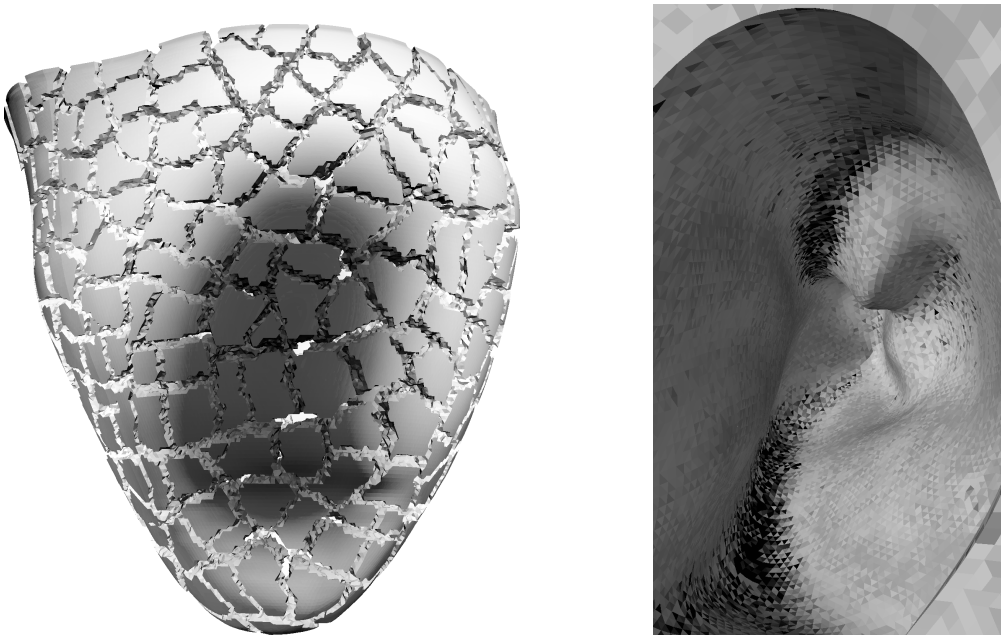

Figure 7.8: The left picture shows the displacement field of the rabbit heart with pressure applied in the right ventricle and the decomposition in 480 subdomains. Point of view is from below showing the apex of the heart at the bottom. To the right we have the stress magnitude (7.5) in the right ventricle. Point of view is from above looking inside the right ventricle. Dark colors indicate high values and lighter gray colors indicate low values.

1 643 040 degrees of freedom is solved by a Newton scheme, where the FETI approach is used in each Newton step. For this specific example the Newton scheme needed four to six iterations. Due to the non-uniformity of the subdomains the efficiency of a global preconditioner becomes more important. The vast differences between the all-floating and the classical FETI method in Table 7.15 are explained with the characteristic of the decomposition where some subdomains only have very few or even only one point located at the Dirichlet boundary, see Figure 7.7. In this special case there are three points on the Dirichlet boundary which leads to higher condition numbers and hence more iterations of the global itertive method for the classical FETI approach compared to the all-floating FETI approach.

All-floating								
κ	Identity prec.		Lumped prec.		Dirichlet prec.		BETI prec.	
0.833	261 it	100 s	113 it	59 s	63 it	61 s	106 it	63 s
3.333	368 it	136 s	162 it	74 s	80 it	70 s	150 it	85 s
33.330	944 it	296 s	387 it	140 s	162 it	110 s	432 it	225 s
333.300	– it	– s	870 it	287 s	351 it	202 s	– it	– s
3333.000	– it	– s	– it	– s	910 it	474 s	– it	– s
Classical								
κ	Identity prec.		Lumped prec.		Dirichlet prec.		BETI prec.	
0.833	868 it	256 s	470 it	154 s	239 it	139 s	393 it	206 s
3.333	– it	– s	628 it	198 s	275 it	157 s	542 it	282 s
33.330	– it	– s	– it	– s	486 it	231 s	– it	– s
333.300	– it	– s	– it	– s	933 it	470 s	– it	– s
3333.000	– it	– s	– it	– s	– it	– s	– it	– s

Table 7.15: Iteration numbers per Newton step (it) and computational times per Newton step (s) for the for all-floating and classical FETI using **linear** ansatz functions comparing the four considered preconditioners. The column κ gives the setting of the bulk modulus. Mesh: rabbit heart subdivided in 256 subdomains, computed with 256 cores. '– it' and '– s' indicate that the global CG method did not converge within 1000 iterations.

As for the academic example in Section 7.2.1 the sophisticated Dirichlet preconditioner and all-floating FETI seem to be the best choice to solve the system. For the proposed parameter setting with $\kappa = 3333\,\text{kPa}$ the CG method needed 910 iterations and the solving time of one Newton step (assembling and solving) lasted 474 seconds, see Table 7.15. The Jacobian $J = \det(\mathbf{F})$, a measure of the compressibility, varied within the interval $(0.9972, 1.0001)$ for $\kappa = 0.8333\,\text{kPa}$ and within the interval $(0.999987, 1.00001)$ for $\kappa = 3333\,\text{kPa}$.

Using quadratic ansatz functions we have a total number of 12 188 296 degrees of freedom. In order to not infringe the memory limitations on the *VSC2* cluster we

have to use a decomposition into 480 subdomains, see Figure 7.8. Using all-floating FETI and the Dirichlet preconditioner we needed 862 iterations for the global CG method and a total solving time of 986 seconds per Newton step, see Table 7.16. The Jacobian $J = \det(\mathbf{F})$ varied within the interval $(0.99988, 1.00045)$ for $\kappa = 0.8333\,\text{kPa}$ and was ≈ 1 in each tetrahedral element for $\kappa = 3333\,\text{kPa}$. As supposed, we can clearly see that quadratic ansatz functions resolve the incompressible elastic behavior much better than linear ansatz functions, see also Section 5.1.4. Hence, a much lower κ than the proposed value of 3333 kPa should be sufficient to simulate the nearly incompressible behavior of the myocardium. Nonetheless, the numbers in this table show as well, that the convergence of the CG method within the FETI approaches chosen in this simulation, is still dependent on the bulk modulus κ.

All-floating

κ	Identity prec.		Lumped prec.		Dirichlet prec.	
0.833	229 it	253 s	112 it	185 s	65 it	232 s
3.333	266 it	275 s	155 it	209 s	68 it	237 s
33.330	535 it	452 s	401 it	375 s	108 it	282 s
333.300	– it	– s	– it	– s	300 it	527 s
3333.000	– it	– s	– it	– s	862 it	986 s

Classical

κ	Identity prec.		Lumped prec.		Dirichlet prec.	
0.833	407 it	360 s	265 it	275 s	134 it	309 s
3.333	483 it	420 s	366 it	345 s	149 it	325 s
33.330	941 it	705 s	916 it	709 s	215 it	406 s
333.300	– it	– s	– it	– s	455 it	684 s
3333.000	– it	– s	– it	– s	– it	– s

Table 7.16: Iteration numbers per Newton step (it) and computational times per Newton step (s) for the all-floating and the classical FETI approach with *quadratic* ansatz functions comparing the different preconditioners. The column κ gives the setting of the bulk modulus. Mesh: rabbit heart, subdivided in 480 subdomains, calculated with 480 cores. '– it' and '– s' indicate that the global CG method did not converge within 1000 iterations.

7.2.4 Scaling for Nonlinear Elasticity

In this section we analyze our computational framework with respect to strong scaling efficiency (7.4). In particular, we consider the meshes of the carotid artery and the aorta as in Section 7.2.2, both subdivided into 512 subdomains. We apply the anisotropic arterial model with the parameters from Table 7.9 and use a $\kappa = 100\,\text{kPa}$ with the lumped preconditioner and linear ansatz functions. For the aorta we used all-floating FETI and needed an average of 324 global CG iterations to reach an absolute error of $\varepsilon = 1e-08$ and 5 Newton steps to reach an absolute error of $1e-06$. In the case of the carotid artery and classical FETI we needed 674 global CG iterations and also 5 Newton steps to reach the same error limits as above.

In the following we present the following numbers: the *local time* is the sum of all assembling and local factorization times during the solution steps. The factorization of the local problems was performed with the direct solver package Pardiso. In most cases we observed a super-linear speedup, and hence an efficiency greater than 1 for

P	Local time	eff	Global CG time	eff	Total time	eff
16	407.7 s	1.000	1311.7 s	1.000	2028.6 s	1.000
32	203.1 s	1.004	666.4 s	0.984	1054.2 s	0.962
64	101.7 s	1.002	345.4 s	0.949	562.0 s	0.902
128	50.5 s	1.009	184.7 s	0.888	316.7 s	0.801
256	25.3 s	1.007	103.8 s	0.790	192.8 s	0.658
512	12.7 s	1.000	67.6 s	0.606	161.0 s	0.394

Table 7.17: Computational time (s) and efficiency (eff) according to (7.4) for a nonlinear elastic problem using a varying number of processing units P. The time is measured for 1 time step with 5 Newton steps for all-floating FETI and the lumped preconditioner.

P	Local time	eff	Global CG time	eff	Total time	eff
16	726.0 s	1.000	4725.8 s	1.000	6519.7 s	1.000
32	351.3 s	1.033	2368.2 s	0.998	3497.0 s	0.932
64	170.5 s	1.065	1262.9 s	0.936	1991.2 s	0.819
128	90.7 s	1.001	694.5 s	0.851	1194.1 s	0.682
256	47.3 s	0.960	443.6 s	0.666	914.4 s	0.446
512	23.9 s	0.949	297.2 s	0.497	667.4 s	0.305

Table 7.18: Computational time (s) and efficiency (eff) according to (7.4) for a nonlinear elastic problem on the carotid artery mesh using a varying number of processing units P. The time is measured for 1 time steps with 5 Newton steps for classical FETI and the lumped preconditioner.

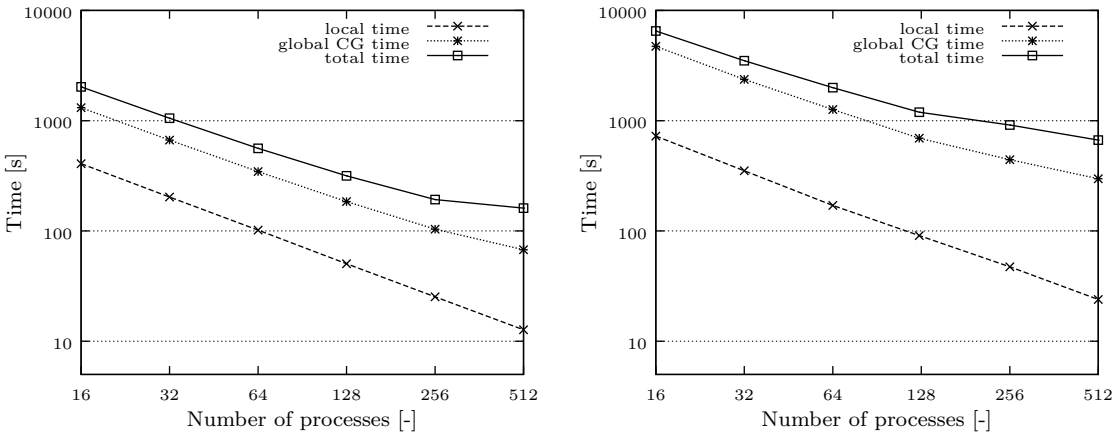

Figure 7.9: Computational times (s) for an artery simulation with the aorta mesh (left) and the carotis mesh (right) using a varying number of cores.

this value. This is due to memory issues, mainly so-called cache effects. For more information on this well-known phenomenon, see, e.g., Hennessy and Patterson [74]. The *global CG time* is the duration of all CG solution steps together. We see that this value scales very well up to 256 cores for the aorta and up to 128 cores for the carotid artery. The *total time* is the total computational time including input and output functions. It also scales admissibly well up to 256 processing units for the aorta, and up to 128 cores for the carotid artery, see Tables 7.17 and 7.18, and Figure 7.9. For a higher number of cores, at least for the specific examples, the speedup is rather low. Possibilities to overcome this problem are, for example, the usage of parallel solver packages such as *Hypre* and a more efficient assembling of the coarse system of the FETI method. It also needs a more elaborate strategy with MPI and the memory management. Note that at some point the subdomains get too small and the increasingly dominant MPI communication impedes further strong scaling. As expected, the nonlinear elasticity case scales better than the linear case, compare Table 7.8. Note that using a larger amount of subdomains or a larger amount of local degrees of freedom improves the scaling properties of the problem. This is again due to memory issues and cache effects. Unfortunately, due to the memory restrictions on *VSC2*, larger problems are not taken into account; they are no longer solvable using $p = 16$ cores. In Figure 7.10 we compare the scaling properties for the aorta mesh dependent on the preconditioner. As expected the time needed to set up the local system is a little bit higher using the Dirichlet preconditioner. In comparison to the lumped preconditioner we have to set up the local Schur complements as described in Definition 6.2. On the other hand, due to the better convergence, the global CG time is significantly lower for Dirichlet preconditioner. The time to set up the coarse system, which are not mentioned in the figure are comparable for both preconditioners.

At last, we analyze the scaling for the all-floating and the classical FETI methods in 7.11. Here we also measure the realization of the coarse system, i.e. the assembling and the inversion of $\mathbf{G}^\top\mathbf{G}$, see (6.16). We see that this part of the computation is scaling the least. This is, as already mentioned before, to the relatively large communication involved there. In this experiment we have a better convergence and hence less computational time for the global CG method for the all-floating approach. On the other hand the realization of the coarse system is faster for classical FETI. There the coarse system is smaller compared to all-floating FETI. In total the computational times are almost the same.

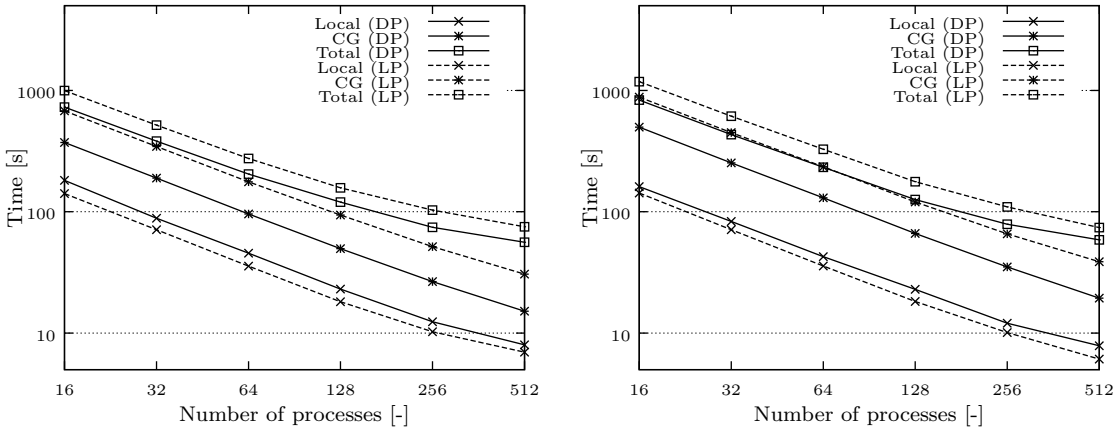

Figure 7.10: Computational times (s) for a simulation of the arterial model with the aorta mesh comparing the lumped preconditioner (LP) and the Dirichlet preconditioner (DP) for all-floating (left) and classical (right) FETI. *Local* is the sum of all assembling and local factorization times, *CG* is the duration of the global CG method and *total* is the total computational time. Note that the coarse time is neglected since it is the same for the lumped and the Dirichlet preconditioner.

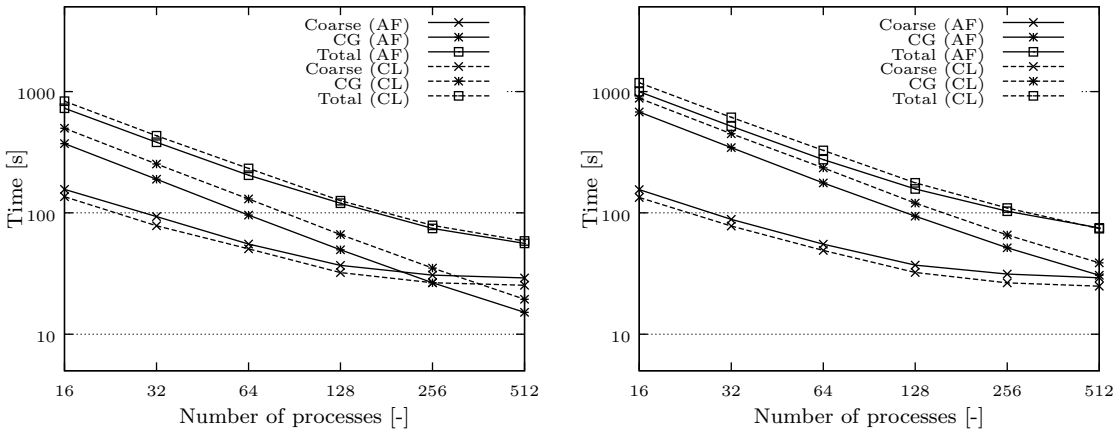

Figure 7.11: Computational times (s) for a simulation of the arterial model with the aorta mesh comparing the different FETI methods, i.e. all-floating FETI (AF) and classical FETI (CL) for the Dirichlet (left) and the lumped (right) preconditioner. *Coarse* is the time needed for the realization of the coarse system, *CG* is the duration of the global CG method and *total* is the total computational time. Note that the local time is almost the same for both FETI approaches, so it was neglected in this figure.

8 CONCLUSIONS AND OUTLOOK

We have shown the application of the finite element tearing and interconnecting method to elasticity problems, in particular to the simulation of the nonlinear elastic behavior of biological tissues, such as the myocardium and the artery. The models to simulate these materials were described in detail. Furthermore, we presented the requirements for the existence of a solution of the nonlinear equations and outlined convergence properties of the necessary Newton method. The main ideas of domain decomposition methods were summarized and the classical and the all-floating FETI approach were discussed in detail.

Illustrated by numerical examples we have shown certain advantages of the all-floating FETI method compared to the classical FETI approach. To the best of our knowledge the application of the all-floating approach to nonlinear orthotropic elasticity problems is not yet to be found in literature. For sure the mentioned advantages are influenced by the mesh structure and the choice of the boundary conditions and hence the method to choose depends on the specific problem.

We have presented and compared different techniques of preconditioning: the lumped preconditioner, the optimal Dirichlet preconditioner and a, in such applications, new BEM-preconditioner (to the best of our knowledge), which is based on the hypersingular integral operators. We have shown that the iteration numbers of the global iterative method behave like expected from the theory: due to the spectral equivalence of the local hypersingular operators to the local Steklov–Poincaré operators, the BEM preconditioner yields iteration numbers that lie in between the numbers obtained with the optimal Dirichlet preconditioner and the numbers obtained with the simple lumped preconditioner. Nonetheless, the numerical examples show that the implementation of the hypersingular operator still needs some work and improvements to achieve competitive or even better computational times compared to the sophisticated direct solver packages.

Furthermore, the numerical examples exposed some instabilities of the global iterative method for incompressible material parameters, i.e. for a very large bulk modulus κ. These problems were resolved in the past for linear elasticity problems but to the best of our knowledge are still an open task in nonlinear elasticity. Here we were able to present, like it was also shown in earlier contributions, that quadratic ansatz functions resolve the incompressible elastic behavior much better than linear ansatz functions.

Future work may include the coupling of the nonlinear elasticity problem with fluid dynamics to simulate the blood flow through cardiovascular vessels. Other interesting topics are the coupling of the electric activity in the heart with the mechanical behavior of the myocardium or contact problems, which occur while simulating certain surgery techniques such as artery stenting. FETI methods for such coupled problems are very demanding and hence still in their infancy. But beyond doubt these topics deserve closer attention.

A APPENDIX

A.1 Tensor Calculus

This section gives a general introduction to the calculus of vectors, matrices and tensors. Basic relations are omitted, for more information to tensor calculus see the books [44, 98]. A great overview including derivatives of tensors and many identities is [142]. Many formulas needed for the modeling of nonlinear elasticity are given in [80, Chapter 1] and in the publications of Itskov [97, 99].

To simplify matters *Einstein's summation convention* is used, which implies the summation over all the values of an index that appears twice in a single term.

A tensor of order n is defined by

$$\mathbf{A}_{i_1 i_2 \dots i_n} \mathbf{e}_{i_1} \otimes \mathbf{e}_{i_2} \otimes \cdots \otimes \mathbf{e}_{i_n},$$

with an orthonormal basis $\{\mathbf{e}_{i_j}\}, . = 1, \cdots, n$.

The *double contraction* of two second-order tensors $\mathbf{A}$ and $\mathbf{B}$, characterized by two dots, yields a scalar and is defined as

$$\mathbf{A} : \mathbf{B} = \mathrm{tr}(\mathbf{A}^\top \mathbf{B}) = \mathrm{tr}(\mathbf{B}^\top \mathbf{A}) = \mathbf{B} : \mathbf{A} = A_{ij} B_{ij}. \tag{A.1}$$

The *tensor product* or *dyadic product* of two vectors $\mathbf{u}$ and $\mathbf{v}$, each having the same dimension, is denoted by $\mathbf{A} = \mathbf{u} \otimes \mathbf{v}$. It results in a tensor of order two and rank one. The components A_{ij} of the dyadic product may be defined as

$$A_{ij} = (\mathbf{u} \otimes \mathbf{v})_{ij} = u_i v_j.$$

The *dyadic product* of two second-order tensors results in a tensor of forth-order

$$\mathbb{D} = \mathbf{A} \otimes \mathbf{B}, \quad D_{ijkl} = A_{ij} B_{kl}. \tag{A.2}$$

Additionally, we define the dot tensor product

$$\mathbb{D} = \mathbf{A} \odot \mathbf{B}, \quad D_{ijkl} = \frac{1}{2}(A_{ik} B_{jl} + A_{il} B_{jk}) \tag{A.3}$$

and the box tensor product

$$\mathbb{D} = \mathbf{A} \boxtimes \mathbf{B}, \quad D_{ijkl} = (A_{ik} A_{jl}). \tag{A.4}$$

The contraction of a forth-order and a second-order tensor is given by

$$\mathbf{B} = \mathbb{D} : \mathbf{A}, \quad B_{ij} = D_{ijkl} A_{kl}, \quad \text{and} \quad \mathbf{B} = \mathbf{A} : \mathbb{D}, \quad B_{ij} = A_{kl} D_{klij}, \tag{A.5}$$

respectively. Finally, the tensor product of two forth-order tensors is defined as

$$\mathbb{C} = \mathbb{A}\mathbb{B}, \quad C_{ijkl} = A_{ijmn} B_{mnkl}. \tag{A.6}$$

We define the forth-order unit tensors by

$$[\mathbb{I}]_{abcd} = (\delta_{ac}\delta_{bd}), \quad [\bar{\mathbb{I}}]_{abcd} = (\delta_{ad}\delta_{bc}). \tag{A.7}$$

and the symmetric unit tensor which fulfills major and minor symmetries 3.8.1 by

$$\mathbb{S} = \mathbf{I} \odot \mathbf{I} = \frac{1}{2}(\mathbb{I} + \bar{\mathbb{I}}). \tag{A.8}$$

Every second-order tensor $\mathbf{A}$ can be decomposed into its so-called *spherical* and its *deviatoric part* by

$$\mathbf{A} = \frac{1}{3}\operatorname{tr}(\mathbf{A})\mathbf{I} + \operatorname{dev}\mathbf{A},$$

with the deviatoric operator

$$\operatorname{dev}(\bullet) = (\bullet) - \frac{1}{3}\operatorname{tr}(\bullet)\mathbf{I}.$$

The deviatoric operator in the Lagrangian description reads

$$\operatorname{Dev}(\bullet) = (\bullet) - \frac{1}{3}[(\bullet) : \mathbf{C}]\,\mathbf{C}^{-1},$$

with the right Cauchy-Green tensor $\mathbf{C} = \mathbf{F}^{\top}\mathbf{F}$.

Two important properties of the deviatoric operator are

$$\operatorname{tr}(\operatorname{dev}\mathbf{A}) = 0,$$
$$\operatorname{dev}\mathbf{A} = (\mathbb{S} - \frac{1}{3}\mathbf{I} \otimes \mathbf{I}) : \mathbf{A},$$

with $\mathbb{S}$ from (A.8).

The unique transpose of a forth-order tensor $\mathbb{A}$ is denoted by $\mathbb{A}^\top$ and defined as

$$\left(\mathbb{A}^\top\right)_{ijkl} = A_{klij}. \tag{A.9}$$

Lemma A.1. *Given the second-order tensors* $\mathbf{A}, \mathbf{B}, \mathbf{C}, \mathbf{D}$*, we can state*

$$(\mathbf{A}\otimes\mathbf{B}) : \mathbf{C} = \mathbf{A}(\mathbf{B} : \mathbf{C}) = (\mathbf{B} : \mathbf{C})\mathbf{A}, \tag{A.10}$$
$$(\mathbf{A}\otimes\mathbf{B})(\mathbf{C}\otimes\mathbf{D}) = (\mathbf{B} : \mathbf{C})(\mathbf{A}\otimes\mathbf{D}) = (\mathbf{A}\otimes\mathbf{D})(\mathbf{B} : \mathbf{C}), \tag{A.11}$$
$$(\mathbf{A}\otimes\mathbf{B})^\top = \mathbf{B}\otimes\mathbf{A}, \tag{A.12}$$
$$\mathbf{AB} : \mathbf{C} = \mathbf{B} : \mathbf{A}^\top\mathbf{C}. \tag{A.13}$$

For the forth-order tensor $\mathbb{A}$ *and the forth-order unit tensor* $\mathbb{I}$ *it holds*

$$\mathbb{A} = \left(\mathbb{A}^\top\right)^\top, \tag{A.14}$$
$$\mathbf{A} = \mathbb{I} : \mathbf{A} = \mathbf{A} : \mathbb{I}, \tag{A.15}$$
$$\mathbb{A} : \mathbf{B} = \mathbf{B} : \mathbb{A}^\top, \tag{A.16}$$
$$\mathbf{B} : \mathbb{A}^\top : \mathbf{C} = \mathbf{C} : \mathbb{A} : \mathbf{B} = (\mathbb{A} : \mathbf{B}) : \mathbf{C}, \tag{A.17}$$
$$\mathbb{A}\mathbb{I} = \mathbb{I}\mathbb{A} = \mathbb{A}. \tag{A.18}$$

Proof. We prove these identities using Einstein's notation and the definitions from above:

$$[(\mathbf{A}\otimes\mathbf{B}) : \mathbf{C}]_{ij} = A_{ij}B_{kl}C_{kl} = A_{ij}(\mathbf{B} : \mathbf{C}) = (\mathbf{B} : \mathbf{C})A_{ij},$$

since $\mathbf{B} : \mathbf{C}$ is scalar valued. For (A.11) additionally use (A.6).

$$[(\mathbf{A}\otimes\mathbf{B})^\top]_{ijkl} = A_{kl}B_{ij} = [\mathbf{B}\otimes\mathbf{A}]_{ijkl},$$

using the definition of the dyadic product (A.2) and the transposed of a forth-order tensor (A.9). Following the same pattern (A.13)-(A.17) can easily be shown. For (A.18) the definitions (A.6) and (A.7) are used. □

Remark A.1.1. *Note that for symmetric second-order tensors* $\mathbf{C}$ *it holds, additionally to* (A.15)*,*

$$\mathbb{S} : \mathbf{C} = \mathbf{C} : \mathbb{S} = \mathbf{C}.$$

Lemma A.2. *Given the second-order tensors* $\mathbf{A}, \mathbf{B}$ *and the vectors* $\mathbf{a}, \mathbf{b}$ *it holds*

$$(\mathbf{A}^\top\mathbf{B}) : (\mathbf{a}\otimes\mathbf{b}) = \mathbf{a}\cdot(\mathbf{A}^\top\mathbf{B}\mathbf{b}) = (\mathbf{A}\mathbf{a})\cdot(\mathbf{B}\mathbf{b}),$$
$$\mathbf{A}(\mathbf{a}\otimes\mathbf{b})\mathbf{B} = (\mathbf{A}\mathbf{a})\otimes(\mathbf{B}^\top\mathbf{b}).$$

Proof. The first equation is proved by

$$\mathbf{A}^\top\mathbf{B} : (\mathbf{a}\otimes\mathbf{b}) = A_{ki}B_{kj}a_ib_j = a_iA_{ki}B_{kj}b_j = a_i[\mathbf{A}^\top\mathbf{B}\mathbf{b}]_i = \mathbf{a}\cdot(\mathbf{A}^\top\mathbf{B}\mathbf{b})$$
$$\mathbf{A}^\top\mathbf{B} : (\mathbf{a}\otimes\mathbf{b}) = A_{ki}B_{kj}a_ib_j = A_{ki}a_iB_{kj}b_j = [\mathbf{A}\mathbf{a}]_k[\mathbf{B}\mathbf{b}]_k = (\mathbf{A}\mathbf{a})\cdot(\mathbf{B}\mathbf{b})$$

and the second equation by

$$\begin{aligned}[\mathbf{A}(\mathbf{a}\otimes\mathbf{b})\mathbf{B}]_{ij} &= [\mathbf{A}(\mathbf{a}\otimes\mathbf{b})]_{ik}B_{kj} = A_{il}(\mathbf{a}\otimes\mathbf{b})_{lk}B_{kj} = A_{il}a_lb_kB_{kj} = [\mathbf{A}\mathbf{a}]_i[\mathbf{B}^\top\mathbf{b}]_j \\ &= [(\mathbf{A}\mathbf{a})\otimes(\mathbf{B}^\top\mathbf{b})]_{ij}.\end{aligned}$$

□

A.1.1 Derivatives

The derivative of a function $\mathbf{A} : \mathbb{R} \to \mathbb{R}^{n\times m}$ with respect to a scalar x is defined as

$$\left[\frac{\partial\mathbf{A}}{\partial x}\right]_{ij} = \frac{\partial A_{ij}}{\partial x}. \tag{A.19}$$

The derivative of the scalar function $f : \mathbb{R}^{n\times m} \to \mathbb{R}$ with respect to a tensor $\mathbf{B} \in \mathbb{R}^{n\times m}$ is defined by convention as

$$\left[\frac{\partial f}{\partial\mathbf{B}}\right]_{ij} = \frac{\partial f}{\partial B_{ij}}. \tag{A.20}$$

The derivative of a second-order tensor valued function $\mathbf{A} : \mathbb{R}^{n\times m} \to \mathbb{R}^{p\times q}$ with respect to a second-order tensor $\mathbf{B}$ is a tensor of forth order is defined in accordance with (A.19) and (A.20) by

$$\left[\frac{\partial\mathbf{A}}{\partial\mathbf{B}}\right]_{ijkl} = \frac{\partial A_{ij}}{\partial B_{kl}}. \tag{A.21}$$

Using (A.20) and (A.21) we get for the second order derivative

$$\left[\frac{\partial^2 f}{\partial\mathbf{B}^2}\right]_{ijkl} = \frac{\partial^2 f}{\partial B_{ij}\partial B_{kl}}. \tag{A.22}$$

Corollary A.1. *Let* $\mathbf{A}$ *be a second-order tensor and let* $\mathbf{C}$ *be a symmetric second-order tensor. Then*

$$\frac{\partial\mathbf{A}}{\partial\mathbf{A}} = \mathbb{I}, \quad \frac{\partial\mathbf{C}}{\partial\mathbf{C}} = \mathbb{S},$$

for the unit tensors given in (A.7) *and* (A.8).

Proof. Following (A.21) we obtain

$$\left(\frac{\partial \mathbf{A}}{\partial \mathbf{A}}\right)_{ijkl} = \frac{\partial A_{ij}}{\partial A_{kl}} = \delta_{ik}\delta_{jl}.$$

The latter is the definition of $\mathbb{I}$, cf. (A.7).

$$\left(\frac{\partial \mathbf{C}}{\partial \mathbf{C}}\right)_{ijkl} = \frac{\partial C_{ij}}{\partial C_{kl}} = \frac{1}{2}\left(\frac{\partial C_{ij}}{\partial C_{kl}} + \frac{\partial C_{ji}}{\partial C_{kl}}\right) = \frac{1}{2}(\delta_{ik}\delta_{jl} + \delta_{il}\delta_{jk}),$$

which is the definition of $\mathbb{S}$, cf. (A.8). □

Corollary A.2. *Let* $\mathbf{A}$ *be an invertible second-order tensor. Then*

$$\frac{\partial \det \mathbf{A}}{\partial \mathbf{A}} = \mathbf{A}^{-\top} \det \mathbf{A}.$$

Proof. Using Laplace's formula for the determinant of an $n \times n$ matrix and Jacobi's formula of matrix calculus we can write

$$\frac{\mathrm{d}\det(\mathbf{A})}{\mathrm{d}x} = \det(\mathbf{A}) \operatorname{tr}\left(\mathbf{A}^{-1}\frac{\mathrm{d}\mathbf{A}}{\mathrm{d}x}\right).$$

From this it follows with (A.19)-(A.22), Corollary A.1, the identities (A.15, A.16) and properties of the trace that

$$\begin{aligned}\left[\frac{\partial \det(\mathbf{A})}{\partial \mathbf{A}}\right]_{ij} &= \frac{\partial \det(\mathbf{A})}{\partial A_{ij}} = \det(\mathbf{A}) \operatorname{tr}\left(\mathbf{A}^{-1}\frac{\partial \mathbf{A}}{\partial A_{ij}}\right) = \det(\mathbf{A})[\mathbf{A}^{-1}]_{km}\frac{\partial A_{mk}}{\partial A_{ij}} \\ &= \det(\mathbf{A})[\mathbf{A}^{-\top}]_{mk}\left[\frac{\partial \mathbf{A}}{\partial \mathbf{A}}\right]_{mkij} = \det(\mathbf{A})\left[\mathbf{A}^{-\top} : \frac{\partial \mathbf{A}}{\partial \mathbf{A}}\right]_{ij} = [\mathbf{A}^{-\top}]_{ij} \det \mathbf{A}.\end{aligned}$$

□

Corollary A.3 (Chain rules in tensor calculus)**.** *For the second-order tensors* $\mathbf{A}, \mathbf{B}, \mathbf{C}$ *and the scalar valued function* f *the following chain rules hold*

$$\frac{\partial f}{\partial \mathbf{A}} = \frac{\partial f}{\partial \mathbf{B}} : \frac{\partial \mathbf{B}}{\partial \mathbf{A}}, \tag{A.23}$$

$$\frac{\partial \mathbf{A}}{\partial \mathbf{B}} = \frac{\partial \mathbf{A}}{\partial \mathbf{C}} : \frac{\partial \mathbf{C}}{\partial \mathbf{B}}, \tag{A.24}$$

$$\frac{\partial \phi \mathbf{A}}{\partial \mathbf{C}} = \mathbf{A} \otimes \frac{\partial \phi}{\partial \mathbf{C}} + \phi \frac{\partial \mathbf{A}}{\partial \mathbf{C}}, \tag{A.25}$$

$$\frac{\partial (\mathbf{A} : \mathbf{B})}{\partial \mathbf{C}} = \mathbf{A} : \frac{\partial \mathbf{B}}{\partial \mathbf{C}} + \mathbf{B} : \frac{\partial \mathbf{A}}{\partial \mathbf{C}}. \tag{A.26}$$

$$\frac{\partial(\mathbf{AB})}{\partial \mathbf{C}} : \mathbf{D} = \left(\frac{\partial \mathbf{A}}{\partial \mathbf{C}} : \mathbf{D}\right)\mathbf{B} + \mathbf{A}\left(\frac{\partial \mathbf{B}}{\partial \mathbf{C}} : \mathbf{D}\right) \tag{A.27}$$

Proof. (A.23) holds according to the definitions (A.20), (A.21) and $(A.5)_1$. (A.24) analogous using (A.6). For (A.25), (A.26) and (A.27) additionally use the definitions for the dyadic product (A.2) and the double contraction (A.1) and (A.5), respectively. □

Corollary A.4. *Let* $\mathbf{A}$ *be an invertible second-order tensor. Then*

$$\left[\frac{\partial \mathbf{A}^{-1}}{\partial \mathbf{A}}\right]_{ijkl} = \frac{\partial A^{-1}_{ij}}{\partial A_{kl}} = -A^{-1}_{ik} A^{-1}_{lj}.$$

For symmetric tensors $\mathbf{A}$ *we get with definition* (A.3)

$$\frac{\partial A^{-1}_{ij}}{\partial A_{kl}} = -\frac{1}{2}(A^{-1}_{ik} A^{-1}_{jl} + A^{-1}_{il} A^{-1}_{jk}), \quad \frac{\partial \mathbf{A}^{-1}}{\partial \mathbf{A}} = -\mathbf{A}^{-1} \odot \mathbf{A}^{-1}.$$

Proof. Let $\mathbf{B}$ be an second-order tensor. Recall that

$$\frac{\partial \mathbf{A}^{-1}\mathbf{A}}{\partial \mathbf{A}} : \mathbf{B} = \mathbf{0}.$$

With (A.27) this is

$$\frac{\partial(\mathbf{A}^{-1}\mathbf{A})}{\partial \mathbf{A}} : \mathbf{B} = \left(\frac{\partial \mathbf{A}^{-1}}{\partial \mathbf{A}} : \mathbf{B}\right)\mathbf{A} + \mathbf{A}^{-1}\left(\frac{\partial \mathbf{A}}{\partial \mathbf{A}} : \mathbf{B}\right) = \mathbf{0},$$

and thus with $(A.5)_1$

$$\left(\frac{\partial \mathbf{A}^{-1}}{\partial \mathbf{A}} : \mathbf{B}\right) = \mathbf{A}^{-1}\mathbf{B}\mathbf{A}^{-1} \quad \text{or} \quad \frac{\partial A^{-1}_{ij}}{\partial A_{kl}} B_{kl} = A^{-1}_{ik} B_{kl} A^{-1}_{lj}$$

which concludes the proof. See also [80, Section 1.7]. □

Corollary A.5 (Derivative of traces)**.** *For the second-order tensors* $\mathbf{A}, \mathbf{B}, \mathbf{C}$ *we obtain*

$$\frac{\partial \mathrm{tr}(\mathbf{A})}{\partial \mathbf{A}} = \mathbf{I}, \quad \frac{\partial \mathrm{tr}(\mathbf{A}^2)}{\partial \mathbf{A}} = 2\mathbf{A}^\top.$$

Proof. First part follows immediately form (A.26). For the second part use (A.19)-

(A.22), Corollary A.1 and properties of the trace

$$\left[\frac{\partial \operatorname{tr}(\mathbf{AA})}{\partial \mathbf{A}}\right]_{ij} = \frac{\partial A_{kl}A_{lk}}{\partial A_{ij}} = \frac{\partial A_{kl}}{\partial A_{ij}}A_{lk} + A_{kl}\frac{\partial A_{lk}}{\partial A_{ij}}$$
$$= \left[\frac{\partial \mathbf{A}}{\partial \mathbf{A}}\right]_{klij}[\mathbf{A}^\top]_{kl} + [\mathbf{A}^\top]_{kl}\left[\frac{\partial \mathbf{A}}{\partial \mathbf{A}}\right]_{lkij} = 2\left[\mathbf{A}^\top : \mathbb{I}\right]_{ij}$$

□

A.1.2 Special Derivatives of Mechanical Quantities

In the following let $\mathbf{F}$ be the deformation gradient, $J = \det(\mathbf{F})$ the Jacobian, $\mathbf{C} = \mathbf{F}^\top\mathbf{F}$ the right Cauchy–Green tensor.

Corollary A.6.

$$\frac{\partial J}{\partial \mathbf{C}} = \frac{J}{2}\mathbf{C}^{-1} \quad , \quad \frac{\partial J^{-2/3}}{\partial \mathbf{C}} = -\frac{1}{3}J^{-2/3}\mathbf{C}^{-1}.$$

Proof. With $\det(\mathbf{C}) = \det(\mathbf{F}^\top)\det(\mathbf{F}) = J^2$, Corollary A.2 and the symmetry of $\mathbf{C}$ we obtain

$$\frac{\partial J^2}{\partial \mathbf{C}} = \frac{\partial \det \mathbf{C}}{\partial \mathbf{C}} = \det(\mathbf{C})\mathbf{C}^{-\top} = J^2\mathbf{C}^{-1}.$$

Using the chain rule we get

$$\frac{\partial J^2}{\partial \mathbf{C}} = 2J\frac{\partial J}{\partial \mathbf{C}} \quad \Rightarrow \quad 2J\frac{\partial J}{\partial \mathbf{C}} = J^2\mathbf{C}^{-1} \quad \Rightarrow \quad \frac{\partial J^{-2/3}}{\partial \mathbf{C}} = -\frac{2}{3}J^{-5/3}\frac{\partial J}{\partial \mathbf{C}} = -\frac{1}{3}J^{-2/3}\mathbf{C}^{-1},$$

which concludes the proof. □

Corollary A.7. *We introduce the forth-order projection tensors* $\mathbb{P}$ *and* $\mathbb{p}$ *as*

$$\mathbb{P} := \mathbb{S} - \frac{1}{3}\mathbf{C}^{-1}\otimes\mathbf{C}, \quad \mathbb{p} := \mathbb{S} - \frac{1}{3}\mathbf{I}\otimes\mathbf{I},$$

with $\mathbf{C}$ *the right Cauchy–Green tensor. It holds*

$$\mathbb{P}^\top = \left(\mathbb{S} - \frac{1}{3}\mathbf{C}\otimes\mathbf{C}^{-1}\right), \quad \mathbb{p}^\top = \mathbb{p}$$

and

$$\mathbf{A} : \mathbb{P}^\top = \mathbb{P} : \mathbf{A} = \operatorname{Dev}(\mathbf{A}), \quad \mathbf{A} : \mathbb{p} = \mathbb{p} : \mathbf{A} = \operatorname{dev}(\mathbf{A}), \quad \frac{\partial \overline{\mathbf{C}}}{\partial \mathbf{C}} = J^{-2/3}\mathbb{P}^\top$$

using $\overline{\mathbf{C}} = J^{-2/3}\mathbf{C}$ *in accordance with* (3.28).

Proof. With the equations (A.12) and (A.14) we obtain

$$\mathbb{P} = \left(\mathbb{P}^\top\right)^\top = \left(\mathbb{S} - \frac{1}{3}\mathbf{C}\otimes\mathbf{C}^{-1}\right)^\top = \mathbb{S}^\top - \frac{1}{3}(\mathbf{C}\otimes\mathbf{C}^{-1})^\top = \mathbb{S} - \frac{1}{3}\mathbf{C}^{-1}\otimes\mathbf{C}.$$

The properties of Dev(•) and dev(•) hold due to (A.10), (A.15) and (A.16). Finally, we get

$$\frac{\partial\overline{\mathbf{C}}}{\partial\mathbf{C}} = \frac{\partial J^{-2/3}\mathbf{C}}{\partial\mathbf{C}} = J^{-2/3}\frac{\partial\mathbf{C}}{\partial\mathbf{C}} + \mathbf{C}\otimes\frac{\partial J^{-2/3}}{\partial\mathbf{C}} = J^{-2/3}\mathbb{S} - \mathbf{C}\otimes\frac{1}{3}J^{-2/3}\mathbf{C}^{-1}$$

with (A.25) and Corollary A.6. □

Let $\chi_*(\bullet)$ denote a push-forward operation. With (A.3) we denote

$$\frac{\partial\mathbf{C}^{-1}}{\partial\mathbf{C}} = -\mathbf{C}^{-1}\odot\mathbf{C}^{-1}.$$

The push-forward of this tensor product is

$$\chi_*\left(\mathbf{C}^{-1}\odot\mathbf{C}^{-1}\right) = J^{-1}F_{aA}F_{bB}F_{cC}F_{dD}\left[\mathbf{C}^{-1}\odot\mathbf{C}^{-1}\right]_{ABCD} = J^{-1}\mathbf{I}\odot\mathbf{I} = J^{-1}\mathbb{S}.$$

With (A.2) we express

$$\left[\mathbf{C}^{-1}\otimes\mathbf{C}^{-1}\right]_{ABCD} = C^{-1}_{AB}C^{-1}_{CD}.$$

The push-forward of this dyad tensor product is

$$\chi_*\left(\mathbf{C}^{-1}\otimes\mathbf{C}^{-1}\right) = J^{-1}F_{aA}F_{bB}F_{cC}F_{dD}\left[\mathbf{C}^{-1}\otimes\mathbf{C}^{-1}\right]_{ABCD} = J^{-1}\mathbf{I}\otimes\mathbf{I}.$$

Other push-forwards are

$$\chi_*(\mathbb{I}) = J^{-1}\mathbf{B}\boxtimes\mathbf{B}, \quad \chi_*(\mathbf{I}\otimes\mathbf{I}) = J^{-1}\mathbf{B}\otimes\mathbf{B}, \quad \chi_*(\mathbb{S}) = \chi_*(\mathbf{I}\odot\mathbf{I}) = J^{-1}\mathbf{B}\odot\mathbf{B}.$$

Corollary A.8 (Derivative of invariants)**.** *Let A be a second-order tensor. Then for the invariants defined in 3.4 it holds*

$$\frac{\partial I_1}{\partial\mathbf{A}} = \mathbf{I}, \quad \frac{\partial I_2}{\partial\mathbf{A}} = I_1\mathbf{I} - \mathbf{A}^\top, \quad \frac{\partial I_3}{\partial\mathbf{A}} = I_3\mathbf{A}^{-\top}.$$

Proof. The derivative of the first invariant gives with A.26

$$\frac{\partial I_1}{\partial\mathbf{A}} = \frac{\partial\operatorname{tr}\mathbf{A}}{\partial\mathbf{A}} = \frac{\partial(\mathbf{I}:\mathbf{A})}{\partial\mathbf{A}} = \mathbf{I}.$$

By means of Corollary A.5 we get for the derivative of the second invariant

$$\frac{\partial I_2}{\partial \mathbf{A}} = \frac{1}{2}\frac{\partial(\mathrm{tr}(\mathbf{A})^2 - \mathrm{tr}(\mathbf{A}^2)}{\partial \mathbf{A}} = \frac{1}{2}\left(2\,\mathrm{tr}\,\mathbf{A}\frac{\partial \mathrm{tr}(\mathbf{A})}{\partial \mathbf{A}} - (2\mathbf{A}^\top)\right) = I_1\mathbf{I} - \mathbf{A}^\top.$$

The third part follows immediately from Corollary A.2. □

A.2 Numerical Derivatives

The computation of the isochoric part of the elasticity tensor may be very complicated, since it involves a lot of matrix manipulations, cf. Section 3.13.3. Numerical derivatives is a possibility to simplify the computation of the elasticity tensor. In the following, we will outline the basic concepts of this topic. For more information and error estimates see [48, 144].

Starting point is the symmetrized form of the differential quotient

$$f'(x) \approx \frac{f(x+h) - f(x-h)}{2h}.$$

Since this is no exact computation there are two main sources of errors that have to be taken into consideration. First, we notice a *truncation error* e_t which results from higher-order terms in the Taylor series expansion of the function $f(x \pm h)$. We can state that $e_\mathrm{t} \sim h^2 f'''$. The other error is the so-called *roundoff error* e_r. It may be estimated by $e_\mathrm{r} \sim \epsilon_\mathrm{f}|f(x)/h|$, where ϵ_f is the accuracy with which f is computed. As an optimal choice for h, in order to minimize the total error $e_\mathrm{r} + e_\mathrm{t}$, we have

$$h \sim \left(\frac{\epsilon_\mathrm{f} f}{f'''}\right)^{1/3} \sim \epsilon_\mathrm{f}^{1/3} x_\mathrm{c}.$$

Here, we denote by $x_\mathrm{c} = (f/f'')^{1/2}$ a measure of the curvature of the function f.

Consequently, the mixed derivative formula for a function of two dimensions it

$$\frac{\partial^2 f}{\partial x \partial y} \approx \frac{[f(x+h,y+h) - f(x+h,y-h)] - [f(x-h,y+h) - f(x-h,y-h)]}{4h^2}. \tag{A.28}$$

The optimal scaling in this case is

$$h \sim \epsilon_\mathrm{f}^{1/4} x_\mathrm{c}.$$

This leads us to the case of the scalar-valued strain-energy function Ψ and its derivative with respect to a tensor. Following (A.20) we can state

$$\left[\frac{\partial \Psi(\mathbf{C})}{\partial \mathbf{C}}\right]_{ij} = \frac{\partial \Psi(\mathbf{C})}{\partial C_{ji}} = \frac{\partial \Psi(\mathbf{C})}{\partial C_{ij}}.$$

Hence, we get for the numerical derivative

$$\left[\frac{\partial \Psi(\mathbf{C})}{\partial \mathbf{C}}\right]_{ij} \approx \frac{\Psi(\mathbf{C}^{ij}_{+h}) - \Psi(\mathbf{C}^{ij}_{-h})}{2h}, \tag{A.29}$$

where the second order tensor $\mathbf{C}^{ij}_a$ is defined as

$$\left[\mathbf{C}^{ij}_a\right]_{kl} = \begin{cases} \mathbf{C}_{kl} & \text{for } kl \neq ij \\ \mathbf{C}_{kl} + a & \text{for } kl = ij \end{cases}.$$

With (A.29) and Corollary 3.2 we may calculate an approximate of the stress tensors in the reference and the current configuration, respectively.

The second derivative of the strain-energy function with respect to the tensor $\mathbf{C}$ yields a forth-order tensor. Using (A.22) we get for the entries of this value

$$\left[\frac{\partial^2 \Psi(\mathbf{C})}{\partial \mathbf{C}^2}\right]_{ijkl} = \frac{\partial^2 \Psi(\mathbf{C})}{\partial C_{ij} \partial C_{kl}}.$$

The numerical derivative is obtained in an analogous way as (A.28) and yields for the entries of the forth-order tensor

$$\left[\frac{\partial^2 \Psi(\mathbf{C})}{\partial \mathbf{C}^2}\right]_{ijkl} = \frac{(\Psi(^{kl}_{+h}\mathbf{C}^{ij}_{+h}) - \Psi(^{kl}_{+h}\mathbf{C}^{ij}_{-h})) - (\Psi(^{kl}_{-h}\mathbf{C}^{ij}_{+h}) - \Psi(^{kl}_{-h}\mathbf{C}^{ij}_{-h}))}{4h^2}.$$

BIBLIOGRAPHY

[1] PR Amestoy, IS Duff, JY L'Excellent, and J Koster. "A Fully Asynchronous Multifrontal Solver Using Distributed Dynamic Scheduling". In: *SIAM J Matrix Anal Appl* 23.1 (2001), pp. 15–41.

[2] PR Amestoy, A Guermouche, JY L'Excellent, and S Pralet. "Hybrid scheduling for the parallel solution of linear systems". In: *Parallel Comput* 32.2 (2006), pp. 136–156.

[3] Aneurisk-Team. *AneuriskWeb project website*. `http://ecm2.mathcs.emory.edu/aneuriskweb/`. [Online; accessed 19-February-2015]. 2012.

[4] SS Antman. "The eversion of thick spherical shells". In: *Arch Rational Mech Anal* 70.2 (1979), pp. 113–123.

[5] DN Arnold. "Discretization by finite elements of a model parameter dependent problem". In: *Numer Math* 37.3 (1981), pp. 405–421.

[6] SF Ashby, TA Manteuffel, and PE Saylor. "A taxonomy for conjugate gradient methods". In: *SIAM J Numer Anal* 27.6 (1990), pp. 1542–1568.

[7] CM Augustin, GA Holzapfel, and O Steinbach. "Classical and All-floating FETI Methods for the Simulation of Arterial Tissues". In: *Int J Numer Meth Eng* 99.4 (2014), pp. 290–312.

[8] CM Augustin and O Steinbach. "FETI methods for the simulation of biological tissues". In: *Domain Decomposition Methods in Science and Engineering XX*. Ed. by R Bank, M Holst, O Widlund, and J Xu. Vol. 91. Lect Notes Comput Sci Eng. Berlin: Springer, 2013, pp. 503–510.

[9] O Axelsson. *Iterative solution methods*. Cambridge: Cambridge University Press, 1994, pp. xiv+654.

[10] I Babuška. "The finite element method with Lagrangian multipliers". In: *Numer Math* 20 (1972/73), pp. 179–192.

[11] I Babuška and M Suri. "Locking effects in the finite element approximation of elasticity problems". In: *Numer Math* 62.4 (1992), pp. 439–463.

[12] M Baker and JL Ericksen. "Inequalities restricting the form of the stress deformation relations for isotropic elastic solids and Reiner–Rivlin fluids". In: *J Wash Acad Sci* 44 (1954), pp. 33–35.

[13] JM Ball. "Constitutive inequalities and existence theorems in nonlinear elastostatics". In: *Nonlinear analysis and mechanics: Heriot-Watt Symposium (Edinburgh, 1976), Vol. I*. London: Pitman, 1977, 187–241. Res. Notes in Math., No. 17.

[14] JM Ball. “Convexity conditions and existence theorems in nonlinear elasticity”. In: *Arch Rational Mech Anal* 63.4 (1976/77), pp. 337–403.

[15] JM Ball. “Some open problems in elasticity”. In: *Geometry, mechanics, and dynamics*. Springer, 2002, pp. 3–59.

[16] D Balzani, D Böse, D Brands, R Erbel, A Klawonn, O Rheinbach, and J Schröder. “Parallel simulation of patient-specific atherosclerotic arteries for the enhancement of intravascular ultrasound diagnostics”. In: *Eng Comput (Swansea)* 29.8 (2012), pp. 888–906.

[17] D Balzani, D Brands, A Klawonn, O Rheinbach, and J Schröder. “On the mechanical modeling of anisotropic biological soft tissue and iterative parallel solution strategies”. In: *Arch Appl Mech* 80.5 (2010), pp. 479–488.

[18] D Balzani, P Neff, J Schröder, and GA Holzapfel. “A polyconvex framework for soft biological tissues. Adjustment to experimental data”. In: *Int J Solids Struct* 43 (2006), pp. 6052–6070.

[19] JD Bayer, RC Blake, G Plank, and NA Trayanova. “A novel rule-based algorithm for assigning myocardial fiber orientation to computational heart models”. In: *Ann Biomed Eng* 40.10 (2012), pp. 2243–2254.

[20] H Benhassine and A Bendali. “A non-overlapping domain decomposition method for continuous-pressure mixed finite element approximations of the Stokes problem”. In: *ESAIM Math Model Numer Anal* 45.4 (2011), pp. 675–696.

[21] C Bernardi, Y Maday, and A Patera. “A new nonconforming approach to domain decomposition: the mortar element method”. In: *Nonlinear partial differential equations and their applications. Collège de France Seminar, Vol. XI (Paris, 1989–1991)*. Vol. 299. Pitman Res Notes Math Ser. Harlow: Longman Sci. Tech., 1994, pp. 13–51.

[22] D Boffi, F Brezzi, and M Fortin. “Finite elements for the Stokes problem”. In: *Mixed Finite Elements, Compatibility Conditions, and Applications*. Springer, 2008, pp. 45–100.

[23] D Boffi, F Brezzi, and M Fortin. *Mixed finite element methods and applications*. Vol. 44. Springer Series in Computational Mathematics. Springer, Heidelberg, 2013, pp. xiv+685.

[24] J Bonet and RD Wood. *Nonlinear continuum mechanics for finite element analysis*. Second. Cambridge University Press, Cambridge, 2008, pp. xx+318.

[25] D Braess. *Finite elements*. Third. Theory, fast solvers, and applications in elasticity theory. Cambridge University Press, Cambridge, 2007, pp. xviii+365.

[26] JH Bramble, JE Pasciak, and J Xu. “Parallel multilevel preconditioners”. In: *Math Comput* 55.191 (1990), pp. 1–22.

[27] D Brands, A Klawonn, O Rheinbach, and J Schröder. “Modelling and convergence in arterial wall simulations using a parallel FETI solution strategy”. In: *Comput Methods Biomech Biomed Engin* 11.5 (2008), pp. 569–583.

[28] D Brands, J Schröder, A Klawonn, O Rheinbach, D Böse, and R Erbel. "Numerical Simulations of Arterial Walls Based on IVUS-Data". In: *Proc Appl Math Mech* 9.1 (2009), pp. 75–78.

[29] SC Brenner and R Scott. *The mathematical theory of finite element methods*. Vol. 15. Texts in Applied Mathematics. New York: Springer-Verlag, 1994, pp. xii+294.

[30] F Brezzi. "On the existence, uniqueness and approximation of saddle-point problems arising from Lagrangian multipliers". In: *ESAIM Math Model Numer Anal* 8.R2 (1974), pp. 129–151.

[31] S Brinkhues, A Klawonn, O Rheinbach, and J Schröder. "Augmented Lagrange methods for quasi-incompressible materials—Applications to soft biological tissue". In: *Int J Numer Methods Biomed Eng* 29.3 (2013), pp. 332–350.

[32] T Brzobohatý, Z Dostál, T Kozubek, P Kovář, and A Markopoulos. "Cholesky decomposition with fixing nodes to stable computation of a generalized inverse of the stiffness matrix of a floating structure". In: *Int J Numer Methods Eng* 88.5 (2011), pp. 493–509.

[33] R Bustamante and GA Holzapfel. "Methods to compute 3D residual stress distributions in hyperelastic tubes with application to arterial walls". In: *Int J Eng Sci* 48.11 (2010), pp. 1066–1082.

[34] C Calgaro and J Laminie. "On the domain decomposition method for the generalized Stokes problem with continuous pressure". In: *Numer Methods Partial Differ Equ* 16.1 (2000), pp. 84–106.

[35] É Chamberland, A Fortin, and M Fortin. "Comparison of the performance of some finite element discretizations for large deformation elasticity problems". In: *Comput Struct* 88.11-12 (2010), pp. 664–673.

[36] P Charrier, B Dacorogna, B Hanouzet, and P Laborde. "An existence theorem for slightly compressible materials in nonlinear elasticity". In: *SIAM J Math Anal* 19.1 (1988), pp. 70–85.

[37] CJ Chuong and YC Fung. "Three-dimensional stress distribution in arteries". In: *J Biomech Engr* 105 (1983), pp. 268–274.

[38] PG Ciarlet. *Mathematical elasticity. Vol. I*. Vol. 20. Studies in Mathematics and its Applications. Three-dimensional elasticity. Amsterdam: North-Holland Publishing Co., 1988, pp. xlii+451.

[39] PG Ciarlet. *The finite element method for elliptic problems*. Studies in Mathematics and its Applications, Vol. 4. Amsterdam: North-Holland Publishing Co., 1978, pp. xix+530.

[40] KD Costa, JW Holmes, and AD McCulloch. "Modeling cardiac mechanical properties in three dimensions". In: *Phil Trans R Soc Lond A* 359 (2001), pp. 1233–1250.

[41] M Crouzeix and PA Raviart. "Conforming and nonconforming finite element methods for solving the stationary Stokes equations I". In: *ESAIM Math Model Numer Anal* 7.R3 (1973), pp. 33–75.

[42] B Dacorogna. *Direct methods in the calculus of variations*. Vol. 78. Applied Mathematical Sciences. Berlin: Springer-Verlag, 1989, pp. x+308.

[43] B Dacorogna. *Direct methods in the calculus of variations*. Second. Vol. 78. Applied Mathematical Sciences. New York: Springer, 2008, pp. xii+619.

[44] DA Danielson. *Vectors and tensors in engineering and physics*. Second. Boulder, CO: Westview Press, 2003, pp. vi+282.

[45] TA Davis. "A column pre-ordering strategy for the unsymmetric-pattern multifrontal method". In: *ACM Trans Math Software* 30.2 (2004), pp. 167–195.

[46] TA Davis. "Algorithm 832: UMFPACK V4.3 – an unsymmetric-pattern multifrontal method". In: *ACM Trans Math Software* 30.2 (2004), pp. 196–199.

[47] H Demiray. "A note on the elasticity of soft biological tissues". In: *J Biomech* 5 (1972), pp. 309–311.

[48] JE Dennis Jr and RB Schnabel. *Numerical methods for unconstrained optimization and nonlinear equations*. Prentice Hall Series in Computational Mathematics. Englewood Cliffs, NJ: Prentice Hall Inc., 1983, pp. xiii+378.

[49] P Deuflhard. *Newton methods for nonlinear problems*. Vol. 35. Springer Series in Computational Mathematics. Springer, Heidelberg, 2011, pp. xii+424.

[50] S Dokos, BH Smaill, AA Young, and IJ LeGrice. "Shear properties of passive ventricular myocardium". In: *Am J Physiol Heart Circ Physiol* 283 (2002), H2650–H2659.

[51] Z Dostál, D Horák, and R Kučera. "Total FETI - an easier implementable variant of the FETI method for numerical solution of elliptic PDE". In: *Comm Numer Methods Eng* 22 (2006), pp. 1155–1162.

[52] TSE Eriksson, AJ Prassl, G Plank, and GA Holzapfel. "Influence of myocardial fiber/sheet orientations on left ventricular mechanical contraction". In: *Math Mech Solids* 18.6 (2013), pp. 592–606.

[53] C Farhat, M Lesoinne, P LeTallec, K Pierson, and D Rixen. "FETI-DP: a dual-primal unified FETI method. I. A faster alternative to the two-level FETI method". In: *Int J Numer Methods Eng* 50.7 (2001), pp. 1523–1544.

[54] C Farhat, J Mandel, and FX Roux. "Optimal convergence properties of the FETI domain decomposition method". In: *Comput Methods Appl Mech Eng* 115 (1994), pp. 365–385.

[55] C Farhat and FX Roux. "A method of finite element tearing and interconnecting and its parallel solution algorithm". In: *Int J Numer Methods Eng* 32 (1991), pp. 1205–1227.

[56] C Farhat and FX Roux. "Implicit parallel processing in structural mechanics". In: *Comput Mech Adv* 2.1 (1994), p. 124.

[57] PJ Flory. "Thermodynamic relations for high elastic materials". In: *Trans Faraday Soc* 57 (1961), pp. 829–838.

[58] M Fortin and F Brezzi. *Mixed and hybrid finite element methods*. Vol. 15. Springer Series in Computational Mathematics. New York: Springer-Verlag, 1991, pp. x+350.

[59] YC Fung. "Elasticity of soft tissues in simple elongation". In: *American Journal of Physiology* 213 (1967), pp. 1532–1544.

[60] YC Fung. "Stress-strain-history relations of soft tissues in simple elongation". In: *Biomechanics: Its Foundations and Objectives*. Ed. by YC Fung, N Perrone, and M Anliker. Englewood Cliffs.: New Jersey: Prentice-Hall, Inc., 1971. Chap. 7, pp. 181–208.

[61] BG Galerkin. "Series solution of some problems of elastic equilibrium of rods and plates". Russian. In: *Vest Inzh Tech* 19 (1915), pp. 897–908.

[62] TC Gasser, RW Ogden, and GA Holzapfel. "Hyperelastic modelling of arterial layers with distibuted collagen fibre orientations". In: *J R Soc Interface* 3 (2006), pp. 15–35.

[63] C Geuzaine and JF Remacle. "Gmsh: a three-dimensional finite element mesh generator with built-in pre- and post-processing facilities". In: *Int J Numer Methods Eng* 79.11 (2009), pp. 1309–1331.

[64] V Girault and PA Raviart. *Finite element methods for Navier–Stokes equations*. Vol. 5. Springer Series in Computational Mathematics. Theory and algorithms. Berlin: Springer-Verlag, 1986, pp. x+374.

[65] R Glowinski and MF Wheeler. "Domain decomposition and mixed finite element methods for elliptic problems". In: *First International Symposium on Domain Decomposition Methods for Partial Differential Equations (Paris, 1987)*. Philadelphia, PA: SIAM, 1988, pp. 144–172.

[66] A Greenbaum. *Iterative methods for solving linear systems*. Vol. 17. Frontiers in Applied Mathematics. Philadelphia, PA: Society for Industrial and Applied Mathematics (SIAM), 1997, pp. xiv+220.

[67] JM Guccione, KD Costa, and AD McCulloch. "Finite element stress analysis of left ventricular mechanics in the beating dog heart". In: *J Biomech* 28.10 (1995), pp. 1167–1177.

[68] ME Gurtin. *An introduction to continuum mechanics*. Vol. 158. Mathematics in Science and Engineering. New York: Academic Press Inc. [Harcourt Brace Jovanovich Publishers], 1981, pp. xi+265.

[69] ME Gurtin. "The linear theory of elasticity". In: *Handbuch der Physik*. Ed. by S Flügge and C Truesdell. Vol. VIa/2. Berlin: Springer, 1972, pp. 1–295.

[70] G Haase. *Parallelisierung numerischer Algorithmen für partielle Differentialgleichungen*. Stuttgart: B. G. Teubner, 1999, p. 175.

[71] W Hackbusch. *Iterative Lösung großer schwachbesetzter Gleichungssysteme*. B. G. Teubner, Stuttgart, 1991, p. 382.

[72] W Hackbusch. *Multigrid methods and applications*. Vol. 4. Springer Series in Computational Mathematics. Berlin: Springer-Verlag, 1985, pp. xiv+377.

[73] S Hartmann and P Neff. "Polyconvexity of generalized polynomial-type hyperelastic strain energy functions for near-incompressibility". In: *Int J Solids Struct* 40.11 (2003), pp. 2767–2791.

[74] JL Hennessy and DA Patterson. *Computer architecture: a quantitative approach*. Elsevier, 2012, pp. xxvii+708.

[75] H Heuser. *Lehrbuch der Analysis. Teil 2*. 14th ed. Wiesbaden: Vieweg+Teubner, 2008, p. 737.

[76] I Hlaváček and J Nečas. "On inequalities of Korn's type. I. Boundary-value problems for elliptic system of partial differential equations". In: *Arch Rational Mech Anal* 36 (1970), pp. 305–311.

[77] I Hlaváček and J Nečas. "On inequalities of Korn's type. II. Applications to linear elasticity". In: *Arch Rational Mech Anal* 36 (1970), pp. 312–334.

[78] GA Holzapfel. "Collagen in Arterial Walls: Biomechanical Aspects". In: *Collagen. Structure and Mechanics*. Ed. by P Fratzl. Springer-Verlag, 2008. Chap. 11, pp. 285–324.

[79] GA Holzapfel. "Determination of material models for arterial walls from uniaxial extension tests and histological structure". In: *J Theoret Biol* 238.2 (2006), pp. 290–302.

[80] GA Holzapfel. *Nonlinear Solid Mechanics. A Continuum Approach for Engineering*. Chichester: John Wiley & Sons Ltd, 2000, pp. xiv+455.

[81] GA Holzapfel. "Structural and numerical models for the (visco)elastic response of arterial walls with residual stresses". In: *Biomechanics of Soft Tissue in Cardiovascular Systems*. Ed. by GA Holzapfel and RW Ogden. Vienna: Springer, 2003, pp. 109–184.

[82] GA Holzapfel, TC Gasser, and RW Ogden. "A new constitutive framework for arterial wall mechanics and a comparative study of material models". In: *J Elast* 61 (2000). Soft tissue mechanics, pp. 1–48.

[83] GA Holzapfel, TC Gasser, and RW Ogden. "Comparison of a multi-layer structural model for arterial walls with a Fung-type model, and issues of material stability". In: *J Biomech Eng* 126 (2004), pp. 264–275.

[84] GA Holzapfel and RW Ogden. "Constitutive modelling of arteries". In: *Proc R Soc Lond Ser A Math Phys Eng Sci* 466.2118 (2010), pp. 1551–1596.

[85] GA Holzapfel and RW Ogden. "Constitutive modelling of passive myocardium: a structurally based framework for material characterization". In: *Philos Trans R Soc Lond Ser A Math Phys Eng Sci* 367.1902 (2009), pp. 3445–3475.

[86] GA Holzapfel and RW Ogden. "Modelling the layer-specific 3D residual stresses in arteries, with an application to the human aorta". In: *J R Soc Interface* 7 (2010), pp. 787–799.

[87] GA Holzapfel, G Sommer, M Auer, P Regitnig, and RW Ogden. "Layer-specific 3D residual deformations of human aortas with non-atherosclerotic intimal thickening". In: *Ann Biomed Eng* 35 (2007), pp. 530–545.

[88] GA Holzapfel and HW Weizsäcker. "Biomechanical behavior of the arterial wall and its numerical characterization". In: *Comp Biol Med* 28 (1998), pp. 377–392.

[89] GC Hsiao and WL Wendland. *Boundary integral equations*. Vol. 164. Applied Mathematical Sciences. Berlin: Springer-Verlag, 2008, pp. xx+618.

[90] TJR Hughes. *The Finite Element Method: Linear Static and Dynamic Finite Element Analysis*. New York: Dover, 2000, pp. xxii+682.

[91] JD Humphrey. "An evaluation of pseudoelastic descriptors used in arterial mechanics." In: *J Biomech Eng* 121 (1999), pp. 259–262.

[92] JD Humphrey. *Cardiovascular Solid Mechanics. Cells, Tissues, and Organs*. New York: Springer-Verlag, 2002, pp. xvi+757.

[93] JD Humphrey. "Mechanics of the arterial wall: review and directions." In: *Crit Rev in Biomed Eng* 23 (1995), pp. 1–162.

[94] JD Humphrey and GA Holzapfel. "Mechanics, mechanobiology, and modeling of human abdominal aorta and aneurysms". In: *J Biomech* 45.5 (2012), pp. 805–814.

[95] JD Humphrey and FCP Yin. "On constitutive relations and finite deformations of passive cardiac tissue. Part I. A pseudo-strain energy function". In: *J Biomech Eng* 109 (1987), pp. 298–304.

[96] AD Ioffe and VM Tihomirov. *Theory of extremal problems*. Vol. 6. Studies in Mathematics and its Applications. Translated from the Russian by Karol Makowski. Amsterdam: North-Holland Publishing Co., 1979, pp. xii+460.

[97] M Itskov. "On the theory of fourth-order tensors and their applications in computational mechanics". In: *Comput Methods Appl Mech Eng* 189.2 (2000), pp. 419–438.

[98] M Itskov. *Tensor algebra and tensor analysis for engineers*. Springer, 2007.

[99] M Itskov. "The Derivative with respect to a Tensor: some Theoretical Aspects and Applications". In: *Z Angew Math Mech* 82 (2002), pp. 535–544.

[100] M Jung and U Langer. *Methode der finiten Elemente für Ingenieure*. Stuttgart, Leipzig, Wiesbaden: Teubner, 2001.

[101] L Kantorovich. "On Newton's method for functional equations". Russian. In: *Dokl Akad Nauk SSSR* 59 (1948), pp. 1237–1249.

[102] G Karypis and V Kumar. "A fast and high quality multilevel scheme for partitioning irregular graphs". In: *SIAM J Sci Comput* 20.1 (1999), pp. 359–392.

[103] N Kechkar and D Silvester. "Analysis of locally stabilized mixed finite element methods for the Stokes problem". In: *Math Comp* 58.197 (1992), pp. 1–10.

[104] A Klawonn and LF Pavarino. "Overlapping Schwarz methods for mixed linear elasticity and Stokes problems". In: *Comput Methods Appl Mech Eng* 165.1-4 (1998), pp. 233–245.

[105] A Klawonn and O Rheinbach. "A parallel implementation of dual-primal FETI methods for three-dimensional linear elasticity using a transformation of basis". In: *SIAM J Sci Comput* 28.5 (2006), 1886–1906 (electronic).

[106] A Klawonn and O Rheinbach. "Highly scalable parallel domain decomposition methods with an application to biomechanics". In: *ZAMM Z Angew Math Mech* 90.1 (2010), pp. 5–32.

[107] A Klawonn and OB Widlund. "A domain decomposition method with Lagrange multipliers and inexact solvers for linear elasticity". In: *SIAM J Sci Comput* 22.4 (2000), pp. 1199–1219.

[108] A Klawonn and OB Widlund. "Dual and dual-primal FETI methods for elliptic problems with discontinuous coefficients in three dimensions". In: *Domain decomposition methods in sciences and engineering (Chiba, 1999).* DDM.org, Augsburg, 2001, 29–39 (electronic).

[109] A Klawonn and OB Widlund. "Dual-primal FETI methods for linear elasticity". In: *Comm Pure Appl Math* 59.11 (2006), pp. 1523–1572.

[110] A Klawonn and OB Widlund. "FETI and Neumann-Neumann iterative substructuring methods: connections and new results". In: *Comm Pure Appl Math* 54.1 (2001), pp. 57–90.

[111] A Klawonn and OB Widlund. "Selecting constraints in dual-primal FETI methods for elasticity in three dimensions". In: *Domain decomposition methods in science and engineering.* Vol. 40. Lect. Notes Comput. Sci. Eng. Berlin: Springer, 2005, pp. 67–81.

[112] A Korn. "Über einige Ungleichungen, welche in der Theorie der elastischen und elektrischen Schwingungen eine Rolle spielen". In: *Bull Intern Cracovie Akad Umiejet, Classe des Sciences Math, et Naturelles* (1909), pp. 705–724.

[113] OA Ladyzhenskaya. *The mathematical theory of viscous incompressible flow.* Second English edition, revised and enlarged. Translated from the Russian by Richard A. Silverman and John Chu. Mathematics and its Applications, Vol. 2. New York: Gordon and Breach Science Publishers, 1969, pp. xviii+224.

[114] U Langer and O Steinbach. "Boundary element tearing and interconnecting methods". In: *Computing* 71.3 (2003), pp. 205–228.

[115] U Langer and O Steinbach. "Coupled finite and boundary element domain decomposition methods". In: *Boundary element analysis.* Vol. 29. Lect Notes Appl Comput Mech. Berlin: Springer, 2007, pp. 61–95.

[116] IJ LeGrice, PJ Hunter, and BH Smaill. "Laminar structure of the heart: a mathematical model". In: *Am J Physiol Heart Circ Physiol* 272 (1997), H2466–H2476.

[117] IJ LeGrice, BH Smaill, LZ Chai, SG Edgar, JB Gavin, and PJ Hunter. "Laminar structure of the heart: ventricular myocyte arrangement and connective tissue architecture in the dog". In: *Am J Physiol Heart Circ Physiol* 269 (1995), H571–H582.

[118] Y Maday, C Mavriplis, and A Patera. "Nonconforming mortar element methods: application to spectral discretizations". In: *Domain decomposition methods (Los Angeles, CA, 1988)*. Philadelphia, PA: SIAM, 1989, pp. 392–418.

[119] J Mandel and R Tezaur. "Convergence of a substructuring method with Lagrange multipliers". In: *Numer Math* 73.4 (1996), pp. 473–487.

[120] E Marchandise, C Geuzaine, and JF Remacle. "Cardiovascular and lung mesh generation based on centerlines". In: *Int J Numer Method Biomed Eng* 29.6 (2013), pp. 665–682.

[121] JE Marsden and TJR Hughes. *Mathematical Foundations of Elasticity*. New York: Dover, 1994.

[122] WCH McLean. *Strongly elliptic systems and boundary integral equations*. Cambridge: Cambridge University Press, 2000, pp. xiv+357.

[123] S Mendis, P Puska, and B Norrving, eds. *Global Atlas on cardiovascular disease prevention and control*. World Health Organization, 2011.

[124] J Merodio and RW Ogden. "Instabilities and loss of ellipticity in fiber-reinforced compressible non-linearly elastic solids under plane deformation". In: *Int J Solids Struct* 40.18 (2003), pp. 4707–4727.

[125] J Merodio and RW Ogden. "The influence of the invariant I8 on the stress deformation and ellipticity characteristics of doubly fiber-reinforced non-linearly elastic solids". In: *Int J Nonlinear Mech* 41.4 (2006), pp. 556–563.

[126] NG Meyers. "Quasi-convexity and lower semi-continuity of multiple variational integrals of any order". In: *Trans Amer Math Soc* 119 (1965), pp. 125–149.

[127] C Miehe. "Aspects of the formulation and finite element implementation of large strain isotropic elasticity". In: *Int J Numer Methods Eng* 37.12 (1994), pp. 1981–2004.

[128] C Miehe and E Stein. "A Canonical Model of Multiplicative Elasto-Plasticity. Formulation and Aspects of the Numerical Implementation". In: *Eur J Mech A Solids* 11 (1992), pp. 25–43.

[129] M Mooney. "A theory of large elastic deformation". In: *J Appl Phys* 11 (1940), pp. 582–592.

[130] CB Morrey. *Multiple integrals in the calculus of variations*. Die Grundlehren der mathematischen Wissenschaften, Band 130. Springer-Verlag New York, Inc., New York, 1966, pp. ix+506.

[131] CB Morrey. "Quasi-convexity and the lower semicontinuity of multiple integrals". In: *Pacific J Math* 2 (1952), pp. 25–53.

[132] JC Nagtegaal, DM Parks, and JR Rice. "On numerically accurate finite element solutions in the fully plastic range". In: *Comput Methods Appl Mech Eng* 4.2 (1974), pp. 153–177.

[133] J Nečas and I Hlaváček. *Mathematical theory of elastic and elasto-plastic bodies: an introduction*. Vol. 3. Studies in Applied Mechanics. Amsterdam: Elsevier Scientific Publishing Co., 1980, p. 342.

[134] P Neff. "Mathematische Analyse multiplikativer Viskoplastizit". PhD thesis. Technische Universität Darmstadt, 2000.

[135] JA Nitsche. "On Korn's second inequality". In: *RAIRO Anal Numér* 15.3 (1981), pp. 237–248.

[136] G Of. "BETI-Gebietszerlegungsmethoden mit schnellen Randelementverfahren und Anwendungen". PhD thesis. Universität Stuttgart, 2006.

[137] G Of. "The all-floating BETI method: numerical results". In: *Domain decomposition methods in science and engineering XVII*. Vol. 60. Lect Notes Comput Sci Eng. Berlin: Springer, 2008, pp. 295–302.

[138] G Of and O Steinbach. "The all-floating boundary element tearing and interconnecting method". In: *J Numer Math* 17.4 (2009), pp. 277–298.

[139] RW Ogden. *Non-linear Elastic Deformations*. New York: Dover, 1997.

[140] C Pechstein and R Scheichl. "Analysis of FETI methods for multiscale PDEs". In: *Numer Math* 111.2 (2008), pp. 293–333.

[141] C Pechstein. *Finite and Boundary Element Tearing and Interconnecting Solvers for Multiscale Problems*. Vol. 90. Lecture Notes in Computational Science and Engineering. Springer, 2013.

[142] KB Petersen, MS Pedersen, et al. "The matrix cookbook". In: *Technical University of Denmark* 450 (2008), pp. 7–15.

[143] AJ Prassl, F Kickinger, H Ahammer, V Grau, JE Schneider, E Hofer, EJ Vigmond, NA Trayanova, and G Plank. "Automatically generated, anatomically accurate meshes for cardiac electrophysiology problems". In: *IEEE Trans Biomed Eng* 56.5 (May 2009), pp. 1318–1330.

[144] WH Press, SA Teukolsky, WT Vetterling, and BP Flannery. *Numerical recipes*. Third. The art of scientific computing. Cambridge: Cambridge University Press, 2007, pp. xxii+1235.

[145] A Quarteroni and A Valli. *Domain decomposition methods for partial differential equations*. Numerical Mathematics and Scientific Computation. Oxford Science Publications. New York: The Clarendon Press Oxford University Press, 1999, pp. xvi+360.

[146] A Raoult. "Symmetry groups in nonlinear elasticity: An exercise in vintage mathematics". In: *Comm Pure Appl Math* 8.1 (2009), pp. 435–456.

[147] O Rheinbach. "Parallel iterative substructuring in structural mechanics". In: *Arch Comput Methods Eng* 16.4 (2009), pp. 425–463.

[148] W Ritz. "Über eine neue Methode zu Lösung gewisser Variationsprobleme der mathematischen Physik". In: *J Reine Angew Math* 135 (1908), pp. 1–61.

[149] RS Rivlin. "Large elastic deformations of isotropic materials. I. Fundamental concepts". In: *Philos Trans Roy Soc London Ser A* 240 (1948), pp. 459–490.

[150] RS Rivlin. "Large elastic deformations of isotropic materials. IV. Further developments of the general theory". In: *Philos Trans Roy Soc London Ser A* 241 (1948), pp. 379–397.

[151] RS Rivlin. "Large elastic deformations of isotropic materials. V. The problem of flexure". In: *Proc Roy Soc London Ser A* 195 (1949), pp. 463–473.

[152] RS Rivlin. "Large elastic deformations of isotropic materials. VI. Further results in the theory of torsion, shear and flexure". In: *Philos Trans Roy Soc London Ser A* 242 (1949), pp. 173–195.

[153] DJ Rixen and C Farhat. "A simple and efficient extension of a class of substructure based preconditioners to heterogeneous structural mechanics problems". In: *Int J Numer Methods Eng* 44.4 (1999), pp. 489–516.

[154] MR Roach and AC Burton. "The reason for the shape of the distensibility curve of arteries". In: *Canad J Biochem Physiol* 35 (1957), pp. 681–690.

[155] TR Rockafellar. *Convex Analysis*. Princeton, NJ: Princeton Univ Press, 1972.

[156] J Rodin. "The architecture of the vessel wall". In: *Handbook of Physiology*. Ed. by DF Bohr, AD Somlyo, and HV Sparks. Vol. 2. Bethesda: American Physiological Society, 1980, pp. 1–31.

[157] Y Saad and MH Schultz. "GMRES: a generalized minimal residual algorithm for solving nonsymmetric linear systems". In: *SIAM J Sci Statist Comput* 7.3 (1986), pp. 856–869.

[158] GB Sands, DA Gerneke, DA Hooks, CR Green, B Smaill, and IJ LeGrice. "Automated imaging of extended tissue volumes using confocal microscopy". In: *Microsc Res Tech* 67 (2005), pp. 227–239.

[159] K Schellbach. "Probleme der Variationsrechnung". In: *J Reine Angew Math* 41 (1851), pp. 293–363.

[160] O Schenk and K Gärtner. "On fast factorization pivoting methods for sparse symmetric indefinite systems". In: *Elec Trans Numer Anal* 23 (2006), pp. 158–179.

[161] O Schenk and K Gärtner. "Solving Unsymmetric Sparse Systems of Linear Equations with PARDISO". In: *Future Gener Comp Sy* 20.3 (2004), pp. 475–487.

[162] H Schmid, MP Nash, AA Young, and PJ Hunter. "Myocardial material parameter estimation—a comparative study for simple shear". In: *J Biomech Eng* 128 (2006), pp. 742–750.

[163] H Schmid, P O'Callaghan, MP Nash, W Lin, IJ LeGrice, BH Smaill, AA Young, and PJ Hunter. "Myocardial material parameter estimation: a non-homogeneous finite element study from simple shear tests". In: *Biomech Model Mechanobiol* 7 (2008), pp. 161–173.

[164] J Schröder and P Neff. "Invariant formulation of hyperelastic transverse isotropy based on polyconvex free energy functions". In: *Int J Solids Struct* 40 (2003), pp. 401–445.

[165] CAJ Schulze-Bauer, P Regitnig, and GA Holzapfel. "Mechanics of the human femoral adventitia including high-pressure response". In: *Am J Physiol Heart Circ Physiol* 282 (2002).

[166] HA Schwarz. "Über einen Grenzübergang durch alternierendes Verfahren". In: *Vierteljahrsschrift der Naturforschenden Gesellschaft in Zürich* (1870).

[167] K Schweizerhof and E Ramm. "Displacement Dependent Pressure Loads in Nonlinear Finite Element Analyses". In: *Comput Struct* 18 (1984), pp. 1099–1114.

[168] AA Shabana. *Computational continuum mechanics*. Cambridge: Cambridge University Press, 2008, pp. xii+335.

[169] JC Simo. "Numerical analysis and simulation of plasticity". In: *Handbook of numerical analysis, Vol. VI*. Handb Numer Anal, VI. Amsterdam: North-Holland, 1998, pp. 183–499.

[170] JC Simo, RL Taylor, and KS Pister. "Variational and projection methods for the volume constraint in finite deformation elasto-plasticity". In: *Comput Methods Appl Mech Eng* 51.1-3 (1985). FENOMECH '84, Part I, II (Stuttgart, 1984), pp. 177–208.

[171] J Šístek, B Sousedík, P Burda, J Mandel, and J Novotný. "Application of the parallel BDDC preconditioner to the Stokes flow". In: *Comput Fluids* 46.1 (2011), pp. 429–435.

[172] BF Smith, PE Bjørstad, and WD Gropp. *Domain decomposition*. Parallel multilevel methods for elliptic partial differential equations. Cambridge: Cambridge University Press, 1996, pp. xii+224.

[173] AJM Spencer. "Constitutive theory for strongly anisotropic solids". In: *Continuum Theory of the Mechanics of Fibre-Reinforced Composites*. Ed. by AJM Spencer. Vol. 282. Springer, 1984, pp. 1–32.

[174] AJM Spencer. "Theory of invariants". In: *Continuum Physics*. Ed. by AC Eringen. Vol. I. Academic Press, 1971.

[175] G Starke. "Field-of-values analysis of preconditioned iterative methods for nonsymmetric elliptic problems". In: *Numer Math* 78.1 (1997), pp. 103–117.

[176] O Steinbach. *Numerical approximation methods for elliptic boundary value problems*. Finite and boundary elements, Translated from the 2003 German original. New York: Springer, 2008, pp. xii+386.

[177] O Steinbach. *Stability estimates for hybrid coupled domain decomposition methods*. Vol. 1809. Lecture Notes in Mathematics. Berlin: Springer-Verlag, 2003, pp. vi+120.

[178] A Toselli and O Widlund. *Domain decomposition methods – algorithms and theory*. Vol. 34. Springer Series in Computational Mathematics. Berlin: Springer, 2005, pp. xvi+450.

[179] F Tröltzsch. *Optimal control of partial differential equations*. Vol. 112. Graduate Studies in Mathematics. Providence, RI: American Mathematical Society, 2010.

[180] C Truesdell and W Noll. *The nonlinear field theories of mechanics*. Second. Berlin: Springer-Verlag, 1992, pp. x+591.

[181] C Truesdell. "Some Challenges Offered to Analysis by Rational Thermomechanics". In: *North-Holland Mathematics Studies* 30 (1978), pp. 495–603.

[182] T Valent. *Boundary value problems of finite elasticity: local theorems on existence, uniqueness, and analytic dependence on data*. Springer Publishing Company, Incorporated, 2011.

[183] R Verfürth. "Error estimates for a mixed finite element approximation of the Stokes equations". In: *RAIRO Anal Numér* 18.2 (1984), pp. 175–182.

[184] J Vossoughi, RN Vaishnav, and DJ Patel. "Compressibility of the myocardial tissue". In: *Advances in bioengineering*. Ed. by VC Mow. New York: American Society of Mechanical Engineers, 1980, pp. 45–48.

[185] JP Whiteley, MJ Bishop, and DJ Gavaghan. "Soft Tissue Modelling of Cardiac Fibres for Use in Coupled Mechano-Electric Simulations". In: *Bull Math Biol* 69 (2007), pp. 2199–2225.

[186] BI Wohlmuth. "A mortar finite element method using dual spaces for the Lagrange multiplier". In: *SIAM J Numer Anal* 38.3 (2000), pp. 989–1012.

[187] P Wriggers. *Nichtlineare Finite-Element-Methoden*. Berlin: Springer-Verlag, 2001.

[188] UM Yang et al. "BoomerAMG: a parallel algebraic multigrid solver and preconditioner". In: *Applied Numerical Mathematics* 41.1 (2002), pp. 155–177.

[189] FCP Yin. "Ventricular wall stress". In: *Circ Res* 49 (1981), pp. 829–842.

[190] K Yosida. "Functional analysis, Vol. 123 of Grundlehren der Mathematischen Wissenschaften". In: *Springer-Verlag, Berlin,* 56 (1980), p. 100.

[191] AA Young, IJ LeGrice, MA Young, and BH Smaill. "Extended confocal microscopy of myocardial laminae and collagen network". In: *J Microsc* 192 (1998), pp. 139–150.

[192] OC Zienkiewicz. *The finite element method in engineering science*. London: McGraw-Hill, 1971, pp. xiv+521.

Monographic Series TU Graz

Computation in Engineering and Science

Vol. 1 Steffen Alvermann

Effective Viscoelastic Behaviour of Cellular Auxetic Materials

2008

ISBN 978-3-902465-92-4

Vol. 2 Sendy Fransiscus Tantono

The Mechanical Behaviour of a Soilbag under Vertical Compression

2008

ISBN 978-3-902465-97-9

Vol. 3 Thomas Rüberg

Non-conforming FEM/BEM Coupling in Time Domain

2008

ISBN 978-3-902465-98-6

Vol. 4 Dimitrios E. Kiousis

Biomechanical and Computational Modeling of Atherosclerotic Arteries

2008

ISBN 978-3-85125-023-7

Vol. 5 Lars Kielhorn

A Time-Domain Symmetric Galerkin BEM for Viscoelastodynamics

2009

ISBN 978-3-85125-042-8

Vol. 6 Gerhard Unger

Analysis of Boundary Element Methods for Laplacian Eigenvalue Problems

2009

ISBN 978-3-85125-081-7

Monographic Series TU Graz

Computation in Engineering and Science

Vol. 7 Gerhard Sommer

Mechanical Properties of Healthy and Diseased Human Arteries
2010
ISBN 978-3-85125-111-1

Vol. 8 Mathias Nenning

Infinite Elements for Elasto- and Poroelastodynamics
2010
ISBN 978-3-85125-130-2

Vol. 9 Thanh Xuan Phan

Boundary Element Methods for Boundary Control Problems
2011
ISBN 978-3-85125-149-4

Vol. 10 Loris Nagler

Simulation of Sound Transmission through Poroelastic Plate-like Structures
2011
ISBN 978-3-85125-153-1

Vol. 11 Markus Windisch

Boundary Element Tearing and Interconnecting Methods for Acoustic and Electromagnetic Scattering
2011
ISBN: 978-3-85125-152-4

Monographic Series TU Graz

Computation in Engineering and Science

Vol. 12 Christian Walchshofer

Analysis of the Dynamics at the Base of a Lifted Strongly Buoyant Jet Flame Using Direct Numerical Simulation
2011
ISBN 978-3-85125-185-2

Vol. 13 Matthias Messner

Fast Boundary Element Methods in Acoustics
2012
ISBN 978-3-85125-202-6

Vol. 14 Peter Urthaler

Analysis of Boundary Element Methods for Wave Propagation in Porous Media
2012
ISBN 978-3-85125-216-3

Vol. 15 Peng Li

Boundary Element Method for Wave Propagation in Partially Saturated Poroelastic Continua
2012
ISBN 978-3-85125-236-1

Vol. 16 Andreas J. Schriefl

Quantification of Collagen Fiber Morphologies in Human Arterial Walls
2012
ISBN 978-3-85125-238-5

Vol. 17 Thomas S. E. Eriksson

Cardiovascular Mechanics
2013
ISBN 978-3-85125-277-4

Monographic Series TU Graz

Computation in Engineering and Science

Vol. 18 Jianhua Tong

Biomechanics of Abdominal Aortic Aneurysms
2013
ISBN 978-3-85125-279-8

Vol. 19 Jonathan Rohleder

Titchmarsh–Weyl Theory and Inverse Problems for Elliptic Differential Operators
2013
ISBN 978-3-85125-283-5

Vol. 20 Martin Neumüller

Space-Time Methods
2013
ISBN 978-3-85125-290-3

Vol. 21 Michael J. Unterberger

Microstructurally-Motivated Constitutive Modeling of Cross-Linked Filamentous Actin Networks
2013
ISBN 978-3-85125-303-0

Vol. 22 Vladimir Lotoreichik

Singular Values and Trace Formulae for Resolvent Power Differences of Self-Adjoint Elliptic Operators
2013
ISBN 978-3-85125-304-7

Vol. 23 Michael Meßner

A Fast Multipole Galerkin Boundary Element Method for the Transient Heat Equation
2014
ISBN 978-3-85125-350-4

Monographic Series TU Graz

Computation in Engineering and Science

Vol. 24 Lorenz Johannes John

Optimal Boundary Control in Energy Spaces
2014
ISBN 978-3-85125-373-3

Vol. 25 Hannah Weisbecker

Softening and Damage Behavior of Human Arteries
2014
ISBN 978-3-85125-370-2

Vol. 26 Bernhard Kager

Efficient Convolution Quadrature based Boundary Element Formulation for Time-Domain Elastodynamics
2015
ISBN 978-3-85125-382-5

Vol. 27 Christoph M. Augustin

Classical and All-floating FETI Methods with Applications to Biomechanical Models
2015
ISBN 978-3-85125-418-1